Universitat Autònoma de Barcelona

Development of Carbon Nanocapsules for Biomedical Applications

Magdalena Kierkowicz

Universitat Autònoma de Barcelona

Development of Carbon Nanocapsules for Biomedical Applications

Magdalena Kierkowicz

Tesis Doctoral
Programa de Doctorado en Ciencia de Materiales

Director: Dr. Gerard Tobias Rossell
Tutor: Dr. Lluis Escriche Martinez

Departamento de Química
Facultad de Ciencias

2017

This dissertation is presented for graduation as Doctor by Magdalena Kierkowicz. To this effect, Dr. Gerard Tobias Rossell (PhD supervisor, ICMAB-CSIC) and Dr. Lluis Escriche Martinez (tutor, UAB) sign this certificate.

.....
Dr. Gerard Tobias Rossell (PhD supervisor)

.....
Dr. Lluis Escriche Martinez (tutor)

.....
Magdalena Kierkowicz

Belaterra, 14/06/2017

ACKNOWLEDGMENTS

You take a breath,
You make a step,
You start a path...
The people you meet are important part of your journey.

I would like to express my gratitude to my supervisor Dr. Gerard Tobias for his guidance, patience and scientific discussions. I also thank tutor of my thesis Dr. Luis Escriche Martínez and examination committee.

I owe thank to current and past members of Solid State Chemistry Department, colleagues from ICMAB, and administrative personnel. In particular, I want thank to my special person, dear friend, co-fellow, companion of laughter and misery Markus Martincic.

This thesis would not be possible without fruitful networking in the frame of RADDEL project, which has received funding from the People Programme (Marie Curie Actions) of the European Union's Seventh Framework Programme FP7/2007-2013/ under REA grant agreement n° 290023. I am grateful to all project members for a unique chance to work in a highly stimulating multidisciplinary environment and to our project manager, expert in problem solving, Dr. Jorge Perez.

I would like commemorate: Dr. Belén Ballesteros, Elzbieta Pach, Dr. Judith Oro, Prof. Gustaaf van Tendeloo and Prof. Sara Bals for electron microcopy measurements, Dr. Martin Kalbáč and Ana Santidrian for advanced Raman studies, Dr. Jose Miguel González-Domínguez for help with optimization of washing protocol of $LuCl_3$ filled SWCNTs, Julio Fraile and Prof. Concha Domingo for BET analysis and NLDFT calculations, Ester Tobias-Rossell for box plot analysis of steam treated SWCNTs and DWCNTs and Dr. Chris Serpell for being the best guest researcher I had pleasure to work with so far. I highly appreciate technical support from Marixa Arnedillo, Roberta Ceravola, Mar Estelles, Enrique Irissari, Dr. Bernat Bozzo, Amable Bernabe, Dr. Tariq Jawhari, Dr. Fabio Hollan and Claudio Gamboz.

My sincere acknowledgment goes to Prof. Maurizio Prato who accepted me for secondment at University of Trieste (Italy), where I performed covalent functionalization of carbon nanotubes. I would like express my appreciation to

Prof. Tatiana Da Ros for numerous advices in the field of organic chemistry, enthusiasm and hospitality. Many thanks to Dr. Agnieszka Gajewska, her kindness and help in the lab were priceless. I am grateful to all members of Carbon Nanotechnology Group for friendly welcome.

PhD studies were a valuable experience. Many people (each of them on their own way) had inspired me in research and life through our interactions during the long hours in the lab and after work. Therefore, I would like to thank: Muling, Simo, Ivy, Dejan, Pengfei, Wojtek, Allessandro, Marta, Marcos, Cristina, Davide, Adem, Laura, Stefania, Ashley, Alex, Cinzia, Mateusz, Siming, Vale, Melodie, Wenjie, Rafa, Maria, Tanja, Arturito, Aurelio, Eleonora, Zois, Siddhi, Estela, Cica, Christiano, Mara, Carlos and Mandy.

Warm thanks to my ICN girls: Ela, Karolina and Marianna, and team Caraterra de Barcelona: Sonia, Adri and Tanit for the continuous support, friendship and great memories. I also would like thank my Family. I am because you are.

My special acknowledgment goes to Mrs. Jolanta Stasiewicz, my first chemistry teacher, an amazing educator and great human being. She saw in me potential and helped me discover passion for chemistry.

Last but not least, I am grateful to everyone who made an effort and read the entire manuscript (!).

ABSTRACT

The high surface area and hollow core of carbon nanotubes (CNTs) make them ideal candidates for the development of smart nanovectors in nanomedicine. Their inner cavity can be employed to host selected payloads for either diagnosis or therapeutic purposes while the external walls can be modified to increase their biocompatibility and even for targeting purposes. A major challenge to turn the potential of CNT based devices into customer applications is to reduce or eliminate their toxicity. Taking into account health and safety concerns, intensified research efforts are conducted to improve the biocompatibility of CNTs, including the development of new shortening and purification strategies.

The first part of this thesis focused on the influence of steam on the length, purity, and sidewall integrity of chemical vapor deposition (CVD) and arc discharge single-walled carbon nanotubes (SWCNTs). In order to obtain individualized carbon nanotubes we developed a protocol that consisted of dispersing the samples in *ortho*-dichlorobenzene and employed scanning electron microscopy (SEM) to acquire the images. Short CVD CNTs with median length of ca. 200 nm can be obtained after 10 h of steam treatment, whereas arc discharged CNTs show low reactivity towards steam. The efficiency of other commonly employed shortening methods, namely ball milling, sulfuric/nitric acids, and piranha was also investigated for both SWCNT and multi-walled CNTs (MWCNTs) grown by CVD. A combination of piranha and steam turned out to be the most efficient for SWCNTs, and a combined sulfuric/nitric acids and steam for MWCNTs. These protocols provide a good balance between length distribution, sidewall integrity and purity of samples with a high yield of production.

In the second part, we report on the encapsulation of selected metal halides, of interest for both imaging and therapy, inside CVD and arc discharge SWCNTs. The role of temperature on the degree of end-closing has been investigated, which has allowed the preparation of closed-ended metal halide filled CNTs. Bulk filling of carbon nanotubes results in samples that contain a large amount of non-encapsulated material, external to the carbon nanotubes, which can affect and even dominate the properties of filled carbon nanotubes. Therefore, we developed a straight forward approach that allows the removal of non-

encapsulated compounds in a time efficient and environmentally friendly manner, using water as a “green” solvent in a Soxhlet setup, while minimizing the residual waste.

The last part of the thesis describes the external modification of previously filled CNTs. SWCNTs have been covalently functionalized via Tour and Prato reactions, the former resulting in a higher degree of functionalization. To complete the study, lutetium chloride filled MWCNTs were externally decorated with gold nanoparticles. The developed hybrid nanocapsules hold potential to be employed as dual agents for diagnosis and therapy.

To summarize, this thesis brings new insights in the preparation of carbon nanocapsules, i.e. close-ended filled carbon nanotubes with chosen payloads, for the development of the next generation of theranostic agents.

RESUMEN

La alta superficie y el hueco interior de los nanotubos de carbono (CNTs; del inglés “carbon nanotubes”) los convierte en candidatos ideales para el desarrollo de nanovectores inteligentes para su aplicación en nanomedicina. Su cavidad interna puede emplearse para alojar compuestos seleccionados para propósitos de diagnóstico o terapéuticos, mientras que las paredes externas pueden modificarse para aumentar su biocompatibilidad e incluso para su direccionamiento. Un reto importante para trasladar los sistemas basados en CNT a su uso clínico es la reducción o eliminación de su toxicidad. Teniendo en cuenta la preocupación sobre salud y seguridad de nanomateriales, se han intensificado los esfuerzos de investigación para mejorar la biocompatibilidad de los CNTs, incluyendo el desarrollo de nuevas estrategias para el acortamiento y purificación de los mismos.

La primera parte de esta tesis se enfoca en el estudio de la influencia del vapor de agua sobre la longitud, pureza y la integridad de las paredes de los nanotubos de carbono monocapa (SWCNTs; del inglés “single-walled carbon nanotubes”) producidos tanto por deposición catalítica en fase de vapor (CVD; del inglés “catalytic vapor deposition”) como por descarga de arco. Para obtener nanotubos de carbono individualizados desarrollamos un protocolo que consiste en dispersar las muestras en *orto*-diclorobenceno y hemos empleado microscopía electrónica de barrido (SEM; del inglés “scanning electron microscopy”) para adquirir las imágenes. CVD CNTs cortos con una longitud media de aprox. 200 nm se obtienen después de 10 h de tratamiento con vapor de agua, mientras que los CNT sintetizados por descarga de arco muestran una baja reactividad frente el vapor de agua. También se investigó la eficiencia de otros métodos de acortamiento comúnmente empleados, como son la molienda de bolas, una mezcla de ácido sulfúrico/nítrico y el tratamiento con piraña, tanto para SWCNTs como para CNTs multicapa (MWCNT; del inglés multi-walled carbon nanotubes) producidos por CVD. La combinación de piraña y vapor de agua resultó ser la más eficiente para el acortamiento de SWCNTs, y la combinación de ácido sulfúrico/nítrico con vapor de agua para MWCNTs. Estos protocolos proporcionan un buen equilibrio entre la obtención de nanotubos cortos con una distribución de

longitud pequeña, la integridad de la paredes y la pureza de las muestras con un alto rendimiento de producción.

En la segunda parte, estudiamos la encapsulación de distintos haluros metálicos, de interés tanto para imagen como para terapia, dentro de SWCNTs preparados por CVD y por descarga de arco. Se ha investigado el papel que juega la temperatura de calientamiento en el grado de cierre de las puntas de los nanotubos de carbono. Este estudio ha permitido la preparación de CNTs llenos con haluros metálicos de forma eficiente. El llenado de nanotubos de carbono da lugar a muestras que contienen una gran cantidad de material no encapsulado, externo a los nanotubos de carbono, que puede afectar e incluso dominar las propiedades de los nanotubos de carbono llenos. Por lo tanto, desarrollamos un protocolo que permite la eliminación de compuestos no encapsulados en poco tiempo y respetuoso con el medio ambiente, utilizando agua como solvente "verde" en un sistema Soxhlet, a la vez que se minimiza la cantidad de agua residual.

La última parte de la tesis describe la modificación de las paredes externas de CNTs llenos. SWCNTs se han funcionalizado covalentemente a través de las reacciones de Tour y Prato, la primera resultando en un grado de funcionalización mayor. Para completar el estudio, las paredes externas de MWCNT llenos con cloruro de lutecio fueron decoradas con nanopartículas de oro. Estas nanocápsulas híbridas tienen interés para su uso como agentes duales para el diagnóstico y la terapia.

En resumen, esta tesis aporta nuevos conocimientos sobre la preparación de nanocápsulas de carbono, és decir, nanotubos de carbono cerrados y rellenos con materiales seleccionados, para el desarrollo de la siguiente generación de agentes teranósticos.

STRUCTURE OF THE THESIS

This thesis is organized in eight chapters, including a general introduction **(Chapter 1)**, objectives **(Chapter 2)**, an experimental part based on the main results and discussion **(Chapters 3-7)**, and the general conclusions **(Chapter 8)**.

In the experimental part, we tackle different aspects that are essential for the production of carbon nanocapsules (closed-ended filled carbon nanotubes), namely purification and shortening, endohedral filling and external functionalization. Initially, we studied the role of time on the length distribution and structure of carbon nanotubes treated with steam **(Chapter 3)**, and also compared and combined different methods commonly used in the literature **(Chapter 4)** in order to achieve samples of carbon nanotubes characterized by high purity, short lengths with a narrow distribution and well preserved tubular structure. The latter is of particular interest for the efficient encapsulation and confinement of materials in the interior of carbon nanotubes, which was the aim of the following chapter **(Chapter 5)**.

Several metal halides (NaI, $EuCl_3$, $LuCl_3$, $LuBr_3$, LuI_3), of interest for biomedical imaging and therapy were employed to develop carbon nanocapsules, and special emphasis was paid to understand the role of temperature on the degree of end closing. To complete the study, the as-prepared carbon nanocapsules were covalently functionalized via Tour and Prato reactions **(Chapter 6),** and the decoration of the external walls with gold nanoparticles **(Chapter 7)** was investigated to achieve a dual agent that contained inorganic materials both in the inner cavities and the external walls of carbon nanotubes.

As mentioned, the general conclusions that have been drawn from the chapters dealing with the results and discussion will be summarized in the last chapter **(Chapter 8)**.

Three Annexes have also been included that contain methods **(Annex A)**, instrumentation **(Annex B)** and a list of publications **(Annex C)**.

TABLE OF CONTENTS

PART III ANNEXES

LIST OF SYMBOLS AND ABBREVIATIONS

^{1}H-NMR - nuclear magnetic resonance
A - absorption
AFM - atomic force microscopy
ARTEM - atomic resolution transmission electron microscopy
AuNPs - gold nanoparticles
BBB - blood-brain barrier
BET - Brunauner, Emmett and Teller
BWF - Breit-Wigner-Fano
CCFs - carboxylated carbonaceous fragments
C_h - chiral vector
CNTs - carbon nanotubes
CT - computerized tomography
CVD - chemical vapor deposition
DLS - dynamic light scatering
d_t - diameter of carbon nanotube
DWCNTs - double-walled carbon nanotubes
ε- extinction coefficient
EDX - energy dispersive X-ray spectroscopy
E_{ii} - transition energy
E_{laser} - laser energy
ESI-MS - electrospray ionization mass spectrometry
f-CNTs -functionalized carbon nanotubes
fdpr-CNTs - functionalized carbon nanotubes with cleaved protecting group
FET - field effect transistor
FY -filling yield
H_0 - null hypothesis
HAADF - high angle annular dark field
HRTEM - high resolution transmission electron microscopy
I_D/I_G-intensity ratio D to G band
IQR - interquartile range
I-Vis - optical imaging
l - length of optical path
m - mass of the sample

M -metallic carbon nanotube
MNPs - metal nanoparticles
MRI - magnetic resonance imaging
MW - molar weight
MWCNTs - multi-walled carbon nanotubes
MX - metal halide
MXNTs - inorganic nanotubes of metal halides
N - number of measured CNTs (or AuNPs)
NIR - near-infrared region
NIRF- near-infrared fluorescence
NLDFT - non-local density functional theory
PAT - photoacoustic tomography
PDI -polydisperisty
PET - positron emission tomography
PTT - photothermal therapy
Q1 - 25^{th} percentile
Q3 - 75^{th} percentile
RBM -radial breathing mode
S - semiconducting carbon nanotube
SBET - specific surface area
SEM - scanning electron microscopy
SERS - surface enhanced Raman scattering
SPECT - photon emission computed tomography.
SPR - surface plasmon resonance
SQUID - superconducting quantum interference device
STEM - scanning transmission electron microscopy
SWCNTs -single-walled carbon nanotubes
TEM - transmission electron microscopy
TFTs - thin-film transistors
TGA - thermogravimetric analysis
TLC - thin layer chromatography
V_A - accumulated pore volume up to 1.25 nm
ω - frequency of RBM
X@CNTs -filled carbon nanotubes

LIST OF FIGURES

LIST OF SCHEMES

LIST OF TABLES

PART I

INTRODUCTION

AND

OBJECTIVES

CHAPTER 1

INTRODUCTION

Sumio Iijima, Japanese scientist credited for discovery of carbon nanotubes (CNTs), once asked, ¨How did you find carbon nanotubes?¨, answered after some thought, ¨Logic or Rationale¨.[1] Three carbon allotropes were known at the time: diamond, graphite and fullerenes. Iijima was interested in the mechanism of fullerenes growth. He studied under electron microscope carbon materials from different sources. In summer 1991 he observed needle-like structures coexisting on the grid with fullerenes obtained from graphitic soot. EUREKA!!! THE BIG DISCOVERY WAS MADE. The new nanostructures described by Iijima as ¨helical microtubules of graphitic carbon¨, were later coined as carbon nanotubes. The same year, in November, the results of his work were published in the journal Nature.[2] It thrilled the world of science. Since then, nanotubes found numerous commercial and potential applications, just to name a few: biosensors, supercapacitors, sollar cells, water filters,[3] gecko inspired adhesives,[4] flexible electronics[5] etc. The carbon nanotube community blossomed, but other exciting materials as graphene[6] also appeared…

25 years later the question arises: **What makes carbon nanotubes interesting thus far?** During this time much progress in their synthesis has been made. Besides physical and chemical properties the impact on human health of carbon nanotubes has been broadly studied. We know their strengths and disadvantages, which enables us to fully exploit the potential of these nanomaterials.

In this chapter an overview of carbon nanotubes with strong emphasis on their biomedical applications is presented.

1.1. Carbon allotropes

Carbon is the fourth most abundant element in the universe by mass and the key ingredient for life on Earth.[7, 8] It is nonmetallic and tetravalent - making four electrons available to form covalent chemical bonds. Carbon atoms between themselves readily adopt sp^2 or sp^3 bonding arrangements, which result in different structures.[9] Varying forms of an element with different physical properties are called allotropes. Carbon has several of them. Here, we focus on selected examples (Fig. 1.1). Among the allotropes of carbon, diamond and graphite have been known since ancient times. The nano-forms: fullerenes, nanotubes and graphene, have been discovered relatively recently.[7, 10, 11]

Diamond consists of a rigid three-dimensional array of carbon atoms. In contrast, graphite forms from stacked planes of covalently bonded hexagonal rings of carbon atoms that can slide across one another easily. Graphene is a single sheet of graphite, and carbon nanotubes can be seen as seamlessly rolled up layers of graphene. Finally, fullerenes are spherical or ellipsoidal molecules with six- and five-membered rings of carbon atoms.[8, 12]

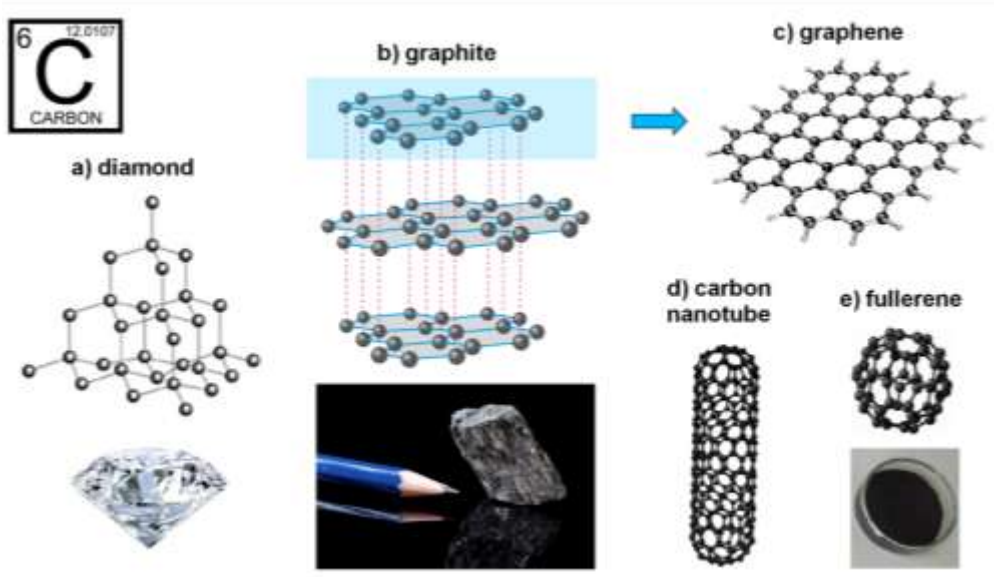

Figure 1.1. Selected allotropes of carbon: a) diamond, b) graphite, c) graphene, d) carbon nanotube, e) fullerene.

Carbon allotropes have distinct characteristics, which are summarized in Table 1.1. For example, diamond is a colorless, transparent, crystalline solid and one of the hardest materials known to date. Graphite is black and shiny but soft. Diamond is an electric insulator while graphite reveals good electric conductivity. Nanocarbons have unique properties and appear as black or dark brown soot-like powders.[13] For instance, an image of fullerene powder is presented in the bottom part of Figure 1.1e. Next, an overview on carbon nanotubes is presented since they are the main focus of this thesis.

Table 1.1. Important parameters of selected carbon allotropes. Adapted from [10].

Allotrope	Diamond	Graphite	Graphene	Nanotube	Fullerene
Dimension	3D	3D	2D	1D	0D
Hybridization (bond arrangement)	sp^3	sp^2	sp^2	sp^2	sp^2
Density (g/cm^3)	3.5	2.1-2.3	2.3	1.2-2.0	1.7
Electronic properties	Insulator	Conductor	Zero-gap semi conductor	Meta/ semi conductor	Semi conductor

1.2. Carbon nanotubes

1.2.1. Structure

CNTs are one of the allotropes of sp^2 hybridized carbon, characterized by cylindrical elongated shape. They are made of rolled-up honeycomb carbon lattice of graphene (Fig. 1.2a). According to the number of layers carbon nanotubes are classified as single- and multi-walled nanotubes (denoted as SWCNTs and MWCNTs). A specific category are double-walled carbon nanotubes (DWCNTs) composed of exactly two concentric layers. They show intermediate properties between both single-walled and multi-walled nanotubes, but are characterized by higher chemical and mechanical resistance compared to the former.

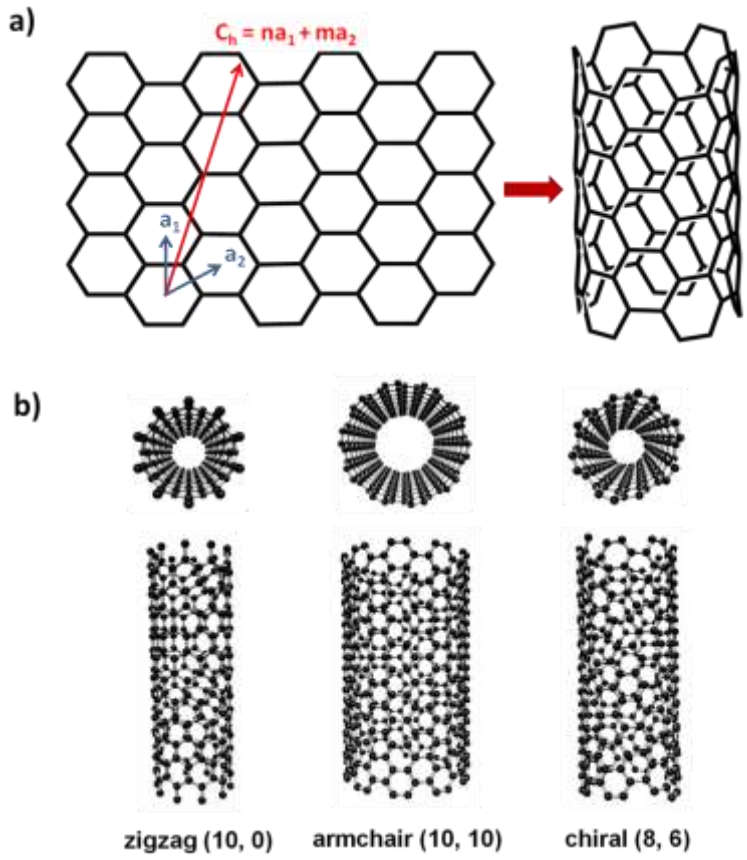

Figure 1.2. a) Schematic representation of SWCNT as the result of rolling up a sheet of graphene, b) different geometries of SWCNTs: zigzag, armchair and chiral.

Depending on the wrapping of the original hexagonal lattice SWCNTs occur in three different forms, namely zigzag, armchair and chiral (Fig. 1.2b). These are determined by the chiral vector (C_h), which connects the centers of two adjoining hexagons. The chiral vector is defined as: $C_h = na_1 + ma_2$, where n and m are integers, and a_1 and a_2 are basis vectors of the hexagonal sheet. The (n, 0) nanotube is called zigzag and the (n, n) structure is referred to armchair. Finally, if $n > m > 0$ the nanotube will be chiral. The chirality predetermines not only electronic structure but also many physical properties of the nanotubes.[14-17] SWCNTs can be metallic ($n = m$ *or* n-m divisible by 3) or semi-conducting (n-m non divisible by 3) depending on the n and m values.[18]

CNTs are usually closed at the ends with hemispherical fullerene-like caps, but some might appear open-ended after the synthesis (Fig. 1.3). Typically, the diameters of SWCNTs range from 0.4 to 3 nm and MWCNTs from few nm to 100 nm. Length of CNTs varies from tens of nanometers to several centimeters. [3, 19, 20] However, they may differ dramatically in size, morphology and chemical composition, either by design or as a result of contamination during production.

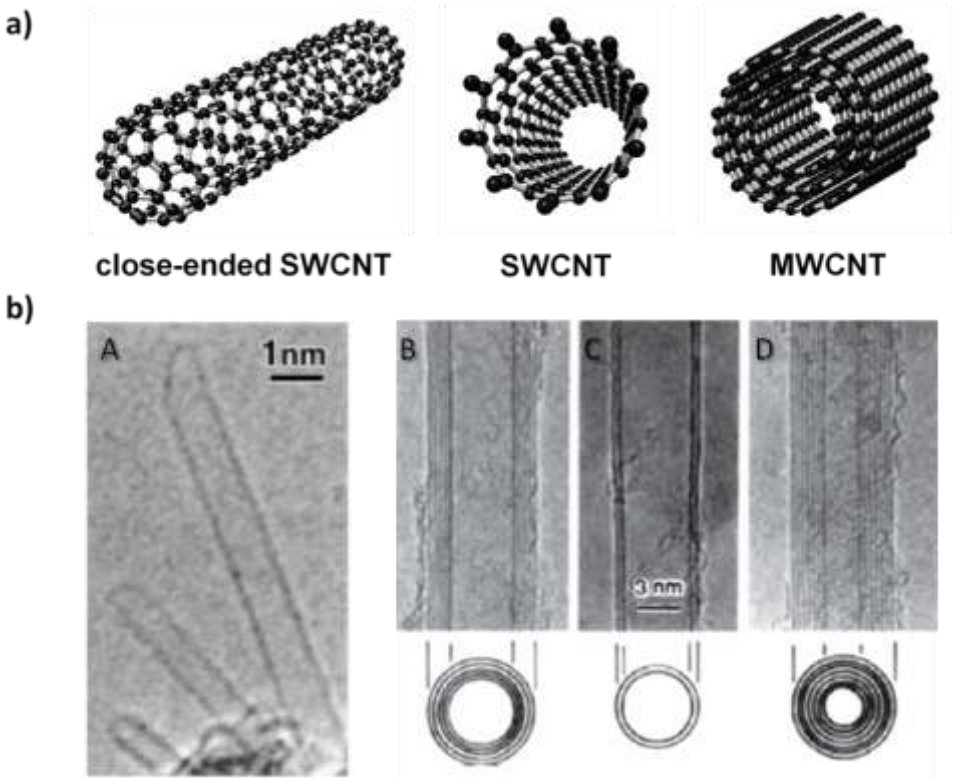

Figure 1.3. a) Models of different forms of CNTs: closed-ended SWCNT, open-ended SWCNT and MWCNT, respectively. b) High-resolution transmission electron microscopy (HRTEM) images of: SWCNTs with closed tips (A),[21] and MWCNTs (B-D).[2] The inner space corresponds to the diameter of the inner hollow cavity of the tube. The separation between the closely spaced fringes in the MWCNTs (B-D) is 0.34 nm, close to the spacing between graphite planes. Every layer in the image (fringe) corresponds to the edges of each cylinder in the nanotube assembly. A cross-section of each tubule is illustrated. (B) Tube consisting of five graphitic sheets, diameter 6.7 nm. (C) Two sheets tube, diameter 5.5 nm. (D) Seven sheet tube, diameter 6.5 nm, which has the smallest hollow diameter (2.2 nm).[2]

1.2.2. Synthesis

The three oldest and the most known methods of CNTs synthesis are arc discharge,[22, 23] laser vapor ablation[24] and chemical vapor deposition (CVD).[25] It is worth to mention that many new approaches are investigated, for example: sonochemical, hydrothermal and electrolysis.[26]

Regardless of the method of production, the basic elements for the formation of nanotubes are a catalyst, a source of carbon, and a source of energy. Both arc discharge and laser vaporization involve high energy sources and high temperature to induce assembly of gaseous carbon atoms into CNTs. They lead to reduced number of defects during growth process.[26] Still, production is limited, because they require continuous replacement of the graphitic target.[14] A subsequent purification step from fullerenes, catalyst particles and amorphous carbon present as impurities is also mandatory. In some cases it is possible to generate MWCNTs without catalyst.[27, 28] The laser vaporization provides higher yield, better crystallinity and narrower size distribution of CNTs in comparison to arc discharge, but the cost of synthesis is really high. On the other hand CVD provides good quality material and it has been proven as the best method for commercial purposes.[19, 29]

CVD synthesis involves passing a hydrocarbon through a hot tubular reactor, where a catalyst is placed (Fig. 1.4). The most common catalysts are Fe,[30] Ni[31] and Co.[32]

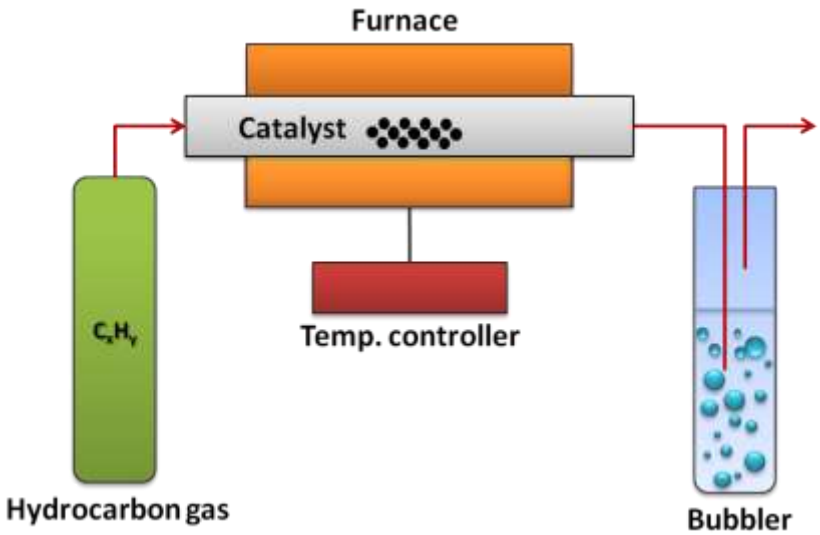

Figure 1.4. Schematic diagram of a CVD setup in its simplest form. Adapted from [33].

Usually, the source of carbon is a hydrocarbon gas (eg. methane[34, 35]). When a liquid hydrocarbon (benzene,[36] alcohol,[37] etc.) is used, it is heated and purged with an inert gas, which serves as a carrier of the hydrocarbon vapor into the reaction zone. In order to decompose the hydrocarbon sufficiently high temperature (500-1200 °C) needs to be achieved.[37, 38] Catalyst particles present in the reaction chamber are the nucleation sites to initiate growth of nanotubes. They might also accelerate the carbon feedstock decomposition.[39]

1.3. Properties and applications of carbon nanotubes

Carbon nanotubes are important players in the emerging field of nanotechnology. Comparing to other materials they show unique combination of mechanical, electrical, thermal and optical properties (Table 1.2). These are leading to numerous studies of their potential applications. [14, 18, 40-42]

Table 1.2. Physical properties of CNTs.

Properties	Parameters	Values	Ref.
Mechanical	Young´s modulus [TPa]	≈ 1 SWCNTs 1.28 MWCNTs	[19]
	Tensile strength [TPa]	≈ 0.1	
Electrical	Electrical character of SWCNTs	Metallic (n-m divisible by 3) Semiconducting (n-m non divisible by 3)	[19]
	Resistivity [Ω·m]	10^{-4} SWCNTs (at RT)	
Thermal	Ballistic conduction [$W \cdot m^{-1} \cdot K^{-1}$]	1800- 6000 (at RT)	[42]
Optical	Fundamental gap of SWCNTs [eV]	0 Metallic ≈ 0.5 Semiconducting	[19]

Transfer of CNTs to technology can be conventionally dated at 1998, when researchers in IBM developed the first nanotube transistors that operated at room temperature.[43] CNTs are commonly incorporated as reinforcement in professional sport equipment like bikes and golf club shafts.[3, 44] They were also

used in NASA's Juno spacecraft to protect critical components against electrostatic discharge.[3, 43] A spectacular example of nanotechnology is a handheld carbon nanotube biosensor multiplex assay for the detection of Lassa, Dengue and Ebola virus hemorrhagic fevers, developed and patented by Nanomix, Inc.[43, 45] Moreover CNTs hold great promise in electronics, for example as the channel materials for thin-film transistors (TFTs) for flexible and stretchable devices. [3, 46, 47] Nowadays, exist more than 700 companies, including IBM, Intel, NASA, NEC, Samsung and Showa Denko, which employ CNTs into their products.[48] Commercial applications are wide ranging from aerospace and defense, automotive parts, composites and coatings, energy, environmental, electronics and semiconductors, medical, batteries and capacitors to textile (Fig. 1.5).[3] In fact, CNTs are used mainly in polymers, which represented in 2014 more than 60% of industrial fabrication shares.[49] Currently, the worldwide commercial CNTs production capacity exceeds several thousand tons per year accounting for 28% of overall nanomaterials market.[48] A continuous growth in CNTs demand can be observed (Fig. 1.6) and its primarily driven by MWCNTs.[49, 50]

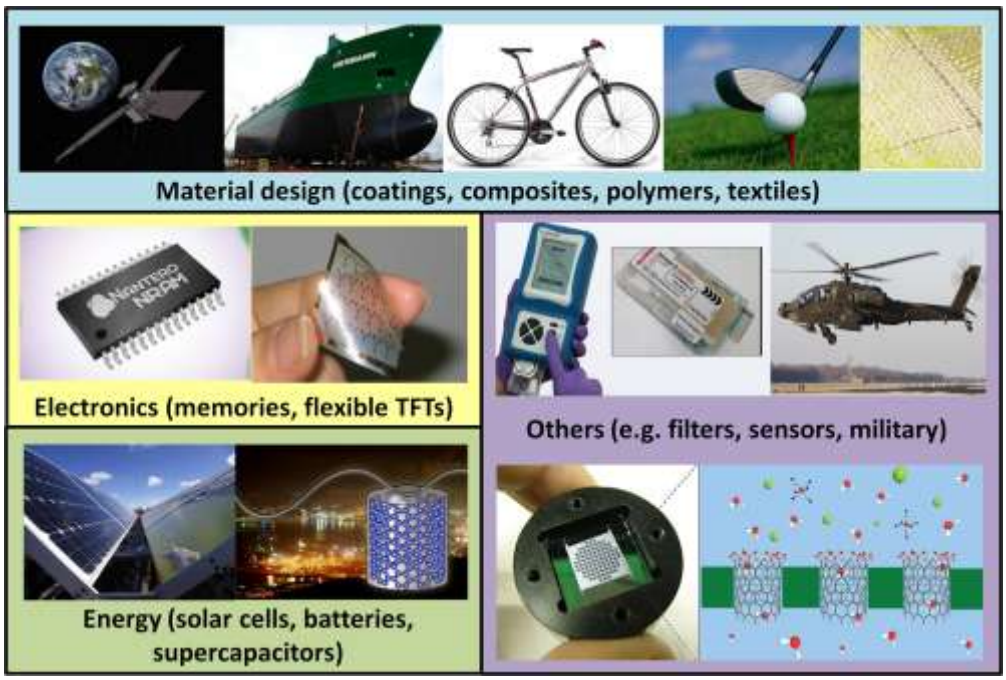

Figure 1.5. Illustrative example of several areas of CNTs applications: material design, electronics, energy and others.

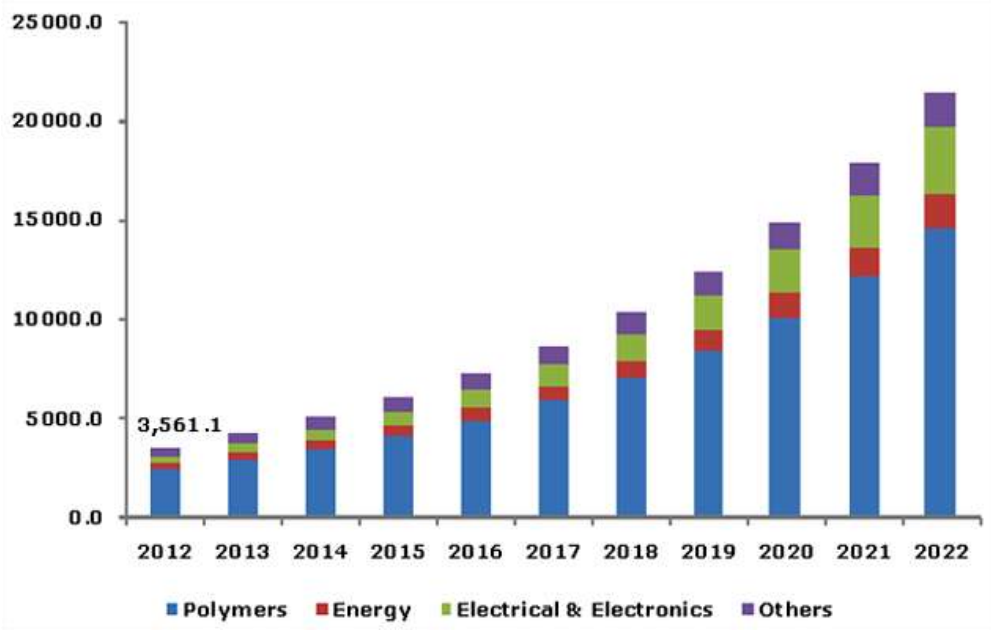

Figure 1.6. Global carbon nanotubes market estimates and forecast, by application, 2012-2022 (Tons).[49]

1.4. Applications of carbon nanotubes in the biomedical field

Carbon nanotubes for medical applications require in-depth scientific studies and still face many challenges. Also the industrial market reveals a gap in this field. [49] Table 1.3 summarizes a few key factors determining the biomedical potential of CNTs.

CNTs are primarily explored in three areas: cellular growth and tissue engineering, sensors, and as nanovectors for both imaging/diagnosis and therapeutic applications (Fig. 1.7).

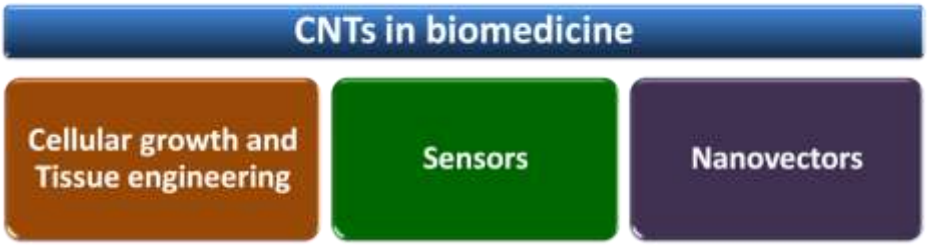

Figure 1.7. Classification of the major biomedical applications of carbon nanotubes.

Table 1.3. Pros and cons of using CNTs for biomedical applications. Adapted from [51].

PROS	CONS
• Unique mechanical properties offer *in vivo* stability • Extremely large aspect ratio, offers template for development of multimodal devices • Capacity to readily cross biological barriers: novel delivery systems • Unique electrical and semiconducting properties; constitute advanced competences for *in vivo* devices • Hollow, fibrous, light structure with different flow dynamics properties; advantageous *in vivo* transport kinetics • Mass production - low cost; attractive for drug development • Simultaneous filling and external decoration with selected payloads	• Controversial studies on biodegrability • Large available surface area for protein opsonization • As-produced material insoluble in most solvents; need to surface treat preferably by covalent functionalization to confer aqueous solubility (i.e. biocompatibility) • Bundling; large structures with less than optimum biological behavior • Healthy tissue tolerance and accumulation; unknown parameters that require toxicological profiling of material • Great variety of CNTs types; makes standardization and toxicological evaluation cumbersome

1.4.1. Cellular growth and tissue engineering

CNTs are one of the strongest and the stiffest materials known to date. Their high tensile strength results from the covalent sp^2 bonds between carbon atoms. Through a fibril structure and high elasticity they resemble collagen, the main component of connective tissue relevant for bone growth.[52, 53] These attributes enable the use CNTs for stem cell related therapies: preparation of nanoscaffolds and reinforcement of prosthetic composite materials.[54-56] It has

been proven that CNTs promote bone formation *in vivo*. [53, 57] Their high electrical conductivity and corrosion resistance make them promising candidates for nerve tissue engineering.[58-60] CNTs based substrates promote neuronal differentiation.[61, 62] Recent *in vivo* findings reveal CNTs induced stimulation of nerve regeneration processes without toxic response in a rat sciatic injury model.[63] Other studies propose the employment of nanotubes as actuators in artificial muscles.[64, 65]

1.4.2. Sensors

The combination of small size, high strength, and high electrical and thermal conductivity makes CNTs interesting for the development of CNTs based materials.[3, 66, 67] There are two kinds of CNTs biosensors. The first type are the CNT optical sensors, which mechanism depends on the response of the band-gap fluorescence shift of SWCNTs to the environment or on the Raman scattering properties of nanotubes. The second type are electronic and electrochemical mediated sensors which work principle is based on the "gating molecules". These molecules bind to the surface of nanotubes and act as the modulators of the conductance of semi-conducting SWCNTs. This phenomena is employed in field effect transistor (FET) devices.[68]

NIR fluorescence is used to detect blood glucose, the conformational polymorphism of DNA, fluorescent detection of cellular ATP, sensing single-molecule H_2O_2 and nitric oxide to name some. Raman and surface enhanced Raman scattering (SERS) biosensors can for instance signal proteins. Electronic sensors are employed to monitor various chemical and biological molecules such as ammonia, nitrogen dioxide, DNA, etc. Electrochemical biosensors detect for instance DNA, viruses and antigens. Also dual-mode biosensors for electrical and surface plasmon resonance (SPR) measurements have been reported.[69-71]

1.4.3. Nanovectors

The high surface area and hollow core make CNTs ideal candidates for the development of nanocarriers where CNTs act as vectors for the attachment of targeting ligands, therapeutic agents, and biomolecules.[72, 73] Moreover, CNTs are easily internalized by cells. Their biodistribution and pharmacokinetic

properties can be tuned by controlling the size, the surface chemistry, and targeting groups.[74, 75]

CNTs based vehicles are intensively explored as new arsenal for the theranostics applications.[40, 76, 77] An schematic example of sophisticated CNT-based multimodal platform is showed in the figure below (Fig. 1.8).

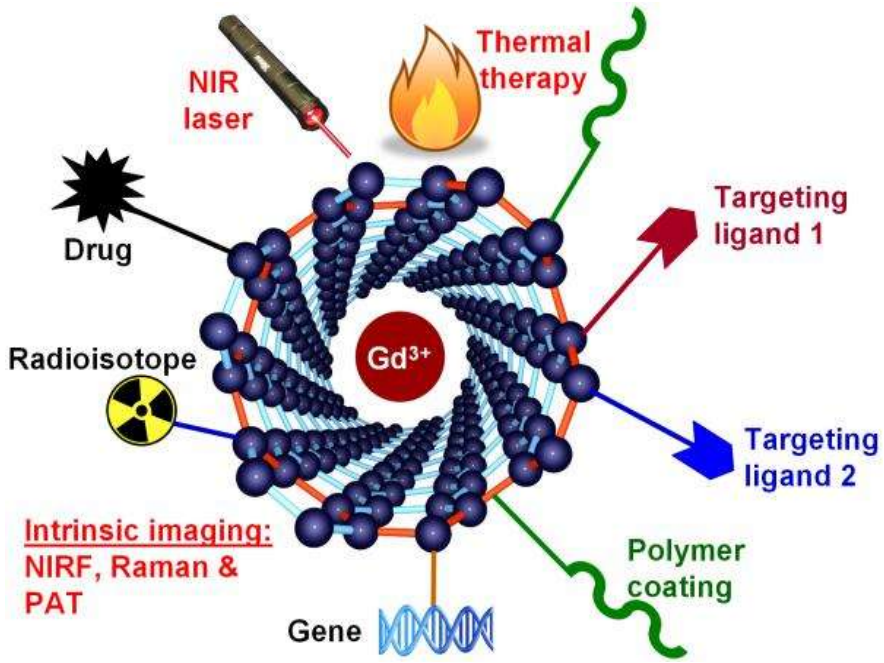

Figure 1.8. A multifunctional SWCNT-based platform incorporating multiple receptor targeting, multimodality imaging, and multiple therapeutic entities. Not all functional moieties will be necessary and only suitably selected components are needed for each individual application.[78]

Owing to their good optical absorbance in the near-infrared region (NIR) CNTs have been successfully applied in thermal therapy of tumors.[79-81] Upon NIR radiation CNTs emit heat and kill cancer cells. It has been proven effective for the treatment of a wide variety of cancer types both *in vitro* and *in vivo*.[82] Heat-based cancer therapy enables to eliminate cancer stem cells, resistant to traditional chemo- and radiotherapy, in a noninvasive manner.[83] Moreover, it can be joint with targeted drug delivery, which was demonstrated on functionalized doxorubicine loaded SWCNTs.[84] Besides cancer, CNTs-mediated photothermal ablation was studied in athlerosclerosis treatment[85] and control of gene expression[86] in mice models.

The quasi one-dimensional semi-conducting SWCNTs are characterized by fluorescence emission in near-infrared region (NIRF). This phenomenon has been

studied for *in vivo* imaging and *in vitro* detection of disease related-biomarkers with limited autofluorescence in this region.[87-92] CNTs exhibit unique resonance Raman scattering and emission of photoacoustic signals used in Raman imaging[93-97] and photoacoustic tomography (PAT),[95, 98-101] respectively. Attachment of dye molecules onto the surface of CNTs might enhance these properties. For example, SWCNTs with adsorbed indocyanine green revealed 300 times higher photoacoustic contrast in living tissues compared to non-functionalized nanotubes.[102] Bismuth (III) filled nanotubes have potential as X-ray contrast agents,[103] and CNTs filled with gadolinium (III) salts can be employed in magnetic resonance imaging (MRI).[104-106] An alternative to fill nanotubes, in order to develop novel contrast agents, is their external decoration with ferromagnetic materials, for instance with iron oxide.[107, 108] Even a high amount of metal catalyst present in as-synthesized CNTs might provide already sufficient contrast.[95] In addition, radionuclides filled or conjugated onto the surface of CNTs are used as positron emission tomography (PET) or single photon emission computed tomography (SPECT) agents.[109-113] Comparison of CNTs based imaging modalities is presented in Table 1.4.

Table 1.4. Summary of CNTs based imaging modalities.

Modality*	Contrast agent	Resolution	Sensitivity	Penetration	References
MRI	Gd^{3+}, Fe_2O_3	High	Low	Good	[95, 104-108, 114, 115]
X-ray	Bi^{3+}	High	Medium	Good	[103]
NIRF	SWCNT	Medium	Medium	Poor	[88-92, 108]
Raman	SWCNT	Low	Medium	Poor	[93-97]
PAT	SWCNT	High	Medium	Poor	[95, 98-101]
PET/SPECT	Radioisotopes	Medium	High	Good	[109, 110, 112, 113]

*** MRI - magnetic resonance imaging, NIRF - near-infrared fluorescence, PAT - photoacoustic tomography, PET - positron emission tomography, SPECT - photon emission computed tomography**

An increased amount of publications is focused on gene therapy using nanocarriers. DNA or siRNA can be attached to CNTs via: i) covalent functionalization, ii) loading on cationic molecule functionalized CNTs, iii) direct wrapping. These delivery systems enable cell penetration in contrast to free nucleic acids, which are macromolecules. CNTs based gene vectors can be employed for

the treatment of cancer,[116-119] restenosis, HIV,[120, 121] myelogenous leukemia[122] and insulin resistance.[123]

Many authors have reported *in vitro* and *in vivo* studies of CNTs platforms for drug deliver (Table 1.5). For example, cisplatin loaded nanotubes can be used in testicular, bladder, lung, gullet (oesophagus), stomach and ovarian cancer therapy. Paclitaxel conjugated CNTs are studied to cure breast tumors.[124-128]

Table 1.5. Examples of anticancer drugs delivered using CNTs.

Name of drug	SWCNT/ MWCNT	Reference
Cisplatin	SWCNT MWCNT	[124, 125, 129] [126, 127]
Carboplatin	SWCNT	[130]
Paclitaxel	SWCNT MWCNT	[131] [132]
Gemcitabine	SWCNT	[133]
Doxorubicin	SWCNT MWCNT	[134] [84, 135-137]
Mitoxatrone	MWCNT	[138]
Methotrexate	MWCT	[139, 140]
Quercitin	SWCNT	[129]
Folic acid	MWCNT	[140]

CNTs might be especially valuable in the treatment of brain cancers: naplastic astrocytomas and glioblastomas. Most of the drugs used currently in chemotheraphy resist the penetration of the blood-brain barrier (BBB), while functionalized MWCNTs can be distributed into the brain.[73, 141] For instance, it has been described PEGylated MWCNTs loaded with the targeting ligand angiopep2 and drug doxorubicin. The resulting conjugate targets low density lipoprotein receptor, which is overexpressed on the BBB and C6 glioma cells.[137] Covalently functionalized CNTs have been investigated for antiviral and tumor vaccination using immuneactivating peptides (FMDV-derived peptide, AMA-1 peptide) and lysate proteins, respectively.[142]

1.4.4. Toxicity and safety concerns

Nanotechnology and its applications have already become part of our everyday lives. Therefore, it is pushing the scientific community for more investigation and regulation of related hazards.

Toxicity of nanomaterials depends on their size, surface area, shape and elemental composition.[73] Carbon nanotubes due to their fibrous nature and needle like shape show similarities to asbestos, which may induce carcinogenesis.[143] This raised serious health concerns. However, we know that CNTs and asbestos differ in chemical composition, weigh and surface properties. Therefore, they have different toxicological profile.[144] Knowledge of the *in vivo* biodistribution and pharmacokinetics of CNTs is essential to determine their use in biomedical applications. CNTs accumulation sites can be determined using radiolabelling, Raman spectroscopy and optical imaging (I-Vis). CNTs concentration, length, purity and functionalization have considerable impact on cell viability and proliferation.[145] As-produced nanotubes tend to form bundles, while functionalized CNTs disperse much better. Recent studies revealed that reduction of length and chemical modification results in safe material, which might be stably suspended in biological fluids without aggregation.[75] For instance PEG-functionalized, biocompatible SWCNTs injected into mice were cleared from blood in one day and from other organs in about two months. Relatively low uptake in the reticuloendothelial system suggested that properly modified SWCNTs are safe for biological use.[146] Also removal of metal catalyst decreases toxicity of CNTs.[147] Despite of all these studies, clear regulatory aspects for the employment CNTs in medical field do not exist so far, although there is an increased interest on the use of CNTs based therapeutics by the pharmaceutical industry.

1.5. Purification of carbon nanotubes

The presence of impurities in samples of CNTs may not only induce toxicity, but also hinder the unique properties of CNTs. The purity of nanotubes is extremely important for the development of many of their commercial applications, particularly in: nanomedicine, electronics and energy storage.[148] Bulk synthesized CNTs usually contain residual material from the metal catalyst and supports employed along with carbonaceous materials that are formed as side-product (Fig. 1.9).

.

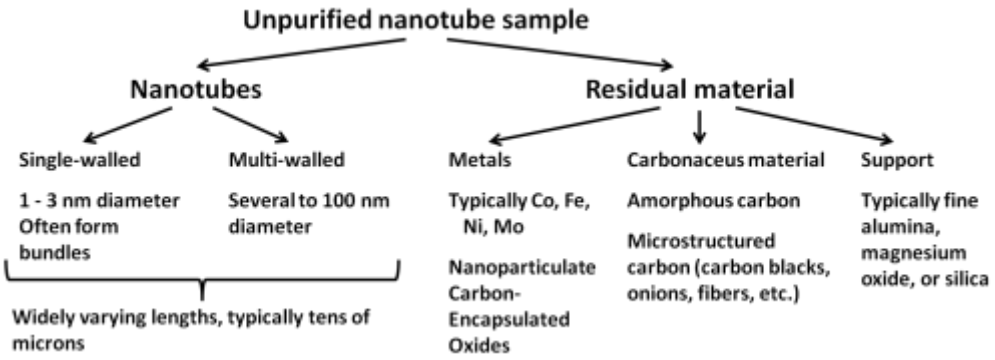

Figure 1.9. Possible components in a sample of unpurified CNTs. Adapted from [149].

The amount, structure, composition and morphology of impurities vary depending on the synthesis protocols. Hence, there is no customized universal method for creating high-quality CNTs samples.

The key for a successful purification is to benefit from the different physical/chemical properties between CNTs and impurities. Therefore **purification methods can be classified as chemical and physical.**

The chemical methods separate impurities based on their reactivity. They involve oxidation of CNTs in liquid or gas environment. The carbonaceous impurities and free catalyst particles are removed first, because they in general are more susceptible to oxidation. During this process, if the oxidants have sufficient power, tips of nanotubes become open and impurities can be removed also from their internal cavities. The most commonly used oxidants are: mineral acids (H_2SO_4, HNO_3, HCl), potassium permanganate ($KMnO_4$), hydrogen peroxide (H_2O_2), and air.[150-156] In order to obtain stronger oxidation effects mixtures of oxidants are employed: piranha solution, H_2SO_4/HNO_3, HNO_3/HCl.[157] On the other hand, water steam is reported as mild oxidant.[158, 159] Whereas liquid oxidation in general might result in a larger damage of the CNTs´ structure than gas oxidation, the latter is more difficult to control.

Most physical methods separate impurities based on their size or weight. In this group, commonly employed routes are ultrasonication, filtration, extraction, centrifugation, and size-exclusive chromatography.[155, 160-162] For example, CS_2 and toluene extractions are used to remove fullerenes and aromatic carbons. Nitric acid pre-treated SWCNTs have negative surface charge which can be used to separate them from carbonaceous impurities and carbon nanoparticles by centrifugation. Many works explore high temperature annealing for removal of metal catalyst at the ends of

nanotubes or from their cavity (when caps are removed). It has been also reported that high temperature annealing (depending of conditions) might improve nanotubes crystallinity or cause their collisions. In brief, physical purification is less efficient than chemical, but it minimizes the alteration of the tubular structure of CNTs.

Quite often both physical and chemical purification routes are combined in order to obtain the optimal product. Further, CNTs can be sorted according to length or conductivity to fulfill the desired criteria depending on the final application. The figure below (Fig. 1.10) shows representative procedures based on the function and characteristics of the purification. The purification approach should be optimized for minimum time, cost and energy.

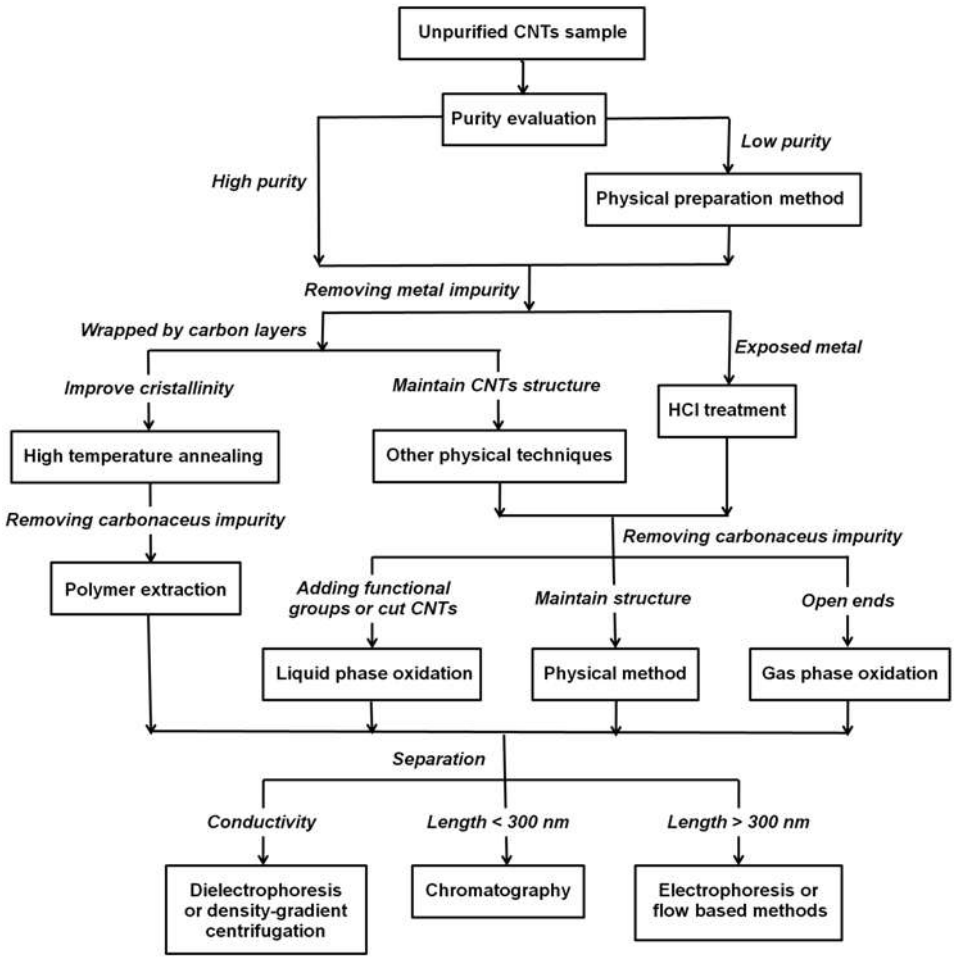

Figure 1.10 A flow chart showing representative procedures based on the function and characteristics of the purifications. Adapted from [163].

1.6. Shortening of carbon nanotubes

As-produced CNTs have length up to few tens of micrometers.[3] However, in order to tune their properties, a shortening process is often required. For example, short nanotubes reveal better thermal end electrical conductivity.[164-166] They are also characterized by higher biocompatibility and better cellular uptake.[167, 168] Moreover, biopersistence tests, which can be an indicator of toxicity of nanoparticles, prove that short CNTs are faster cleared from lungs.[169] **Shortening can be achieved via chemical or physical methods.**

The mechanism of **chemical cutting** involves attack on nanotube defects such as non-six member carbon rings, graphitic edges, kinks, and highly reactive ends. As a result functionalized and open-ended nanotubes are obtained. The first attempt on etching nanotubes was by refluxing the sample with concentrated H_2SO_4/HNO_3 (3:1 mixture).[170] Frequently employed methods are: acid treatment,[165, 171-174] ozonolysis,[175, 176] fluorination,[177, 178] thermal oxidative cutting[179, 180] and steam shortening.[158, 181]

Physical shortening includes different types of radiation,[182, 183] electron beam etching,[184] sonication[185-188] and mechanical cutting[189]. Mechanical approaches involve use of shear forces, for example: ball milling[189-205], high-speed agitation[206], cryogenic crush.[207]

Chemical methods do not only allow cutting the nanotubes, but also introduce functional groups, which facilitate the dispersion of nanotubes and their further functionalization. Acid treatment often involves harmful and aggressive chemicals which can damage the structure if CNTs are exposed to strong oxidants. Thermal oxidation is a safe and direct method, but it might be difficult to control. Mechanical treatment enables a quick reduction of the length, but without precision of the cutting. Besides, some physical methods require either expensive equipment (f.i. electron beam etching with TEM) or are difficult to scale up (f.i. radiation). Combined approaches are also explored, but are usually time-consuming. As in the case of purification, **the choice of CNTs shortening route will depend on the final application.**

1.7. Functionalization of carbon nanotubes

Functionalization is a common way to tailor CNTs´ properties, i. a.: to reduce their hydrophobicity, tune conductivity or improve mechanical performance of their composites.[208-210]

Functionalization methods of carbon nanotubes can be categorized as follows (Fig. 1.11):

1. Covalent chemical functionalization of the external walls (and tips) that leads to a permanent change of the CNT surface.
2. Non-covalent functionalization which does not involve the covalent chemical bond formation between a molecule and the surface of CNT.
3. Endohedral filling which benefits of the internal cavity of nanotubes.
4. Exohedral (external) decoration with inorganic nanoparticles:
   i) *Ex situ*, where nanoparticles are presynthesized,
   ii) *In situ*, where nanoparticles are formed directly onto the CNT surface. [211-213]

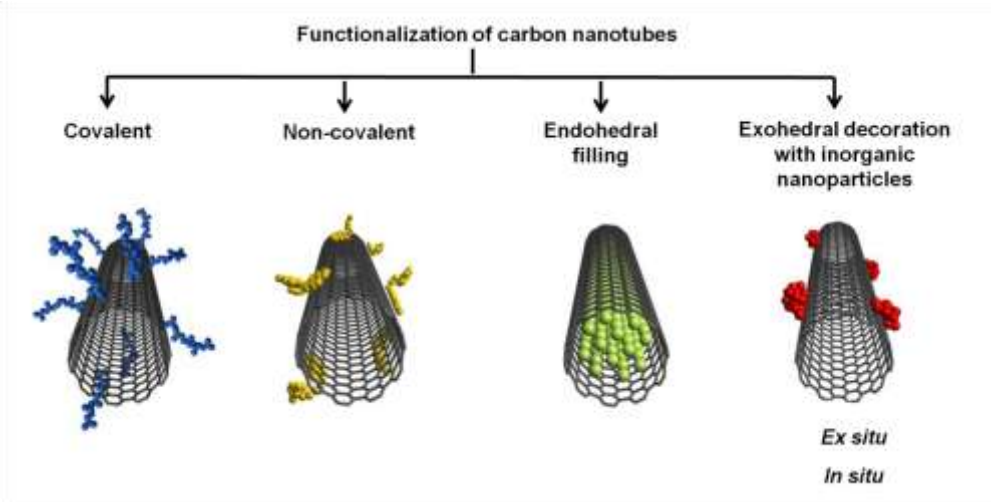

Figure 1.11. Chart summarizing different strategies of functionalization of carbon nanotubes.

1.7.1. Covalent approaches

Carbon atoms in nanotubes are bonded to only three other atoms so they can form a fourth stable covalent bond with different elements. Covalent functionalization occurs by attaching functional groups to the nanotube ends or defects by various reactions (Fig. 1.12). The tips of nanotubes are more reactive due to presence of pentagonal and hexagonal rings in their structure. Often, the first step of functionalization involves introduction of carboxyl and hydroxyl groups via oxidation reaction.[214, 215] Next, they undergo further derivatization via amidation or esterification, and/or can provide sites for coordination chemistry.[211, 215, 216] However, organic moieties can be also attached directly onto the nanotube sidewalls, by addition chemistry, which includes cycloadditions, electrophilic and nucleophilic or radical additions, halogenations, etc.[213, 217]

Covalent modification of CNTs induces structural defects. SWCNTs are more sensitive to functionalization than MWCNTs. Their double bonds are irreversibly lost, which causes perturbation of electronic structure. Nevertheless, functionalization remains a powerful tool to modify CNTs´ properties. For instance, hydrogenation of CNTs has been reported to debundle and disperse CNTs in organic solvents, but also the hydrogenated CNTs with covalent C-H bonds are proved as a stable form of hydrogen storage at room temperature.[218] Grafting of polymers is employed to improve dispersibility of samples.[219] Ozonolysis is a method of shortening nanotubes,[220, 221] but at the same time it might be an intermediate step for further derivatization.[211, 222]

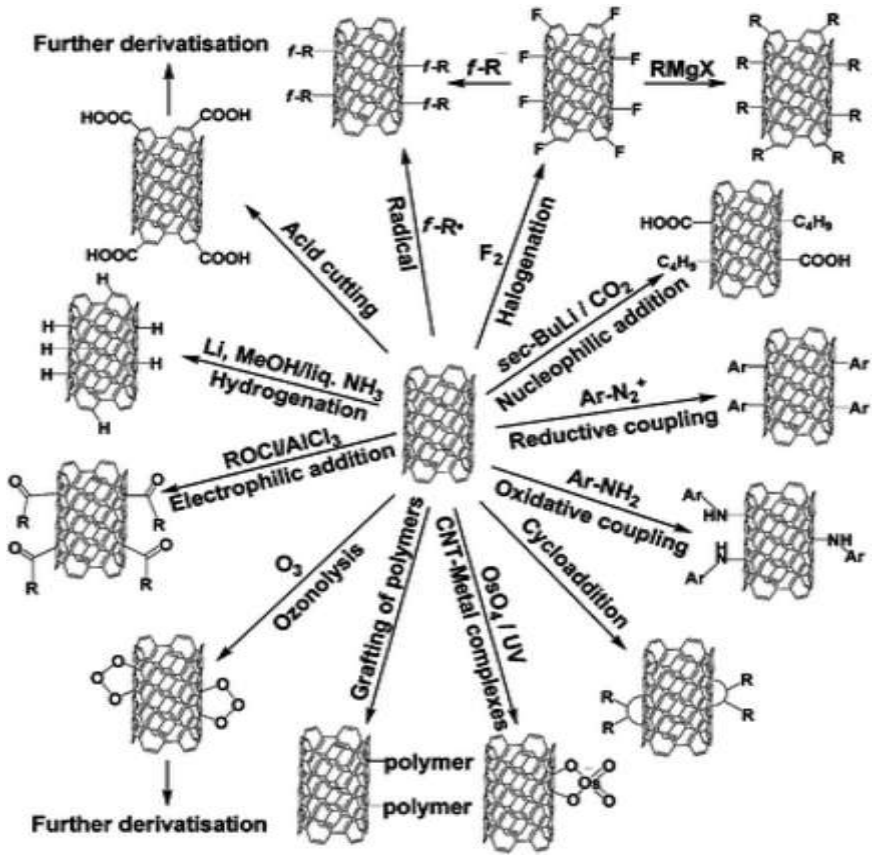

Figure 1.12. Surface covalent functionalization of carbon nanotubes.[212]

1.7.2. Non-covalent functionalization

The non-covalent functionalization is based on van der Waals forces and π-π interactions, electrostatic forces, hydrogen bonding and hydrophobic interactions. These attractive forces enable adsorption of aromatic molecules, polymers, surfactants and biocompounds onto the surface of CNTs. Using this approach the structure of nanotubes remains unchanged. Non-covalent functionalization is out of scope of this thesis and will not be further discussed.

1.7.3. Endohedral filling

Filled nanotubes (X@CNTs, where X represents the filling material) contain in their cavities encapsulated payloads (Fig. 1.13) leading to the production of materials with different properties and characteristics. Payloads are found in the form of one-dimensional (1D) crystals, isolated atoms/molecules, chains or nanowires. In Table 1.6 are listed examples of materials which have been inserted in SWCNTs. The concept of filling nanotubes was introduced for the first time by the theoretical work by Broughton and Pederson back in 1992.[223] A year later Ajayan and Iijima reported the filling MWCNTs with Pb by heating a mixture of CNTs and Pb above the melting point of the metal,[224] and since then these hybrid materials have been broadly studied.[225-229]

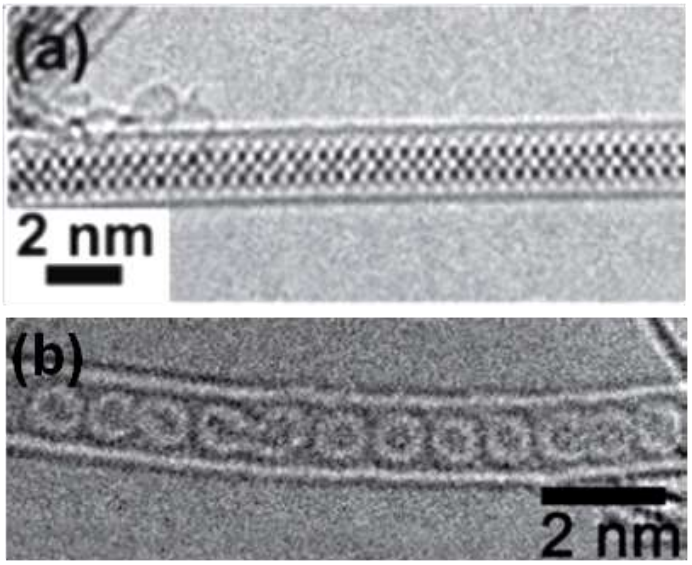

Figure 1.13. HRTEM images of SWCNTs filled with a) $PbTe_xI_{2-2x}$, b) fullerenes.[230]

Table 1.6. Selected examples of various kinds of materials which have been reported as successfully inserted in SWCNTs. Adapted from [231].

Nature of filling materials	Morphology (as encapsulated)	Compound
Atoms	Single atom chains or isolated	I, Cs
Molecules	Mainly as single molecule chains	*Fullerenes*: C_{60}, C_{70}, C_{78}, C_{80}, C_{84}, C_{90} *Endohedral fullerenes*: $La_2@C_{80}$, $Gd@C_{82}$, NC_{60}, $Sc_3N@C_{80}$, $Sm@C_{82}$, $Dy@C_{82}$, $Tm@C_{82}$, $Ca@C_{82}$, $Sc_2@C_{84}$, $Gd_2@C_{92}$ *Doped fullerenes*: fullerenes combined with elements (e.g. K) or compounds (e.g., $FeCl_3$) *Functionalized fullerenes*: C_{60} grafted with: dicarboxylic acid diethyl ester, 4(pyrrolidin-1-yl) phenol *Organic molecules*: ferrocene, nickelocene, fulvalenes, Zn-diphenyl-1-porphiyrin, H_2O
Elements	Nanowires, 1D-crystals, elongated nanoparticles	*Direct*: Bi, Se *From salt reduction*: Ru, Bi, Ag, Au, Pt, Pd
Compounds	Nanowires, 1D-crystals, elongated nanoparticles	*Halides*: $RuCl_3$, NaCl, TiCl, $CdCl_2$, $FeCl_2$, $CoCl_2$, $TbCl_3$, Al_2Cl_6, $HoCl_3$, $GdCl_3$, Ln(La to Lu)Cl_3, $HfCl_4$, $ThCl_4$, $ZrCl_4$, $ThCl_6$, WCl_6, $(KCl)_x(UCl_4)$, $AgCl_xBr_yI_z$, Cs(Cl/Br/I), (K/Li/Na/Rb/Ag)I, CdI_2, CoI_2, SrI_2, BaI_2, PbI_2, HgI_2, TeI_4, SnI_4, $MoCl_5$ *Oxides*: CrO_3, Sb_2O_3, PbO, Re_xO_y

1.7.3.1. Filling methods

Filling of both SWCNTs and MWCNTs can be accomplished through *in situ* and *ex situ* synthesis routes.[232] Filling *in situ* is a simple method, but the number of payloads that can be used is limited. In this approach, tuning the synthesis conditions of CNTs enables encapsulation of metals and metals carbides. One of the major advantages of the *in situ* filling of CNT is the reduction of production time. On the other hand, post-synthesis filling involves step for opening the ends of

nanotubes usually in an oxidizing environment, which can be performed by one of the purification or shortening methods (see Subchapters 1.5 and 1.6), thus leading to samples of purified (short) open-ended nanotubes. Next, filling of chosen compounds is induced either by capillary forces or by sublimation. For the former, payloads should be characterized by surface tensions in the range of 130-190 $mN \cdot m^{-1}$ for SWCNTs[233] and 100-200 $mN \cdot m^{-1}$ for MWCNTs[231, 234-236] in their molten state or be soluble/dispersible in a suitable solvent. Post-synthesis filling includes high temperature (molten phase, gas phase) and low temperature (solution phase, nanoextraction, supercritical CO_2) methods. [72, 231, 237] Among them the most universal approaches are **filling from melts and solution.**

Filling from melts implies direct insertion of molten payloads into the inner channel of CNTs under vacuum at elevated temperatures.[231, 232] The melting point of chosen materials should be inferior to their sublimation temperature. At the same time the thermal treatment temperature should remain below the temperature at which nanotubes can get damaged and selected payloads should not react with the CNTs. Various CNT composites filled with melted halides, oxides, chalcogenides, fullerenes, elements and hydroxides are reported in the literature.[208, 230, 238] The main advantages of melting filling are continuous filling, and higher filling yields than from solution phase.[231, 235] Furthermore, after annealing at high temperatures the spontaneous closing of SWCNTs´ ends occurs upon cooling, which prevents the leakage of material from the internal cavity.[239]

Filling from solution consist of impregnating open-ended CNTs with either a solution or suspension of selected materials, for instance metal salts, fullerenes, proteins.[230, 240-242] The filling yield is usually quite low (ca. 20%) and correlated with the diameters of nanotubes.[235] It makes MWCNTs better candidates for filling from solution due to their higher diameter and bigger cavities compared to SWCNTs. Noteworthy, opening and filling may be achieved in one or two steps (Fig. 1.14). One of the initially employed strategies consisted of refluxing CNTs in concentrated nitric acid containing precursor salt. I this way CNTs can be opened and filled simultaneously.[234] Another approach implies opening the nanotubes (by either wet or dry chemistry) and then transferring them into the solution containing the material to be filled. The excess of solvent is removed by filtration or evaporation. A posterior treatment might be required to close the ends or to obtain a crystalline payload.

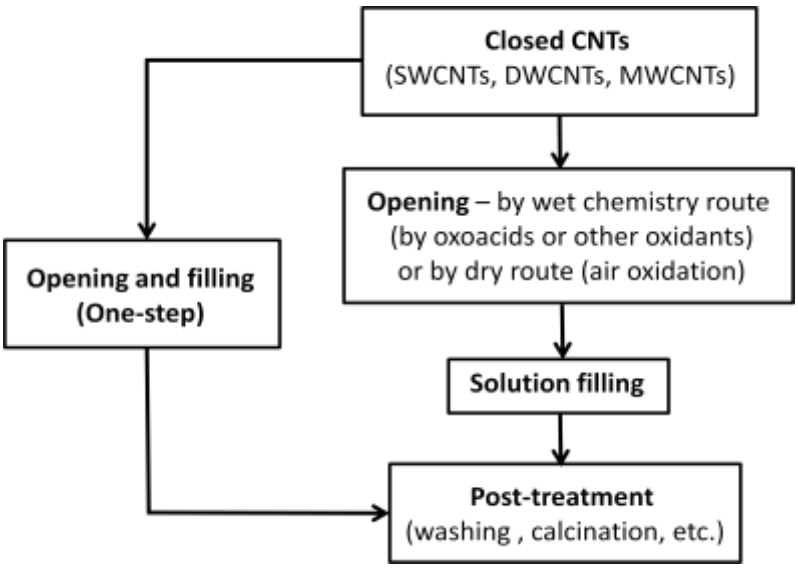

Figure 1.14. Sketch of the main steps for the filling of CNT in solution. Adapted from [235].

1.7.3.2. Removal of non-encapsulated material from samples of filled carbon nanotubes

A suitable solvent should be used to remove the large amount of external material present after the filling step to avoid the loss of material from the internal cavities of CNTs. When the ends of nanotubes remain opened, the best strategy is to use a selective washing. An appropriate solvent should solubilize or disperse the payload, but do not wet nanotubes. For example, Fu and coworkers filled MWCNTs from solution with iron, cobalt and nickel. They used a mixture of chloroform and 1-propanol to obtain exclusively internal metal nanoparticles.[234] Other authors proposed a cold and wet filling chemical procedure for the effective synthesis of CdS@MWCNTs together with the total removal of any residuals deposited outside. First, MWCNTs were dipped in $CdCl_2$ solution and lyophilized. Then, nanotubes were filled with benzene in order to protect them from the washing solvent (water), which rinsed away the external $CdCl_2$. Finally, $CdCl_2$@MWCNTs were reacted with H_2S in order to obtain CdS@MWCNTs.[243] It has been also demonstrated that washing $RhCl_3$@MWCNTs with a bulky micellar medium (dodecylammonium propionate-solubilized water in benzene) causes the selective removal of soluble material exterior to filled nanotubes, whilst leaving the encapsulated material essentially unchanged.[244] In general, cleaning of filled CNTs might be time consuming. Therefore, many authors avoid the washing step, if it is not crucial for the further application of the obtained composites. Recent work

from our group reports on the optimization of the parameters for cleaning closed-ended $SmCl_3$@SWCNTs (and any analogous sample soluble in water), including time, temperature, volume and sonication. The non-encapsulated material can be efficiently removed in less than 1 h from a sample as large as 300 mg when the proposed protocol is employed.[245]

1.7.3.3. Closing the ends of carbon nanotubes

The main obstacle encountered for some of the targeted applications of filled CNTs is how to prevent the leakage of payload. Therefore, several closing/ "corking" strategies have been investigated. Initial studies showed that at high temperatures (≈ 900 °C) the ends of SWCNTs close spontaneously on cooling.[239] MWCNTs have larger diameters than SWCNTs and closing their ends by thermal annealing so far was not been reported. Satishkumar and coworkers investigated blocking MWCNTs with methanol, ethylene glycol and propylene glycol. The authors suggested that the closure of the nanotubes by these hydroxy compounds is probably due to the interaction with the carboxy and the hydroxy groups present in the HNO_3-treated nanotubes leading to formation of ester and ether bonds. Methanol and glycols can also react with isolated double bonds. Hydroxy compounds coverage was resistant to heating in air up to 673 K. In the same work, MWCNTs were closed by reaction with benzene vapor, argon and hydrogen at 1173 K.[246]

The tips of CNTs can be also blocked by various compounds that act as "corks". Fullerenes were used as stoppers for SWCNTs.[247] Noteworthy, this process is reversible. When properly functionalized the fullerene corks can be triggered by changing the pH in a liquid environment.[242] Likewise, silica nanospheres have been used to seal the tips of thiopirydyne functionalized flueresceine filled MWCNTs. The encapsulated die was released using disulfide reducing agents (e.g., 10^{-2} M dithiothreitol) or temperature. Another study reports on thiol terminated nitrogen-doped carbon nanotube cups (NCNCs) corked with gold nanoparticles. Silver nanoparticles also have a strong affinity to thiols and were able to block NCNCs. Furthermore, NCNCs can also be capped in ethanol by polystyrene latex nanoparticles containing aldehyde groups, presumably due to the formation of imine bonds.[248]

The parameters taken into account in "corking via functionalization" are:

- diameter of nanotube and diameter of "cork",
- chemical nature and localization of functionalities,

- solvent in which corking is performed.

The design of perfectly matching nanotubes and "corks" is difficult and in general the efficiency of the process is quite low. Therefore, it is still an interesting and open problem for further studies.

1.7.4. Exohedral decoration with metal nanoparticles

The external walls of CNTs can be decorated with various inorganic materials, including: nitrides, chalcogenides, carbides, metal oxides and metal nanoparticles.[249] The focus of this thesis is on the exohedral decoration of carbon nanotubes with metal nanoparticles (MNPs). The first report on decoration of CNTs with metal clusters dates back to 1994 by Ajayan and coworkers.[250] They dispersed ruthenium nanoparticles on SWCNTs that acted as support. Since then, CNTs decorated with metal nanoparticles have emerged as an important class of hybrid nanomaterials.

CNTs-MNPs can be obtained by employing several procedures, which include CVD *in situ* synthesis, assembling presynthesized nanoparticles on CNTs, controlled heteroagregation, reduction/deposition of metal precursor directly onto CNTs, hydrothermal crystallization and sol-gel based methods.[209, 251, 252] Commonly used nanoparticles are Au, Pt, Ru, Pd, Ag, and more rarely: Ni, Co, Ti and Fe among others.[209, 253, 254] Presynthesized MNPs can be attached to CNTs via chemical bonds or by non-covalent interactions. Functional moieties might be present either on CNTs or less often on the MNPs. The shape and size of individual nanoparticles can be easily tailored by sophisticated synthesis methods prior to their combination with nanotubes.[255-257] The distribution of MNPs in the covalent approach depends on the character and degree of functionalization of the nanotubes. Hence, MNPs can also serve as markers of sidewall defects.[232] In contrast, the non-specificity of non-covalent functionalization promotes uniform coating of nanotubes with a relatively high density of nanoparticles.[252] On the other hand, CNTs can act as a templates to direct the synthesis of MNPs through, for example: reduction of metal precursors (salts or organometalic compounds), or electrodeposition. In this case, MNPs typically bind through van der Waals forces, π–π stacking or electrostatic interactions.[209, 254, 258-260]. CNTs-MNPs composites have promising applications not only in the field of biomedicine, but also in fuel cells, sensors, solar cells, catalysis, and hydrogen storage.

REFERENCES

1. Iijima, S., *The Discovery of Carbon Nanotubes*. 2007 [cited 08.06.2017]. Available from: http://www.balzan.org/en/prizewinners/sumio-iijima/the-discovery-of-carbon-nanotubes-iijima.
2. Iijima, S., *Helical Microtubules of Graphitic Carbon.* Nature, 1991. **354**(6348): p. 56-58.
3. De Volder, M.F.L., et al., *Carbon Nanotubes: Present and Future Commercial Applications.* Science, 2013. **339**(6119): p. 535-539.
4. Qu, L., et al., *Carbon Nanotube Arrays with Strong Shear Binding-On and Easy Normal Lifting-Off.* Science, 2008. **322**(5899): p. 238-242.
5. Jang, S., et al., *Fluoropolymer Coatings for Improved Carbon Nanotube Transistor Device and Circuit Performance.* Applied Physics Letters, 2014. **105**(12): p. 122107.
6. Novoselov, K.S., et al., *Electric Field Effect in Atomically Thin Carbon Films.* Science, 2004. **306**(5696): p. 666.
7. Katsnelson, M.I., *Graphene: Carbon in Two Dimensions.* Materials Today, 2007. **10**(1–2): p. 20-27.
8. Falcao, E.H.L. and F. Wudl, *Carbon Allotropes: Beyond Graphite and Diamond.* Journal of Chemical Technology & Biotechnology, 2007. **82**(6): p. 524-531.
9. Hirsch, A., *The Era of Carbon Allotropes.* Nature Materials, 2010. **9**(11): p. 868-871.
10. Atta, N.F., Galal, A., El-Ads, E.H, *Graphene - A Platform for Sensor and Biosensor Applications*, in *Biosensors - Micro and Nanoscale Applications*, Rinken, T., Editor. 2015, InTech. p. 37-83.
11. Paradise, M., Goswami, T., *Carbon Nanotubes - Production and Industrial Applications.* Materials & Design, 2007. **28**(5): p. 1477-1489.
12. Khalaj, Z., Monajjemi, M., Diudea, M.V., *Main Allotropes of Carbon: A Brief Review*, in *Sustainable Nanosystems Development, Properties, and Applications*, Mirica, M.C., Putz, M.V., Editors. 2016, IGI Global. p. 185-213.
13. Ren, Z., et al., *Introduction to Carbon*, in *Aligned Carbon Nanotubes: Physics, Concepts, Fabrication and Devices*, Ren, Z., Lan, Y., Wang, Y., Editors. 2013, Springer. p. 1-5.
14. Thostenson, E.T., Ren, Z., Chou, T.W., *Advances in the Science and Technology of Carbon Nanotubes and Their Composites: A Review.* Composites Science and Technology, 2001. **61**(13): p. 1899-1912.
15. Saifuddin, N., Raziah, A.Z., Junizah, A.R. *Carbon Nanotubes: A Review on Structure and Their Interaction with Proteins.* Journal of Chemistry, 2013. **2013**: p. 18.
16. Zhang, M., Li, J., *Carbon Nanotube in Different Shapes.* Materials Today, 2009. **12**(6): p. 12-18.

17. Saito, R., Dresselhaus, G., Dresselhaus , M.S., *Structure of a Single-Wall Carbon Nanotube*, in *Physical Properties of Carbon Nanotubes*. 1998, Imperial College Press. p. 35-37.
18. Bandaru, P., *Electrical Properties and Applications of Carbon Nanotube Structures.* Journal of Nanoscience and Nanotechnology, 2007. **7**(4-5): p. 1239-1267.
19. Eatemadi, A., et al., *Carbon Nanotubes: Properties, Synthesis, Purification, and Medical Applications.* Nanoscale Research Letters, 2014. **9**(1): p. 1-13.
20. Ajayan, P.M., *Nanotubes from Carbon.* Chemical Reviews, 1999. **99**(7): p. 1787-1800.
21. Iijima, S., *Growth of Carbon Nanotubes.* Materials Science and Engineering: B, 1993. **19**(1): p. 172-180.
22. Iijima, S., Ichihashi, T., *Single-Shell Carbon Nanotubes of 1-nm Diameter.* Nature, 1993. **363**(6430): p. 603-605.
23. Bethune, D.S., et al., *Cobalt-Catalysed Growth of Carbon Nanotubes with Single-Atomic-Layer Walls.* Nature, 1993. **363**(6430): p. 605-607.
24. Thess, A., et al., *Crystalline Ropes of Metallic Carbon Nanotubes.* Science, 1996. **273**(5274): p. 483-487.
25. José-Yacamán, M., et al., *Catalytic Growth of Carbon Microtubules with Fullerene Structure.* Applied Physics Letters, 1993. **62**(6): p. 657-659.
26. Prasek, J., et al., *Methods for Carbon nanotubes Synthesis - Review.* Journal of Materials Chemistry, 2011. **21**(40): p. 15872-15884.
27. Ebbesen, T.W., Ajayan, P.M., *Large-Scale Synthesis of Carbon Nanotubes.* Nature, 1992. **358**(6383): p. 220-222.
28. Guo, T., et al., *Self-Assembly of Tubular Fullerenes.* The Journal of Physical Chemistry, 1995. **99**(27): p. 10694-10697.
29. Shah, K.A., Tali, B.A., *Synthesis of Carbon Nanotubes by Catalytic Chemical Vapour Deposition: A Review on Carbon Sources, Catalysts and Substrates.* Materials Science in Semiconductor Processing, 2016. **41**: p. 67-82.
30. Chakraborty, A.K., et al., *Chemical Vapor Deposition Growth of Carbon Nanotubes on Si Substrates Using Fe Catalyst: What Happens at the Nanotube/Fe/Si Interface.* Journal of Applied Physics, 2006. **100**(8): p. 0843
31. Kakehi, K., et al., *Supported Ni Catalysts from Nominal Monolayer Grow Single-Walled Carbon Nanotubes.* Chemical Physics Letters, 2006. **428**(4–6): p. 381-385.
32. Chatterjee, A.K., et al., *CVD Synthesis of Carbon Nanotubes Using a fFnely Dispersed Cobalt Catalyst and Their Use in Double Layer Electrochemical Capacitors.* Electrochimica Acta, 2003. **48**(23): p. 3439-3446.
33. Kumar, M., Ando, Y., *Chemical Vapor Deposition of Carbon Nanotubes: A Review on Growth Mechanism and Mass Production.* Journal of Nanoscience and Nanotechnology, 2010. **10**(6): p. 3739-3758.

34. Guofang, Z., et al., *Low Temperature Synthesis of Extremely Dense and Vertically Aligned Single-Walled Carbon Nanotubes.* Japanese Journal of Applied Physics, 2005. **44**(4R): p. 1558.
35. Toshiaki, K., Rikizo, H., Kazuyuki, T., *Diffusion Plasma Chemical Vapour Deposition Yielding Freestanding Individual Single-Walled Carbon Nanotubes on a Silicon-Based Flat Substrate.* Nanotechnology, 2006. **17**(9): p. 2223.
36. Liu, W.-W., et al., *Synthesis of Single-Walled Carbon Nanotubes: Effects of Active Metals, Catalyst Supports, and Metal Loading Percentage.* Journal of Nanomaterials, 2013.
37. Maruyama, S., et al., *Low-Temperature Synthesis of High-Purity Single-Walled Carbon Nanotubes from Alcohol.* Chemical Physics Letters, 2002. **360**(3–4): p. 229-234.
38. Nikolaev, P., et al., *Gas-Phase Catalytic Growth of Single-Walled Carbon Nanotubes from Carbon Monoxide.* Chemical Physics Letters, 1999. **313**(1–2): p. 91-97.
39. Kumar, M., *Carbon Nanotube Synthesis and Growth Mechanism*, in *Carbon Nanotubes - Synthesis, Characterization, Applications*, Yellampalli, S., Editor. 2011, InTech. p. 147-170.
40. Gong, H., Peng, R., Liu, Z., *Carbon Nanotubes for Biomedical Imaging: The Recent Advances.* Advanced Drug Delivery Reviews, 2013. **65**(15): p. 1951-1963.
41. Saeed, K., Khan, I., *Carbon Nanotubes - Properties and Applications: A Review.* Carbon Letters, 2013. **14**(3): p. 131-144.
42. Varshney, K., *Carbon Nanotubes: A Review on Synthesis, Properties and Applications.* International Journal of Engineering Research and General Science, 2014. **2**(4): p. 660-677.
43. Davenport, M., *They Will Be Called Wonder Material.* Chemical & Engineering News 2015. **93**(23): p. 10-15.
44. Lim, Y., Jang, J., Choi, Y., *Development of Golf Shaft with Carbon Nanotubes and Marketing Strategy.* International Journal of Software Engineering and Its Applications, 2014. **8**(12): p. 165-170.
45. Jones, A., et al., *Field Testing of Ebola Multiplex in Sierra Leone,* 2012 [cited 08.06.2017]. Available from: http://www.nano.com/news.php#.
46. Cai, L., Wang, C., *Carbon Nanotube Flexible and Stretchable Electronics.* Nanoscale Research Letters, 2015. **10**(1): p. 320.
47. Chen, K., et al., *Printed Carbon Nanotube Electronics and Sensor Systems.* Advanced Materials, 2016. **28**(22): p. 4397-4414.
48. *Production and Applications of Carbon Nanotubes, Carbon Nanofibers, Fullerenes, Graphene and Nanodiamonds: A Global Technology Survey and Market Analysis*. 2011, Innovative Research and Products, Inc.
49. *Carbon Nanotubes (CNT) Market Analysis By Product (Single Walled Carbon Nanotubes (SWCNT), Multi Walled Carbon Nanotubes (MWCNT)), By*

Application (Polymers, Energy, Electrical & Electronics) And Segment Forecasts To 2022. 2015, Grand View Research, Inc.

50. Basu-Dutt, S., et al., *Chemistry of Carbon Nanotubes for Everyone.* Journal of Chemical Education, 2012. **89**(2): p. 221-229.
51. Lacerda, L., et al., *Cell-Penetrating CNTs for Delivery of Therapeutics.* Nano Today, 2007. **2**(6): p. 38-43.
52. Mooney, E., et al., *Carbon Nanotubes and Mesenchymal Stem Cells: Biocompatibility, Proliferation and Differentiation.* Nano Letters, 2008. **8**(8): p. 2137-2143.
53. Usui, Y., et al., *Carbon Nanotubes with High Bone-Tissue Compatibility and Bone-Formation Acceleration Effects.* Small, 2008. **4**(2): p. 240-246.
54. Sitharaman, B., et al., *In vivo Biocompatibility of Ultra-Short Single-Walled Carbon Nanotube/Biodegradable Polymer Nanocomposites for, Bone Tissue Engineering.* Bone, 2008. **43**(2): p. 362-370.
55. Veetil, J.V., Ye, K., *Tailored Carbon Nanotubes for Tissue Engineering Applications.* Biotechnology Progress, 2009. **25**(3): p. 709-721.
56. Edwards, S.L., Werkmeister, J.A., Ramshaw, J.A.M., *Carbon Nanotubes in Scaffolds for Tissue Engineering.* Expert Review of Medical Devices, 2009. **6**(5): p. 499-505.
57. Bhattacharya, M., et al., *Bone Formation on Carbon Nanotube Composite.* Journal of Biomedical Materials Research Part A, 2011. **96A**(1): p. 75-82.
58. Bosi, S., et al., *Carbon Nanotubes: a Promise for Nerve Tissue Engineering?* Nanotechnology Reviews, 2013. **2**(1): p. 47-57.
59. Bosi, S., et al., *Carbon Based Substrates for Interfacing Neurons: Comparing Pristine with Functionalized Carbon Nanotubes Effects on Cultured Neuronal Networks.* Carbon, 2016. **97**: p. 87-91.
60. Mattson, M.P., Haddon, R.C., Rao, A.M., *Molecular Functionalization of Carbon Nanotubes and Use as Substrates for Neuronal Growth.* Journal of Molecular Neuroscience, 2000. **14**(3): p. 175-182.
61. Jan, E., Kotov, N.A., *Successful Differentiation of Mouse Neural Stem Cells on Layer-by-Layer Assembled Single-Walled Carbon Nanotube Composite.* Nano Letters, 2007. **7**(5): p. 1123-1128.
62. Chen, C.-S., et al., *Human Stem Cell Neuronal Differentiation on Silk-Carbon Nanotube Composite.* Nanoscale Research Letters, 2012. **7**(1): p. 126.
63. Ahn, H.-S., et al., *Carbon-Nanotube-Interfaced Glass Fiber Scaffold for Regeneration of Transected Sciatic Nerve.* Acta Biomaterialia, 2015. **13**: p. 324-334.
64. Ebron, V.H., et al., *Fuel-Powered Artificial Muscles.* Science, 2006. **311**(5767): p. 1580-1583.
65. Foroughi, J., et al., *Torsional Carbon Nanotube Artificial Muscles.* Science, 2011. **334**(6055): p. 494-497.
66. Meyyappan, M., *Carbon Nanotube-Based Chemical Sensors.* Small, 2016. **12**(16): p. 2118-2129.

67. Tan, C.W., et al., *Energy and Environmental Applications of Carbon Nanotubes.* Environmental Chemistry Letters, 2012. **10**(3): p. 265-273.
68. Wang, X. and Z. Liu, *Carbon Nanotubes in Biology and Medicine: An Overview.* Chinese Science Bulletin, 2012. **57**(2): p. 167-180.
69. Koh, J., et al., *Nanotube-Based Chemical and Biomolecular Sensors.* Journal of Materials Science & Technology, 2008. **24**(4): p. 578-588.
70. Sinha, N., Ma, J.Z., Yeow, J.T.W., *Carbon Nanotube-Based Sensors.* Journal of Nanoscience and Nanotechnology, 2006. **6**(3): p. 573-590.
71. Yum, K., et al., *Single-Walled Carbon Nanotube-Based Near-Infrared Optical Glucose Sensors toward In Vivo Continuous Glucose Monitoring.* Journal of Diabetes Science and Technology, 2013. **7**(1): p. 72-87.
72. Martincic, M., Tobias, G., *Filled Carbon Nanotubes in Biomedical Imaging and Drug Delivery.* Expert Opinion on Drug Delivery, 2015. **12**(4): p. 563-581.
73. Beg, S., et al., *Advancement in Carbon Nanotubes: Basics, Biomedical Applications and Toxicity.* Journal of Pharmacy and Pharmacology, 2011. **63**(2): p. 141-163.
74. Ali-Boucetta, H., Kostarelos, K., *Pharmacology of Carbon Nanotubes: Toxicokinetics, Excretion and Tissue Accumulation.* Advanced Drug Delivery Reviews, 2013. **65**(15): p. 2111-2119.
75. Al-Jamal, K.T., et al., *Degree of Chemical Functionalization of Carbon Nanotubes Determines Tissue Distribution and Excretion Profile.* Angewandte Chemie-International Edition, 2012. **51**(26): p. 6389-6393.
76. Lim, E.-K., et al., *Nanomaterials for Theranostics: Recent Advances and Future Challenges.* Chemical Reviews, 2015. **115**(1): p. 327-394.
77. Cortezon-Tamarit, F., et al., *Chapter Eight - Carbon Nanotubes and Related Nanohybrids Incorporating Inorganic Transition Metal Compounds and Radioactive Species as Synthetic Scaffolds for Nanomedicine Design*, in *Inorganic and Organometallic Transition Metal Complexes with Biological Molecules and Living Cells*. Kam-Wing Lo, K., Editor. 2017, Academic Press. p. 245-327.
78. Hong, H., Gao, T., Cai, W., *Molecular Imaging with Single-Walled Carbon Nanotubes.* Nano Today, 2009. **4**(3): p. 252-261.
79. Iancu, C. and L. Mocan, *Advances in Cancer Therapy Through the Use of Carbon Nanotube-Mediated Targeted Hyperthermia.* International Journal of Nanomedicine, 2011. **6**: p. 1675-1684.
80. Zhou, F., et al., *Cancer Photothermal Therapy in the Near-Infrared Region by using Single-Walled Carbon Nanotubes.* Journal of Biomedical Optics, 2009. **14**(2).
81. Zhou, F., et al., *Mitochondria-Targeting Single-Walled Carbon Nanotubes for Cancer Photothermal Therapy.* Small, 2011. **7**(19): p. 2727-2735.
82. Singh, R., Torti, S.V., *Carbon Nanotubes in Hyperthermia Therapy.* Advanced Drug Delivery Reviews, 2013. **65**(15): p. 2045-2060.

83. Kam, N.W.S., et al., *Carbon Nanotubes as Multifunctional Biological Transporters and Near-Infrared Agents for Selective Cancer Cell Destruction.* Proceedings of the National Academy of Sciences of the United States of America, 2005. **102**(33): p. 11600-11605.
84. Jeyamohan, P., et al., *Accelerated Killing of Cancer Cells Using a Multifunctional Single-Walled Carbon Nanotube-Based System for Targeted Drug Delivery in Combination with Photothermal therapy.* International Journal of Nanomedicine, 2013. **8**: p. 2653-2667.
85. Kosuge, H., et al., *Carbon Nanotubes Enable Optical Ablation of Vascular Macrophages.* Circulation, 2011. **124**(21).
86. Miyako, E., et al., *Photothermic Regulation of Gene Expression Triggered by Laser-Induced Carbon Nanohorns.* Proceedings of the National Academy of Sciences of the United States of America, 2012. **109**(19): p. 7523-7528.
87. Serpell, C.J., Kostarelos, K., Davis, B.G., *Can Carbon Nanotubes Deliver on Their Promise in Biology? Harnessing Unique Properties for Unparalleled Applications.* ACS Central Science, 2016. **2**(4): p. 190-200.
88. Huang, H., et al., *Near-Infrared Fluorescence Spectroscopy of Single-Walled Carbon Nanotubes and Its Applications.* TrAC Trends in Analytical Chemistry, 2011. **30**(7): p. 1109-1119.
89. Roxbury, D., et al., *Hyperspectral Microscopy of Near-Infrared Fluorescence Enables 17-Chirality Carbon Nanotube Imaging.* Scientific Reports, 2015. **5**.
90. Cherukuri, P., et al., *Mammalian Pharmacokinetics of Carbon Nanotubes Using Intrinsic Near-Infrared fFuorescence.* Proceedings of the National Academy of Sciences of the United States of America, 2006. **103**(50): p. 18882-18886.
91. Welsher, K., et al., *Selective Probing and Imaging of Cells with Single Walled Carbon Nanotubes as Near-Infrared Fluorescent Molecules.* Nano Letters, 2008. **8**(2): p. 586-590.
92. Leeuw, T.K., et al., *Single-Walled Carbon Nanotubes in the Intact Organism: Near-IR Imaging and Biocompatibility Studies in Drosophila.* Nano Letters, 2007. **7**(9): p. 2650-2654.
93. Keren, S., et al., *Noninvasive Molecular Imaging of Small Living Subjects Using Raman Spectroscopy.* Proceedings of the National Academy of Sciences of the United States of America, 2008. **105**(15): p. 5844-5849.
94. Gaufres E. , et al., *Giant Raman Scattering from J-Aggregated Dyes Inside Carbon Nanotubes for Multispectral Imaging.* Nature Photonics, 2014. **8**(1): p. 72-78.
95. Wang, C., et al., *Protamine Functionalized Single-Walled Carbon Nanotubes for Stem Cell Labeling and In Vivo Raman/Magnetic Resonance/Photoacoustic Triple-Modal Imaging.* Advanced Functional Materials, 2012. **22**(11): p. 2363-2375.

96. Zavaleta, C., et al., *Noninvasive Raman Spectroscopy in Living Mice for Evaluation of Tumor Targeting with Carbon Nanotubes.* Nano Letters, 2008. **8**(9): p. 2800-2805.
97. Liu, Z., et al., *Multiplexed Multi-Color Raman Imaging of Live Cells with Isotopically Modified Single Walled Carbon Nanotubes.* Journal of the American Chemical Society, 2008. **130**(41): p. 13540-13541.
98. De la Zerda, A., et al., *Carbon Nanotubes as Photoacoustic Molecular Imaging Agents in Living Mice.* Nature Nanotechnology, 2008. **3**(9): p. 557-562.
99. Kim, J.-W., et al., *Golden Carbon Nanotubes as Multimodal Photoacoustic and Photothermal High-Contrast Molecular Agents.* Nature Nanotechnology, 2009. **4**(10): p. 688-694.
100. Zanganeh, S., et al., *Photoacoustic Imaging Enhanced by Indocyanine Green-Conjugated Single-Wall Carbon Nanotubes.* Journal of Biomedical Optics, 2013. **18**(9).
101. Wang, L.V., *Prospects of Photoacoustic Tomography.* Medical Physics, 2008. **35**(12): p. 5758-5767.
102. De la Zerda, A., et al., *Ultrahigh Sensitivity Carbon Nanotube Agents for Photoacoustic Molecular Imaging in Living Mice.* Nano Letters, 2010. **10**(6): p. 2168-2172.
103. Rivera, E.J., et al., *Bismuth@US-Tubes as a Potential Contrast Agent for X-Ray Imaging Applications.* Journal of Materials Chemistry B, 2013. **1**(37): p. 4792-4800.
104. Sethi, R., Mackeyev, Y., Wilson, L.J., *The Gadonanotubes Revisited: A New Frontier in MRI Contrast Agent Design.* Inorganica Chimica Acta, 2012. **393**: p. 165-172.
105. Ma, Q., et al., *The Gadonanotubes: Structural Origin of Their High-Performance MRI Contrast Agent Behavior.* Journal of Materials Chemistry B, 2013. **1**(42): p. 5791-5797.
106. Tang, A.M., et al., *Cellular Uptake and Imaging Studies of Gadolinium-Loaded Single-Walled Carbon Nanotubes as MRI Contrast Agents.* Contrast Media & Molecular Imaging, 2011. **6**(2): p. 93-99.
107. Cabana, L., et al., *The Shortening of MWNT-SPION Hybrids by Steam Treatment Improves Their Magnetic Resonance Imaging Properties In Vitro and In Vivo.* Small, 2016. **12**(21): p. 2893-905.
108. Choi, J.H., et al., *Multimodal Biomedical Imaging with Asymmetric Single-Walled Carbon Nanotube/Iron Oxide Nanoparticle Complexes.* Nano Letters, 2007. **7**(4): p. 861-867.
109. Hong, S.Y., et al., *Filled and Glycosylated-Carbon Nanotubes for In Vivo Radioemitter Localization and Imaging.* Nature Materials, 2010. **9**(6): p. 485-490.
110. Liu, Z., et al., *In Vivo Biodistribution and Highly Efficient Tumour Targeting of Carbon Nanotubes in Mice.* Nature Nanotechnology, 2007. **2**(1): p. 47-52.

111. McDevitt, M.R., et al., *PET Imaging of Soluble Yttrium-86-Labeled Carbon Nanotubes in Mice.* Plos One, 2007. **2**(9).
112. Liu, Z., et al., *In Vivo Biodistribution and Highly Efficient Tumour Targeting of Carbon Nanotubes in Mice.* Nature Nanotechnology, 2007. **2**(1): p. 47-52.
113. McDevitt, M.R., et al., *Tumor Targeting with Antibody-Functionalized, Radiolabeled Carbon Nanotubes.* Journal of Nuclear Medicine, 2007. **48**(7): p. 1180-1189.
114. Sitharaman, B., et al., *Superparamagnetic Gadonanotubes are High-Performance MRI Contrast Agents.* Chemical Communications, 2005(31): p. 3915-3917.
115. Hartman, K.B., et al., *Gadonanotubes as Ultrasensitive pH-Smart Probes for Magnetic Resonance Imaging.* Nano Letters, 2008. **8**(2): p. 415-419.
116. Karmakar, A., et al., *Ethylenediamine Functionalized-Single-walled Nanotube (f-SWNT)-Assisted In Vitro Delivery of the Oncogene Suppressor p53 Gene to Breast Cancer MCF-7 Cells.* International Journal of Nanomedicine, 2011. **6**: p. 1045-1055.
117. Ahmed, M., et al., *Cationic Glyco-Functionalized Single-Walled Carbon Nanotubes as Efficient Gene Delivery Vehicles.* Bioconjugate Chemistry, 2009. **20**(11): p. 2017-2022.
118. Pantarotto, D., et al., *Functionalized Carbon Nanotubes for Plasmid DNA Gene Delivery.* Angewandte Chemie-International Edition, 2004. **43**(39): p. 5242-5246.
119. Zhang, Z., et al., *Delivery of Telomerase Reverse Transcriptase Small Interfering RNA in Complex with Positively Charged Single-Walled Carbon Nanotubes Suppresses Tumor Growth.* Clinical Cancer Research, 2006. **12**(16): p. 4933-4939.
120. Liu, Z., et al., *siRNA Delivery Into Human T Cells and Primary Cells with Carbon-Nanotube Transporters.* Angewandte Chemie-International Edition, 2007. **46**(12): p. 2023-2027.
121. Krajcik, R., et al., *Functionalization of Carbon Nanotubes Enables Non-Covalent Binding and Intracellular Delivery of Small Interfering RNA for Efficient Knock-Down of Genes.* Biochemical and Biophysical Research Communications, 2008. **369**(2): p. 595-602.
122. Wang, X., Ren, J., Qu, X., *Targeted RNA Interference of Cyclin A2 Mediated by Functionalized Single-Walled Carbon Nanotubes Induces Proliferation Arrest and Apoptosis in Chronic Myelogenous Leukemia K562 Cells.* ChemMedChem, 2008. **3**(6): p. 940-945.
123. Lanner, J.T., et al., *Knockdown of TRPC3 with siRNA Coupled to Carbon Nanotubes Results in Decreased Insulin-Mediated Glucose Uptake in Adult Skeletal Muscle Cells.* Faseb Journal, 2009. **23**(6): p. 1728-1738.
124. Heister, E., et al., *Triple Functionalisation of Single-walled Carbon Nanotubes with Doxorubicin, a Monoclonal Antibody, and a Fuorescent Marker for Targeted Cancer Therapy.* Carbon, 2009. **47**(9): p. 2152-2160.

125. Zhang, X., et al., *Targeted Delivery and Controlled Release of Doxorubicin to Cancer Cells Using Modified Single Wall Carbon Nanotubes.* Biomaterials, 2009. **30**(30): p. 6041-6047.
126. Li, J., et al., *Carbon Nanotube Bottles for Incorporation, Release and Enhanced Cytotoxic Effect of Cisplatin.* Carbon, 2012. **50**(4): p. 1625-1634.
127. Li, J., et al., *In Vivo Biodistribution of Platinum-Based Drugs Encapsulated into Multi-Walled Carbon Nanotubes.* Nanomedicine-Nanotechnology Biology and Medicine, 2014. **10**(7): p. 1465-1475.
128. Madani, S.Y., et al., *A New Era of Cancer Treatment: Carbon Nanotubes as Drug Delivery Tools.* International Journal of Nanomedicine, 2011. **6**: p. 2963-2979.
129. Vittorio, O., et al., *Novel Functional Cisplatin Carrier Based on Carbon Nanotubes-Quercetin Nanohybrid Induces Synergistic Anticancer Activity Against Neuroblastoma In Vitro.* RSC Advances, 2014. **4**(59): p. 31378-31384.
130. Hampel, S., et al., *Carbon Nanotubes Filled with a Chemotherapeutic Agent: a Nanocarrier Mediates Inhibition of Tumor Cell Growth.* Nanomedicine, 2008. **3**(2): p. 175-182.
131. Wu, C.H., et al., *Trojan-Horse Nanotube On-Command Intracellular Drug Delivery.* Nano Letters, 2012. **12**(11): p. 5475-5480.
132. Zhong, T., et al., *Functionalized Multiwalled Carbon Nanotubes-Anticancer Drug Carriers: Synthesis, Targeting Ability and Antitumor Activity.* Nano Biomedicine and Engineering, 2011. **3**(3): p. 157-162.
133. Singh, R., et al., *Gemcitabine-Loaded Smart Carbon Nanotubes for Effective Targeting to Cancer Cells.* Journal of Drug Targeting, 2013. **21**(6): p. 581-592.
134. Liu, Z., et al., *Supramolecular Stacking of Doxorubicin on Carbon Nanotubes for In Vivo Cancer Therapy.* Angewandte Chemie-International Edition, 2009. **48**(41): p. 7668-7672.
135. Ali-Boucetta, H., et al., *Multiwalled Carbon Nanotube-Doxorubicin Supramolecular Complexes for Cancer Therapeutics.* Chemical Communications, 2008(4): p. 459-461.
136. Farahani, B.V., Behbahani, G.R., Javadi, N., *Functionalized Multi Walled Carbon Nanotubes as a Carrier for Doxorubicin: Drug Adsorption Study and Statistical Optimization of Drug Loading by Factorial Design Methodology.* Journal of the Brazilian Chemical Society, 2016. **27**: p. 694-705.
137. Ren, J., et al., *The Targeted Delivery of Anticancer Drugs to Brain Glioma by PEGylated Oxidized Multi-Walled Carbon Nanotubes Modified with Angiopep-2.* Biomaterials, 2012. **33**(11): p. 3324-3333.
138. Risi, G., et al., *In vitro Study of Multiwall Carbon Nanotubes (MWCNTs) with Adsorbed Mitoxantrone (MTO) as a Drug Delivery System to Treat Breast Cancer.* RSC Advances, 2014. **4**(36): p. 18683-18693.

139. Samori, C., et al., *Enhanced Anticancer Activity of Multi-walled Carbon Nanotube-Methotrexate Conjugates Using Cleavable Linkers.* Chemical Communications, 2010. **46**(9): p. 1494-1496.
140. Das, M., et al., *Augmented Anticancer Activity of a Targeted, Intracellularly Activatable, Theranostic Nanomedicine Based on Fluorescent and Radiolabeled, Methotrexate-Folic Acid-Multiwalled Carbon Nanotube Conjugate.* Molecular Pharmaceutics, 2013. **10**(7): p. 2543-2557.
141. Kafa, H., et al., *The Interaction of Carbon Nanotubes with an In Vitro Blood-Brain Barrier Model and Mouse Brain In Vivo.* Biomaterials, 2015. **53**: p. 437-452.
142. Kostarelos, K., Bianco, A., Prato,M., *Promises, Facts and Challenges for Carbon Nanotubes in Imaging and tTherapeutics.* Nature Nanotechnology, 2009. **4**(10): p. 627-633.
143. Poland, C.A., et al., *Carbon Nanotubes Introduced into the Abdominal Cavity of Mice Show Asbestos-Like Pathogenicity in a Pilot Study.* Nature Nanotechnology, 2008. **3**(7): p. 423-428.
144. Nagai, H., Toyokuni, S., *Differences and Similarities between Carbon Nanotubes and Asbestos Fibers during Mesothelial Carcinogenesis: Shedding Light on Fiber Entry Mechanism.* Cancer Science, 2012. **103**(8): p. 1378-1390.
145. Yang, S.T., et al., *Pharmacokinetics, Metabolism and Toxicity of Carbon Nanotubes for Biomedical Purposes.* Theranostics, 2012. **2**(3): p. 271-282.
146. Liu, Z., et al., *Circulation and Long-Term Fate of Functionalized, Biocompatible Single-Walled Carbon Nanotubes in Mice Probed by Raman Spectroscopy.* Proceedings of the National Academy of Sciences, 2008. **105**(5): p. 1410-1415.
147. Meng, L., et al., *Single Walled Carbon Nanotubes as Drug Delivery Vehicles: Targeting Doxorubicin to Tumors.* Biomaterials, 2012. **33**(6): p. 1689-1698.
148. Popov, V.N., *Carbon Nanotubes: Properties and Application.* Materials Science & Engineering R-Reports, 2004. **43**(3): p. 61-102.
149. Donaldson, K., et al., *Carbon Nanotubes: A Review of Their Properties in Relation to Pulmonary Toxicology and Workplace Safety.* Toxicological Sciences, 2006. **92**(1): p. 5-22.
150. Datsyuk, V., et al., *Chemical Oxidation of Multiwalled Carbon Nanotubes.* Carbon, 2008. **46**(6): p. 833-840.
151. He, F.A., Fan, J.T, *An Effective Approach for Purifying, Cutting, and Functionalising of Multi-Walled Carbon Nanotubes.* Materials Science and Technology, 2013. **29**(12): p. 1423-1429.
152. Liu, Y., et al., *A Multi-Step Strategy for Cutting and Purification of Single-Walled Carbon Nanotubes.* Carbon, 2007. **45**(10): p. 1972-1978.
153. Pelalak, R., Baniadam, M., Maghrebi, M., *Controllable Purification, Cutting and Unzipping of Multi-Walled Carbon Nanotubes with a Microwave Method.* Applied Physics A, 2013. **111**(3): p. 951-957.

154. Hamwi, A., et al., *Fluorination of Carbon Nanotubes.* Carbon, 1997. **35**(6): p. 723-728.
155. Mohsen Jahanshahi, A.D.K., *Fabrication, Purification and Characterization of Carbon Nanotubes: Arc-Discharge in Liquid Media (ADLM)*, in *Syntheses and Applications of Carbon Nanotubes and Their Composites*, Suzuki, S. Editor. 2013, InTech. p. 55-75.
156. Ko, F.-H., et al., *Purification of Multi-Walled Carbon Nanotubes Through Microwave Heating of Nitric Acid in a Closed Vessel.* Carbon, 2005. **43**(4): p. 727-733.
157. Li, Y., et al., *Purification of CVD Synthesized Single-Wall Carbon Nanotubes by Different Acid Oxidation Treatments.* Nanotechnology, 2004. **15**(11): p. 1645-1649.
158. Tobias, G., et al., *Purification and Opening of Carbon Nanotubes Using Steam.* Journal of Physical Chemistry B, 2006. **110**(45): p. 22318-22322.
159. Ballesteros, B., et al., *Steam Purification for the Removal of Graphitic Shells Coating Catalytic Particles and the Shortening of Single-Walled Carbon Nanotubes.* Small, 2008. **4**(9): p. 1501-1506.
160. Yang, Y., et al., *Purification and Length Separation of Single-Walled Carbon Nanotubes Using Chromatographic Method.* Synthetic Metals, 2005. **155**(3): p. 455-460.
161. Ismail, A.F., et al., *A Review of Purification Techniques for Carbon Nanotubes.* Nano, 2008. **03**(03): p. 127-143.
162. Zhang, H., et al., *Purification of Multiwalled Carbon Nanotubes by Annealing and Extraction Based on the Difference in van der Waals Potential.* Journal of Physical Chemistry B, 2006. **110**(19): p. 9477-9481.
163. Hou, P.-X., C. Liu, and H.-M. Cheng, *Purification of carbon nanotubes.* Carbon, 2008. **46**(15): p. 2003-2025.
164. Javey, A., et al., *High-Field Quasiballistic Transport in Short Carbon Nanotubes.* Physical Review Letters, 2004. **92**(10): p. 106804.
165. Barros, E.B., et al., *Charge Transfer Effects in Acid Treated Single-Wall Carbon Nanotubes.* Carbon, 2005. **43**(12): p. 2495-2500.
166. Onoa, G.B., et al., *Bulk Production of Singly Dispersed Carbon Nanotubes with Prescribed Ñengths.* Nanotechnology, 2005. **16**(12): p. 2799.
167. Smart, S.K., et al., *The Biocompatibility of Carbon Nanotubes.* Carbon, 2006. **44**(6): p. 1034-1047.
168. Kolosnjaj-Tabi, J., et al., *In Vivo Behavior of Large Doses of Ultrashort and Full-Length Single-Walled Carbon Nanotubes after Oral and Intraperitoneal Administration to Swiss Mice.* ACS Nano, 2010. **4**(3): p. 1481-1492.
169. Muller, J., et al., *Respiratory Toxicity of Multi-Wall Carbon Nanotubes.* Toxicology Applied Pharmacology, 2005. **207**(3): p. 221-231.
170. Liu, J., et al., *Fullerene Pipes.* Science, 1998. **280**(5367): p. 1253-1256.
171. Ziegler, K.J., et al., *Cutting Single-Walled Carbon Nanotubes.* Nanotechnology, 2005. **16**(7): p. S539-S544.

172. Pistone, A., et al., *Morphological Modification of MWCNTs Functionalized with HNO_3/H_2SO_4 Mixtures.* Journal of Nanoscience and Nanotechnology, 2012. **12**(6): p. 5054-60.
173. Forrest, G.A., Alexander, A.J., *A Model for the Dependence of Carbon Nanotube Length on Acid Oxidation Time.* Journal of Physical Chemistry C, 2007. **111**(29): p. 10792-10798.
174. Shuba, M.V., et al., *Soft Cutting of Single-Wall Carbon Nanotubes by Low Temperature Ultrasonication in a Mixture of Sulfuric and Nitric Acids.* Nanotechnology, 2012. **23**(49): p. 495714.
175. Chen, Z.Y., et al., *Cutting of Single-Walled Carbon Nanotubes by Ozonolysis.* Journal of Physical Chemistry B, 2006. **110**(24): p. 11624-11627.
176. Chen, Z.Y., Hauge, R.H., Smalley, R.E., *Ozonolysis of Functionalized Single-Walled Carbon Nanotubes.* Journal of Nanoscience and Nanotechnology, 2006. **6**(7): p. 1935-1938.
177. Gu, Z., et al., *Cutting Single-Wall Carbon Nanotubes Through Fluorination.* Nano Letters, 2002. **2**(9): p. 1009-1013.
178. Kang, J., et al., *Fluorination and Defluorination of Carbon Nanotubes: A Nanoscale Perspective.* Chemical Physics Letters, 2012. **534**(0): p. 43-47.
179. Tran, M.Q., et al., *Thermal Oxidative Cutting of Multi-Walled Carbon Nanotubes.* Carbon, 2007. **45**(12): p. 2341-2350.
180. Marega, R., et al., *Cap Removal and Shortening of Double-Walled and Very-Thin Multi-Walled Carbon Nanotubes Under Mild Oxidative Conditions.* Carbon, 2009. **47**(3): p. 675-682.
181. Cabana, L., et al., *The Role of Steam Treatment on the Structure, Purity and Length Distribution of Multi-Walled Carbon Nanotubes.* Carbon, 2015. **93**: p. 1059-1067.
182. Banhart, F., *Irradiation Effects in Carbon Nanostructures.* Reports on Progress in Physics, 1999. **62**(8): p. 1181.
183. Sun, H., *γ Radiation Cutting and Photoacoustic Effect of Single-Walled Carbon Nanotubes.* Yuanzineng Kexue Jishu/Atomic Energy Science and Technology, 2011. **45**(4): p. 474-478.
184. Banhart, F., Li, J., Terrones, M., *Cutting Single-Walled Carbon Nanotubes with an Electron Beam: Evidence for Atom Migration Inside Nanotubes.* Small, 2005. **1**(10): p. 953-956.
185. Zhou, J., et al., *Tailoring Multi-Wall Carbon Nanotubes for Smaller Nanostructures.* Carbon, 2009. **47**(3): p. 829-838.
186. Jeong, S.H., et al., *Preparation of Aligned Carbon Nanotubes with Prescribed Dimensions: Template Synthesis and Sonication Cutting Approach.* Chemistry of Materials, 2002. **14**(4): p. 1859-1862.
187. Liu, P., Wang, T., *Ultrasonic-Assisted Chemical Oxidative Cutting of Multiwalled Carbon Nanotubes with Ammonium Persulfate in Neutral Media.* Applied Physics A, 2009. **97**(4): p. 771.

188. Park, H.J., et al., *The Effect of Pre-Treatment Methods on Morphology and Size Distribution of Multi-Walled Carbon Nanotubes.* Nanotechnology, 2008. **19**(33): p. 335702.
189. Rubio, N., et al., *Ball-Milling Modification of Single-Walled Carbon Nanotubes: Purification, Cutting, and Functionalization.* Small, 2011. **7**(5): p. 665-674.
190. Ahn, J.H., et al., *Structural Modification of Carbon Nanotubes by Various Ball Milling.* Journal of Alloys and Compounds, 2007. **434–435**(0): p. 428-432.
191. Chen, L., et al., *Cutting of Carbon Nanotubes by a Two-Roller Mill.* Materials Letters, 2006. **60**(2): p. 241-244.
192. Darsono, N., Yoon, D.-H., Kim, J., *Milling and Dispersion of Multi-Walled Carbon Nanotubes in Texanol.* Applied Surface Science, 2008. **254**(11): p. 3412-3419.
193. Kim, Y.A., et al., *Effect of Ball Milling on Morphology of Cup-Stacked Carbon Nanotubes.* Chemical Physics Letters, 2002. **355**(3–4): p. 279-284.
194. Kukovecz, Á., et al., *Long-Time Low-Impact Ball Milling of Multi-Wall Carbon Nanotubes.* Carbon, 2005. **43**(5): p. 994-1000.
195. Liu, F., et al., *Preparation of Short Carbon Nanotubes by Mechanical Ball Milling and Their Hydrogen Adsorption Behavior.* Carbon, 2003. **41**(13): p. 2527-2532.
196. Ma, P.C., Tang, B.Z., Kim, J.-K., *Conversion of Semiconducting Behavior of Carbon Nanotubes Using Ball Milling.* Chemical Physics Letters, 2008. **458**(1–3): p. 166-169.
197. Oh, Y., et al., *The Effects of Ball Milling Process on the Diameter Dependent Fracture of Single Walled Carbon Nanotubes.* Scripta Materialia, 2007. **56**(9): p. 741-744.
198. Sun, Y.F., et al., *The Investigation of Adsorptive Performance on Modified Multi-Walled Carbon Nanotubes by Mechanical Ball Milling.* Materials Chemistry and Physics, 2007. **101**(1): p. 30-34.
199. Tucho, W.M., et al., *The Effects of Ball Milling Intensity on Morphology of Multiwall Carbon Nanotubes.* Scripta Materialia, 2010. **63**(6): p. 637-640.
200. Zapata-Massot, C., Le Bolay, N., *Effect of Ball Milling in a Tumbling Ball Mill on the Properties of Multi-Wall Carbon Nanotubes.* Chemical Engineering and Processing: Process Intensification, 2008. **47**(8): p. 1350-1356.
201. Forró, L., et al., *Tuning the Length Dispersion of Multi-Walled Carbon Nanotubes by Ball Milling.* AIP Advances, 2013. **3**(9): p. -.
202. Papp, I., et al., *Effect of Planetary Ball Milling Process Parameters on the Nitrogen Adsorption Properties of Multiwall Carbon Nanotubes.* Adsorption, 2013. **19**(2-4): p. 687-694.
203. Munkhbayar, B., et al., *Influence of Dry and Wet Ball Milling on Dispersion Characteristics of the Multi-Walled Carbon Nanotubes in Aqueous Solution with and without Surfactant.* Powder Technology, 2013. **234**: p. 132-140.

204. Munkhbayar, B., et al., *Effect of Grinding Speed Changes on Dispersibility of the Treated Multi-Walled Carbon Nanotubes in Aqueous Solution and Its Thermal Characteristics.* Chemical Engineering and Processing: Process Intensification, 2012. **61**(0): p. 36-41.
205. Munkhbayar, B., et al., *An Experimental Study of the Planetary Ball Milling Effect on Dispersibility and Thermal Conductivity of MWCNTs-Based Aqueous Nanofluids.* Materials Research Bulletin, 2012. **47**(12): p. 4187-4196.
206. Park, K.C., et al., *Inter-Collisional Cutting of Multi-Walled Carbon Nanotubes by High-Speed Agitation.* Journal of Physics and Chemistry of Solids, 2008. **69**(10): p. 2481-2486.
207. Lee, J., et al., *Short Carbon Nanotubes Produced by Cryogenic Crushing.* Carbon, 2006. **44**(14): p. 2984-2989.
208. Kharlamova, M.V., *Advances in Tailoring the Electronic Properties of Single-Walled Carbon Nanotubes.* Progress in Materials Science, 2016. **77**: p. 125-211.
209. Georgakilas, V., et al., *Decorating Carbon Nanotubes with Metal or Semiconductor Nanoparticles.* Journal of Materials Chemistry, 2007. **17**(26): p. 2679-2694.
210. Meng, L., C. Fu, and Q. Lu, *Advanced Technology for Functionalization of Carbon Nanotubes.* Progress in Natural Science, 2009. **19**(7): p. 801-810.
211. Karousis, N., N. Tagmatarchis, and D. Tasis, *Current Progress on the Chemical Modification of Carbon Nanotubes.* Chemical Reviews, 2010. **110**(9): p. 5366-5397.
212. Wu, H.-C., et al., *Chemistry of Carbon Nanotubes in Biomedical Applications.* Journal of Materials Chemistry, 2010. **20**(6): p. 1036-1052.
213. Jeon, I.-Y., et al., *Functionalization of Carbon Nanotubes*, in *Carbon Nanotubes - Polymer Nanocomposites*, Yellampalli, S., Editor. 2011, InTech. p. 91-110.
214. Chiang, Y.-C., Lin, W.-H., Chang, Y.-C., *The Influence of Treatment Duration on Multi-Walled Carbon Nanotubes Functionalized by H_2SO_4/HNO_3 Oxidation.* Applied Surface Science, 2011. **257**(6): p. 2401-2410.
215. Tasis, D., et al., *Chemistry of Carbon Nanotubes.* Chemical Reviews, 2006. **106**(3): p. 1105-1136.
216. Axet, M.R., et al., *Coordination Chemistry on Carbon Surfaces.* Coordination Chemistry Reviews, 2016. **308, Part 2**: p. 236-345.
217. Georgakilas, V., et al., *Organic Functionalization of Carbon Nanotubes.* Journal of the American Chemical Society, 2002. **124**(5): p. 760-761.
218. Tang, X., et al., *Hydrogenation of Multi-walled Carbon Nanotubes in Ethylenediamine.* Fullerenes, Nanotubes and Carbon Nanostructures, 2010. **18**(1): p. 14-23.
219. Tsubokawa, N., *Preparation and Properties of Polymer-grafted Carbon Nanotubes and Nanofibers.* Polymer Journal, 2005. **37**(9): p. 637-655.

220. Chen, Z., et al., *Cutting of Single-Walled Carbon Nanotubes by Ozonolysis.* Journal of Physical Chemistry B, 2006. **110**(24): p. 11624-11627.
221. Hemraj-Benny, T., Bandosz, T.J., Wong, S.S., *Effect of Ozonolysis on the Pore Structure, Surface Chemistry, and Bundling of Single-Walled Carbon Nanotubes.* Journal of Colloid and Interface Science, 2008. **317**(2): p. 375-382.
222. Sun, Y.-P., et al., *Functionalized Carbon Nanotubes: Properties and Applications.* Accounts of Chemical Research, 2002. **35**(12): p. 1096-1104.
223. Pederson, M.R., Broughton, J.Q., *Nanocapillarity in Fullerene Tubules.* Physical Review Letters, 1992. **69**(18): p. 2689-2692.
224. Ajayan, P.M., Iijima, S. *Capillarity-Induced Filling of Carbon Nanotubes.* Nature, 1993. **361**(6410): p. 333-334.
225. Andrei, A.E., et al., *Preparation and Properties of Single-Walled Nanotubes Filled with Inorganic Compounds.* Russian Chemical Reviews, 2009. **78**(9): p. 833.
226. Sloan, J., et al., *Integral Atomic Layer Architectures of 1D Crystals Inserted into Single Walled Carbon Nanotubes.* Chemical Communications, 2002(13): p. 1319-1332.
227. Spinato, C., et al., *Design of Antibody-Functionalized Carbon Nanotubes Filled with Radioactivable Metals Towards a Targeted Anticancer Therapy.* Nanoscale, 2016.
228. Marega, R., Bonifazi, D., *Filling Carbon Nanotubes for Nanobiotechnological Applications.* New Journal of Chemistry, 2014. **38**(1): p. 22-27.
229. Gautam, U.K., et al., *Recent Developments in Inorganically Filled Carbon Nanotubes: Successes and Challenges.* Science and Technology of Advanced Materials, 2010. **11**(5).
230. Eliseev, A., et al., *One-Dimensional Crystals inside Single-Walled Carbon Nanotubes: Growth, Structure and Electronic Properties*, in *Electronic Properties of Carbon Nanotubes*, Marulanda, J.M., Editor. 2011, InTech. p. 127-156.
231. Monthioux, M., Flahaut, E., *Meta- and Hybrid-CNTs: A Clue for the Future Development of Carbon Nanotubes.* Materials Science and Engineering: C, 2007. **27**(5–8): p. 1096-1101.
232. Tobias, G., Mendoza, E., Ballesteros, B., *Functionalisation of Carbon Nanotubes*, in *Encyclopedia of Nanotechnology*, Bhushan, B., Editor. 2012, Springer. p. 911-919.
233. Dujardin, E., et al., *Wetting of Single Shell Carbon Nanotubes.* Advanced Materials, 1998. **10**(17): p. 1472-1475.
234. Fu, Q., et al.,, *Selective Filling of Carbon Nanotubes with Metals by Selective Washing.* New Carbon Materials, 2008. **23**(1): p. 17-20.
235. Lukanov, P., et al.,, *Filling of Carbon Nanotubes with Compounds in Solution or Melted Phase*, in *Carbon Nanotubes for Biomedical Applications*, Rüdiger Klingeler, R.B.S., Editor. 2011, Springer.

236. Dujardin, E., et al., *Capillarity and Wetting of Carbon Nanotubes.* Science, 1994. **265**(5180): p. 1850.
237. Ujjal, K.G., et al., *Recent Developments in Inorganically Filled Carbon Nanotubes: Successes and Challenges.* Science and Technology of Advanced Materials, 2010. **11**(5): p. 054501.
238. Ballesteros, B., et al., *Quantitative Assessment of the Amount of Material Encapsulated in Filled Carbon Nanotubes.* Journal Physical Chemistry C., 2009. **113**(7): p. 2653-2656.
239. Shao, L., et al., *Reversible Filling of Single Walled Carbon Nanotubes Opened by Alkali Hydroxides.* Carbon, 2006. **44**(13): p. 2855-2858.
240. Bortolamiol, T., et al., *Double-Walled Carbon Nanotubes: Quantitative Purification Assessment, Balance Between Purification and Degradation and Solution Filling as an Evidence of Opening.* Carbon, 2014. **78**: p. 79-90.
241. De Jongh, P.E., Eggenhuisen, T.M,*Melt Infiltration: an Emerging Technique for the Preparation of Novel Functional Nanostructured Materials.* Advanced Materials, 2013. **25**(46): p. 6672-6690.
242. Luksirikul, P., et al., *pH-Triggered Release of Materials from Single-Walled Carbon Nanotubes using Dimethylamino-Functionalized Fullerenes as Removable "Corks".* Carbon, 2010. **48**(7): p. 1912-1917.
243. Capobianchi, A., et al., *Controlled Filling and External Cleaning of Multi-Wall Carbon Nanotubes Using a Wet Chemical Method.* Carbon, 2007. **45**(11): p. 2205-2208.
244. Cook, J., et al., *Purification of Rhodium-Filled Carbon Nanotubes Using Reversed Micelles.* Chemical Communications, 1996(23): p. 2673-2674.
245. Martincic, M., et al., *Quantitative Monitoring of the Removal of Non-Encapsulated Material External to Filled Carbon Nanotube Samples.* ChemPhysChem, 2015. **17**: p. 31662-31669.
246. Satishkumar, B.C., et al., *Novel Experiments with Carbon Nanotubes: Opening, Filling, Closing and Functionalizing Nanotubes.* Journal of Physics B: Atomic, Molecular and Optical Physics, 1996. **29**(21): p. 4925.
247. Tobias, G., et al., *Carbon Nanocapsules: Blocking Materials Inside Carbon Nanotubes.* Physica Status Solidi C, 2010. **7**(11-12): p. 2739-2742.
248. Zhao, Y., et al., *Corking Carbon Nanotube Cups with Gold Nanoparticles.* ACSNano, 2012. **6**(8): p. 6912-6923.
249. Eder, D., *Carbon Nanotube–Inorganic Hybrids.* Chemical Reviews, 2010. **110**(3): p. 1348-1385.
250. Planeix, J.M., et al., *Application of Carbon Nanotubes as Supports in Heterogeneous Catalysis.* Journal of the American Chemical Society, 1994. **116**(17): p. 7935-7936.
251. Chen, J., Lu, G., *Carbon Nanotube-Nanoparticle Hybrid Structures*, in *Carbon Nanotubes*, Marulanda, J.M., Editor. 2010, InTech. p. 611-633.
252. Peng, X., et al., *Carbon Nanotube-Nanocrystal Heterostructures.* Chemical Society Reviews, 2009. **38**(4): p. 1076-1098.

253. Kharisov, B.I., et al., *Decoration of Carbon Nanotubes With Metal Nanoparticles: Recent Trends.* Synthesis and Reactivity in Inorganic Metal-Organic and Nano-Metal Chemistry, 2016. **46**(1): p. 55-76.
254. Satishkumar, B.C., et al., *The Decoration of Carbon Nanotubes by Metal Nanoparticles.* Journal of Physics D, 1996. **29**(12): p. 3173.
255. Coleman, K.S., et al., *Functionalization of Single-Walled Carbon Nanotubes via the Bingel Reaction.* Journal of the American Chemical Society, 2003. **125**(29): p. 8722-8723.
256. Vilian, A.T.E., et al., *Immobilization of Myoglobin on Au Nanoparticle-Decorated Carbon Nanotube/Polytyramine Composite as a Mediator-Free H_2O_2 and Nitrite Biosensor.* Scientific Reports, 2015. **5**.
257. Li, X., et al., *Ultra-Small Palladium Nanoparticle Decorated Carbon Nanotubes: Conductivity and Reactivity.* ChemPhysChem, 2015. **16**(11): p. 2322-2325.
258. Sun, Z., et al., *Decoration Carbon Nanotubes with Pd and Ru Nanocrystals via an Inorganic Reaction Route in Supercritical Carbon Dioxide–Methanol Solution.* Journal of Colloid and Interface Science, 2006. **304**(2): p. 323-328.
259. Nie, C., et al., *Mussel-Inspired Coatings on Ag Nanoparticle-Conjugated Carbon Nanotubes: Bactericidal Activity and Mammal Cell Toxicity.* Journal of Materials Chemistry B, 2016. **4**(16): p. 2749-2756.
260. Wang, D., Z.-C. Li, and L. Chen, *Templated Synthesis of Single-Walled Carbon Nanotube and Metal Nanoparticle Assemblies in Solution.* Journal of the American Chemical Society, 2006. **128**(47): p. 15078-15079.

CHAPTER 2

OBJECTIVES

There are many articles dedicated to the growth, properties, and applications of CNTs. However, the literature reveals that relatively little is known about filled CNTs. Consequently, this thesis aims to narrow this research gap and it brings new insights into the synthesis and investigation of filled carbon nanotubes.

The main goal of this work was to develop samples of filled carbon nanotubes with a low degree of structural defects, characterized by high purity and a short and narrow length distribution for biomedical applications. In this way carbon nanocapsules were prepared (Fig. 2.1). The nanocapsules were then covalently functionalized in order to improve their dispersion which is essential to render the material biocompatible.

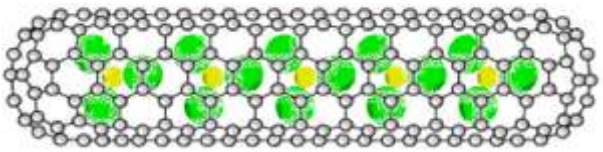

Figure 2.1 Carbon nanocapsule (clean and filled carbon nanotube).

The above aim was accomplished following these specific research objectives:

- ✓ Purification of CNTs in order to remove carbonaceous impurities and decrease the amount of catalyst present in the sample, while preserving the structure of the carbon nanotubes.
- ✓ Shortening of CNTs in a high yield, with a narrow length distribution and a minimal amount of structural defects.
- ✓ Encapsulation of biomedically relevant payloads into carbon nanotubes of interest for nanooncology.
- ✓ To develop an environmentally friendly protocol that allows an efficient removal of the non-encapsulated (radioactive) compounds from samples of filled carbon nanotubes.

- ✓ Investigate the role of temperature on the degree of end-closing of single-walled carbon nanotubes.
- ✓ Modification of the nanocapsules via covalent functionalization of the external walls, while preserving the encapsulated payload.
- ✓ Development of a dual agent via external decoration with gold nanoparticles of previously filled carbon nanotubes.

PART II

RESULTS

AND

DISCUSSION

CHAPTER 3

STEAM SHORTENING OF SINGLE-WALLED AND DOUBLE-WALLED CARBON NANOTUBES

CNTs are characterized by a big aspect ratio and hollow core; hence they have emerged as promising nanovectors for the development of smart diagnosis and therapeutic systems.[1-3] In spite their great potential in nanomedicine, the potential toxicity of CNTs is a prime concern.[4] Toxicity associated to CNTs arises from residual catalytic nanoparticles employed for their synthesis and from the presence of long CNTs in the samples.[5, 6] Therefore, intensified research efforts are conducted to improve their biocompatibility, including the development of new shortening and purification strategies.[7-9] The length of as-produced CNTs is typically in the order of micrometers,[1, 10] and toxic effects arising from the length of CNTs have been reported above 20 μm.[11] Most methods of CNTs´ shortening described in literature involve liquid oxidation with sulfuric or nitric acid which also alters the structure of nanotubes.[12-17] Although the presence of structural defects facilitates the processability and further derivatization of the material, it hinders the use of their inner cavities for the encapsulation and isolation of biomedically relevant payloads. Other popular approaches such as air oxidation or fluorination result in significant losses of sample due to fast etching rates.[18-21] Treating carbon nanotubes with steam (a mild oxidant) enables shortening and purification of the nanotubes, whilst avoiding the formation of defects, which may ultimately affect the properties and applications of CNTs. Early studies showed that once the ends are opened, prolonged steam treatment results in the shortening of the nanotubes. Furthermore, both amorphous carbon and graphitic particles that shield the metal catalyst are also removed. The exposed metal nanoparticles can be then dissolved in HCl.[22, 23] Our group had previously established the length distribution of steam treated MWCNTs for different periods of time.[24] In this chapter we will report on the role of steam on the length and structure of single-walled and double-walled carbon nanotubes.

3.1. Steam treatment protocol

CVD grown Elicarb® carbon nanotubes (Thomas Swan & Co. Ltd.) were employed in these studies. The as-received powder "Elicarb® SWNT" contains a mixture of both SWCNTs and DWCNTs (according to the supplier). Iron nanoparticles (catalyst) coated with graphitic shells and amorphous carbon were also present in the sample. This material will be referred in this chapter as CNTs.

As alternative source of CNTs we employed arc discharge grown SWCNTs (Carbon Nanotechnologies, Inc.). They also contain carbonaceous and iron impurities.

As-received CVD CNTs (400 mg) were finely ground with an agate mortar and pestle and spread inside a silica tube (4 cm in diameter) which served as a sample holder. The silica tube was then placed inside an alumina tube (5 cm in diameter) in the center of a tubular furnace. Steam was introduced at a rate of 0.58 mL/min by a continuous flow of argon (Carburos Metalicos, 99.999% purity) through hot water (98 °C). The experimental setup is shown on the schematic representation on Figure 3.1. The system was initially purged with Ar for 2 h to ensure the complete removal of air. Then, the furnace was annealed at a rate of 300 °C/min and dwelled at 900 °C for selected periods of time, namely 4 h, 10 h, 15 h and 25 h. The temperature was kept constant during the steam process since this parameter has been previously investigated and optimized.[22, 25]

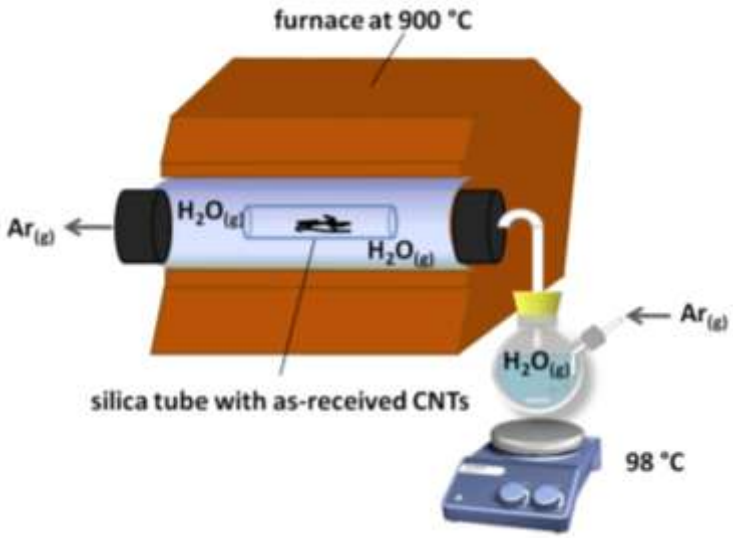

Figure 3.1. Schematic representation of the setup for the steam shortening and purification of CNTs.

According to previous reports, steam removes the amorphous carbon and graphitic shells that stealth the catalytic metal particles employed for the growth of the CNTs.[22] Therefore, each of the steam treated samples was independently refluxed with 6 M HCl overnight. The yellow color that developed in the acid solution indicated the dissolution of exposed iron nanoparticles. The sample was collected by filtration onto a polycarbonate membrane (0.2 μm pore size) and rinsed with distilled water until the pH of the filtrate was neutral. The collected solid powder was dried overnight at 100 °C and used for characterization.

Likewise, were prepared arc discharge SWCNTs. First, they were treated with steam for selected periods of time: 0.5 h, 1 h, 2 h, 3 h, 4 h, and 5 h. Then, they were refluxed with with 6 M HCl following the previously established protocol, and samples were collected by filtration

3.2. Dispersion of single-walled and double-walled carbon nanotubes

A major drawback to determine the length distribution of SWCNTs and DWCNTs is that these nanomaterials are present as aggregates due to van der Waals interactions.[26, 27] In contrast, MWCNTs separate much better. CNTs debundling can be achieved by dispersion in a suitable organic solvent, in aqueous solutions using surfactants or by surface modification with functional groups.[28-30] However, the complete individualization of SWCNTs while their structure is preserved remains a challenge.

Development of a fast and cheap methodology for the length distribution analysis of CNTs is becoming crucially important, for instance to path their way to commercial biomedical and electronic applications. In this area, microscopy techniques are taking the lead. Although atomic force microscopy (AFM)[31-34] and transmission electron microscopy (TEM)[33, 35] have been mostly employed to assess the CNTs' length distribution, the use of scanning electron microscopy (SEM)[8] presents substantial advantages. SEM is in general more accessible than AFM and TEM and provides accurate measurements for wide areas of the sample in an easy and fast manner. Moreover, most SEM samples require minimal preparation. Therefore, we tested several supports and solvents to optimize the dispersion of CNTs, which are summarized in Table 3.1. Various techniques were used in order to disperse raw and shortened samples of CNTs: sonication, centrifugation, spin coating and combined approaches. Next, the dispersed samples

were dropcasted onto the chosen supports and analyzed by SEM. Based on the obtained results we selected the best protocol for the determination of the length distribution of CNT samples, which is described in detail in the next paragraph.

Table 3.1. Summary of supports, solvents and protocols tested for dispersion of CNTs.

Support	Solvent	Protocol	Comments
silica	• Ethanol • 1% Pluronic® P 125 surfactant • hexane • chloroform ($CHCl_3$) • $CHCl_3$	• 30 min sonication • 30 min sonication • 30 min sonication • 30 min sonication • 30 s spin coating 2000 rpm	Spin coating does not work, CNTs absent on support. In case of sonication, in chloroform CNTs present in form of big aggregates, in other solvents various level of dispersion, but not individualized CNTs.
mica	$CHCl_3$	• 30 min sonication, 30 min centrifugation 2000 rpm • 60 s spin coating 2000 rpm	Does not work, impossible to acquire an image.
polycarbonate membrane	Ethanol	30 min sonication and further filtration through membrane which was used for SEM analysis	Good support, but problem when acquiring images for highly dispersed CNTs.
teflon membrane	acetonitryl	30 min sonication and further filtration through membrane which was used for SEM analysis	Impossible to acquire good image.
alumina stub	ethanol	30 min sonication	Impossible to acquire good image.
TEM copper grid coated with formvar/carbon	hexane	30 min sonication, aliquot collected after night	Does not work, very limited dispersion.
TEM copper grid coated with a carbon film	• ethanol • 0.1 and 0.01% sodium dodecyl sulfate (SDS) surfactant • *ortho*-dichlorobenzene (odcb) • odcb • $CHCl_3$ • hexane	• 30 min sonication • 5 min sonication, 30 min centrifugation 2000 rpm • 30 min sonication • 30 min sonication, aliquot collected after night • 30 min sonication • 30 min sonication	In most cases CNTs dispersed, but not individualized. **Individual CNTs observed for sample dispersed in odcb by 30 min of sonication.**

3.2.1. Length measurement procedure

We have developed and optimized a protocol in order to avoid the presence of big CNTs aggregates. Samples were dispersed by sonication of a tiny amount of CNTs in 3 mL of ortho-dichlorobenzene (odcb, Sigma Aldrich, 99%) for 30-45 min until a homogenous pale grey suspension was obtained. Next, the dispersion was dropcasted onto a TEM copper grid coated with a carbon film, and left to dry. Length measurements were performed on individual SWCNTs by SEM. As it can be seen in Figure 3.2, this imaging modality allows to easily discern between bundles and individual CNTs. Figure 3.2a-d correspond to images from optimized protocol, whereas Figure 3.2e corresponds to a non properly dispersed sample.

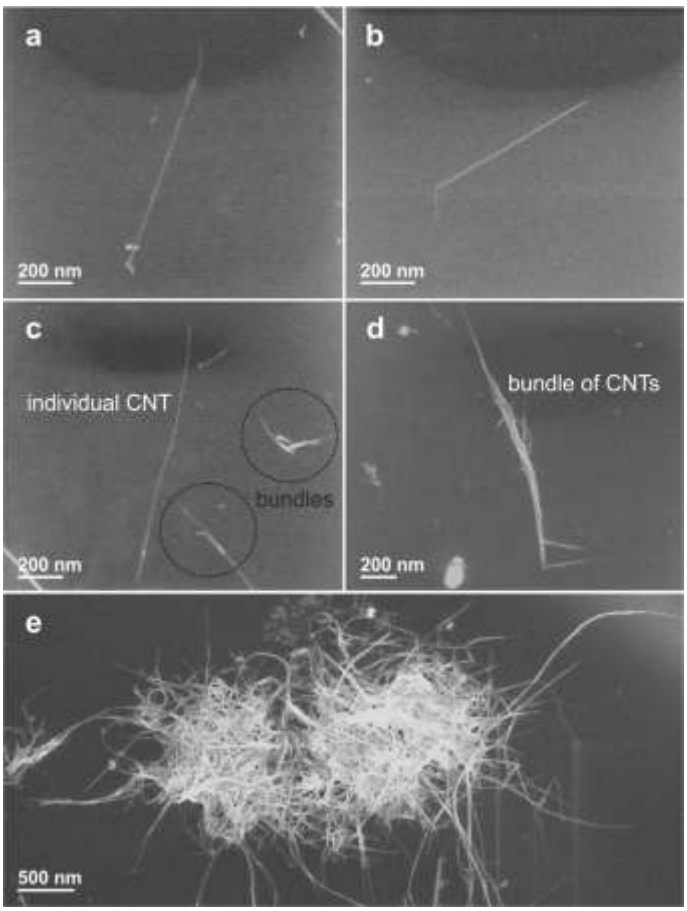

Figure 3.2. SEM images of CVD grown CNTs : a), b) individual nanotubes, c) individual CNT with the presence of small bundles (indicated by black circles), d) bundle of CNTs, e) big aggregate of CNTs in not properly dispersed sample.

High resolution transmission electron microscopy (HRTEM) confirmed that the individual CNTs present on the support were of few nanometers in diameter (Fig. 3.3).

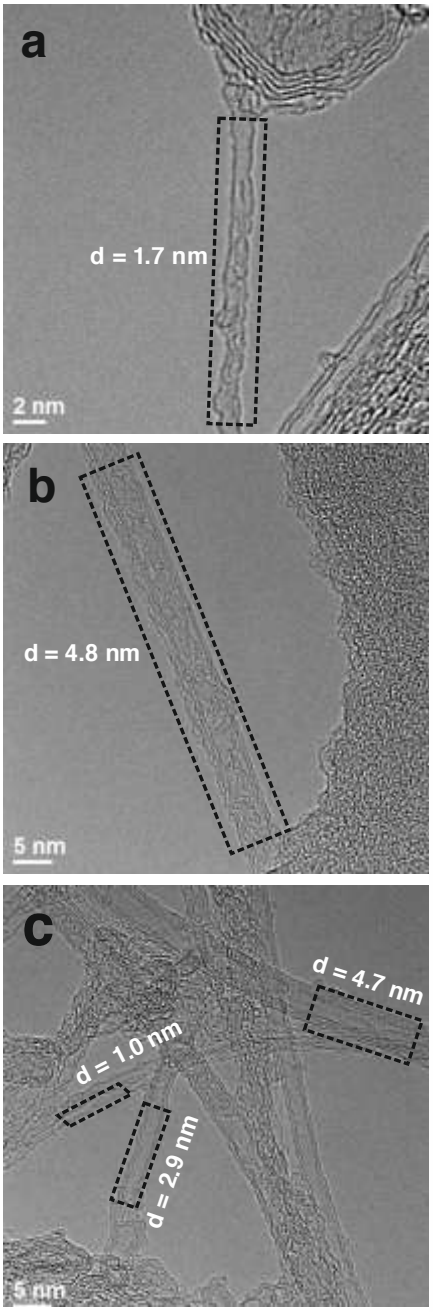

Figure 3.3. HRTEM images showing individual as-received CVD grown CNTs with a few nanometers in diameter: a) SWCNT, b) DWCNT, c) random bundle of CNTs. The tubes with measured diameters are indicated with black rectangles for clarity.

3.3. Results and discussion

As-received CVD CNTs were steam treated at 900 °C for different periods of time (4 h, 10 h, 15 h and 25 h), followed by an HCl wash. Samples were characterized by SEM, HRTEM, Raman spectroscopy and spectroelectrochemistry, thermogravimetric analysis (TGA), magnetic measurements using a superconducting quantum interference device (SQUID) magnetometer and energy dispersive X-ray spectroscopy (EDX).

3.3.1. Effect of steam on length distribution of carbon nanotubes

The length distribution of the samples was assesed from analysis of SEM images using Digital Micrograph software. Individual CNTs were measured for each of the samples, namely control group (as-received) and steam treated groups (steam + HCl). Reliable results are obtained for large populations, so we measured 300 nanotubes per group. Visual inspection of the SEM images and the histograms already reveal that the length of the as-received CNTs decreases after exposing the material to steam (Fig. 3.4).

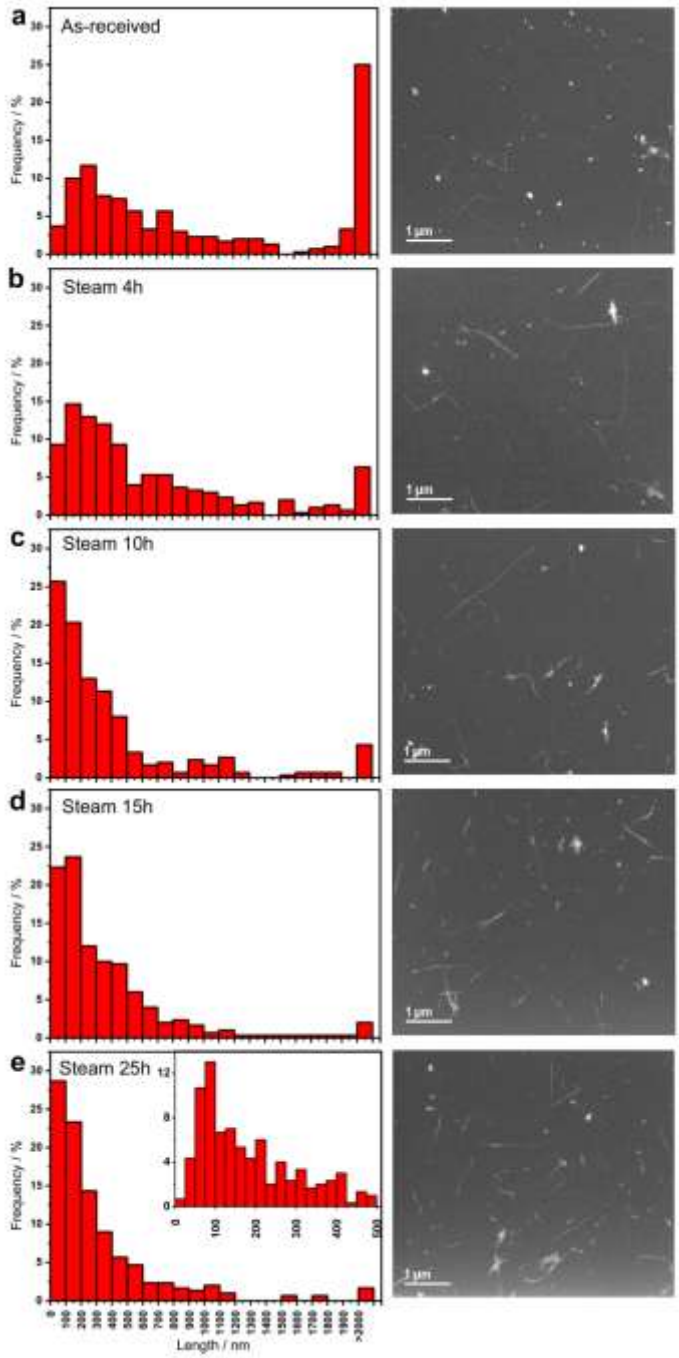

Figure 3.4. Analysis of the length distribution of as-received and steam-treated CVD CNTs for different periods of time: a) as-received, b) 4 h, c) 10 h, d) 15 h and e) 25 h. All steam treated samples were subsequently refluxed with HCl. Histograms are presented on the left panel and representative SEM images on the right panel of the figure. The inset in e) shows the detailed length distribution of the 25 h steam treated sample in the range 0-500 nm.

Statistical examination of the collected data was performed in order to determine the median value and asses the length distribution of each group. Figure 3.5 shows the box plot analysis of both as-received and the steam-treated CNTs, and Table 3.2 contains the descriptive analysis.

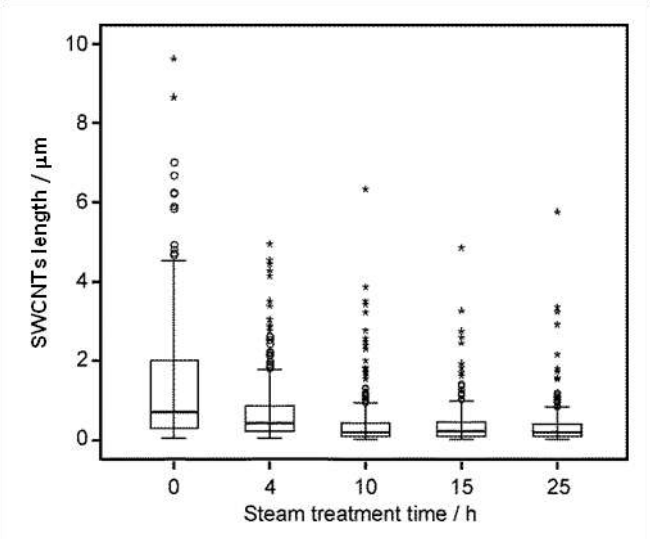

Figure 3.5. Box-plot analysis of the as-received CNTs (0 h) and steam-treated CNTs for 4, 10, 15 and 25 h (after an HCl wash). Empty circles indicate outliers and asterisks far outliers. The lower and maximum adjacent observations are represented with horizontal lines at the end of the whiskers.

We employed nonparametric tests to assess whether the median and the length distribution of two given groups had significant differences or not. The median test was used for the former, and both the U test of Mann–Whitney and the Kolmogorov–Smirnov test, for independent groups, were employed for the latter. The null hypotheses (H_0) were respectively: "medians are the same" and "length distributions are the same". Analyses of the as-received and 4 h steam-treated CNTs gave probability $p < 0.05$ for all the performed tests thus rejecting H_0. This implies that the medians and the length distribution of the CNTs are significantly different. A 40% decrease of the median value is observed between the as-received ($median_{as\text{-}received}$ = 711 nm) and the 4 h steam treated CNTs ($median_{4h}$ = 420 nm), CNTs treated for 4 h and 10 h with steam also present significant differences, with ca. 50% decrease of the median length between both groups ($median_{10h}$ = 198 nm). Interestingly, longer exposure of the CNTs to the steam treatment does not significantly alter the median value and the length distribution of the obtained material.

Table 3.2. Descriptive analysis of the length distribution for as-received CNTs and steam-treated CNTs during 4 h, 10 h, 15 h and 25 h (after an HCl wash).

Sample	N Number of measured CNTs	Median (nm)	Minimum adjacent observation (nm)	Q1 25th percentile (nm)	Q3 75th percentile (nm)	Maximum adjacent observation (nm)	Maximum observation (nm)
As-received	300	711	41	296.8	2009.2	4517	9621
4 h	300	420	33	214.5	845.0	1783	4943
10 h	300	198	15	83.7	423.0	932	6320
15 h	300	223	6	100.8	455.1	985	4857
25 h	300	191	23	91.7	388.0	831	5756

The statistical hypothesis testing of the CNTs treated with steam for 10 h, 15 h and 25 h resulted in $p > 0.05$. Therefore, the steam treatment of as-received CNTs for periods of time ranging between 10 h and 25 h allows the shortening of CNTs to median lengths of ca. 200 nm. Whereas as-received material contained more than 25% of CNTs longer than 2 µm, after 10-25 h of steam treatment ca. 50% nanotubes are shorter than 200 nm and 80% are below 500 nm.

3.3.2. Effect of steam on physical and structural properties of carbon nanotubes

After determining the length distribution, we examined the influence of steam on the physical and structural properties of the CNTs. Samples were studied by Raman spectroscopy and *in situ* Raman spectroelectrochemistry with 3 different excitation energies (1.96 eV (633 nm), 2.33 eV (532 nm) and 2.54 eV (488 nm)). The Raman spectrum of CNTs consists of three major areas: i) the radial breathing mode (RBM) from 100 cm^{-1} to 300 cm^{-1}, ii) the tangential mode (G-band) centered at ca. 1588 cm^{-1}, and iii) G'-band (also known as the 2D-band), centered at ca. 2650 cm^{-1}. Additionally, for samples containing structural defects, the disorder induced mode (D-band) is observed at 1350 cm^{-1}.[36-38]

First, as-received CNTs were analyzed by *in situ* Raman spectroelectrochemistry in order to obtain more detailed information about their electronic structure. The sample was excited at 1.96 eV using acetonitrile as electrolyte solution. Next, electrochemical charging by applying potential from -1.5 V to + 1.5 V in steps 0.3 V was performed to induce doping. The recorded

spectra are shown in Figure 3.6. Applying positive potentials results in p-doping (introduction of holes into π-band), and as consequence the Fermi level is downshifted. The opposite trend occurs when negative potentials are applied, and we can observe n-doping (introduction of electrons into π-band).[39, 40] When an upshift in the Fermi level reaches the van Hove singularity level, the corresponding electronic transition is blocked and the Raman signal is bleached. The Raman spectrum at 0 V after applying the potential recovers its original shape, indicating that the electrochemical doping of the as-received CNTs is a reversible process.

The decrease of the spectral intensity is most pronounced in the RBM area (Fig. 3.6a). Only CNTs with transition energies (denoted as E_{ii}) in resonance or close to the employed laser energy (E_{laser}) appear in the RBM spectrum.[41] The diameter (d_t) of CNTs, can be determined from the frequency of RBM (ω): $\omega = 217/d_t + 15$.[38] Moreover, the Kataura plot indicates the relation between the energy of the band gap (E_{ii}) and the diameter of CNTs. It also differentiates between semiconducting (S) and metallic (M) nanotubes depending on their (n,m) integers.[42-44]

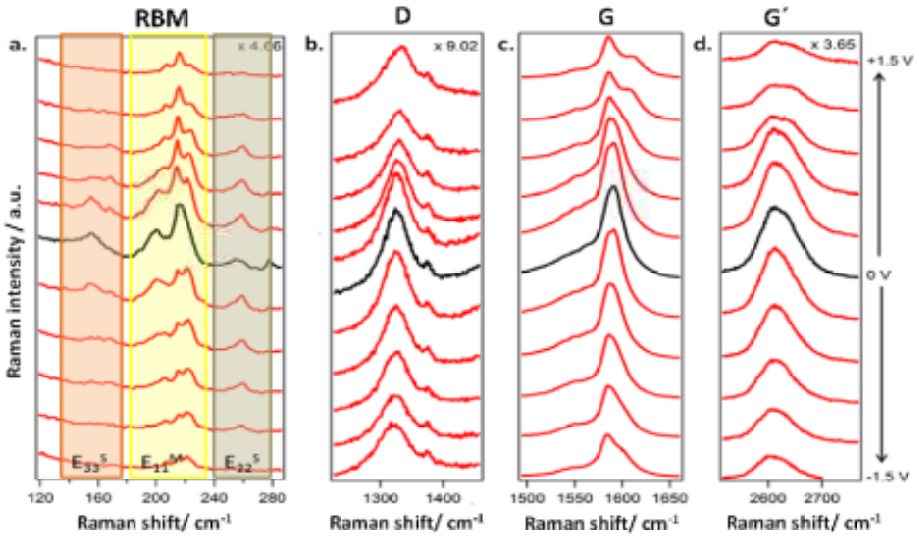

Figure 3.6. Raman spectra of the as-received CNTs at different potentials in the spectral regions of a. RBM, b. D-band, c. G-band, and d. G'-band. The electrode potential range is from -1.5 to 1.5 V vs Ag/Ag^+ (from bottom to top). The spectra in black correspond to the 0 V potential. The electrochemical potential change between the curves in the figure is 0.3 V. The spectra were acquired using 1.96 eV laser excitation energy. The spectra are offset for clarity.

Figure 3.6a is divided into three regions: orange, yellow and grey, each of them corresponding to tubes excited via the electronic transitions of CNTs so-called E_{33}^{S}, E_{11}^{M} and E_{22}^{S}, respectively. The peaks at around 200 cm^{-1} (d_t= 1 nm), 215 cm^{-1} (d_t= 0.94 nm), and 221 cm^{-1} (d_t= 0.92 nm), represent metallic nanotubes, while the peaks at 156 cm^{-1} (d_t= 1.27 nm) and at 259 cm^{-1} (d_t= 0.79 nm), correspond to semiconducting nanotubes. Detailed analysis of the RBM mode indicates the presence of DWCNTs. While the frequencies of the RBM of the DWCNTs are unaffected by changing the potential, their intensities are modified in a different manner for inner and outer tubes. The attenuation observed in the RBM intensity promoted by electrochemical charging is more pronounced for the outer tubes which have larger diameters (156 cm^{-1}) and softer for the inner ones (200 cm^{-1}, 215 cm^{-1}, 221 cm^{-1} and 259 cm^{-1}). The bleaching of the band at 156 cm^{-1}, which corresponds to outer tubes, is observed already at ± 0.3 V, and the bleaching of the inner tubes is postponed.

In Figure 3.6c the G-band appears at 1588 cm^{-1}. At high anodic potentials, the G-band splits into 2 modes, which also reveals the presence of DWCNTs in the sample.[45] The G^{-}-contribution, at around 1583 - 1586 cm^{-1} can be assigned to the inner tube, and the G^{+}, at 1588 - 1611 cm^{-1} to the outer one. The outer tube is more sensitive to electrochemical charging, because it is more exposed. It also exhibits more pronounced shift of the G-band, revealing a higher charge carrier concentration. [45]

In order to study how the steam treatment affects tubes of different diameters we analyzed the radial breathing mode region of the Raman spectra using different laser energies: 1.96 (a), 2.33 (b) and 2.54 eV (c). As previously mentioned, the Kataura plot enables to correlate the energies of the optical transitions with the diameters of the nanotubes.[43]Based on this information, in Figure 3.7a1, the region marked in orange, from 133 to 171 cm^{-1}, is assigned to semiconducting CNTs being in resonance with the third optical transition energy, E_{33}^{S}, and corresponds to a diameter distribution of 1.17 - 1.47 nm (semiconducting nanotubes at 1.96 eV). The yellow region represents the tubes excited via the E_{11}^{M} electronic transition, and it comprises the strong bands at 191 cm^{-1} (d_t= 1.05 nm) and at 215 cm^{-1} (d_t= 0.94 nm), assigned to metallic nanotubes. The grey region represents the RBM intensities that come from the E_{22}^{S} electronic transition, and it contains the band at ca. 255 cm^{-1} (d_t= 0.80 nm), thus corresponding to semiconducting nanotubes.

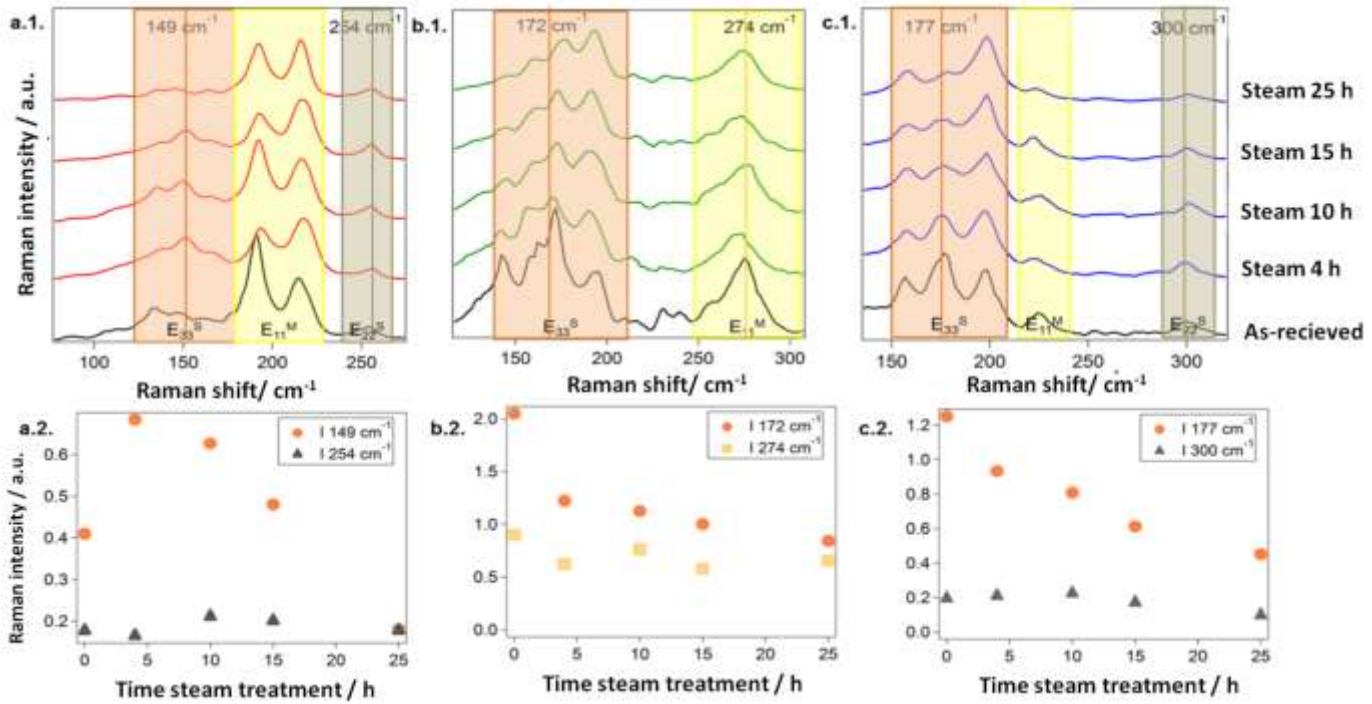

Figure. 3.7. Resonance Raman spectra (RBM region) of pristine CNTs (black line) and steam treated CNTs for different periods of time (HCl washed), excited by different laser lines a. 1.96 eV (633 nm), b. 2.33 eV (532 nm) and c. 2.54 eV (488 nm). In figures a.1, b.1. and c.1., the orange, yellow and grey regions correspond to the E_{33}^{S}, E_{11}^{M} and E_{22}^{S} electronic transitions, respectively. Each spectrum is an average based on 900 (1.96 eV) and 49 spectra (2.33 and 2.54 eV) measured in different points. a.2., b.2. and c.2. show the normalized Raman Intensity of the RBM modes versus time of steam treatment for excitation energies of 1.96 eV, 2.33 eV and 2.54 eV, respectively. Spectra in a.1. and intensities in a.2. were normalized by the RBM band at 215 cm^{-1}. Spectra in b.1. and intensities in b.2. were normalized by the RBM band at 195 cm^{-1}, Spectra in c.1. and intensities in c.2. were normalized by the RBM band at 199 cm^{-1}. The spectra are offset for clarity.

Figure 3.7b1 shows the Raman spectra measured with the 2.33 eV laser line. The bands in the orange region, 142-195 cm^{-1}, correspond to nanotubes of d_t= 1.16-1.38 nm and represent the tubes that belong to the E_{33}^S transition. A strong band, in the yellow region, corresponding to tubes excited via the metallic transition (E_{11}^M) appears at ca. 274 cm^{-1} (d_t= 0.75). Results for the 2.54 eV laser are presented in Figure 3.7c1. The bands in the orange region at ca. 157 cm^{-1} and 177 cm^{-1} (d_t= 1.26 and 1.13 nm) are assigned to semiconducting nanotubes that are in resonance via the E_{33}^S transition. The RBM modes in the yellow region at ca. 225 cm^{-1} (d_t= 0.90) and in the grey region at ca. 300 cm^{-1} (d_t= 0.69 nm) are assigned to metallic and semiconducting CNTs, the former being in resonance with the E_{11}^M and the latter with the E_{22}^S transition. For all the excitation energies, there are abrupt changes in the intensity of the bands assigned to the E_{33}^S transition, which correspond to semiconducting nanotubes with large diameters. This indicates that mainly nanotubes with large diameters that correspond to outer nanotubes seem to be affected by the probed treatments. The bottom panel of Figure 3.7 represents the intensity of the RBM modes normalized by the highest band in each region versus the time of steam treatment for excitation energies of 1.96 eV, 2.33 eV and 2.54 eV, respectively (Fig. 3.7a2, 3.7b2, and 3.7c2). The RBM bands with lower frequency, corresponding to nanotubes with larger diameter, change their intensity more remarkably, further confirming that they might be altered by steam.

Next, we studied D-band and the G-band for the control and steam treated CNTs using 3 different energies: 1.96 eV (633 nm), 2.33 eV (532 nm) and 2.54 eV (488 nm) to examine the steam effect on different diameters (Fig. 3.8). The G-bands are centered at 1588 cm^{-1}. They display widths about 20 cm^{-1}, which is typical for CNT bundles.[46] The broadening of the G-band reveals that semiconducting and metallic carbon nanotubes are in resonance with the used laser excitation energies. The broadening of G^- indicates resonance with the transition of metallic nanotubes.[47]

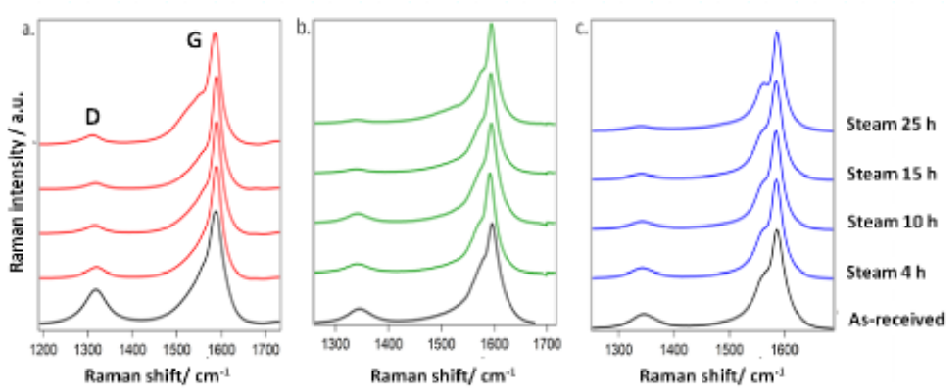

Figure 3.8. Resonance Raman spectra (D and G-band region) of pristine CNTs (black line) and steam treated CNTs for different periods of time (HCl washed), excited by different laser lines a. 1.96 eV (633 nm), b. 2.33 eV (532 nm) and c. 2.54 eV (488 nm). Each spectrum is an average based on 900 (1.96 eV) and 49 spectra (2.33 and 2.54 eV) measured in different points. The spectra are offset for clarity.

The position of the D-band is laser line dependent[48] and it appears at 1347 cm^{-1} using 2.54 eV and 2.33 eV, and at 1320 cm^{-1} using 1.96 eV excitation energy. To evaluate the amount of structural defects in the samples we compared the intensity ratio between D and G-bands (the A_D/A_G ratio), calculated from the integrated areas (A_D and A_G, respectively). As observed in Figure 3.9, the A_D/A_G ratio decreases as the time of treatment increases due to the removal of residual amorphous carbon via purification.[22]

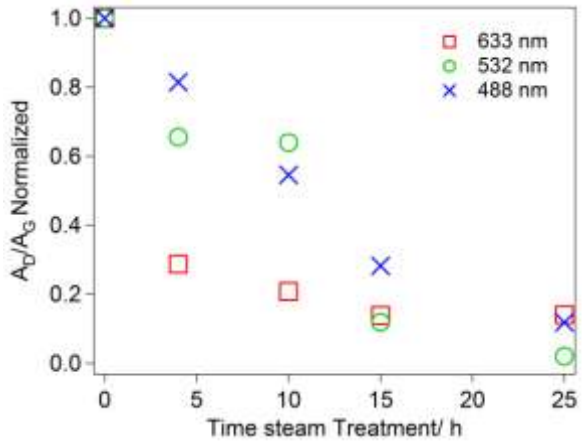

Figure 3.9. A_D/A_G ratio of the as-received CNTs (0 h treatment) and steam treated CNTs (HCl washed) for different periods of time. The samples were excited using 1.96 eV (red squares), 2.33 eV (green circles) and 2.54 eV (blue crosses) laser energies.

HRTEM studies are in agreement with Raman spectroscopy and confirm that no significant morphological changes were induced by the steam treatment (Fig. 3.10).

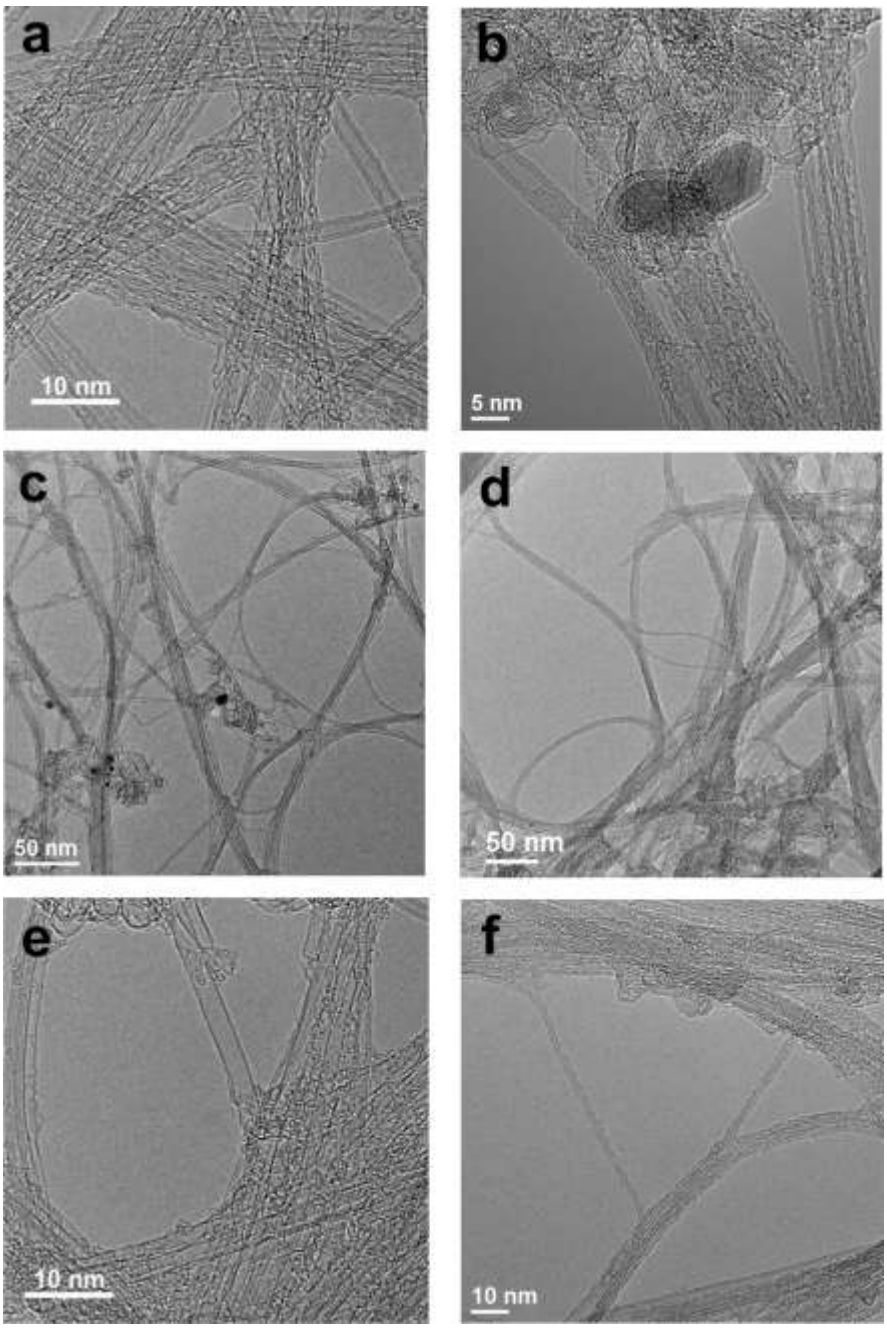

Figure 3.10. High resolution transmission electron microscopy analysis of steam treated samples: a-c) as-received CNTs, d-f) 25 h of steam treated CNTs (after an HCl wash). The black dots in b and c correspond to catalyst nanoparticles sheath with graphitic shells.

3.3.3. Effect of steam and HCl on the removal of inorganic impurities

Visual inspection of the HRTEM confirms the removal of Fe catalyst particles (Fig. 3.10 b,c) after the combined steam and HCl purification. The amount of iron nanoparticles present as impurities in the samples was determined by magnetic measurements using SQUID magnetometer and TGA.

Apart from Fe, according to EDX analysis as-received CNTs also contain inorganic impurities with silicon and oxygen (Fig. 3.11). Silicon and oxygen can be assigned to residual impurities from the silica support used for the processing of CNTs, while as mentioned iron is attributed to remaining catalytic nanoparticles employed for the synthesis of the CNTs.

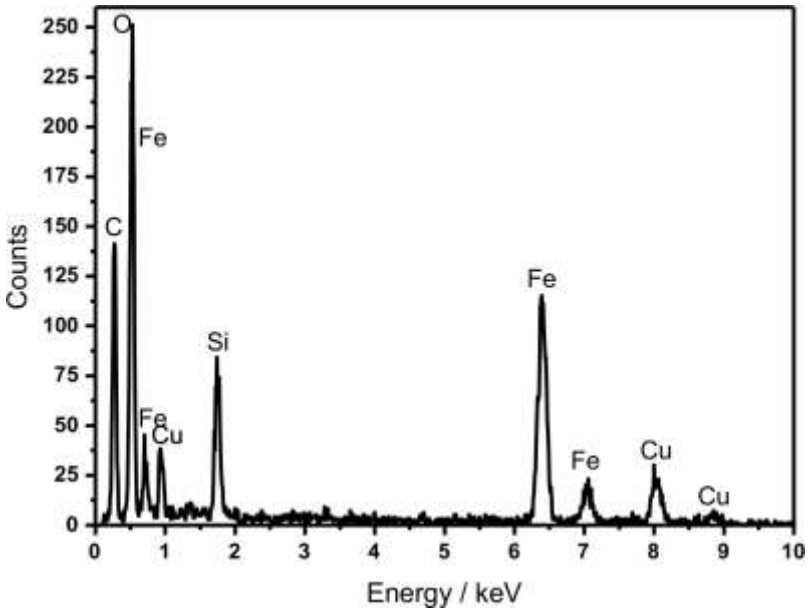

Figure 3.11. EDX analysis of as-received CVD CNTs.

Since the solid residue obtained after the complete combustion of samples in air during TGA corresponds to the mixture of inorganic elements in their oxidized form, a precise estimation of the iron content is impossible using this technique. Therefore, as explained above, the amount of iron present after each steam and HCl treatment was determined from SQUID hysteresis loops (Fig. 3.12a).[49] The amount of Fe in the as-received CNTs is 1.4 wt. % (SQUID). This amount of Fe is converted to Fe_2O_3 during the TGA and would result in a 2.0 wt. % of solid residue after the complete combustion of the sample.

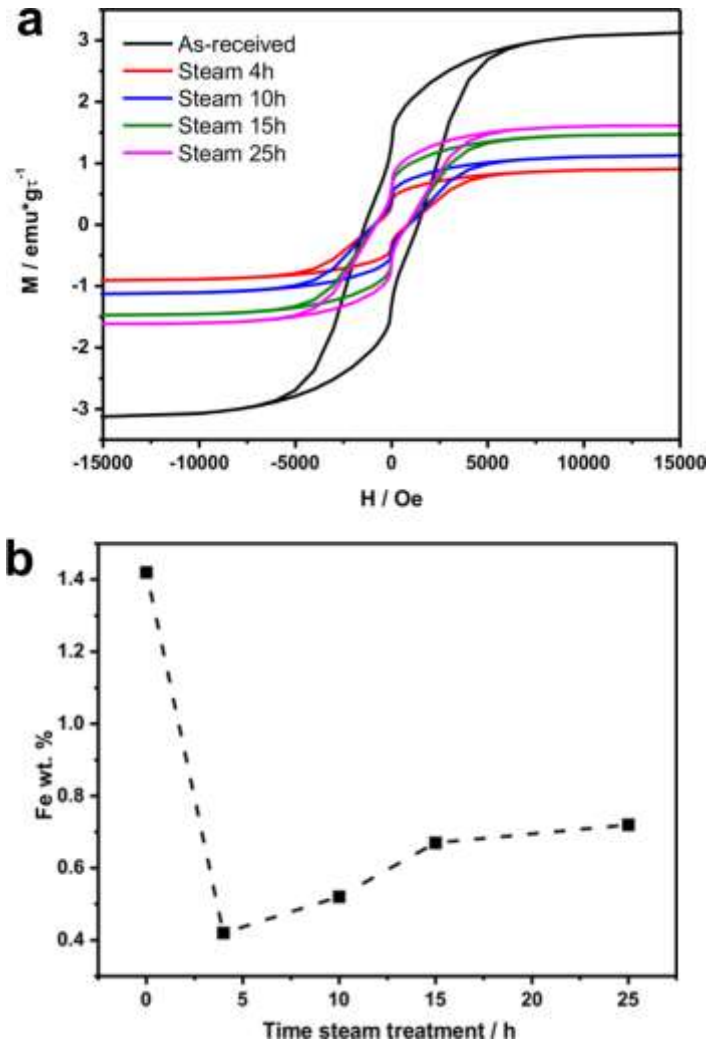

Figure 3.12. a) Hysteresis loops at 10 K, of as-received and steam treated (HCl washed) CNTs for different periods of time. b) The amount of iron in samples (determined by SQUID) plotted versus time of steam treatment.

Therefore, the amount of silica can be determined from the difference between the inorganic solid residue of the as-received material (4.6 wt. % by TGA, Fig.3.13a) and the amount of iron oxide (2.0 wt. %); thus the as-received CNTs contain 2.6 wt. % of silica. Nanotubes treated with steam for 4 h are characterized by the highest purity: 1.8 wt. % inorganic solid residue; 0.4 wt. % Fe. Noteworthy, for samples with longer exposure to steam (10-25 h) the amount of solid residue increases (Fig. 3.13b), while iron content is still relatively low (Fig. 3.12b). After 25 h of steam treatment the sample contains 7.8 wt. % of solid residue and 0.7 wt. % of Fe.

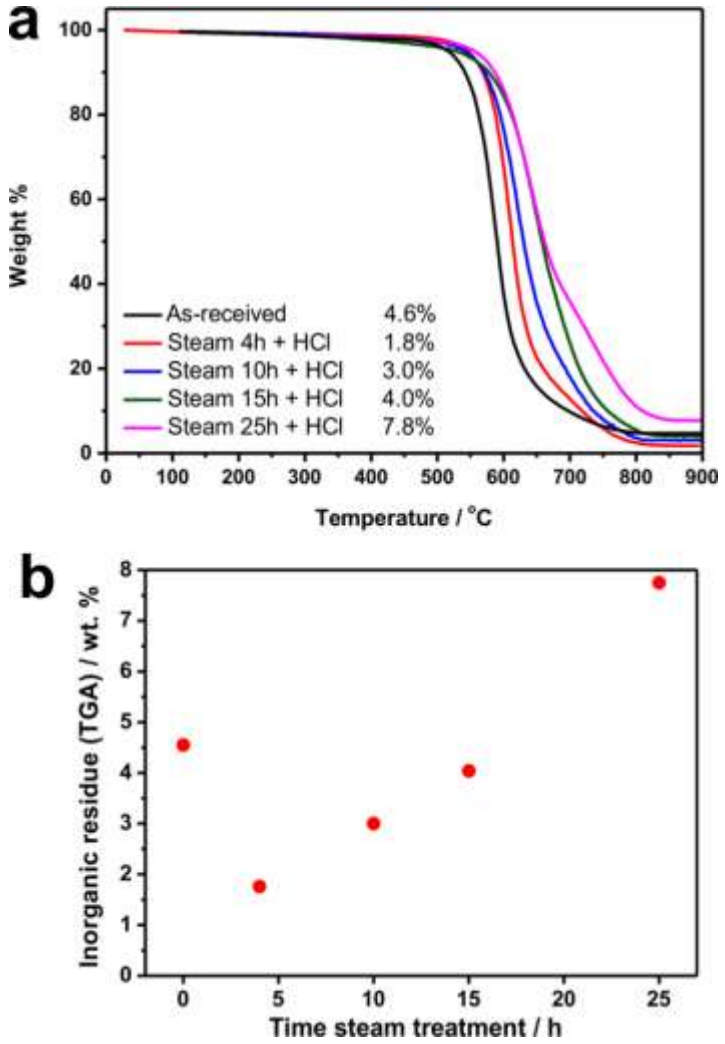

Figure 3.13 a) TGA curves of as-received and steam treated (HCl washed) CVD CNTs for different periods of time. Numbers in the legend correspond to the residue (wt. %) obtained at 900 °C. b) Inorganic solid residue (determined by TGA) plotted versus time of steam treatment.

The presence of amorphous carbon and defective carbon nanotubes also affects the shape of TGA curves (Fig. 3.13a) since they are more reactive toward oxygen than carbon nanotubes presenting a low degree of structural defects. In agreement amples after purification are characterized by a higher onset of carbon combustion.

3.3.4. Effect of steam on shortening and purification of carbon nanotubes from an alternative source of production (arc discharge)

As-received arc discharge SWCNTs were treated with steam at 900 °C for periods of 0.5 h, 1 h, 2 h, 3 h, 4 h and 5 h. The steam treated samples were later independently treated with 6 M HCl. We initially focused on the sample of SWCNTs treated 4 h with steam since from the previous study this period of time seems to be optimal for the removal of metal impurities. Both, raw arc discharge SWCNTs and 4 h steam + HCl treated SWCNTs were dispersed in *ortho*-dichlorobenzene and characterized by SEM to determine the length distribution of individual carbon nanotubes following a previously established protocol (see Subchapter 3.2.1.). Statistical analysis was performed with a sample size of 200 for each of the groups, namely control group (as-received SWCNTs) and 4 h steam and HCl treated SWCNTs. The resulting histograms are displayed on Figure 3.14. The median length distribution of raw arc discharge SWCNTs (537 nm) is reduced to 457 nm after 4 h of steam (and HCl) which corresponds to a 15% reduction of length.

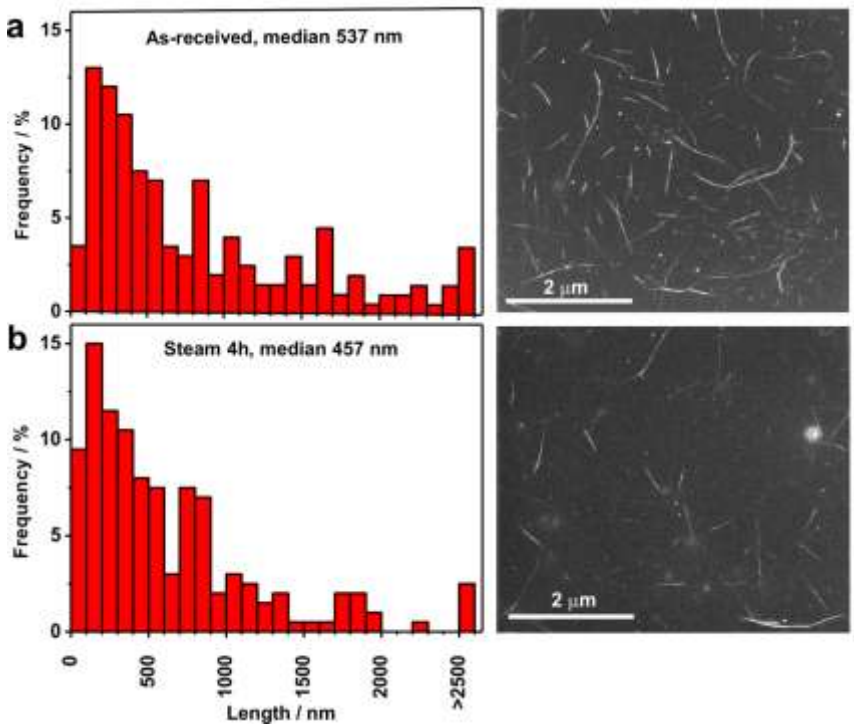

Figure 3.14. Analysis of the length distribution of arc discharge SWCNTs: a) as-received and b) 4 h steam-treated (and HCl washed). Histograms are presented on the left panel and representative SEM images on the right panel of the figure.

Next, Raman spectroscopy with 3 different excitation energies: 1.96 eV (633 nm), 2.33 eV (532 nm) and 2.54 eV (488 nm) was performed to understand the influence of steam on the physical and structural properties of the arc discharge SWCNTs. Figure 3.15 displays the D and G-band area (upper panel), and RBM region (bottom panel) of the Raman spectra of the as-received (raw) and steam treated SWCNTs. No remarkable changes in the RBM area are observed, probing that the nanotube structure is in general preserved.

Looking at the RBM in detail, it can be seen that the bands at low frequency transition, which correspond to nanotubes with large diameters, present a small decrease in intensity. Consequently, mainly nanotubes with large diameter seem to be affected by the probed treatments.

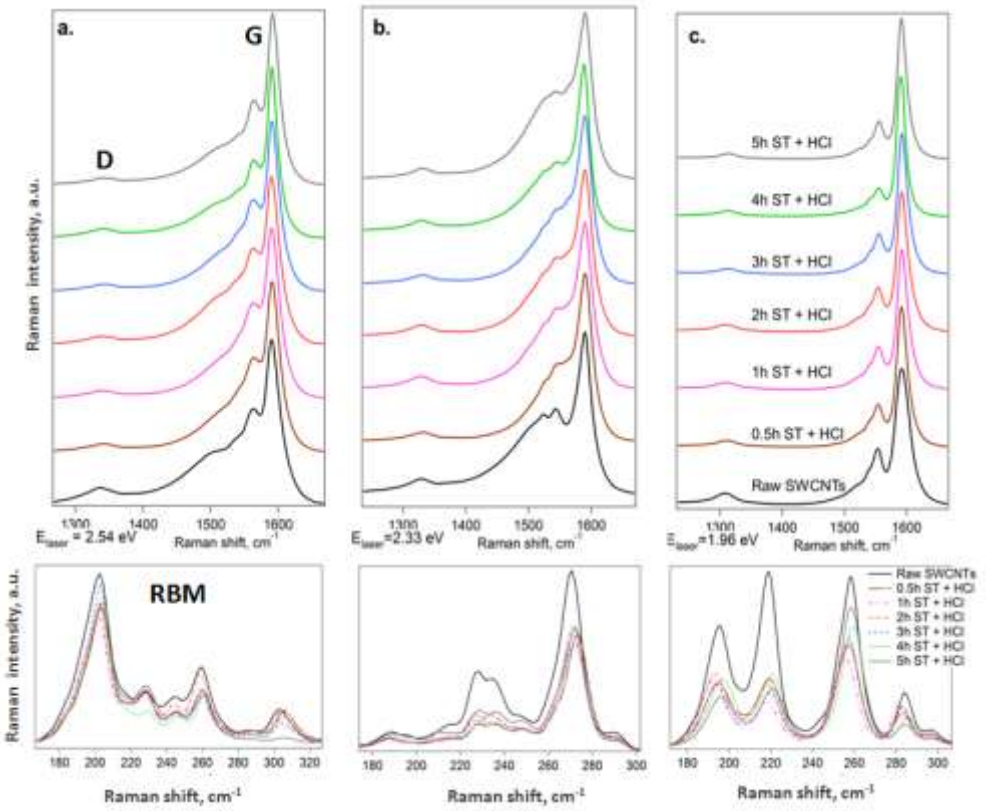

Figure 3.15. Resonance Raman spectra of D and G-band region (top) and the RBM region (bottom), of as received (raw) arc discharge SWCNTs and steam treated SWCNTs for different periods of time (after an HCl wash), excited by different laser lines a. 2.54 eV (488 nm), b. 2.33 eV (532 nm) and c. 1.96 eV (633 nm). Each spectrum is an average based on 900 (1.96 eV) and 49 spectra (2.33 and 2.54 eV) measured at different points. The spectra are offset for clarity.

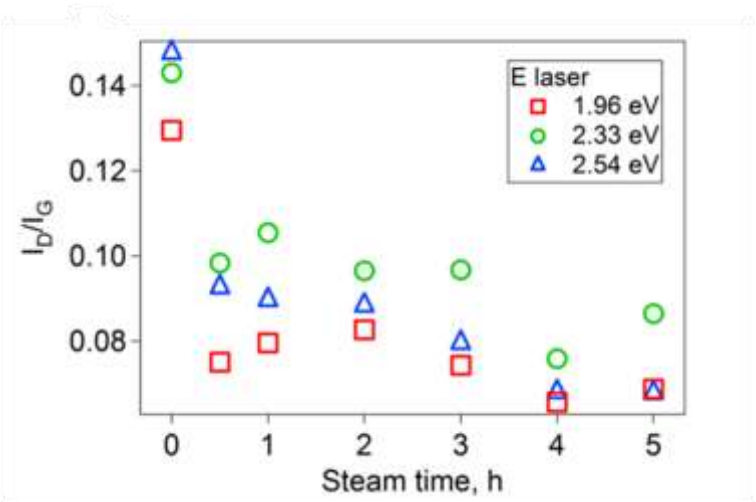

Figure 3.16. I_D/I_G ratio of the as-received arc discharge SWCNTs (0 h treatment) and steam treated SWCNTs for different periods of time (after an HCl wash). The samples were excited using 1.96 eV (red squares), 2.33 eV (green circles) and 2.54 eV (blue triangles) laser energies.

The G-band spectra are typical for CNTs bundles where the widths of the G-band are about 20 cm^{-1} (isolated nanotubes display smaller widths) and are centered at 1590 cm^{-1}. The broad G-band indicates that both semiconducting and metallic carbon nanotubes are in resonance at the used laser excitation energies. The D-band appears at 1337 cm^{-1}, 1330 cm^{-1} and 1310 cm^{-1} using 2.54 eV, 2.33 eV and 1.96 eV as excitation energy, respectively, since as mentioned the frequency of the D-band is laser energy dependent. In order to evaluate the amount of defects in the samples, in Figure 3.16 we represent the intensity ratio between D and G-bands (the I_D/I_G ratio). As observed, the I_D/I_G ratio decreases as the time of treatment increases. This correlation is consistent with the fact that amorphous carbon present in as-received SWCNTs is removed during the steam treatment. Furthermore, the lowering tendency of the I_D/I_G ratio with the time of treatment also indicates that no significant number of new defects is created. Scanning transmission electron microscopy (STEM) inspection of the steam treated CNTs also reveals that the morphology of the SWCNTs has been well preserved after the steam treatment (Fig. 3.17). The amount of catalytic particles, visible as bright dots, has also been reduced.

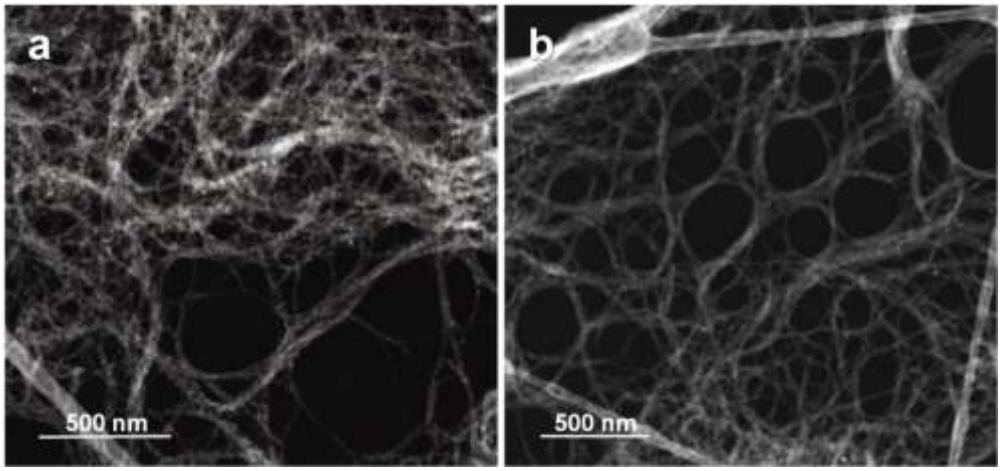

Figure 3.17. STEM images of: a) as-received and b) steam treated for 4 h (after an HCl wash) arc discharge SWCNTs, respectively.

TGA was carried out under flowing air to investigate the amount of metal catalyst present in the samples before and after the different steam purification treatments. EDX analysis of the solid residue obtained after TGA of raw SWCNTs in the air reveals the presence of iron and oxygen in the sample (Fig. 3.18.). Iron is the catalyst used for the growth of SWCNTs and upon oxidation it turns into Fe_2O_3. The iron content in each of the samples (Fig.3.19b) was determined from the TGA residue (Fig.3.19a).

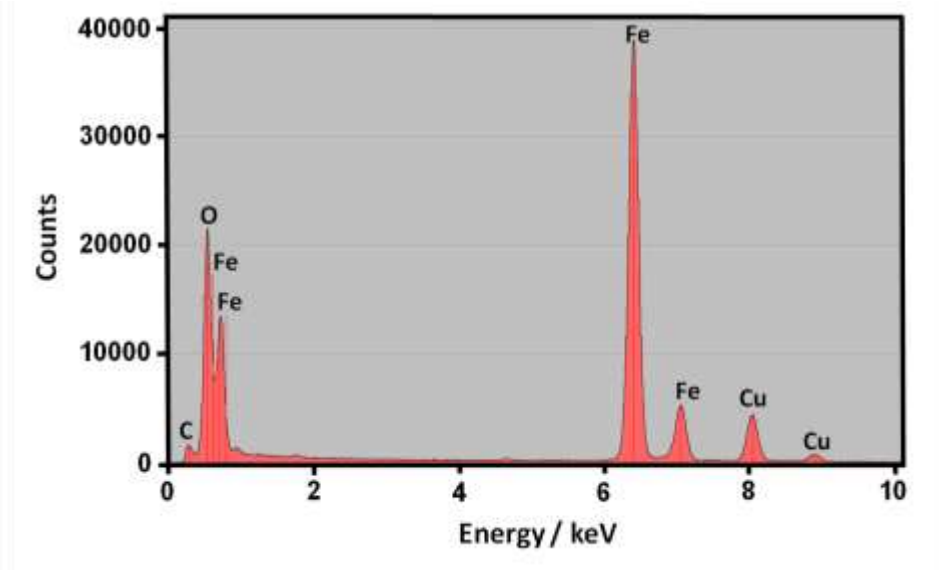

Figure 3.18. EDX analysis of TGA residue after burning raw arc discharge SWCNTs. Sample contains oxygen and iron. Signals assigned to copper and carbon arise from the employed support grid.

Nevertheless, whereas the initial treatments (0.5 h - 3 h steam + HCl) have a high effect on the metal content, treating the as-received SWCNTs with steam for 3 h to 5 h does not have a major influence on the catalyst content. As it can be seen in Figure 3.19, a dramatic decrease of iron nanoparticles is observed after treating the raw material (30.2 wt. % solid residue; 21.1 wt. % Fe) with 0.5 h steam and HCl (12.4 wt. % solid residue; 8.7 wt. % Fe). Longer steam treatments result in a further decrease in the metal content. Therefore, we selected 4 h of steam (and HCl wash) for the purification protocol of arc discharge SWCNTs.

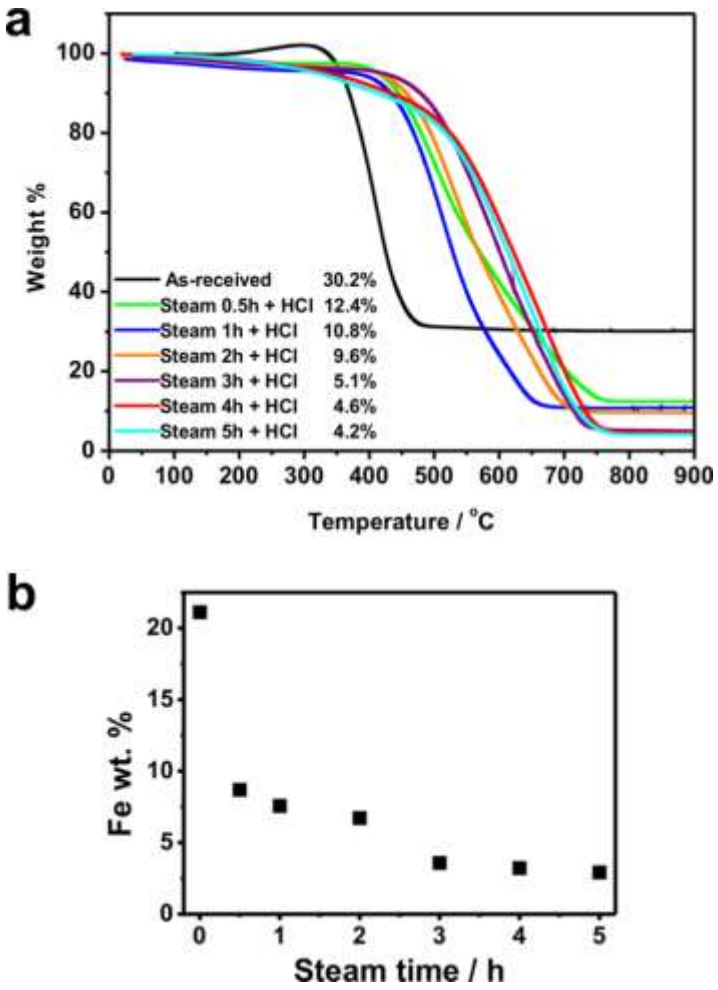

Figure 3.19. a) TGA curves of as-received and steam treated (HCl washed) arc discharge SWCNTs for different periods of time. Numbers in the legend correspond to the residue (wt. %) obtained at 900 °C. b) Amount of iron calculated from the inorganic solid residue (determined by TGA) in the as-received SWCNTs (0 h) and steam treated samples during 0.5 h, 1 h, 2 h, 3 h, 4 h and 5 h (after an HCl wash).

3.4. Conclusions

The influence of steam treatment on the length and wall structure of SWCNTs and DWCNTs has been studied. We have developed a protocol that allows debundling of CNTs, and spread individual CNTs on a support employing *ortho*-dichlorobenzene as a dispersing agent. This allows a fast and easy quantitative SEM determination of the length distribution of carbon nanotubes samples.

The steam treatment allows the modulation of CNTs' length. As-received CVD CNTs are characterized by a median length of ca. 710 nm. After 4 h of steam treatment it is reduced by about 40% (ca. 420 nm median length). Short nanotubes, ca. 200 nm median length, are obtained after 10 h of steam. The length distribution of the samples after 10 h, 15 h and 25 h of steam treatment does not present significant differences. In contrast to CVD grown CNTs, a much smaller effect is observed on the length distribution of arc discharge SWCNTs. After 4 h of steam treatment their length is only reduced about 15%. This indicates a completely different reactivity of the nanotubes towards steam depending on their source of production.

Raman spectroscopy and *in situ* Raman spectroelectrochemistry of CVD CNTs with 3 different excitation energies (1.96 eV (633 nm), 2.33 eV (532 nm) and 2.54 eV (488 nm)) revealed that wider and outer nanotubes exhibit more significant changes in the RBM mode upon the steam treatment, especially in the case of prolonged treatments (25 h). The samples exposed to steam show a continuous decrease in the *D*/*G* band, being an indication of the removal of the more defective nanotubes and amorphous carbon. It also reveals that no significant structural defects are created by the used treatments.

Both as-received and purified CVD nanotubes contain iron catalyst and silica (4.6 wt. % solid residue by TGA). An optimal purification of CNTs is achieved after 4 h of steam treatment and HCl acid reflux (1.8 wt. % solid residue; TGA). In order to determine the contribution arising from iron we performed SQUID magnetic measurements. Iron content in the sample after 4 h of steam and HCl is 0.4 wt. %. All the samples of purified arc discharge SWCNTs present a lower metal content than the raw as-received material. The lowest amount of catalytic particles is achieved in the range of 3 h - 5 h of steam treatment followed by HCl (ca. 3 wt. % of Fe).

To conclude, steam shortened samples are characterized by high purity and minimal amount of structural defects. Therefore they might find applications, in a

variety of fields including nanomedicine, electronic devices and composite materials.

REFERENCES

1. Martincic, M., Tobias, G., *Filled Carbon Nanotubes in Biomedical Imaging and Drug Delivery.* Expert Opinion on Drug Delivery, 2015. **12**(4): p. 563-581.
2. Serpell, C.J., Kostarelos, K., Davis, B.G., *Can Carbon Nanotubes Deliver on Their Promise in Biology? Harnessing Unique Properties for Unparalleled Applications.* Acs Central Science, 2016. **2**(4): p. 190-200.
3. Lacerda, L., et al., *Cell-Penetrating CNTs for Delivery of Therapeutics.* Nano Today, 2007. **2**(6): p. 38-43.
4. Liu, Y., et al., *Understanding the Toxicity of Carbon Nanotubes.* Accounts of Chemical Research , 2012. **46**(3): p. 702-713.
5. Ali-Boucetta, H., et al., *Asbestos-Like Pathogenicity of Long Carbon Nanotubes Alleviated by Chemical Functionalization.* Angewandte Chemie International Edition, 2013. **52**(8): p. 2274-2278.
6. Donaldson, K., et al., *Carbon Nanotubes: A Review of Their Properties in Relation to Pulmonary Toxicology and Workplace Safety.* Toxicology Science, 2006. **92**(1): p. 5-22.
7. Montes-Fonseca, S.L., et al., *Cytotoxicity of Carbon Nanotubes on J774 Macrophages Is a Purification-Dependent Effect.* Journal of Nanomaterials, 2012. **2012**: p. 7.
8. Hamilton, R., et al., *Effect of MWCNT Size, Carboxylation, and Purification on In Vitro and In Vivo Toxicity, Inflammation and Lung Pathology.* Part. Fibre. Toxicol., 2013. **10**(1): p. 57.
9. Liu, X., et al., *Targeted Removal of Bioavailable Metal as a Detoxification Strategy for Carbon Nanotubes.* Carbon, 2008. **46**(3): p. 489-500.
10. Dresselhaus, M.S., Dresselhaus, G., Eklund, P.C., *Science of Fullerenes and Carbon Nanotubes.* Academic Press: New York, USA, 1996.
11. Kostarelos, K., *The Long and Short of Carbon Nanotube Toxicity.* Nature Biotechnology, 2008. **26**(7): p. 774-776.
12. Chen, Z., et al., *Soluble Ultra-Short Single-Walled Carbon Nanotubes.* Journal of the American Chemical Society, 2006. **128**(32): p. 10568-10571.
13. Chiang, Y.C., Lin, W.H., Chang, Y.C., *The Influence of Treatment Duration on Multi-Walled Carbon Nanotubes Functionalized by H_2SO_4/HNO_3 Oxidation.* Applied Surface Science, 2011. **257**(6): p. 2401-2410.
14. Liu, J., et al., *Fullerene Pipes.* Science, 1998. **280**(5367): p. 1253-1256.
15. Li, J.Y., Zhang, Y.C., *Cutting of Multi Walled Carbon Nanotubes.* Applied Surface Science, 2006. **252**(8): p. 2944-2948.

16. Datsyuk, V., et al., *Chemical Oxidation of Multiwalled Carbon Nanotubes.* Carbon, 2008. **46**(6): p. 833-840.
17. Tchoul, M.N., et al., *Effect of Mild Nitric Acid Oxidation on Dispersability, Size, and Structure of Single-Walled Carbon Nanotubes.* Chemisrty of Maertials, 2007. **19**(23): p. 5765-5772.
18. Gu, Z., et al., *Cutting Single-Wall Carbon Nanotubes through Fluorination.* Nano Letters, 2002. **2**(9): p. 1009-1013.
19. Bendjemil, B., et al., *Elimination of Metal Catalyst and Carbon-Like Impurities from Single-Wall Carbon Nanotube Raw Material.* Applied Physics A, 2004. **78**(3): p. 311-314.
20. Hamwi, A., et al., *Fluorination of Carbon Nanotubes.* Carbon, 1997. **35**(6): p. 723-728.
21. Tran, M.Q., et al., *Thermal Oxidative Cutting of Multi-Walled Carbon Nanotubes.* Carbon, 2007. **45**(12): p. 2341-2350.
22. Tobias, G., et al., *Purification and Opening of Carbon Nanotubes Using Steam.* Journal of Physical Chemistry B, 2006. **110**(45): p. 22318-22322.
23. Ballesteros, B., et al., *Steam Purification for the Removal of Graphitic Shells Coating Catalytic Particles and the Shortening of Single-Walled Carbon Nanotubes.* Small, 2008. **4**(9): p. 1501-1506.
24. Cabana, L., et al., *The Role of Steam Treatment on The Structure, Purity and Length Distribution of Multi-Walled Carbon Nanotubes.* Carbon, 2015. **93**: p. 1059–1067.
25. King, S.G., et al., *Highly Aligned Arrays of Super Resilient Carbon Nanotubes by Steam Purification.* Carbon, 2015. **84**: p. 130-137.
26. Grobert, N., *Carbon Nanotubes – Becoming Clean.* Materials Today, 2007. **10**(1–2): p. 28-35.
27. Szabados, A., Biro, L.P., Surjan, P.R. *Intertube Interactions in Carbon Nanotube Bundles.* Physical Review B, 2006. **73**(19): p. 9.
28. Bahr, J.L., et al., *Dissolution of Small Diameter Single-Wall Carbon Nanotubes in Organic Solvents?* Chemical Communications, 2001(2): p. 193-194.
29. Battigelli, A., et al., *Endowing Carbon Nanotubes with Biological and Biomedical Properties by Chemical Modifications.* Advanced Drug Delivery Review, 2013. **65**(15): p. 1899-1920.
30. Tasis, D., et al., *Chemistry of Carbon Nanotubes.* Chemistry Review, 2006. **106**(3): p. 1105-1136.
31. Chen, Z., Hauge, R.H., Smalley, R.E., *Ozonolysis of Functionalized Single-Walled Carbon Nanotubes.* Journal of Nanoscience and Nanotechnology, 2006. **6**(7): p. 1935-1938.
32. Shiren, W., et al., *Statistical Characterization of Single-Wall Carbon Nanotube Length Distribution.* Nanotechnology, 2006. **17**(3): p. 634.

33. Wang, X.X., et al., *Preparation of Short Carbon Nanotubes and Application as an Electrode Material in Li-Ion Batteries.* Advanced Functional Materials, 2007. **17**(17): p. 3613-3618.
34. Fogden, S., et al., *Purification of Single Walled Carbon Nanotubes: The Problem with Oxidation Debris.* Chem. Phys. Lett., 2008. **460**(1–3): p. 162-167.
35. Liu, P., Wang, T., *Ultrasonic-Assisted Chemical Oxidative Cutting of Multiwalled Carbon Nanotubes with Ammonium Persulfate in Neutral Media.* Applied Physics A, 2009. **97**(4): p. 771.
36. Reich, S., Thomsen, C., Maultzsch J., *Carbon Nanotubes: Basic Concepts and Physical Properties*. 2004: John Wiley & Sons.
37. Dresselhaus, M. S., Dresselhaus, G., Saito, R., Jorio, A., *Raman Spectroscopy of Carbon Nanotubes.* Physics Reports, 2005. **409**: p. 47-99.
38. Araujo, P.T., Pesce, P.B.C., Dresselhaus, M.S., Sato, K., Saito, R., Jorio, A., *Resonance Raman Spectroscopy of the Radial Breathing Modes in Carbon Nanotubes.* Journal of Physics E, 2010. **42**(5): p. 1251–1261.
39. Kavan, L., Dunsch, L., *Electrochemistry of Carbon Nanotubes*, in *Carbon Nanotubes*, Jorio, A., Dresselhaus, G., Dresselhaus, M., Editors. 2008, Springer Berlin Heidelberg. p. 567-604.
40. Kavan, L., et al., *Electrochemical Tuning of Electronic Structure of Single-Walled Carbon Nanotubes: In-situ Raman and Vis-NIR Study.* Journal of Physical Chemistry B, 2001. **105**(44): p. 10764-10771.
41. Kalbac, M., Kavan, L., *Influence of the Resonant Electronic Transition on the Intensity of the Raman Radial Breathing Mode of Single Walled Carbon Nanotubes during Electrochemical Charging.* Journal of Physical Chemistry C, 2009. **113**(37): p. 16408-16413.
42. Jorio, A.S., Hafner, R., Lieber, J.H., Hunter, C.M., McClure,T., Dresselhaus, G., Dresselhaus, M. S., *Structural (n, m) Determination of Isolated Single Wall Carbon Nanotubes by Resonant Raman Scattering.* AIP Conference Proceedings, 2001(590): p. 129-132.
43. Kataura, H., et al., *Optical Properties of Single-Wall Carbon Nanotubes.* Synthetic Metals, 1999. **103**(1): p. 2555-2558.
44. Jorio, A., et al., *Structural (n,m) Determination of Isolated Single-Wall Carbon Nanotubes by Resonant Raman Scattering.* Physical Revew Letters, 2001. **86**(6): p. 1118-1121.
45. Kavan, L., et al., *Electrochemical Doping of Double-Walled Carbon Nanotubes: An In Situ Raman Spectroelectrochemical Study.* Phys. Chem. Chem. Phys., 2004. **5**(2): p. 274-277.
46. Jorio, A., et al., *G-band Resonant Raman Study of 62 Isolated Single-Wall Carbon Nanotubes.* Physical Review B, 2002. **65**(15).

CHAPTER 4

COMPARATIVE STUDY OF SHORTENING PROTOCOLS OF CARBON NANOTUBES

As mentioned in the introductory chapter, although as-produced CNTs have lengths up to few tens of micrometers, there are several applications that can benefit from the use of short CNTs. In the biomedical field, that is main focus of this thesis, typically are desired nanotubes with lengths below 300 nm. Short nanotubes are more easily expelled from lungs compared to their long counterparts.[1, 2] In addition, short CNTs reveal higher biocompatibility and better cellular uptake.[3, 4]

Decreasing the length of nanotubes requires additional processing in which they may suffer from yield issues, structural damage and increased impurity. For instance, chemical cutting introduces defects, electron beam etching is difficult to scale up, and mechanically shortened nanotubes tend to collide. In the present chapter, several commonly used shortening approaches have been taken into consideration in order to define the optimal shortening protocols for biomedical applications. We have compared the efficiency of: steam treatment, ball milling, acid cutting and piranha treatment with respect to the length distribution, purity and morphological changes of CNTs. Finally, a combined shortening strategy is suggested for SWCNTs and another one for MWCNTs.

4.1. Shortening protocols

In this work Elicarb® CVD grown SWCNTs and MWCNTs were employed. The as-received CNTs also contained carbonaceous impurities and iron catalyst surrounded by graphitic shells. Initially, the as-received SWCNTs and MWCNTs were independently shortened via the following methods: steam, ball milling, mixture of concentrated sulfuric and nitric acids (H_2SO_4/HNO_3, vol/vol 3:1), and piranha (96% H_2SO_4/ 30% H_2O_2, vol/vol 4:1). Among them the most advantageous approaches were combined with steam treatment to remove any functional groups

or amorphous carbon present in the samples. As it will be discussed in the following sections the combined protocols that will be included in the different performed analysis are piranha and steam in the case of SWCNTs and a mixture of H_2SO_4/HNO_3 with steam in the case of MWCNTs.

4.1.1. Steam treatment

CNTs (400 mg) were finely grinded in an agate mortar with a pestle, and then were loaded into a silica tube and placed in the center of an alumina tube in a tubular furnace. They were treated with water steam under argon atmosphere at 900 °C for the desired amount of time (1, 12 or 25 h) and subsequently refluxed with 6 M HCl overnight. The sample was filtered under vacuum onto a polycarbonate (PC) membrane, rinsed with distilled water until the pH of the filtrate was neutral and dried in the oven at 100 °C.[5, 6]

4.1.2. Acid treatment

CNTs (300 mg) were immersed in 300 mL of the mixture of concentrated H_2SO_4/HNO_3 (vol/vol 3:1) and sonicated for 24 h at temperature between 35 °C and 40 °C as previously reported.[7] We employed a concentration of 1 mg/mL. The resulting suspension was diluted with distilled water and filtered under vacuum onto a PC membrane, rinsed with distilled water until the pH of the filtrate was neutral and dried in the oven at 100 °C.

4.1.3. Piranha reaction

Fresh piranha solution (96% H_2SO_4/ 30% H_2O_2, vol/vol 4:1) was prepared and cooled down to room temperature in an ice bath. Then, CNTs (300 mg) were dispersed in the oxidant mixture (300 mL) and stirred with magnetic bar for 2 h[8]. In order to have comparable results, we used the same concentration of CNTs (1 mg/mL) as in the acid treatment protocol. The reaction was quenched by dilution with distilled water and filtered onto a PC membrane. Then, it was rinsed with distilled water until the pH of the filtrate was neutral and dried in the oven overnight at 100°C.

4.1.4. Ball milling

This protocol was inspired by work of Rubio and coworkers,[9] but we had to adjust the parameters to the possibilities of our equipment. 50 mg of CNTs were put in a 50 mL stainless steel grinding bowl with six stainless steel balls (1 cm diameter). The setup was sealed inside Ar-filled glovebox (Labconco). Next, the bowl container was placed in the planetary mill (Retsch PM 100 Planetary Mill) for 30 min. The rotation speed was 500 rpm and the direction of rotation was reversed each 5 min. Ball milled CNTs were subsequently refluxed with 6 M HCl overnight. The sample was filtered under vacuum onto a polycarbonate (PC) membrane, rinsed with distilled water until the pH of the filtrate was neutral and dried in the oven at 100 °C.

4.1.5. Chemicals and materials

Hydrochloric (37%) and sulfuric (98%) acids were purchased from Panreac Applichem. Nitric acid (65%) and filtration membranes (Whatman Cyclopore, polycarbonate-PC, pore size 0.2 μm) were bought from Fischer Scientific. Hydrogen peroxide (35 %) was purchased from Acros Organics.

4.2. Results and discussion

Both as-received and shortened CNTs were characterized by SEM, Raman spectroscopy, TGA, EDX and magnetic measurements using a SQUID device.

4.2.1. Effect of the shortening treatment on the length distribution of carbon nanotubes

CNTs were dispersed in *ortho*-dichlorobenzene and dropcasted onto a carbon coated copper grid so that individual nanotubes were obtained (see the optimization of the dispersion protocol in Chapter 3), and characterized by SEM. Representative acquired images of the different samples are shown on Figure 4.1 and Figure 4.2. Just by visual inspection we can observe that as-received CNTs have lengths of several μm, which are significantly decreased after the shortening protocols. The length distribution (Fig. 4.3 and Fig. 4.4) was determined by

measuring 200 individual carbon nanotubes for each sample from SEM images using Digital Micrograph software. The fraction of CNTs with lengths below 500 nm is represented on the right panel of Figure 4.3 and Figure 4.4.

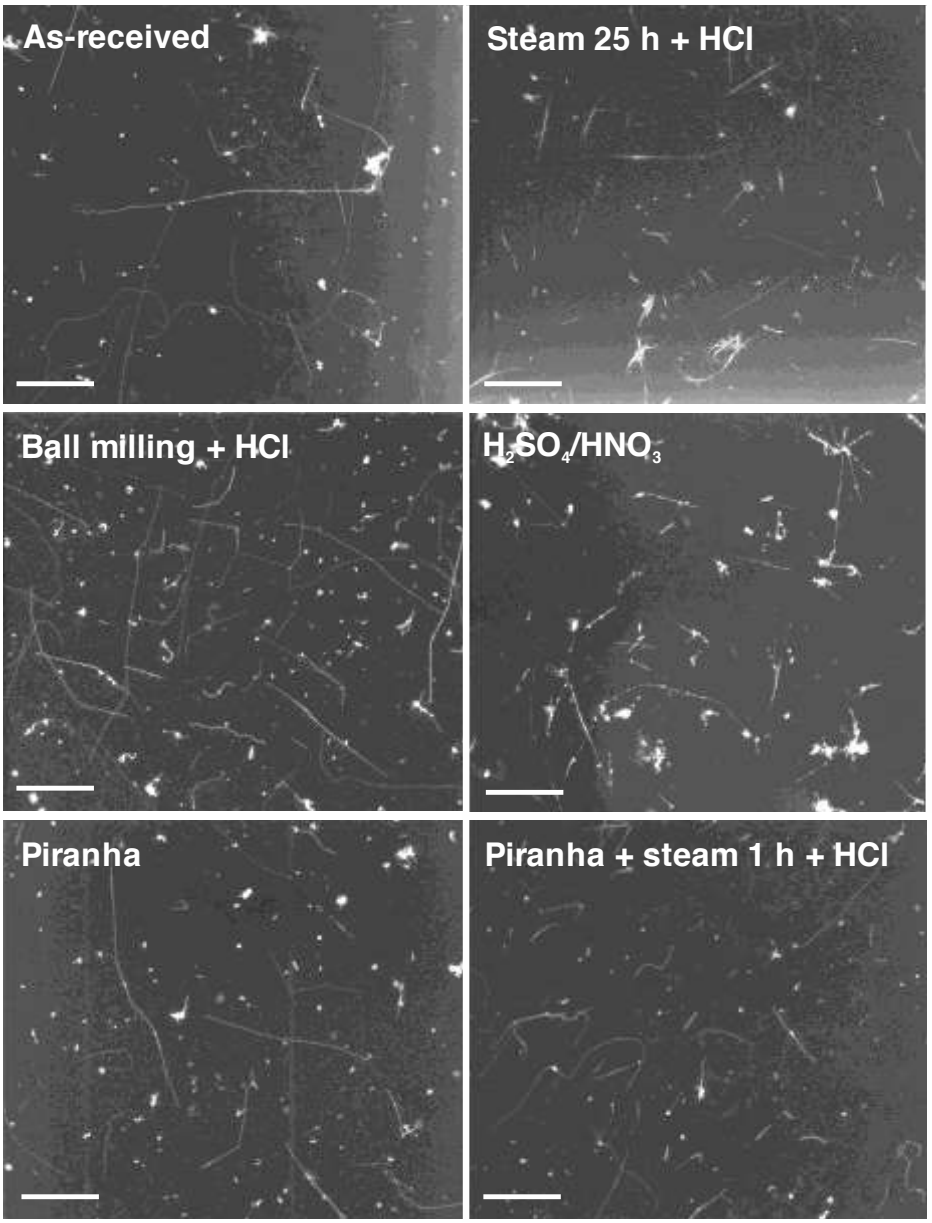

Figure 4.1. SEM images of as-received and shortened SWCNTs. Scale bars correspond to 1μm.

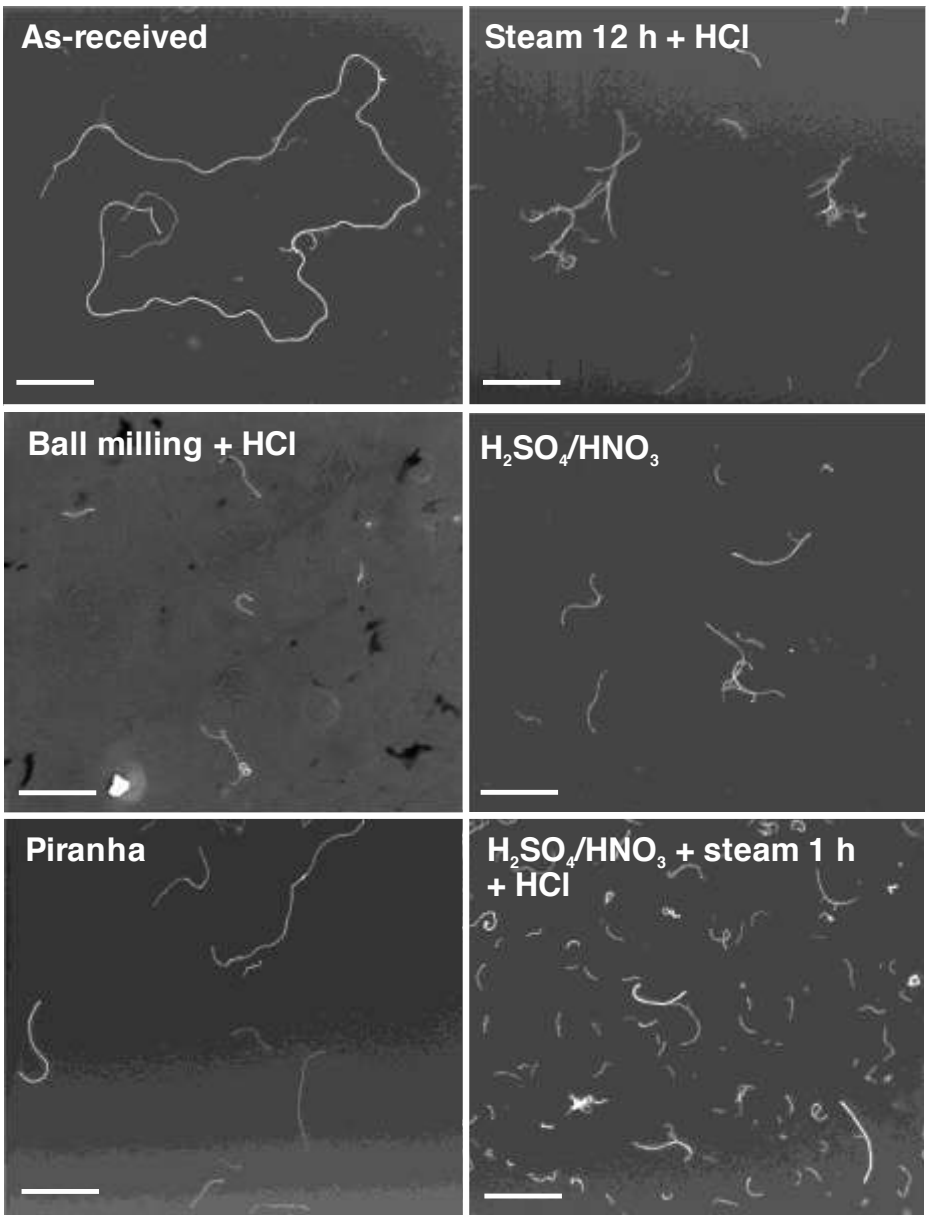

Figure 4.2. SEM images of as-received and shortened MWCNTs. Scale bars correspond to 1μm.

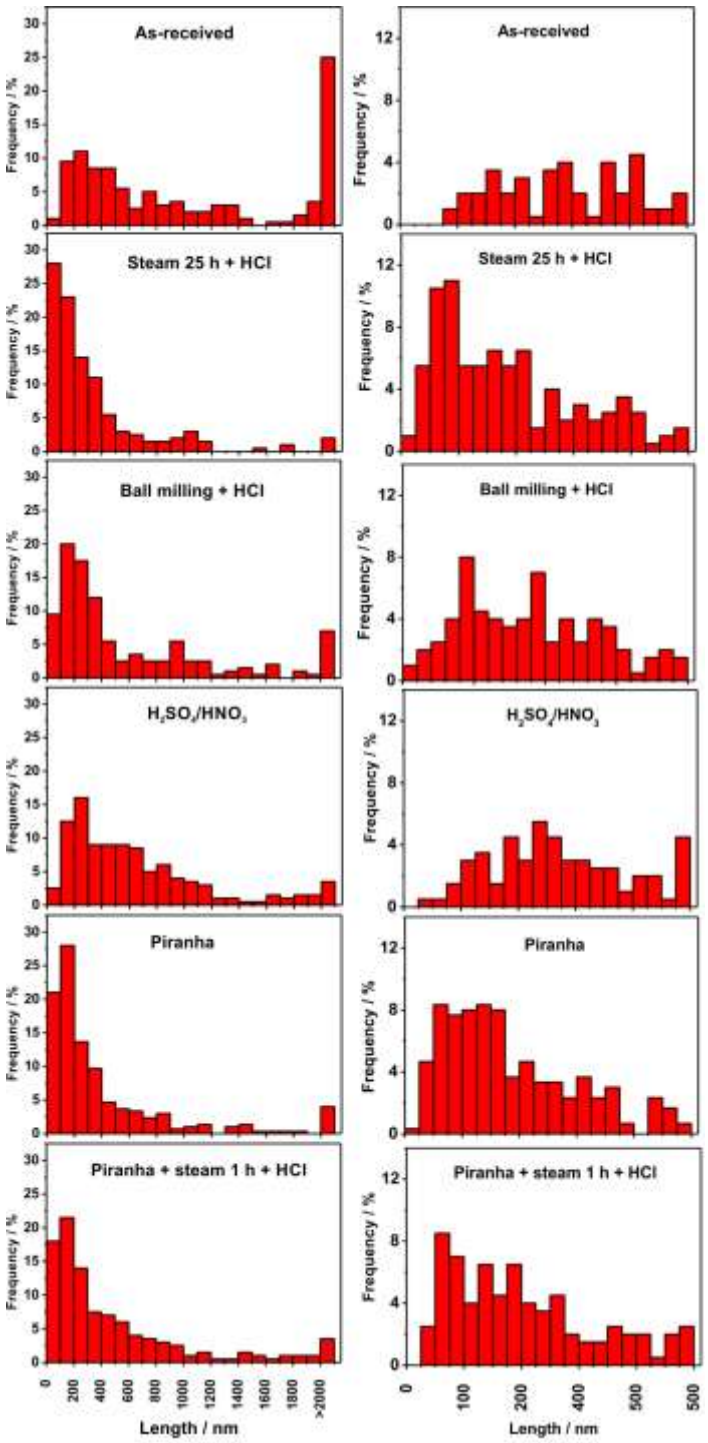

Figure 4.3. Length distribution histograms of as-received and shortened SWCNTs based on SEM image analysis. On the right panel is represented the length distribution of SWCNTs in the range of 0 to 500 nm. 200 CNTs were measured in each sample.

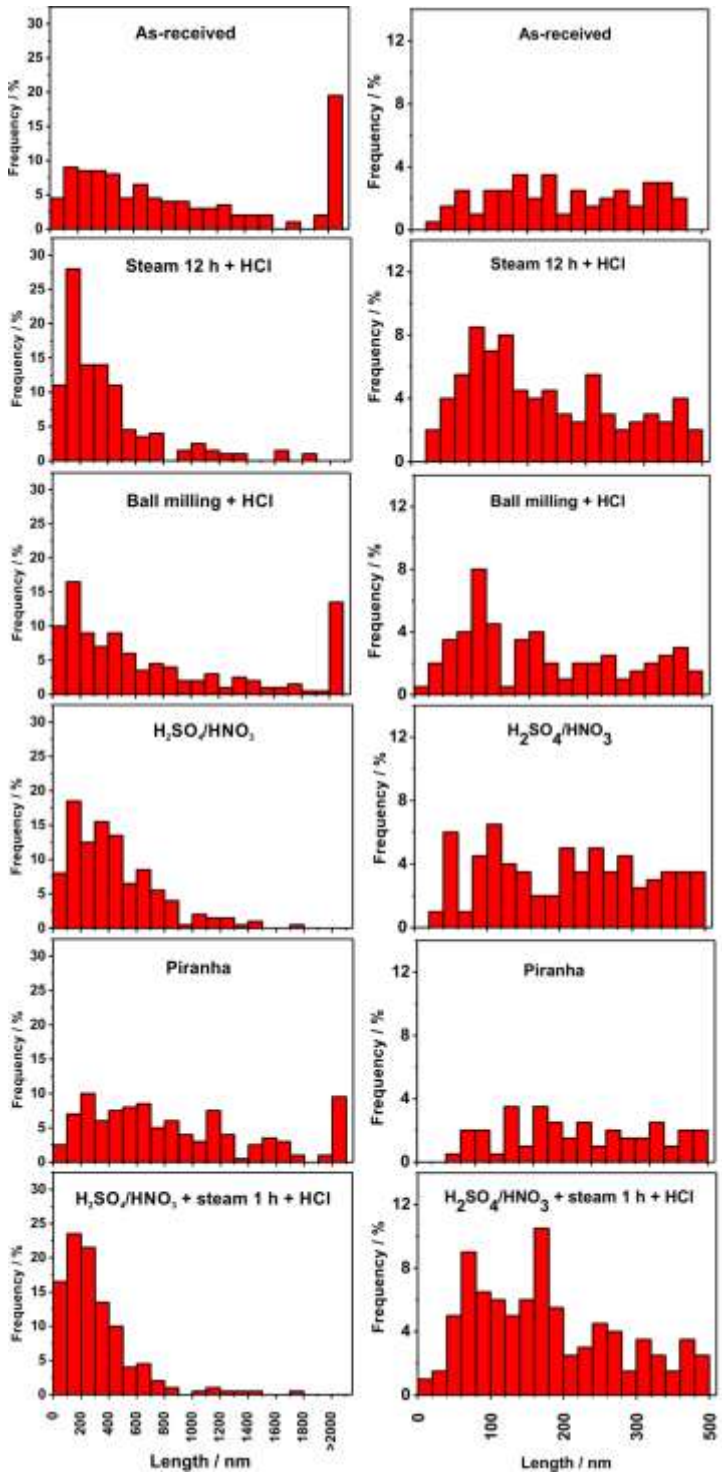

Figure 4.4. Length distribution histograms of as-received and shortened MWCNTs based on SEM image analysis. On the right panel is represented the length distribution of MWCNTs in the range of 0 to 500 nm. 200 CNTs were measured in each sample.

Table 4.1. Descriptive analysis of the length distribution for as-received and shortened CNTs.

Sample	N	Median (nm)	Lower adjacent observation (nm)	Q1 (nm)	Q3 (nm)	IQR (nm)	Maximum adjacent observation (nm)	Maximum observation (nm)
SWCNTs								
as-received	200	768	83	354	2004	1650	4479	9621
steam 25 h + HCl	200	198	23	94	389	295	831	3342
ball milling + HCl	200	328	17	173	883	710	1948	9803
H_2SO_4/HNO_3	200	507	32	258	883	625	1820	5328
Piranha	200	221	19	109	559	450	1234	4977
piranha + steam 1 h + HCl	200	266	32	134	603	469	1306	5537
MWCNTs								
as-received	200	708	27	330	1479	1151	3206	10084
steam 12 h + HCl	200	274	35	145	470	325	958	1899
ball milling + HCl	200	474	24	190	1138	948	2560	7167
H_2SO_4/HNO_3	200	365	31	183	615	469	1319	1779
Piranha	200	714	64	385	1211	826	2450	5101
H_2SO_4/HNO_3 + steam 1 h + HCl	200	225	12	133	399	266	798	1751

N – Number of measured CNTs, Q1 - 25th percentile, Q3 - 75th percentile, IQR - interquartile range.

Table 4.1 contains the descriptive statistical analysis of the different samples and Figure 4.5 displays the corresponding box plot analysis of both as-received and the steam treated CNTs.

As-received SWCNTs had a median length of 768 nm, which decreased drastically after 25 h of steam treatment to 198 nm. However, despite this treatment is very efficient in shortening SWCNTs, it is characterized by a low production yield, around 10 %. This is because steam preferentially reacts through the ends of SWCNTs and "eats" the SWCNTs up through the following reactions[5]:

$$C_{(s)} + H_2O_{(g)} \rightarrow CO_{(g)} + H_{2\,(g)} \quad (1)$$

$$CO_{(g)} + H_2O_{(g)} \rightarrow CO_{2\,(g)} + H_{2\,(g)} \quad (2)$$

In contrast, ball milling is a physical method based on shear forces. Depending on the pressure locally generated by collision of balls different morphologies can be achieved which range from shortened nanotubes[9] to carbonaceous nanoparticles.[10] Therefore, here we employed a short time of milling in order to avoid structural damage of CNTs, but cutting turned out to be not so efficient. The median length of the obtained SWCNTs was 328 nm, but a high fraction of nanotubes above 2 μm was still preserved. Acid H_2SO_4/HNO_3 cutting led to a broader length distribution with a median length of 507 nm. Finally, cutting with piranha enabled to obtain much shorter SWCNT (median 221 nm) than with the acid treatment and with a much higher yield than steam. This could be due the fact that piranha has stronger oxidative power than the mixture of H_2SO_4/HNO_3.[11] During the preparation of piranha the generation of Caro´s acid occurs [8]:

$$H_2SO_4 + H_2O_2 \rightarrow H_2SO_5 + H_2O \quad (3),$$

which decomposes to singlet oxygen:

$$HSO_5^- + SO_5^{2-} \rightarrow HSO_4^- + SO_4^{2-} + {}^1O_2 \quad (4),$$

Singlet oxygen reacts more aggressively with carbon atoms[11] compared to nitronium ion generated by the mixture of sulfuric and nitric acids[12]:

$$HNO_3 + 2H_2SO_4 \leftrightarrow NO_2^+ + H_3O^+ + 2HSO_4^- \quad (5).$$

Our findings that piranha is more efficient in cutting SWCNTs than the mixture of H_2SO_4/HNO_3 are in agreement with the work of Liu et al.[13], although they employed different conditions. Other factors, such as formation of carboxylated carbonaceous fragments that protect the walls of SWCNTs from further oxidation could also play a role.[14] We will discuss this aspect in more detail in the section about MWCNTs samples.

From the statistical analysis performed so far on the length distribution of SWCNTs samples, piranha arises as an appealing option when large amount of samples are needed, because short SWCNTs (ca. 220 nm median) are obtained with good yield. However, the use of strong oxidants may alter the structure of CNTs and add functional groups. In order to remove potentially introduced defects we employed a combined piranha and steam (1 h + HCl) treatment. As a result the median length of SWCNTs was slightly increased to 266 nm. The yield of this shortening process was ca. 70%.

Let us now focus on the effect of the different treatments on MWCNTs. The median length of as-received MWCNTs was 708 nm. Steam treated MWCNTs show a similar trend as in the case of SWCNTs and short nanotubes (median 274 nm) with a narrow length distribution were obtained. It should be emphasized that the time of steam treatment employed for MWCNTs was 12 h and in the case of SWCNTs was 25 h, because in the present case shortening occurs faster.[15] The major drawback of the steam treatment compared to the other employed protocols for the shortening of MWCNTs is that it presents the lowest yield of reaction. MWCNTs processed by ball milling reveal a broad length distribution with a high fraction (ca. 15%) of nanotubes above 2 μm. Short nanotubes, with a median length of 365 nm, were obtained by etching MWCNTs with a mixture of H_2SO_4/HNO_3 at room temperature with a narrow length distribution and a good yield. Interestingly, whereas piranha treatment turned out to be very efficient for shortening of SWCNTs, this is not case for MWCNTs. The as-received MWCNTs do not seem to have suffered any major alteration after the piranha treatment. In fact the median length remains practically unaltered within experimental error (708 nm as-received, 714 nm piranha). Despite, as mentioned before, piranha has a stronger oxidative power than the mixture of H_2SO_4/HNO_3[11], in contrast to SWCNTs, it is by far less efficient than the acid mixture for the shortening of MWCNTs. We should note that CNTs were exposed to H_2SO_4/HNO_3 for 24 h and to piranha for 2 h. Therefore, it seems that a longer oxidative treatment is more efficient, independently of the power of the oxidant used. Further studies would be needed using both piranha and H_2SO_4/HNO_3 for different periods of time on samples of as-

received SWCNTs and MWCNTs to shed some light on the mechanism of the reaction. In terms of reactivity of the samples it is worth noting that apart from the different number of concentric graphitic layers between SWCNTs and MWCNTs, MWCNTs also have a larger amount of structural defects than their single-walled counterparts. On the other hand, SWCNTs present a larger amount of amorphous carbon in the sample than MWCNTs. It has been previously reported that amorphous carbon reacts with strong acids forming carboxylated carbonaceous fragments (CCFs) that non-covalently bind to the walls of the carbon nanotubes thus protecting them from oxidation.[14] Therefore, the formation of CCFs, which is expected in a greater extension on samples of SWCNTs, could also be responsible for the lower efficiency of the acid mixture in cutting SWCNTs compared to MWCNTs.

From the different employed strategies, H_2SO_4/HNO_3 turns out to be the most efficient for the shortening of MWCNTs. Since this treatment is known to introduce functional groups in the sample, we next performed an additional short steam treatment (1 h) followed by HCl. The combined treatment resulted in a decreased median length to 225 nm with 85% of MWCNTs below 500 nm. The yield of cutting was about 75%.

Box plot analyses (Fig. 4.5) show a graphical representation of the distribution of the data, indicating the range where most values fall and which values differ considerably from the norm (atypical values). As-received CNTs are characterized by the highest dispersion and the broadest length distribution: most population of SWCNTs is below 4.4 μm and MWCNTs below 3 μm. In both cases extreme values up to 10 μm can be observed. Average and median length values are different for all samples indicating a non-symmetric length distribution, but they get closer after cutting the CNTs nanotubes, also with narrower length distributions. As expected, there is a clear correlation between the length histograms and the box plot analyses. Is it worth noting the small dispersion of population of the steam treated samples and also of the selected combined treatments.

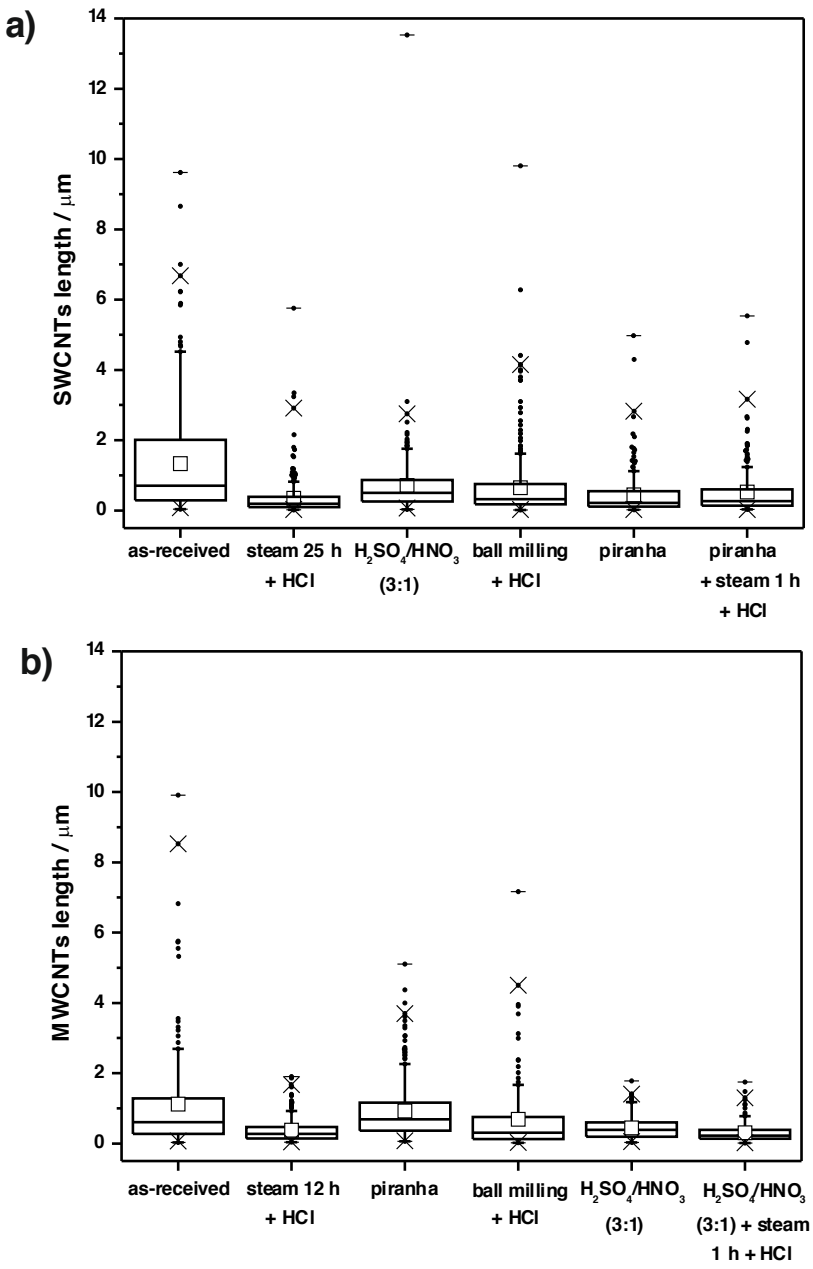

Figure 4.5. Box plot analysis of the as-received and shortened a) SWCNTs, b) MWCNTs. Black dots identify outliers, empty squares correspond to mean length, crosses to border 99% or 1% of population, short line to maximum or minimum length values. The lower and maximum adjacent observations are represented with horizontal lines at the end of the whiskers.

4.3.2. Effect of shortening on physical and structural properties of carbon nanotubes

Raman spectroscopy measurements were performed in order to evaluate the effect of different shortening protocols on the structure of CNTs. As previously described the Raman spectra of CNTs present several features, among which the most intense ones can be found in three spectral regions. First, the radial breathing mode (RBM) that is specific of the SWCNTs and which Raman shift (from 100 cm^{-1} to 300 cm^{-1}) inversely depends on the CNTs´ diameter.[16] Second, the tangential mode (G-band) centered at 1588 cm^{-1}, containing an axial and a circumferential component, which can be used to distinguish between metallic and semiconducting CNTs by its line shape.[17, 18] And third, the second-order Raman mode, the G'-band (also known as the 2D-band), centered at around 2650 cm^{-1}.[19] Additionally, for samples containing structural defects, the disorder induced mode (D-band) is observed at around 1350 cm^{-1}. The D-band is a second-order Raman mode. In this process, the incident photon resonantly excites an electron-hole pair. The electron is subsequently scattered under emission/absorption of a phonon. To satisfy the conservation of momentum, the electron has to be scattered back to a point in k-space where its momentum is near that of the initial hole. For the D mode in the Raman spectrum, the backscattering is achieved by a defect. The intensity of the D-band has been used to analyze the quality of the CNTs as it is sensitive to structural defects in the graphitic sp^2 network. The frequency of the D-band changes with changing laser excitation energy, which is called dispersive behavior.[18]

The D-band is the most employed mode for the characterization of treated and functionalized CNTs since the relative intensity of this mode can provide direct evidence of covalent modification and defect concentration. The intensity ratio I_D/I_G is suggested to be a sensitive measure for the concentration of defect in carbon nanotubes. Figure 4.6. shows the D-band and the G-band spectra of CNTs excited by different laser lines: 1.96 eV (a), 2.33 eV (b) and 2.54 eV (c).

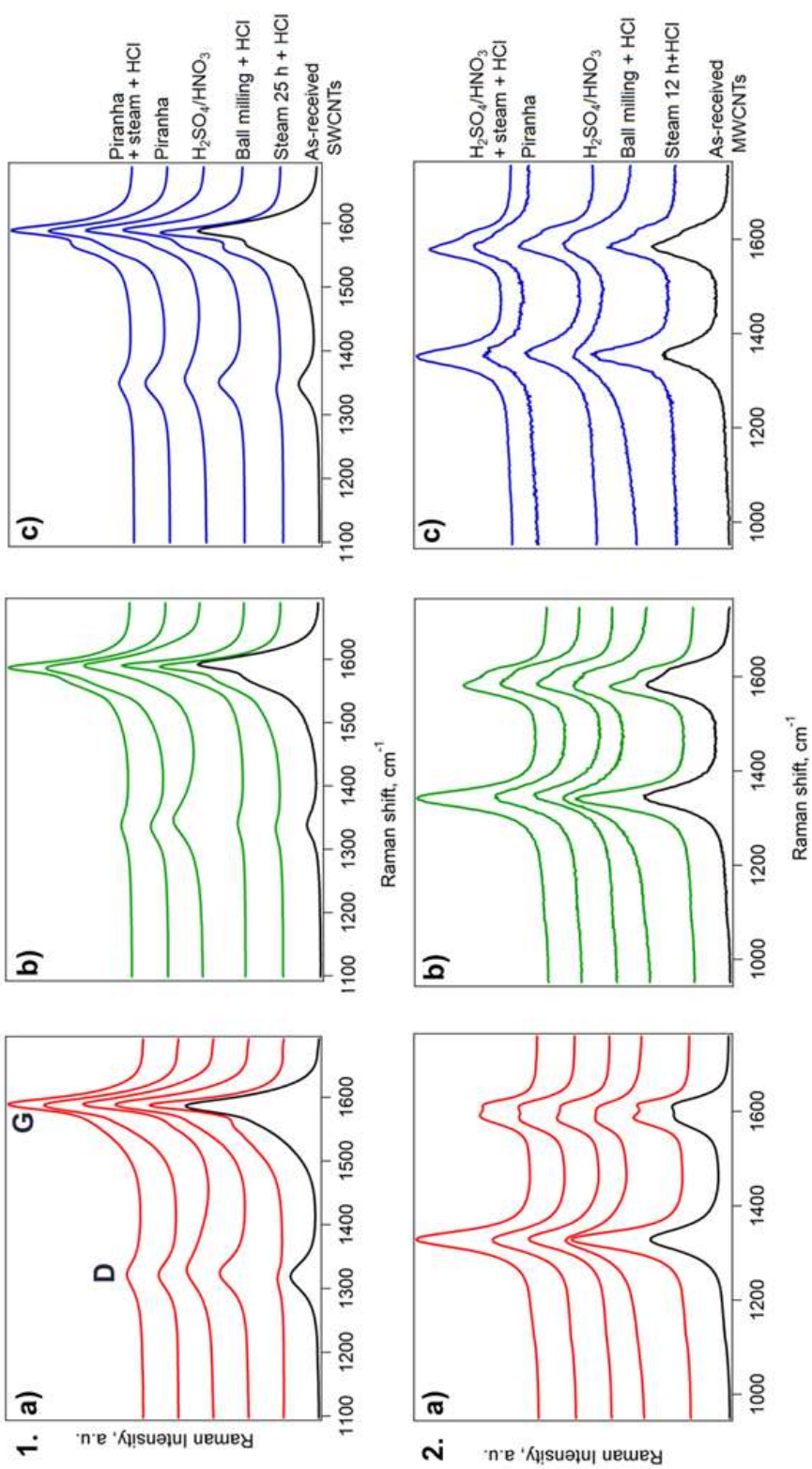

Figure 4.6. 1. SWCNTs, 2. MWCNTs. Resonance Raman spectra (D and G-band region) of as-received (black line) and treated CNTs (colored lines) excited by different laser lines a) 1.96 eV, b) 2.33 eV and c) 2.54 eV. Each spectrum is an average based on 900 (1.96 eV) and 49 spectra (2.33 and 2.54 eV) measured in different points. Spectra were normalized by the G-band. The spectra are offset for clarity.

The shapes of G-bands are typical for CNT bundles where the widths of the G-band are about 20 cm^{-1} (isolated nanotubes display smaller widths) and are centered at 1588 cm^{-1}.[20] The line shape of the G-band indicates that semiconducting and metallic carbon nanotubes are in resonance at the used laser excitation energies. When nanotube bundles are excited in resonance with the transition of metallic nanotubes, the G^- is broadened.[21] The D-band appears at 1347 cm^{-1} using 2.54 eV, at 1343 cm^{-1} using 2.33 eV and at 1320 cm^{-1} using 1.96 eV as excitation energy, since the frequency of the D-band is laser energy dependent.[22] The intensity ratio of the D-band and the G-band (I_D/I_G ratio) reflects the defect density of CNTs (Table 4.2.).

Table 4.2. The intensities I_D/I_G ratio of CNTs tested with shortening protocols normalized to I_D/I_G ratio of as-received CNTs. Raman spectra were recorded using three different laser excitation energies: 633 nm, 532 nm and 488 nm.

Sample	I_D/I_G Laser wavelength (nm)		
	633	532	488
SWCNTs			
as-received	1.00	1.00	1.00
steam 25 h + HCl	0.22	0.60	0.36
ball milling + HCl	1.02	0.61	1.23
H_2SO_4/HNO_3	0.97	2.16	1.08
Piranha	0.69	1.26	1.17
piranha + steam 1 h + HCl	0.56	0.77	0.69
MWCNTs			
as-received	1.00	1.00	1.00
steam 12 h + HCl	1.47	1.34	1.34
ball milling + HCl	1.09	1.08	1.01
H_2SO_4/HNO_3	1.08	1.00	1.05
piranha	1.05	1.03	1.02
H_2SO_4/HNO_3 + steam 1 h + HCl	1.49	1.46	1.30

In the case of SWCNTs, the decrease in the D-band intensity with steam and HCl treatment can be assigned to the removal of amorphous carbon and the more defective SWCNTs. On the other hand, for the acid treatment an increase of the I_D/I_G is observed. This chemical treatment leads to structural damage of the SWCNTs which can even result in the formation of functionalized amorphous carbon (CCF) that will contribute to the D-band. Until now it has not been possible to distinguish between the contribution to the D-band from amorphous carbon and from defects associated with defective nanotubes. Ball milling being a physical approach, should introduce less structural defects than chemical methods. This is in agreement with I_D/I_G ratio that increases slightly for ball milled SWCNTs. Finally, the piranha treated sample is characterized by increased intensity of D-band, which significantly drops down after applying short (1 h) steam treatment. It proofs again that steam enables to remove defective nanotubes and amorphous carbon.

The D-band intensity is not reduced with any of the treatments. Particularly, after the steam treatment, the D-band intensity increases significantly. This observation is in contrast to the steam treatment of SWCNTs, where a decrease of the D-band is observed. It results from the different morphology of MWCNTs with respect to SWCNTs. The number of walls is higher and the diameters are larger for MWCNTs. Also the D-band of MWCNT is typically larger than for SWCNT.

4.3.3. Effect of shortening on the removal of inorganic impurities

The purity of samples was assessed by TGA measurements (Fig. 4.7) under flowing air. The residues after burning the CNTs correspond to the amount of inorganic impurities present in the samples in their oxidized form. Moreover, the onset temperature corresponds to the combustion of the carbon material. As-received SWCNTs result in a 4.6 wt. % of inorganic material after the TGA. The amount of inorganic impurities present after the TGA in air is the highest for steam 25 h + HCl treated samples (7.8 wt. %) and the lowest for piranha cut followed by steam + HCl SWCNTs, 2.2 wt. %. It has been previously reported that with increasing time of steam treatment the consumption of carbon increases, resulting in an apparent increase of the amount of inorganic impurities.[6] In contrast, short time of exposure to steam improves CNTs structure and their thermal stability without affecting significantly the yield of reaction. For the rest of cut SWCNTs

samples we can observe a significant decrease of the amount of inorganic impurities.

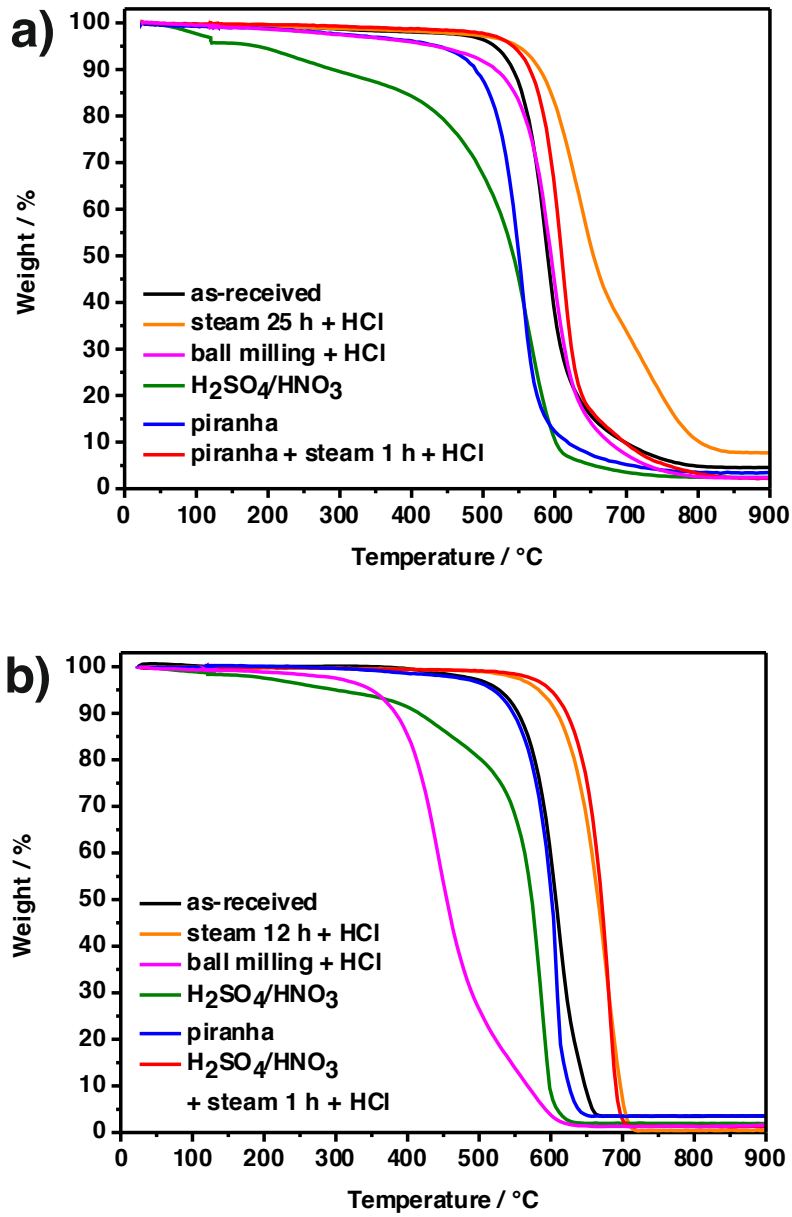

Figure 4.7. TGA of as-received material and CNTs shortened with different methods: a) SWCNTs, b) MWCNTs. Measurements were performed in the air using ramp 10 °C/min up to 900 °C.

Among the different chemical methods, a mixture of H_2SO_4/HNO_3 (3:1) is one of the most commonly used oxidants to introduce oxygen-containing functional groups (mainly carboxyl, and hydroxyl) on the surface of CNTs.[23] Therefore, the sample of SWCNT treated by this acid mixture suffer the highest damage. The TGA curve of this sample is characterized by three different weight drops. The first weight loss at ca. 120 °C corresponds to evaporation of absorbed molecules (including water), the second at ca. 300 °C to the removal carboxylic groups and the third one at 500 °C to the combustion of SWCNTs. Piranha treated SWCNTs also start to lose weight at lower temperatures than other samples and burn at 516 °C. Both H_2SO_4/HNO_3 and piranha have been reported to to selectively eliminate the smaller diameter nanotubes from the material.[13] For the remaining samples the onset temperature of combustion is significantly higher and oscillates in the range of 557 °C - 580 °C.

As-received MWCNTs revealed fewer impurities than SWCNTs, 3.5 wt. %, and burn at 576 °C. Steam treated (12 h) MWCNTs are characterized by the lowest content of inorganic material, only 0.5 wt. % and a high temperature of combustion (631 °C). According to TGA MWCNTs are the most affected by ball milling, as reflected with an onset of combustion temperature at 373 °C. The length distribution and Raman spectroscopy of this sample do not reflect such dramatic changes. A possible explanation of this fact might be that MWCNTs tend to compact rather than shorten due to friction impact during dry mechanical grinding.[24] On the other hand, several works report introduction of oxygen-containing functional groups by ball milling carbon nanotubes under ambient atmosphere,[25, 26] and it is well known that functionalized nanotubes burn at lower temperatures. H_2SO_4/HNO_3 treatment is also creating defects, but when it is combined with steam, nanotubes reveal higher stability than as-received material. After piranha treatment the amount of inorganic material remains the same as in the as-received MWCNTs. Noteworthy, MWCNTs after piranha treatment do not show the continuous weight loss observed for their single-walled counterparts. These results are correlated with the analyses of length distribution of both samples, where piranha was found to be more efficient in shortening of SWCNTs than MWCNTs. H_2SO_4/HNO_3 cut MWCNTs contain 1.9 wt. % of inorganic impurities, which decreased after steam and HCl treatment to 1.3 wt. %. Likewise as for SWCNTs, the onset temperature of combustion indicates that the short steam treatment (1 h) improves the stability of MWCNTs. It is worth noting that the combined protocol developed herein (red TGA curves, Fig. 4.7), for SWCNTS (piranha + steam 1 h + HCl) and for MWCNTs (H_2SO_4/HNO_3 + steam 1 h + HCl) present a higher onset of combustion temperature than the as-received CNTs

(black TGA curve, Fig. 4.7). This indicates the removal of amorphous carbon and the most defective CNTs from the samples and the presence of a low amount of structural defects (including functional groups).

The results of additional TGA measurements under flowing nitrogen (Fig. 4.8) are in agreement with this conclusion. Both SWCNTs and MWCNTs cut by the combined treatment present higher thermal stability in an inert atmosphere than as-received CNTs, indicating the presence of minimal amounts of functional groups. The weight loss of both SWCNTs and MWCNTs above 500 °C - 600 °C is attributed to the oxidation of the samples by traces of oxygen present in the flowing nitrogen employed for the analyses.

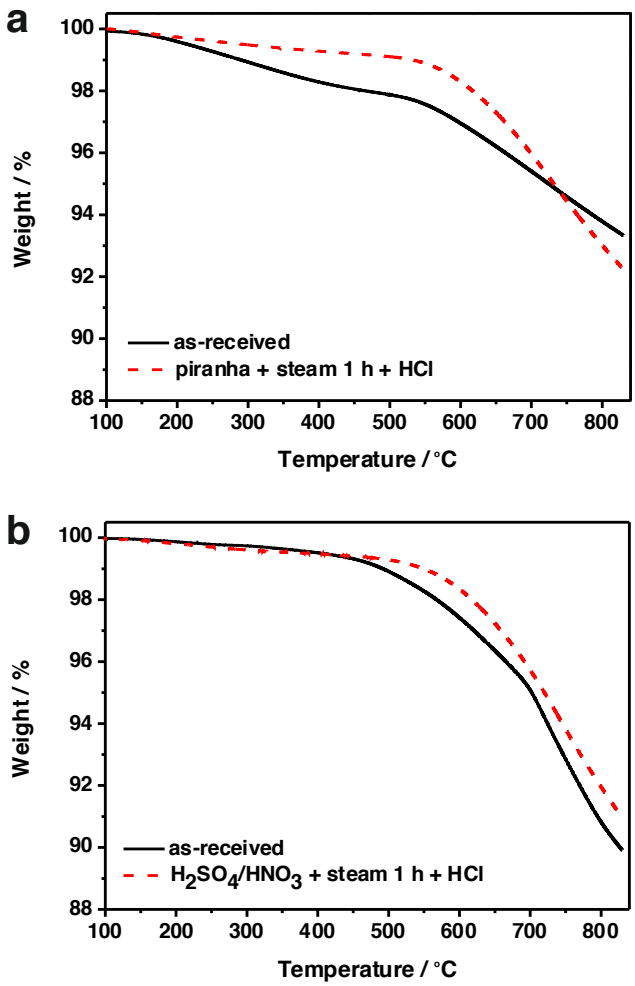

Figure 4.8. TGA in nitrogen of as-received and shortened CNTs with proposed combined protocol: a) SWCNTs, b) MWCNTs.

As described in Chapter 3, as received CNTs also contain silica particles (Fig. 3.11) that together with iron (from the catalyst) will contribute to the inorganic solid residue remaining after TGA in air. In order to evaluate the iron content ($M_{s(Fe)}$ = 221.7 emu·g^{-1}) in the samples magnetization measurements were performed using a superconducting quantum interference device (SQUID). Table 4.3 summarizes the main characteristics of as-received and shortened CNTs, including the iron content determined by SQUID. As it can be seen, as-received material contains 1.43 wt. % and 1.54 wt. % of iron in SWCNTs and MWCNTs, respectively. It has been reported that the presence of a high amount of iron (ca. 40 wt. %) might contribute to CNTs toxicity, because it acts as a catalyst for oxidative stress.[27-29] Therefore, it is an important indicator to assess whether shortened nanotubes might be employed in the biomedical field. Nevertheless, piranha cut SWCNTs, steam, ball milled, and H_2SO_4/HNO_3 and steam treated MWCNTs present a negligible amount of iron.

Table 4.3. Summary of the length, purity and spectroscopic properties of as-received and shortened CNTs. The best parameters obtained after treatment of samples are highlighted in yellow, n.d. = non-detectable.

Sample	Median length (nm)	Fraction below 500 nm (%)	Inorganic impurities (wt. %)[a)]	Iron content (wt. %)[b)]	Onset of combustion (°C) [a)]	Raman I_D/I_G ratio[c)]
SWCNTs						
as-received	768	39	4.6	1.4	557	1.00
steam 25 h + HCl	198	82	7.8	0.8	580	0.22
ball milling + HCl	328	65	2.4	1.4	560	1.02
H_2SO_4/HNO_3	507	49	2.5	0.6	500	0.97
Piranha	221	77	3.5	n.d.	516	0.69
piranha + steam 1 h + HCl	266	68	2.2	0.9	575	0.57
MWCNTs						
as-received	708	39	3.5	1.5	576	1.00
steam 12 h + HCl	274	78	0.5	n.d.	631	1.47
ball milling + HCl	474	52	1.6	n.d.	373	1.09
H_2SO_4/HNO_3	365	68	1.9	0.8	567	1.08
Piranha	714	33	3.6	1.3	535	1.05
H_2SO_4/HNO_3 + steam 1 h + HCl	225	85	1.3	n.d	633	1.50

[a)] based on TGA; [b)] based on magnetic measurements; [c)] spectra were recorded using 633 nm laser excitation energy and normalized to I_D/I_G ratio of as-received CNT

4. 4. Conclusions

We have studied different methods for shortening CNTs: steam treatment, ball milling, H_2SO_4/HNO_3 and piranha, and the protocols providing nanotubes with optimal parameters for biological applications were further combined with steam. Short steam treatment (1 h) enables to remove amorphous carbon, defective nanotubes and sidewall functionalization, and thus improves thermal stability of CNTs.

SEM was used to evaluate the length distribution of carbon nanotubes. The shortest SWCNTs with a median length of 198 nm were obtained after 25 h of steam exposure. However, the yield of reaction was low (about 10%). Piranha cutting led to production SWCNTs with a similar median length (221 nm median), with a negligible amount of iron and with a good yield of production. Therefore, for SWCNTs we tested a combined treatment of piranha and steam (1 h + HCl). In this case, the length distribution of sample slightly changed - median 266 nm, with 0.9 wt. % of iron. For MWCNTs we employed the combination of H_2SO_4/HNO_3 and steam (1 h + HCl). The obtained MWCNTs also present a negligible amount of iron and the shortest median length amongst all protocols in their group (median length 225 nm). Short CNTs are of interest for a broad range of applications, including biomedicine, electronics, water purification and composite materials.

REFERENCES

1. Muller, J., et al., *Respiratory Toxicity of Multi-Wall Carbon Nanotubes.* Toxicolology and Applied Pharmacology, 2005. **207**(3): p. 221-231.
2. Kane, A.B., Hurt, R.H., *Nanotoxicology: The Asbestos Analogy Revisited.* Nature Nanotechnology, 2008. **3**(7): p. 378-379.
3. Smart, S.K., et al., *The Biocompatibility of Carbon Nanotubes.* Carbon, 2006. **44**(6): p. 1034-1047.
4. Kolosnjaj-Tabi, J., et al., *In Vivo Behavior of Large Doses of Ultrashort and Full-Length Single-Walled Carbon Nanotubes after Oral and Intraperitoneal Administration to Swiss Mice.* ACS Nano, 2010. **4**(3): p. 1481-1492.
5. Tobias, G., et al., *Purification and Opening of Carbon Nanotubes Using Steam.* The Journal of Physical Chemistry B, 2006. **110**(45): p. 22318-22322.
6. Ballesteros, B., et al., *Steam Purification for the Removal of Graphitic Shells Coating Catalytic Particles and the Shortening of Single-Walled Carbon Nanotubes.* Small, 2008. **4**(9): p. 1501-1506.
7. Lim, J.K., et al., *Selective Thiolation of Single-Walled Carbon Nanotubes.* Synthetic Metals, 2003. **139**(2): p. 521-527.

8. Ziegler, K.J., et al., *Cutting Single-Walled Carbon Nanotubes.* Nanotechnology, 2005. **16**(7): p. S539-S544.
9. Rubio, N., et al., *Ball-Milling Modification of Single-Walled Carbon Nanotubes: Purification, Cutting, and Functionalization.* Small, 2011. **7**(5): p. 665-674.
10. Li, Y.B., et al., *Transformation of Carbon Nanotubes to Nanoparticles by Ball Milling Process.* Carbon, 1999. **37**(3): p. 493-497.
11. Lange, A., Brauer, H.-D., *On the Formation of Dioxiranes and of Singlet Oxygen by the Ketone-Catalysed Decomposition of Caro's Acid.* Journal of the Chemical Society, Perkin Transitions 2, 1996(5): p. 805-811.
12. Edwards, H.G.M., Turner, J.M.C., Fawcett, V., *Raman Spectroscopic Study of Nitronium Ion Formation in Mixtures of Nitric Acid, Sulfuric Acid and Water.* Journal of the Chemical Society, Faraday Transitions, 1995. **91**(10): p. 1439-1443.
13. Liu, J., et al., *Fullerene Pipes.* Science, 1998. **280**(5367): p. 1253-1256.
14. Salzmann, C.G., et al., *The Role of Carboxylated Carbonaceous Fragments in the Functionalization and Spectroscopy of a Single-Walled Carbon-Nanotube Material.* Advanced Materials, 2007. **19**(6): p. 883-887.
15. Cabana, L., et al., *The Role of Steam Treatment on the Structure, Purity and Length Distribution of Multi-Walled Carbon Nanotubes.* Carbon, 2015. **93**: p. 1059-1067.
16. Araujo, P.T., et al., *Resonance Raman Spectroscopy of the Radial Breathing Modes in Carbon Nanotubes.* Journal of Physics E, 2010. **42**(5): p. 1251-1261.
17. Reich, S., Thomsen, C., Maultzsch, J., *Carbon Nanotubes: Basic Concepts and Physical Properties*. 2004: John Wiley & Sons.
18. Dresselhaus, M.S., et al., *Raman Spectroscopy on Isolated Single Wall Carbon Nanotubes.* Carbon, 2002. **40**(12): p. 2043-2061.
19. Dresselhaus, M.S., et al., *Raman Spectroscopy of Carbon Nanotubes.* Physics Reports, 2005. **409**(2): p. 47-99.
20. Jorio, A., et al., *G-band Resonant Raman Study of 62 Isolated Single-Wall Carbon Nanotubes.* Physics Review B, 2002. **65**(15).
21. Pimenta, M.A., et al., *Raman Modes of Metallic Carbon Nanotubes.* Physics Review B 1998. **58**(24): p. 16016-16019.
22. Pimenta, M.A., et al., *The Anomalous Dispersion of the Disorder-Induced and the Second-order Raman Bands in Carbon Nanotubes.* Brazilian Journal of Physics, 2000. **30**: p. 423-427.
23. Datsyuk, V., et al., *Chemical Oxidation of Multiwalled Carbon Nanotubes.* Carbon, 2008. **46**(6): p. 833-840.
24. Ahn, J.H., et al., *Structural Modification of Carbon Nanotubes by Various Ball Milling.* Journal of Alloys and Compounds, 2007. **434**: p. 428-432.

25. Smart, S.K., et al., *Shortened Double-Walled Carbon Nanotubes by High-Energy Ball Milling.* International Journal of Nanotechnology, 2007. **4**(5): p. 618-633.
26. Park, K.C., et al., *Inter-Collisional Cutting of Multi-Walled Carbon Nanotubes by High-Speed Agitation.* Journal of Physics and Chemistry of Solids, 2008. **69**(10): p. 2481-2486.
27. Kagan, V.E., et al., *Direct and Indirect Effects of Single Walled Carbon Nanotubes on RAW 264.7 macrophages: Role of Iron.* Toxicology Letters, 2006. **165**(1): p. 88-100.
28. Halliwell, B., et al., *Free Radicals in Biology and Medicine*. 1993.
29. Pulskamp, K., Diabaté, S., Krug, H.F., *Carbon Nanotubes Show No Sign of Acute Toxicity But Induce Intracellular Reactive Oxygen Species in Dependence on Contaminants.* Toxicology Letters, 2007. **168**(1): p. 58-74.

CHAPTER 5

ENDOHEDRAL FUNCTIONALIZATION OF CARBON NANOTUBES

Several methods have been developed in order to introduce payloads into the channels of CNTs. Regardless of the method employed, bulk filling of CNTs results in samples that contain a large amount of external (non-encapsulated) material. The presence of external material is not desired since it can influence the behavior and properties of filled tubes, and in the biomedical field it can lead to undesired side effects. If the ends of the CNTs remain opened after the filling experiment, in general, attempts to remove the external material also result in the removal of encapsulated compounds, of the same nature. Having closed or corked ends allows the washing of the external material (using an appropriate solvent) whilst preserving the encapsulated compounds.[1, 2] The molten phase high temperature approach results in the simultaneous formation of filled closed-ended SWCNTs.[3]

The endohedral filling of CNTs is of interest for numerous applications; being materials nanoarchitectonics a hot topic nowadays. The encapsulation of materials inside CNTs usually results in the formation of 1D nanowires, but layered materials can also be grown inside CNTs channels.[4] Layer structures are commonly obtained by soft chemistry[5] and physical methods: Langmuir–Blodgett technique and layer-by-layer assembly of available 2D materials.[6] So far only few examples using CNTs as hosting templates have been reported: the growth of graphene nanoribbons,[7] single-walled lead iodide nanotubes[4] and single-walled boron nitride nanotubes.[8] Significantly, the use of CNTs as templates is a simple and easy-scalable method and has potential to be used for the production of a variety of nanomaterials, which are expected to show distinct properties in comparison to their bulk form.

Another exciting area is the use of filled CNTs in biomedicine [9, 10] One recent application resides in the use of "hot" (radioactive) metal halides as *in vivo* radiotracers. For instance, ultrasensitive imaging and the delivery of an unprecedented amount of radiodose density has been achieved via de the encapsulation of radioactive $Na^{125}I$ inside SWCNTs.[11] Provided that external

functionalization ensured biocompatibility, and a secondary derivatization granted proper targeting, these nanocapsules have proven to be a unique nanoplatform towards the development of a targeted anticancer therapy.[11-13] The removal of non-encaged external material whilst preserving the structural integrity of the nanocapsules becomes even more important when dealing with radioactive species. Besides, given the short half-life times of common clinically used radionuclides, rapidity is a must.

In this chapter we demonstrate few examples of filling SWCNTs with molten metal halides (MX). Formation of MX single-walled nanotubes has been observed inside CVD SWCNTs. As we realized that preparation of clean carbon nanocapsules might be a time-consuming process, we developed an approach that allows an efficient and environmentally friendly cleaning of the non-encapsulated metal halides that remain external to the nanotubes in samples of filled SWCNTs (MX@SWCNTs). Our method could be directly transferable to a large scale production of an equivalent radioactive system. Water was the selected "green" solvent and in order to minimize the radioactive waste, reduction of the volume employed in the cleaning process was also a targeted objective. Lutetium(III) chloride was the material of choice owing to the extended use of its radioisotope ^{177}Lu for the treatment of several cancer types including neuroendocrine tumors.[14] Furthermore, the low water solubility of $LuCl_3$ allowed a better appreciation of the effect that each of the different washing protocols had on the removal of the external $LuCl_3$. To our best knowledge this is the first comparative study on different methodologies for the removal of external, non-encapsulated material from samples of filled CNTs. Finally, we investigated the relation between the degree of end-closing of SWCNTs and the annealing temperature of SWCNTs. We compared the surface area of as-received, purified and annealed (after purification) SWCNTs using nitrogen adsorption. We also analyzed the effect of temperature on the filling yield of $EuCl_3$@SWCNTs prepared by molten phase capillary filling. Europium (III) complexes have unique luminescent properties, [15-17] and several europium (III) based MRI contrast agents have been reported.[18-20] Our studies fill a gap in the literature concerning the production of carbon nanocapsules by high temperature melt filling.

5.1. Experimental details

5.1.1. Chemicals

Chemical vapor deposition (CVD) produced SWCNTs, Elicarb®, were supplied by Thomas Swan and Co. They contained a significant fraction of DWCNTs. According to the supplier the average diameter of carbon nanotubes was 2.1 nm. Carbonaceous impurities and iron catalyst particles surrounded by graphitic shells were also present in the samples. Arc discharge SWCNTs were provided by Carbon Nanotechnologies, Inc. They also contained iron catalyst. Metal halides were purchased from Sigma Aldrich. Lutetium (III) chloride, lutetium (III) bromide, lutetium (III) iodide and europium (III) chloride were anhydrous (99.99% trace metals basis) and sodium iodide was standard reagent grade (98%).

5.1.2. Purification and filling of carbon nanotubes

CNTs were purified with steam (4 h) and hydrochloric acid as it has been previously reported elsewhere.[21, 22] Next, purified CNTs from the same batch were filled with molten metal halides: sodium iodide, europium (III) chloride, lutetium (III) chloride, lutetium (III) bromide, lutetium (III) iodide.

In a typical experiment CNTs were mixed with the chosen salt in weight ratio 1:10 (unless specified otherwise) and grinded with an agate mortar and pestle inside an Ar-filled glovebox (Labconco) until the sample presented a homogeneous color. Then, the mixture was vacuum-sealed inside a silica ampoule. When large amounts of filled CNTs of the same type were prepared, the sample was split into equal amounts in several silica ampoules in order to avoid sample explosion inside the furnace. The ampoules were placed inside a tubular furnace, annealed at given temperature above melting point of the payload and dwelled at this temperature for 12 h. After cooling to room temperature the ampoules were opened on an open bench. The collected material was sonicated and washed in a hot water (NaI@SWCNTs, $EuCl_3$@SWCNTs) at room temperature or water with few drops of HCl (LuX@SWCNTs) in order to remove the non-encapsulated material external to filled CNTs.

5.1.3. Cleaning protocols

$LuCl_3$@SWCNTs employed for the optimization of the washing protocol were prepared by mixing SWCNTs and $LuCl_3$ in a weight ratio 1:7 and employing the above described melt filling protocol. In all the washing protocols large and equal amounts (480 mg) of $LuCl_3$@SWCNTs, collected after the filling experiment, were processed. Milli-Q water was employed in all the washing protocols. All treatments were repeated for up to six days unless a clean sample was already achieved at an early stage. Hot water used in the protocols was in the range of temperature 70 °C - 90 °C. Dialysis sacks (cellulose, 12kDa MWCO) were purchased from Sigma Aldrich. Extraction thimbles (Whatman, cellulose) and filtration membranes (Whatman Cyclopore, polycarbonate, pore size 0.2 μm) were bought from Fischer Scientific

5.1.3.1. Sonication and Filtration (SF)

$LuCl_3$@SWCNTs were dispersed in 150 mL of water at 90 °C by bath sonication for 2 min, and filtered over a polycarbonate membrane. The sample was further rinsed with 900 mL of hot water on top of the filter membrane. The whole process (sonication + filtration + rinsing) was repeated three times. Then, the sample was collected from the top of the membrane, dispersed in 150 mL of water (2 min sonication) and left stirring overnight at 70 °C. Finally the solution was filtered and the solid sample was recovered from the top of the filter membrane. The whole process was repeated 6 times.

5.1.3.2. Sonication and Dialysis (SD)

Filled nanotubes were dispersed in 150 mL of water at 90 °C by bath sonication for 2 min. The suspension was filtered over a polycarbonate membrane. The solid sample was transferred to a cellulose dialysis sack with 40 mL of water. The dialysis sack was placed in a beaker containing 900 mL of hot water, sonicated for 2 minutes and left for 2 hours. Next, the sample was recovered by filtration and transferred again with 40 mL of fresh water to a new dialysis sack. The hot water in the beaker was also replaced. Two additional cycles of dialysis were performed.

The last dialysis step was carried out overnight in water at 70 °C. This procedure was repeated 6 times.

5.1.3.3. Sonication and Centrifugation (SC)

$LuCl_3$@SWCNTs were dispersed in 150 mL of water at 90 °C by bath sonication for 2 min. The sample was transferred to 30 mL tubes and centrifuged at a speed of 4000 r.p.m. for 10 min. The supernatant was separated from the solid sample by decantation. All the steps (sonication + centrifugation + decantation) were repeated three times. The fourth cycle consisted of stirring $LuCl_3$@SWCNTs overnight in 150 mL of water at 70 °C. The complete protocol was repeated systematically for 4 more cycles.

5.1.3.4. Soxhlet with cellulose thimble (Sh)

Filled SWCNTs were placed in a cylindrical cellulose thimble as solid powder and moistened with water. The thimble containing the sample was placed into a Soxhlet apparatus. The round-bottom flask underneath the thimble was filled with 200 mL of water. Water was refluxed using an electric heating mantle (set at 400 °C). The water was allowed to circulate through the system for 5 days, with water replacements every 8-10 h. The sample was not removed from the thimble when placing fresh water, and the same thimble was employed during the whole process. After completing the washing cycles, the thimble with the solid content was placed in the oven at 80 °C and allowed to dry for few hours. $LuCl_3$@SWCNTs were poured out from the thimble as a dry solid powder by holding the thimble upside down.

5.1.3.5. Soxhlet with dialysis sack (DSh)

$LuCl_3$@SWCNTs were placed inside a dialysis sack and dispersed in 40 mL of water. The dialysis sack containing the sample was placed into the Soxhlet apparatus. The round-bottom flask underneath was filled with 200 mL of water and heated, with an electrical mantle (set at 400 °C), to allow the circulation of water through the system. Both, water and the dialysis sack were replaced every 24 h. To do so, the sample was collected from the dialysis sack by filtration onto a

polycarbonate membrane, and then transferred with 40 mL of water to new dialysis sack. The overall process was performed for 4 days.

5.1.4. Lutetium (III) chloride complex with cetylpirydinium chloride/chromeazurol S

Cetylpirydinium chloride (CPC) and chromeazurol S (CAS, dye content 50%) were purchased from Sigma Aldrich. Aqueous solutions of 0.2% (w/v) CPC and CAS were prepared, mixed in 1:1 ratio and diluted to $4 \cdot 10^{-3}$%. A CPC/CAS solution (2 mL) was added to a $LuCl_3$ aqueous solution in the range of concentrations 10^{-2} M to 10^{-8} M, keeping the final volume constant at 30 mL.

5.1.5. Annealing of SWCNTs

Purified CNTs (250 mg) were split into five equal fractions. Each of them (50 mg) was sealed in a silica tube under a vacuum. As control, one sample was directly open after sealing, which will be referred as room temperature, RT CNTs. The other samples were dwelled in the furnace for 12 h in the air at selected temperatures: 400 °C, 700 °C, 800 °C, 900 °C, 1100 °C and 1200 °C.

5.2. Melt filling with selected payloads

The range of substances that can be encapsulated in the SWCNT channels is wide. Metal halides have received special attention, since they can be incorporated in a high yield.[23-25] Here, we demonstrate the filling of SWCNTs from two different sources: CVD and arc discharge, with selected metal halides.

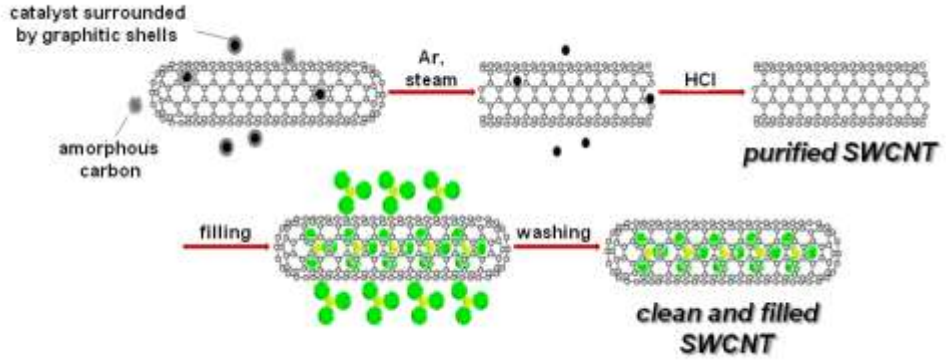

Figure 5.1. Schematic representation of purification and filling of CVD SWCNTs.

Steam-purified SWCNTs have been filled from molten salts and sealed by high temperature treatment, affording close-ended CNTs with the filling material confined in the inner cavity.[3] Non-encapsulated metal halides external to the CNTs were removed by washing in a suitable solvent. Thus, clean and filled SWCNTs (i.e. carbon nanocapsules) were obtained (Fig. 5.1). The source of nanotubes, temperature of annealing and payloads are summarized in the Table 5.1.

Table 5.1. Summary of samples prepared by the melt filling method.

Source of SWCNTs	Payload	Melting temperature (℃) [26]	Annealing temperature (℃)
CVD	NaI	661	900
	$EuCl_3$	632	910
	$LuCl_3$	905	950
	$LuBr_3$	1025	1050
	LuI_3	1050	1100
Arc discharge	$LuCl_3$	905	940
	$LuBr_3$	1025	1050
	LuI_3	1050	1100

Samples were dispersed in ethanol, deposited on a lacey carbon coated copper grid and characterized by electron microscopy techniques. High-angle annular dark-field high resolution scanning electron microscopy (HAADF STEM) images acquired with spatial to atomic resolution clearly show the presence of filling material inside CVD SWCNTs (Fig. 5.2-5.4). HAADF STEM provides image intensity which depends on the atomic number (Z) of the elements present by utilizing thermal diffuse scattering electrons in the sample. Therefore, in this imaging modality bright contrast corresponds to heavier elements. Thus, on our images metal halides appear with a brighter contrast (white strings) than carbon from the nanotubes (pale grey). Apart form filled CNTs, some small bright dots are also visible that correspond to residual inorganic particles, in most cases from the catalyst, still present after the steam and HCl purification. Encapsulated payloads might be present as a continuous filling or as small agglomerates. As is can be seen in the high resolution (HR) STEM microscopy (Figure 5.3), since bulk lutetium halides present a layered structure (van der Waals solids), once encapsulated they can be present inside CVD SWCNTs either as nanowires (green arrows) or nanotubes (yellow arrows). Both forms of filling might also occur simultaneously. Since the ends of SWCNTs close after the filling experiment, closed-ended inorganic nanotubes of metal halides (MXNTs) can be observed on some images (Fig. 3b, d and Fig. 4d, e). This indicates that the filling material wets the inner cavity of the SWCNTs and accommodates to their structure.

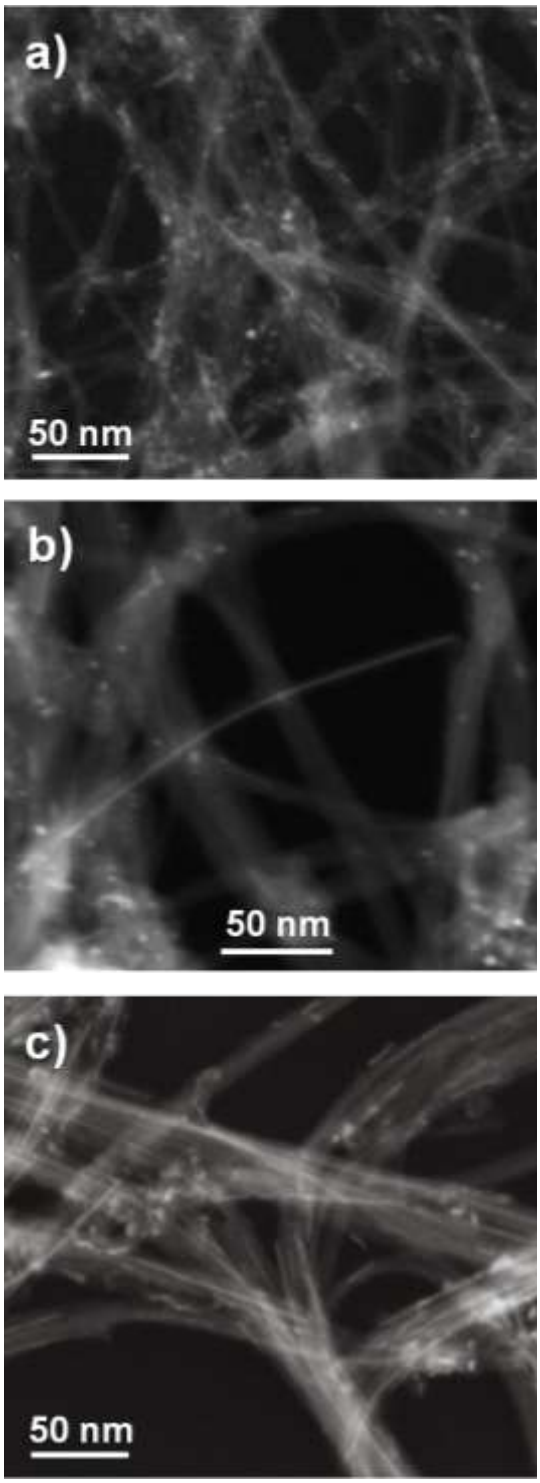

Figure 5.2. HAADF STEM images of filled CVD SWCNTs: a) NaI@SWCNTs; b, c) $EuCl_3$@SWCNTs.

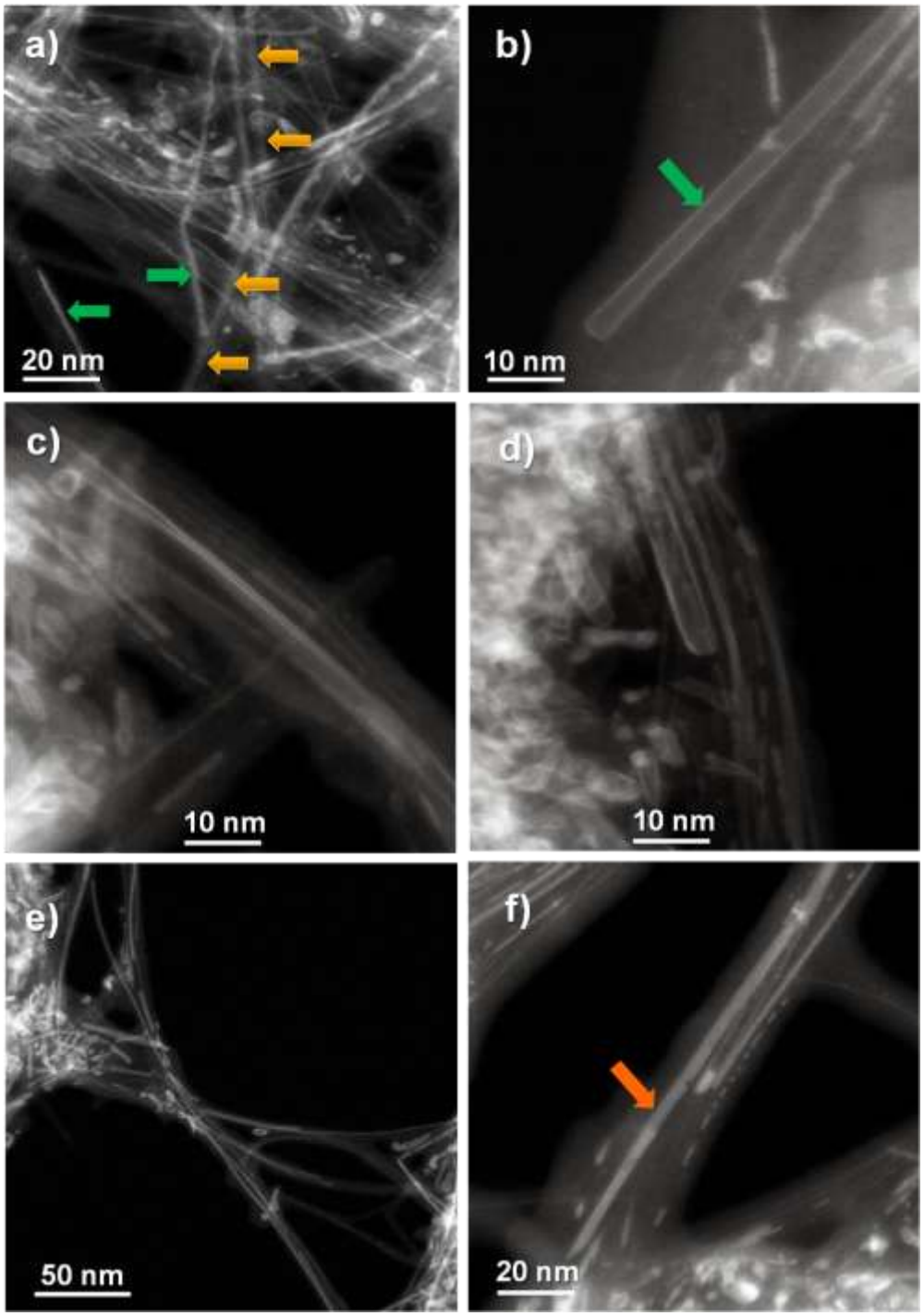

Figure 5.3. HAADF HRSTEM images of filled CVD SWCNTs: a, b) $LuCl_3$@SWCNTs, c, d) $LuBr_3$@SWCNTs, e, f) LuI_3@SWCNTs. As guided to the eye, orange arrows indicate some examples of LuX_3 nanowires and green arrows indicate some examples of LuX_3 nanotubes.

Atomic resolution (AR) images of filled CVD CNTs were obtained using spherical aberration (C_s) corrected STEM in high-angle annular dark-field mode (Fig. 5.4). The microscope used is a state of the art FEI Qu-Ant-EM microscope installed at EMAT, University of Antwerp (Belgium). This is a double aberration corrected FEI Titan G2 80-300 instrument capable of routinely making small probes which enable 0.8 Å resolution at an acceleration voltage of 300 kV. We synthesized mostly single-walled MXNTs, but inside $LuCl_3$@SWCNTs occasionally double-walled MXNTs can also be observed (Fig. 5.4a). As it can be seen in Figure 5.4b, individual lutetium and chloride atoms are clearly visible. They form an hexagonal pattern (hexagonal motif indicated by dotted yellow line), which is confirmed by the masked inversed FFT diffraction pattern (inset in Figure 5.4b). Based on the analysis of multiple images we can conclude that MX nanowires (Fig. 5.4c) are preferably formed in SWCNTs with smaller diameters, while MXNTs (Fig. 5.4a,b and Fig. 5.4d-f) are formed in the bigger SWCNTs.

Figure 5.5 displays lutetium halides filled arc discharge SWCNTs. These nanotubes contain a higher amount of catalyst than the CVD SWCNTs (see Chapter 3), and therefore more bright dots are visible on the images. They are also characterized by smaller diameters comparing to CVD CNTs, making more difficult to observe the filling.

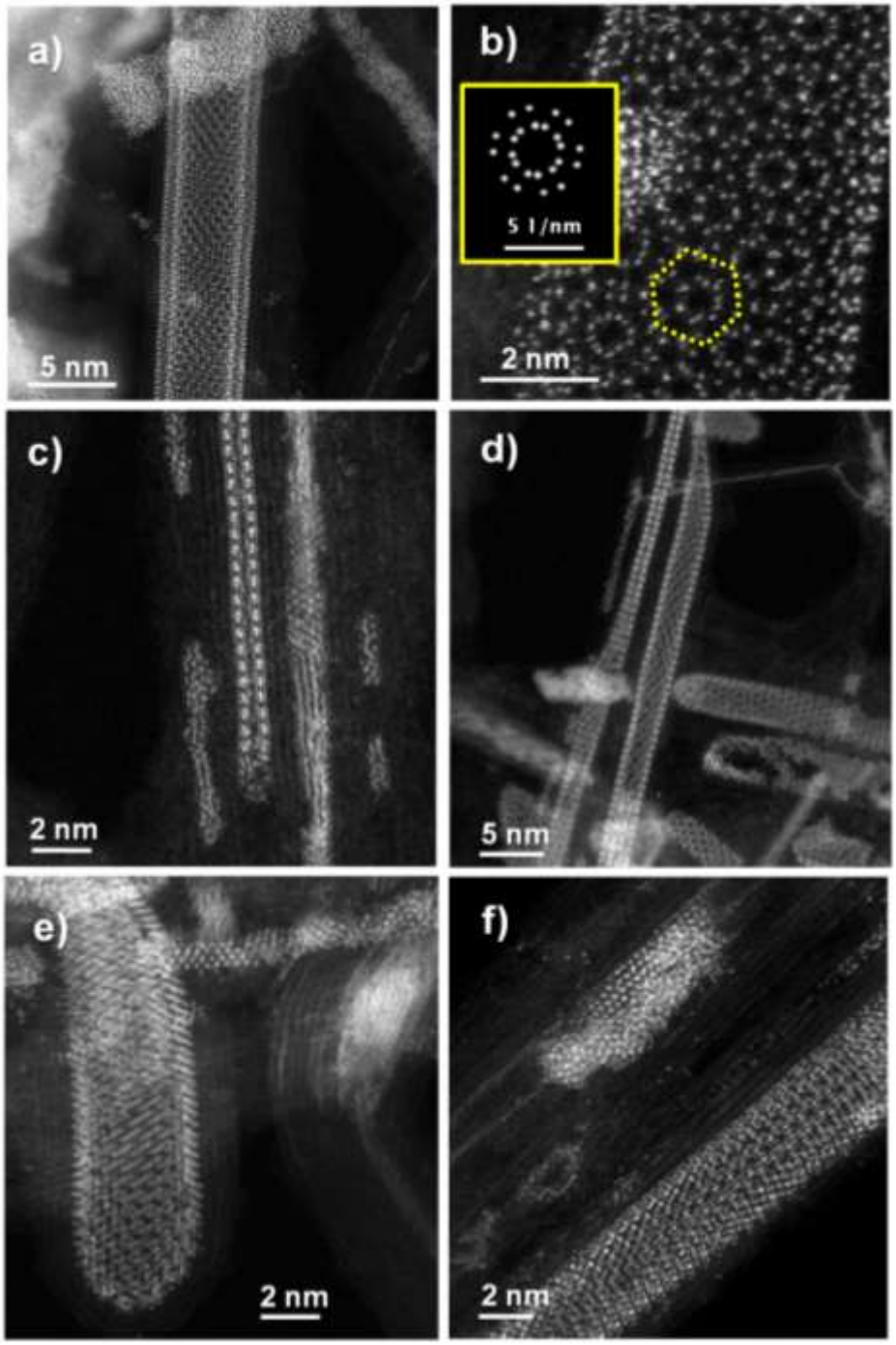

Figure 5.4. HAADF ARSTEM images of filled CVD SWCNTs: a, b) $LuCl_3$@SWCNTs, c, d) $LuBr_3$@SWCNTs, e, f) LuI_3@SWCNTs. In a Figure 5.4b: a yellow dotted hexagon reflects single hexagonal motif in the honeycomb structure of a single-walled $LuCl_3$ nanotube; the inset in a yellow rectangle shows the inversed FFT diffraction pattern with mask.

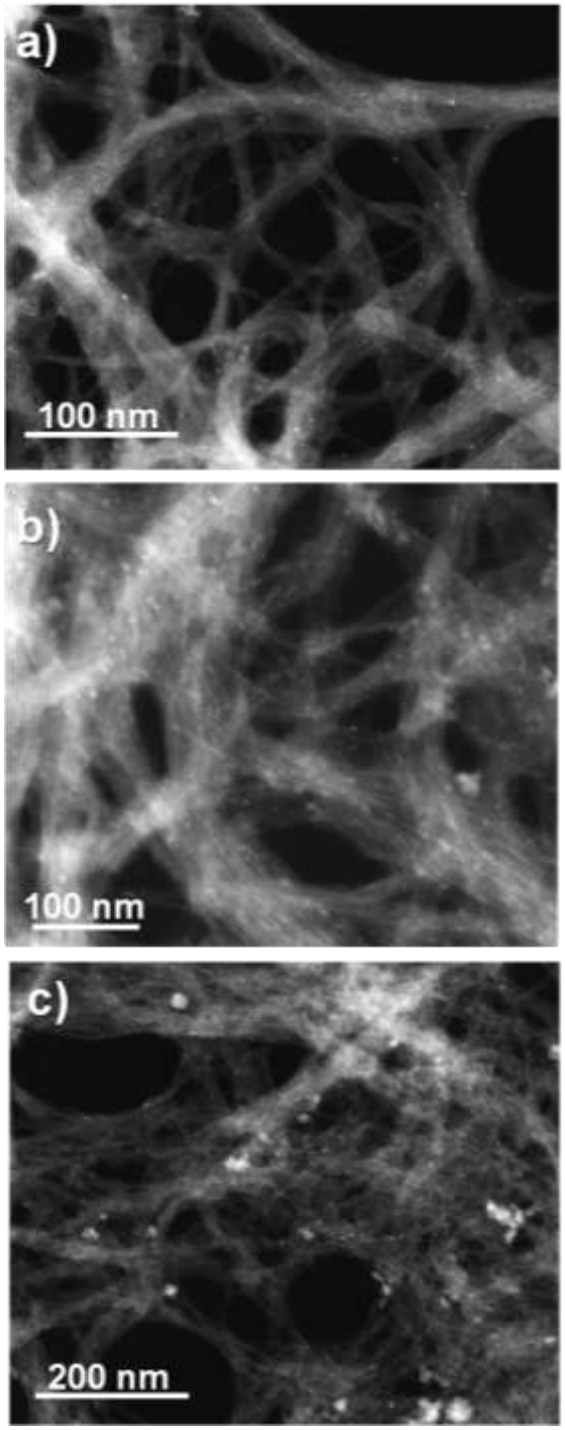

Figure 5.5. HAADF STEM images of filled arc discharge SWCNTs: a) $LuCl_3$@SWCNTs, b) $LuBr_3$@SWCNTs, c) LuI_3@SWCNTs.

5.3. Sustainable production of nanocapsules free of non-encapsulated material - the case of single-walled carbon nanotubes filled with lutetium (III) chloride

As-received SWCNTs were steam (4 h) and HCl treated in order to open their ends and remove carbonaceous and metal impurities, following a previously established protocol.[21, 22] The resulting SWCNTs have a median length of 420 nm, (see Chapter 3) suitable for biomedical applications. The purified material was characterized by thermogravimetric analysis (TGA) and by electron microscopy. A representative HAADF STEM image of the purified sample is presented in Figure 5.6a. Apart from SWCNTs forming a web-like structure, small bright dots of few nanometers are visible, which correspond to the residual Fe catalytic particles remaining after the purification process. These metal particles are employed during the synthesis of SWCNTs and are partially removed by the HCl treatment. The amount of iron nanoparticles still present after the purification step is 1.2 wt. % as determined by TGA. Afterwards, we proceeded to the filling of the SWCNTs with $LuCl_3$ by molten phase capillary wetting. Electron microscopy analysis of the collected material after the filling process reveals the presence of a large amount of non-encapsulated salt (Figure 5.6b). SWCNTs appear to be mostly covered by large crystals of $LuCl_3$.

The protocol employed for the encapsulation of $LuCl_3$ into SWCNTs leads to samples of filled tubes with closed ends.[3] This allows the removal of the non-encapsulated $LuCl_3$ using a solvent in which the salt is soluble, since the nanotubes protect the inner crystals from dissolution. We tested the solubility of $LuCl_3$ and observed that at room temperature it presents a poor solubility in water. A higher solubility was achieved in hot water (≥ 70 °C), which was preserved after cooling. We avoided the use of corrosive mineral acids, such as nitric acid, that can alter the tubular structure of the carbon nanotubes.[27] The presence of defects could result in the release of the encapsulated payload, which is indeed undesirable in the present study. On the other hand we also disregarded the use of surfactants or organic solvents, which have for instance been employed for the purification of filled SWCNTs[28, 29] since the aim was to develop an environmentally friendly protocol. This drove us to the use of boiling water, which is a “green” innocuous solvent, for the cleaning of the non-encapsulated salt.

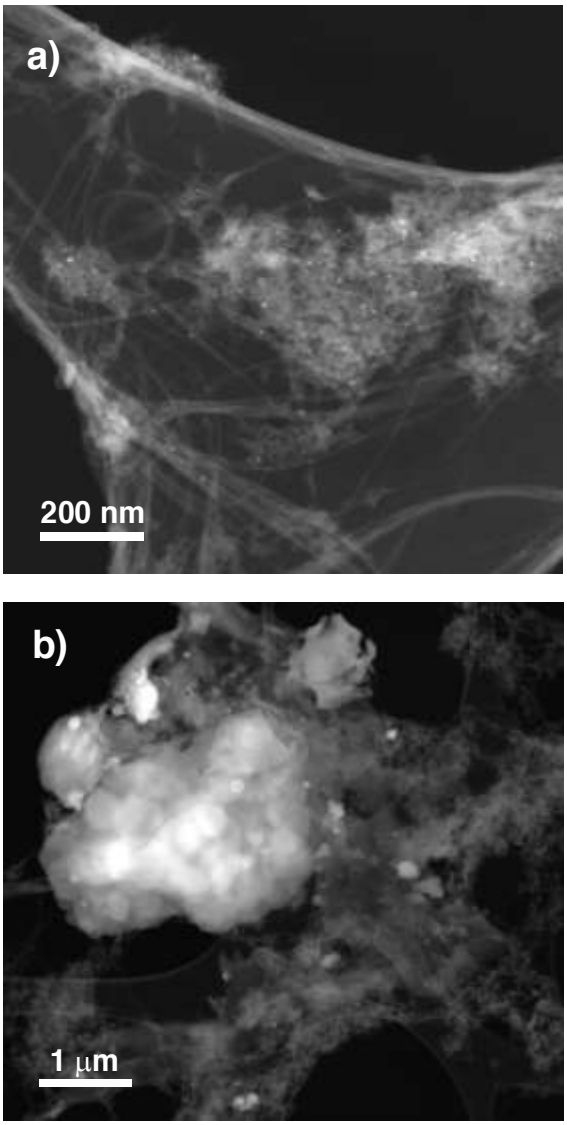

Figure 5.6. a) HAADF STEM image of steam and HCl purified SWCNTs. Small bright dots of few nanometers in diameter correspond to residual iron catalyst remaining after the purification process. b) HAADF STEM image of as-produced $LuCl_3$@SWCNTs (before washing). Huge bright crystals correspond to non-encapsulated $LuCl_3$.

The most common protocol for the removal of external material consists on dispersing the sample of filled SWCNTs in a suitable solvent. After a given amount of time, which can involve or not stirring, the sample is collected as a solid powder by filtration.[28, 30-32] This process might be repeated several times to completely remove the non-encapsulated payload. The quality of the resulting material is in general determined by means of electron microscopy, but since the

filtrate contains the dissolved external material, a fast monitoring of the cleaning process can be performed by visual inspection of the filtrate, provided a colored solution is obtained upon dissolution of the payload. The presence of a colorless filtrate serves then as an indication that the cleaning protocol is completed. This is for instance the case when iron chloride is removed from the exterior of filled tubes using hydrochloric acid, since iron cations give a yellow color to the solution.[33] To benefit from such fast qualitative monitoring, and despite $LuCl_3$ gives a colorless water solution, we used a salt complexation method and added CPC/CAS (Cetylpyridinium chloride/Chromeazurol-S) to the collected filtrates. CPC/CAS complexes have been reported for several metal and rare-metal salts. [30, 34, 35] The color of the solution becomes dark royal blue if the lutetium complex is formed and yellow when the lutetium salt is not present (Fig. 5.7). This allows a quick and non-destructive *on-site* assessment of the removal of external salts.

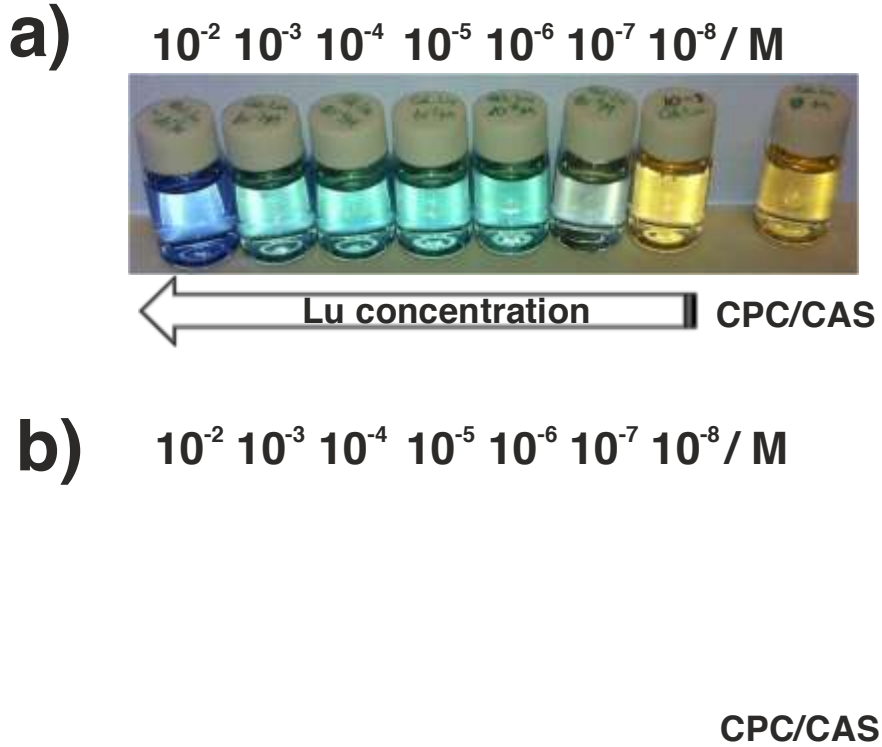

Figure 5.7. Vials containing 10^{-2}-10^{-8} M $LuCl_3$ in the presence of CPC/CAS showing a concentration dependent change of color. A control sample of CPC/CAS is included on the right side of the photograph. The concentration of CPC/CAS is a) $4 \cdot 10^{-3}$% w/v and b) 0.2% w/v.

Two different concentrations of CPC/CAS have been employed. From a qualitative point of view it is interesting to note that regardless of the concentration of CPC/CAS a royal blue color indicates the presence of lutetium chloride (Fig. 5.7), not appreciable in the picture in b, and yellow indicates the absence of the metal salt (CPC/CAS in water has a yellow color). Greenish/reddish colors are observed between both stages.

A large sample of $LuCl_3$ filled SWCNTs (480 mg) was submitted to the above mentioned cleaning protocol, which consisted in sonication of the sample in hot water followed by filtration three times. Then to allow enough time for the salt to get dissolved, the sample was left stirring overnight in water at 70 °C. We will refer to this treatment as "sonication and filtration" (SF). In the present case, cleaning of the sample was stopped after prolonged washing cycles, reaching up to 6 days and 18 fractions. It has been reported that the majority of external material is removed after the first washing step.[30] To check whether this was also the case, we analyzed the sample collected after the initial sonication and filtration step by TGA. Analysis of the obtained data reveals the presence of 15.6 mg of non-encapsulated $LuCl_3$ external to the nanotubes (a filling yield of 23 wt. % was employed to determine this value, which will be determined in the sample washed using the optimized protocol). STEM analysis of the collected sample at the end of this process reveals the presence of contamination from an organic-type material (Fig. 5.8a).

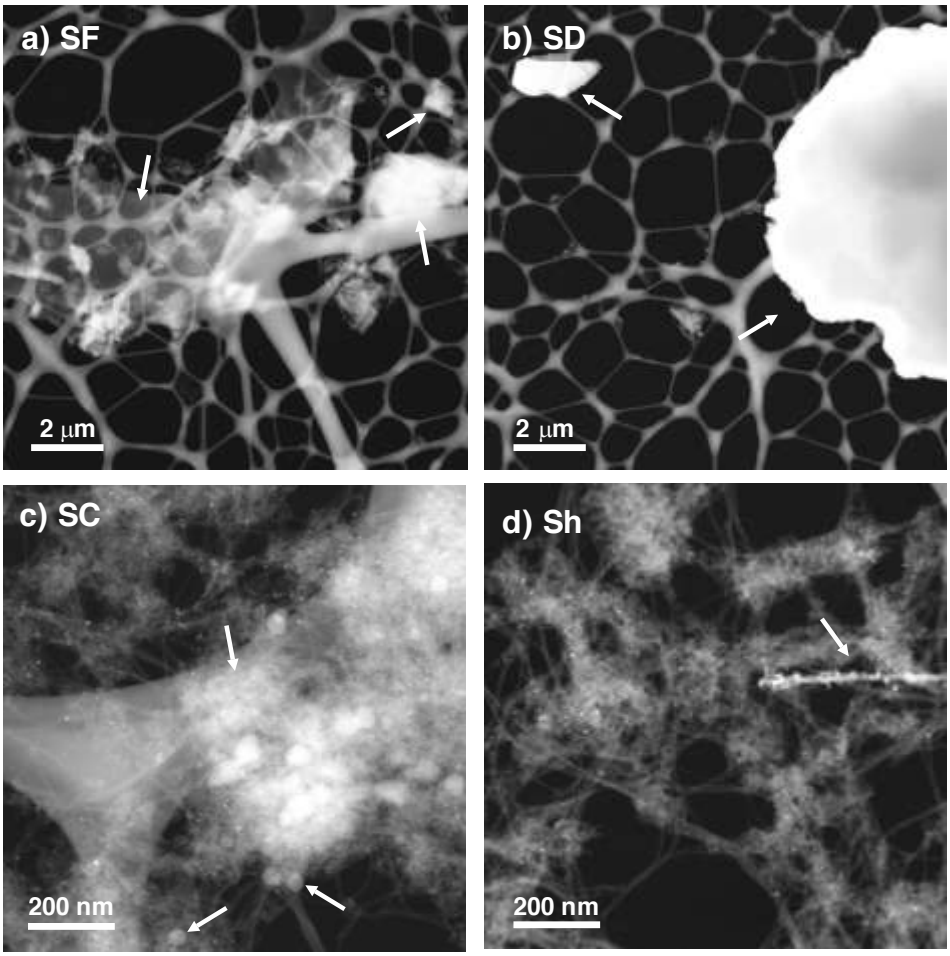

Figure 5.8. a-d) HAADF STEM images of $LuCl_3$@SWCNTs at the final stage of the different washing protocols. a) SF-sonication and filtration; b) SD-sonication and dialysis; c) SC-sonication and centrifugation; d) Sh-Soxhlet with cellulose thimble. Arrows point to external impurities.

It is likely that the sample has been contaminated with polycarbonate from the filter membranes due to the prolonged treatment at which the sample was subjected (18 cycles). The SF is the most classical method employed by most authors, with slight variations, and works well when using a "good" solvent, i.e. a solvent in which the material to be removed presents a high solubility. No previous observations of contamination have been reported using SF. Therefore, the eventual contamination observed in the present case is attributed to the prolonged processing of the material. Much shorter washing cycles are needed when the external material presents a high solubility in the employed solvent.

An alternative cleaning protocol was thus needed. We next tested two variations of the SF, replacing the filtration step by either dialysis or by centrifugation. We will refer to the former as "sonication and dialysis" (SD) and to the latter as "sonication and centrifugation" (SC). The SD method was the least efficient in removing external material as shown in the HAADF STEM image (Fig. 5.8b), where micrometer-sized lumps of non-encapsulated $LuCl_3$ are visible even after several washing cycles. The number of washing fractions, time employed and a brief description of the obtained results are recorded in Table 5.2, for the different explored methods. The SC method seemed to work well at the beginning but a complete cleaning of the sample was not reached even after prolonged treatment. STEM inspection of the final collected sample reveals the presence of external metal halide impurities. A major drawback of this methodology is that requires decantation of the supernatant after centrifugation, which results in a continuous loss of sample between cycles.

The use of a Soxhlet apparatus, which has been employed for the purification of as-produced nanotubes,[36] arises as an interesting alternative. First of all it reduces the amount of waste, since water is recirculated over the sample in a closed cycle. This is key for the envisaged application that aims to develop a “green” process that allows handling of radioactive systems ($^{177}LuCl_3$). On the other hand it requires minimal sample manipulation which is also of interest when dealing with radionuclides. Remarkably, using the Soxhlet approach (Sh) a clean sample was already achieved with only 6 cycles. Unfortunately, due to the difficulty in recovering the nanotubes after the reflux from the cellulose cartridge, contamination of the sample with cellulose seemed to have taken place, as it can be seen in the STEM image of Figure 5.8d. Encouraged by the efficiency of the Soxhlet system, we replaced the generally employed cellulose thimble with a dialysis sack, to facilitate the recovery of the sample and prevent its contamination. A schematic representation of the proposed "Soxhlet with dialysis sack" (DSh) system is presented in Figure 5.9.

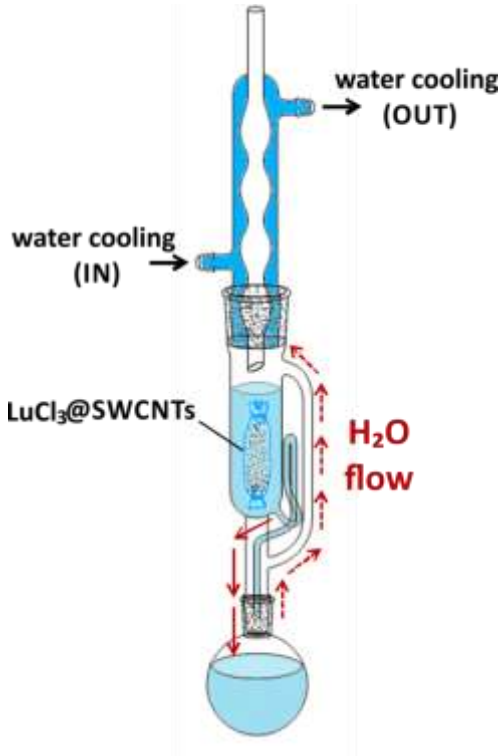

Figure 5.9. Schematic representation of the "Soxhlet with dialysis sack" system. The sample to be cleaned from external material is sealed in a dialysis sack and placed into the Soxhlet apparatus. Boiling water goes through the sample in a continuous flow thus minimizing the amount of liquid waste at the end of the process.

After the initial cycle only 3.6 mg of external non-encapsulated $LuCl_3$ remained in the sample (as determined by TGA - using the filling yield of 23 wt. %) and a clean sample was already achieved with only three cycles of washing. According to the CPC/CAS test, the filtrate of the fourth washing was already free of $LuCl_3$ and thus this final washing would be unnecessary (Fig. 5.10).

Figure 5.10. Photos of aliquots after complexation with CPC/CAS using DSh for the removal of external $LuCl_3$ after first washing (left) and 4^{th} final washing (right). The concentration of CPC/CAS is 0.2% w/v. The total volume of each fraction was 30 mL.

Electron microscopy analyses confirm that a clean sample, free of external $LuCl_3$, was achieved by the DSh protocol (Fig. 5.11). No large lumps of $LuCl_3$ or additional impurities, which could arise from the processing of the sample, were detected either by HAADF STEM or by low magnification TEM imaging. This is further proven by EDX analysis (Fig. 5.11b) as only signals for Lu and Cl (from the encapsulated material), Fe (from the catalyst) and C are detected. Cu peaks arise from the TEM support grid.

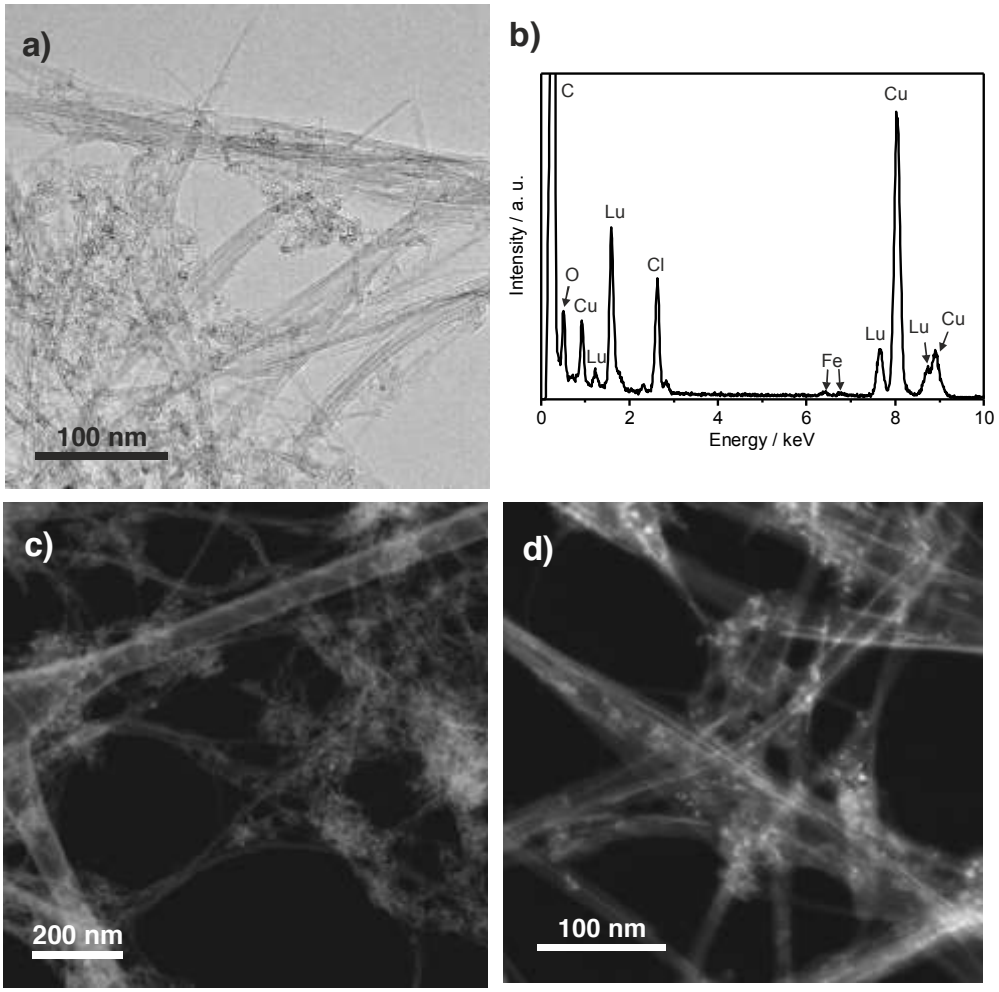

Figure 5.11. Analysis of the sample of $LuCl_3$@SWCNTs washed by the DSh protocol: a) HRTEM image, b) EDX analysis, c,d) HAADF STEM images.

The $LuCl_3$ filling can be more easily seen in the HAADF STEM images. In this imaging modality, heavy elements (such as Lu, Cl) give a higher intensity than light elements (such as C). Therefore, the filled material appears as bright lines following the shape of the SWCNTs, which appear as pale grey. EDX analyses on individual bright dots observed in the HAADF STEM images prove that these correspond either to Fe, from the catalyst impurities remaining after the steam treatment (already observed in the purified sample of empty SWCNTs (Fig. 5.6a), or to $LuCl_3$. The latter can be related to $LuCl_3$ encapsulated into SWCNTs which are perpendicular to the image and are thus seen in cross-section or to $LuCl_3$ in the form of small nanoparticles or clusters.

HRTEM inspection allowed to exclude that these small clusters or nanoparticles of $LuCl_3$ are outside the CNTs. Representative HRTEM images are shown in Figure 10. $LuCl_3$ is only observed inside SWCNTs, either as long nanowires or as small nanoparticles indicated by arrows on Figure 10. b. Once encapsulated, $LuCl_3$ keeps its monoclinic C2/m crystal structure. Interplanar spacings of 3.1 Å, in good agreement with the (002) planes of the monoclinic $LuCl_3$, are clearly visible in the HRTEM image in Figure 5.12.

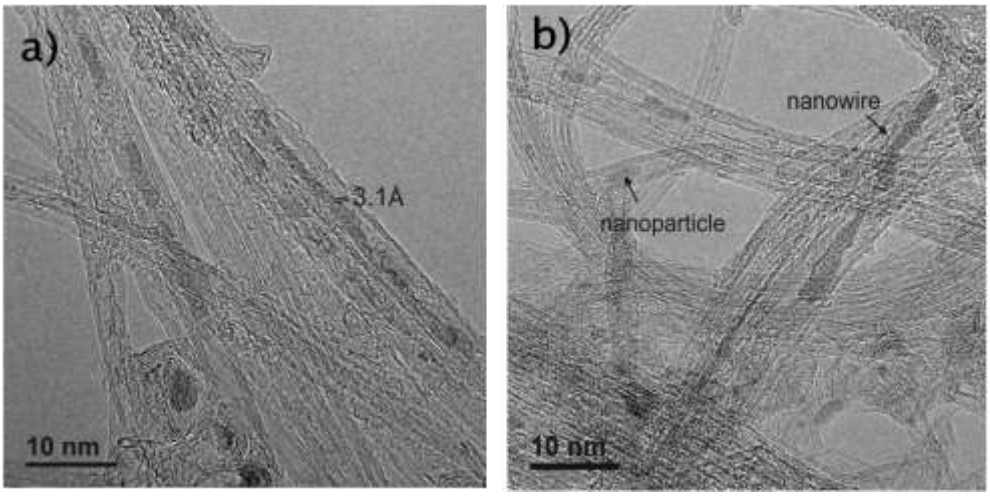

Figure 5.12. HRTEM images of the sample of $LuCl_3$@SWCNTs washed by the DSh protocol. No external material is observed. Examples of small nanoparticles of $LuCl_3$ as well as filling in the form of nanowires are indicated by arrows.

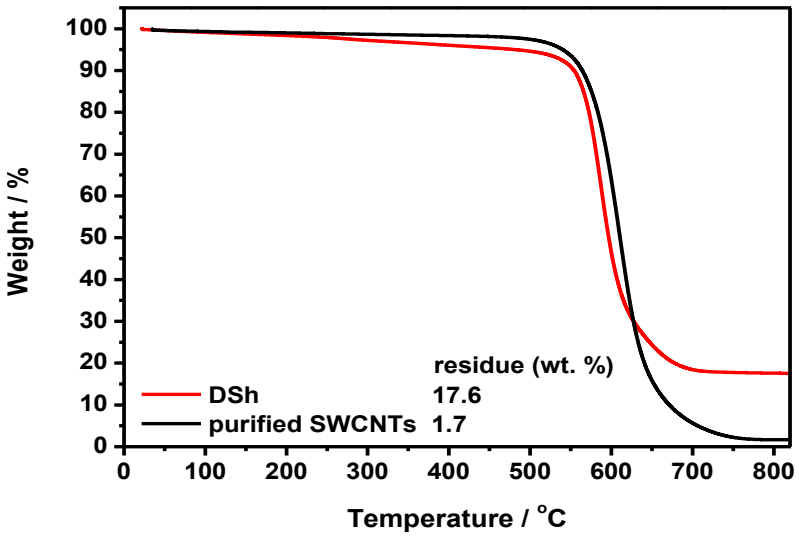

Figure 5.13. TGA of empty purified SWCNTs and $LuCl_3$@SWCNTs after being washed with the DSh protocol. Analyses were performed under flowing air at a heating rate of 10 °C min^{-1}.

A quantitative determination of the filling yield (FY) can be provided by TGA of the sample under flowing air. The TGA curves of the purified (empty) SWCNTs and the DSh cleaned $LuCl_3$@SWCNTs are presented in Figure 5.13. During the TGA in air, carbon species are completely oxidized to CO_2. Thus the solid residue recorded in the sample of empty SWCNTs results from the oxidation of the Fe nanoparticles to Fe_2O_3. A 1.7 wt. % of iron oxide corresponds to a 1.2 wt. % of iron (value previously mentioned at the beginning of section 5.3). The oxidation of the sample of filled tubes will still have a small contribution from these iron nanoparticles, but the main contribution to the inorganic solid residue collected at the end of the experiment will arise from the oxidation of $LuCl_3$ to Lu_2O_3 (17.6 wt. %). Although TEM has been widely employed to estimate the degree of filling, the amount of encapsulated payload (i.e. filling yield) can be quantitatively determined from the TGA residues (see Annex A.1).[33] In this case, the filling yield of $LuCl_3$ turned out to be of 23 wt. %, which is similar to the filling yields achieved with other metal halides (as per TGA). [33]

Thus, only the DSh method was able to provide a clean product with a high filling yield. We believe that the superiority of the DSh method with respect to the other studied protocols lies in the fact that this setup provides a continuous flow of hot water resulting in the constant removal of external material whilst preserving

the tubular structure of the nanocapsules. Furthermore, the use of a dialysis sack prevents sample contamination from the employed materials. Taking into account that we replaced the Soxhlet water every 24 h, we believe that the time employed for dissolving the external material can be further decreased with more frequent water replacements. A remarkable reduction of the liquid waste, which would be contaminated with radioactive materials when using ^{177}Lu, has been achieved with the developed protocol. As previously discussed, the widely employed SF process leads to clean samples when the material to be removed presents a good solubility in the employed solvent. In the present case, even if the SF did not result in a clean sample at the end of the process, the total volume of water employed (18 fractions) amounts to 18.90 L, in contrast to 0.96 L used for the optimized DSh. This represents a 95% reduction in water waste, which gets contaminated with hazardous heavy (radioactive) elements. It is also worth noting that the use of dialysis sacks is compatible with both acidic and basic conditions and a wide range of organic solvents, further expanding the range of application of the proposed process.

Table 5.2 summarizes the different investigated protocols for the removal of material remaining on the exterior of filled SWCNTs after the bulk filling process.

Table 5.2. Comparison of different washing protocols.

Protocol	Brief description	Number of fractions	Time (days)	Comments
SF	sonication and filtration	18	6	Eventual contamination
SD	sonication and dialysis	18	6	Unable to completely clean sample, loss of sample during cleaning
SC	sonication and centrifugation	13	5	Unable to completely clean sample, loss of sample during cleaning
Sh	Soxhlet with cellulose thimble	6	6	Eventual contamination
DSh	Soxhlet with dialysis sack	4	4	Clean sample achieved, high filling

5. 4. Closing the ends of carbon nanotubes by thermal annealing

As-previously mentioned it is well established that thermal annealing of open-ended SWCNTs results in samples of closed-ended SWCNTs,[3] which can be employed to seal materials inside SWCNTs. Defects are reactive at high temperatures and are responsible for closing their ends. Closed- and opened-ended CNTs vary in specific surface area and pore size distribution. There are several potential sides available for gas adsorption on SWCNTs, which include: outer surface, inner channels, interstitial channels and grooves [37, 38] as it is schematically illustrated on the Figure 5.14. However, Wisniewski et al. proved that isolated tubes play the most important role in adsorption by comparing the adsorption from liquid solution and gas phase.[39] The Brunauner, Emmett and Teller (BET) theory enables to calculate specific surface area of cylindrical CNTs, taking into account a model of multimolecular layer adsorption.[40, 41]. The non-local density functional theory (NLDFT) is often used for the pore size/volume analysis from adsorption isotherms for CNTs with micro and mesoporosity considering slit-shaped pores with graphitic walls. The main advantage of this method is that it describes complex systems and physical phenomena associated with them.[42] The presence of impurities, such as amorphous carbon or functional groups may modify the adsorption capacity of CNTs.[43]

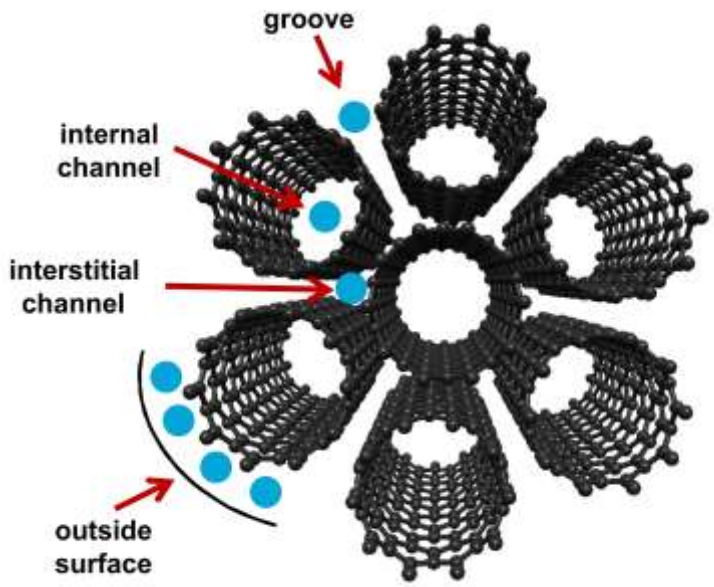

Figure 5.14. A scheme of gas adsorption in a bundle of SWCNTs. Blue dots symbolize molecules adsorbed on accessible sites.

Interestingly, to date there is no systematic study that investigates the role of temperature on the degree of end-closing. Towards this end we have investigated the effect of annealing open-ended SWCNTs at different temperatures by means of nitrogen adsorption because morphological changes of nanotubes can be easily monitored by gas adsorption.[44-47]

Steam and HCl purified SWCNTs were annealed at 400 °C, 700 °C, 800 °C, 900 °C, 1100 °C and 1200 °C under vacuum in a silica ampule and the resulting samples were studied by nitrogen adsorption analysis. The specific surface area (S_{BET}) was determined for as-received SWCNTs and each of the annealed samples by the BET method. An additional sample prepared following the same protocol (sealed in a silica ampoule) but without annealing was included for comparison (RT). Prior to the adsorption-desorption experiments, samples were out gassed at 300 °C during 15 h. Isotherms were recorded at 77 K.

The pore size distribution was further computed using NLDFT model applied to the physical adsorption-desorption data of nitrogen at low temperature (Fig. 5.16) using the Saeius software. This model has been designed for predicting the pore size distribution of carbon materials and was employed over a range of pore sizes between 0.3-3 nm; in agreement with the diameter of the nanotubes employed in this study (mentioned in Experimental section). The accumulated pore volume (V_A) was obtained by limiting the pore distribution to 1.25 nm

All the CNT samples are characterized by type IV isotherms (Fig 5.15 a), which classifies them as mesoporous material. The capillary condensation of nitrogen is accompanied by a hysteresis loop type H2. This loop occurs for more complex pore structures in which network effects are important, which is in agreement with the natural tendency of carbon nanotubes to form bundles.[48]

Figure 5.15b shows that as-received material has a much lower specific surface area than purified RT CNTs. After treatment with steam the ends of the CNTs become open which is reflected in the increase of the specific surface from 790 m^2g^{-1} (as-received) to 1245 m^2g^{-1} (RT CNTs). Annealing of purified open-ended nanotubes at 800 °C and above results in a progressive decrease of the specific surface area. This trend could be an indication that after annealing the samples at 800 °C and above the ends of the CNTs can become closed upon cooling.

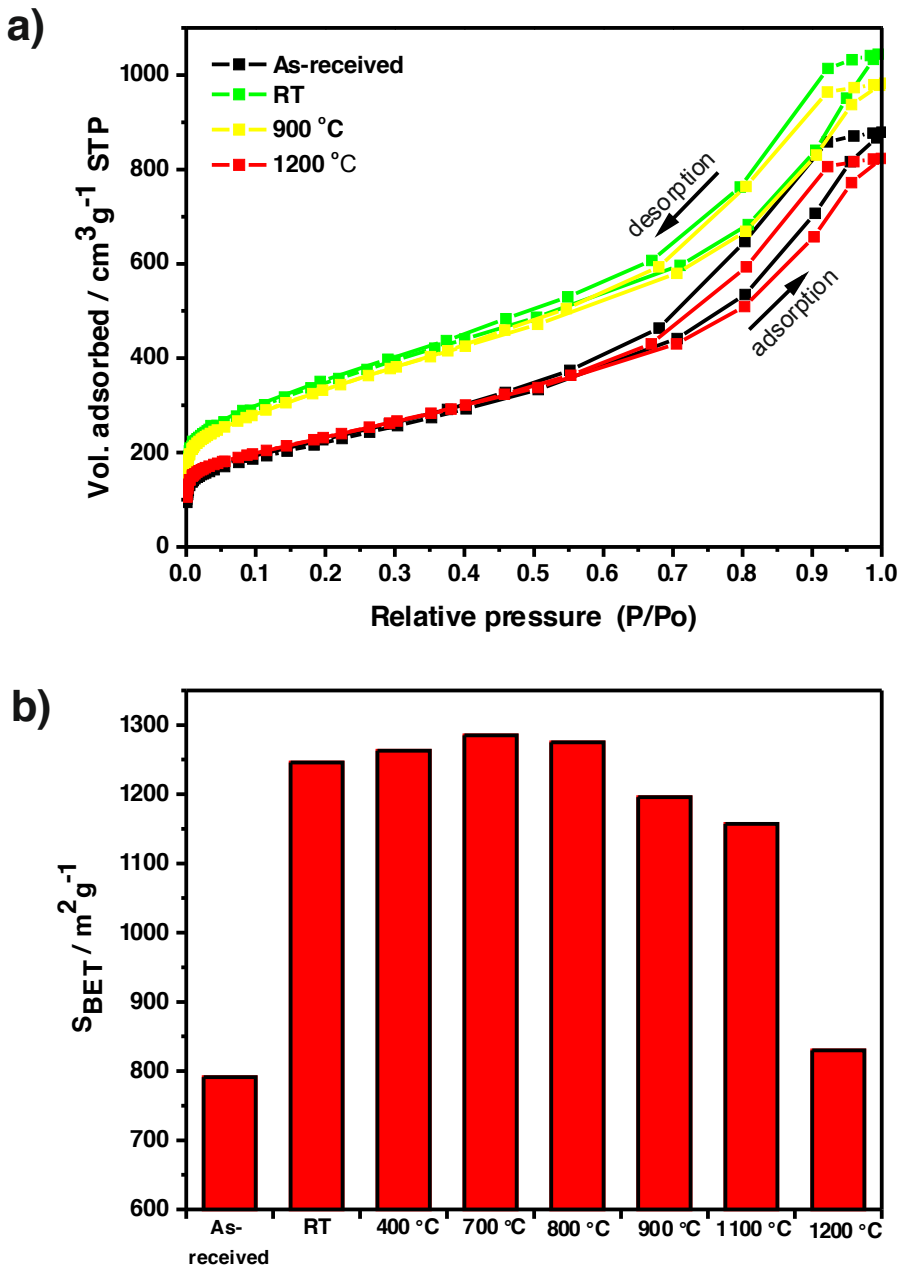

Figure 5.15. a) Nitrogen adsorption isotherms of as-received SWCNTs, purified (RT), and thermally annealed samples (after purification) at 900 °C and 1200 °C at 77 K. b) Histogram of specific surface area (S_{BET}) of as-received SWCNTs, purified (RT), and thermally annealed samples (after purification) at 400 °C, 700 °C, 800 °C, 900 °C, 1100 °C and 1200 °C.

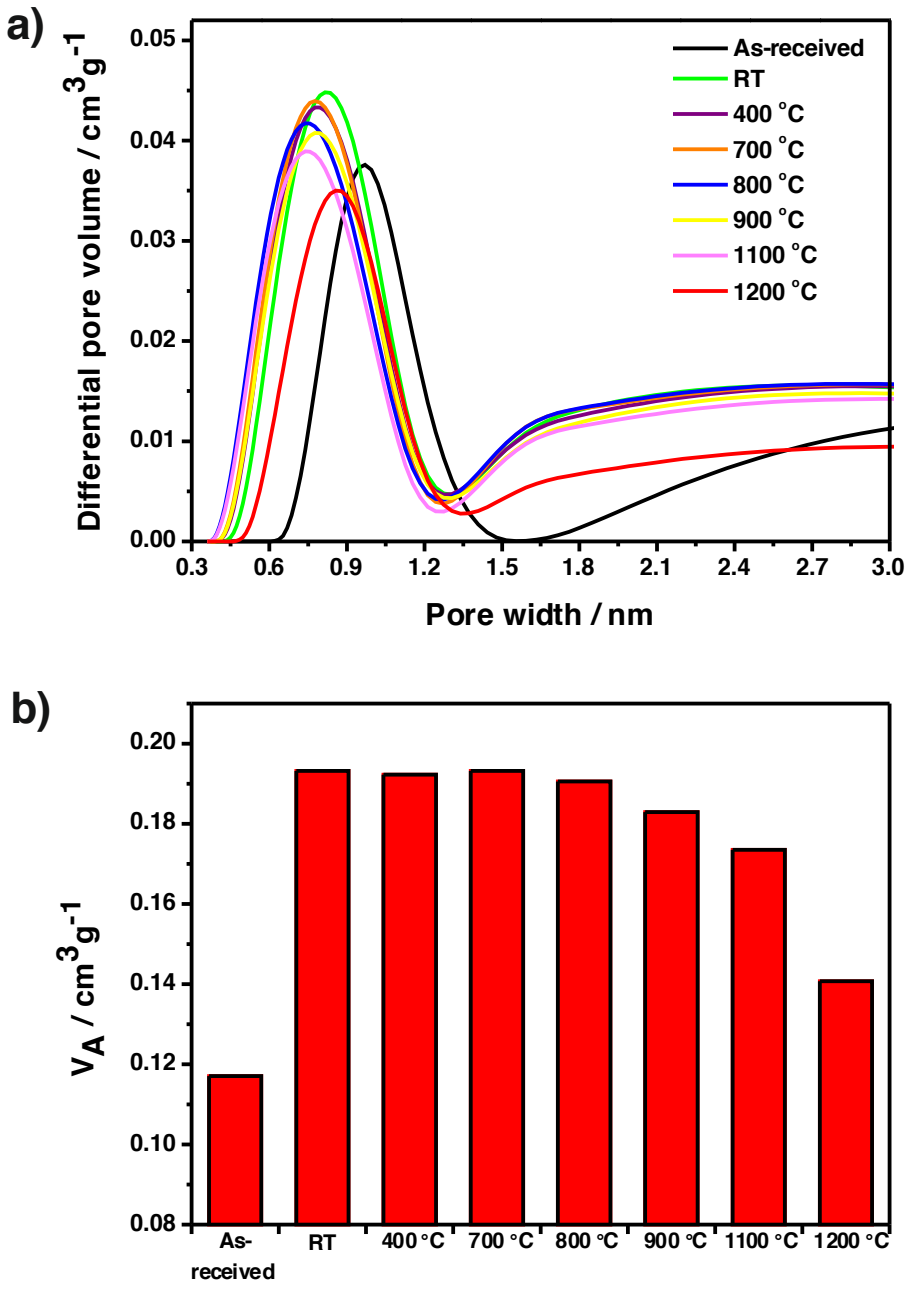

Figure 5.16. a) NLDFT calculations of differential pore volume up to 3 nm and b) accumulated pore volume (V_A) histogram up to 1.25 nm of as-received SWCNTs, purified (RT), and thermally annealed samples (after purification) at 400 °C, 700 °C, 800 °C, 900 °C, 1100 °C and 1200 °C.

NLDFT model was used to describe the distribution of the pores including two parameters: differential pore volume and pore width. According to the supplier, the average diameter of the as-received carbon nanotubes was 2.1 nm, so we calculated the pore size distribution in the range of 0.3 nm to 3 nm. In this area majority of pores are concentrated between 0.3 nm and 1.25 nm. The differential pore volume of purified SWCNTs (RT) is higher than for as-received material, and decreases for samples annealed at 800 °C and 1200 °C. This is in agreement with the end-closing of SWCNTs at high temperatures. It is worth noting that even after annealing the samples at 1200 °C, V_A presents a higher value than as-received material. This can imply that even after annealing at 1200 °C some of SWCNTs remain opened. We did not explore temperatures higher than 1200 °C to avoid recrystallization of the silica tubes employed for annealing experiments.

Both, NLDFT pore volume and BET surface data (Table 5.3) follow a similar trend. Nitrogen adsorption increases after purification (end-opening) and decreases after annealing samples at 800 °C and 1200 °C indicating a decreasing amount of accessible surface due to the formation of caps at the ends of SWCNTs.

Table 5.3. Descriptive analysis of the specific surface area and pore volume of as-received , purified (RT), and annealed samples (after purification) calculated using BET and DFT models from nitrogen adsorption.

Sample	S_{BET} (m^2g^{-1})	V_A (cm^2g^{-1})
As-received	791	0.12
RT	1246	0.19
400 °C	1263	0.19
700 °C	1285	0.19
800 °C	1275	0.19
900 °C	1196	0.18
1100 °C	1157	0.17
1200 °C	830	0.14

S_{BET} - specific surface area, V_A – accumulated pore volume up to 1.25 nm.

Raman spectroscopy (Fig. 5.17) did not reveal significant differences between the different analyzed samples. The I_D/I_G ratio is similar in all cases in the range of 0.11 and 0.14. This suggests that annealing does not alter the tubular structure of the nanotubes. Since SWCNTs have a high aspect ratio the closure of the SWCNTs ends is not detected by Raman spectroscopy.

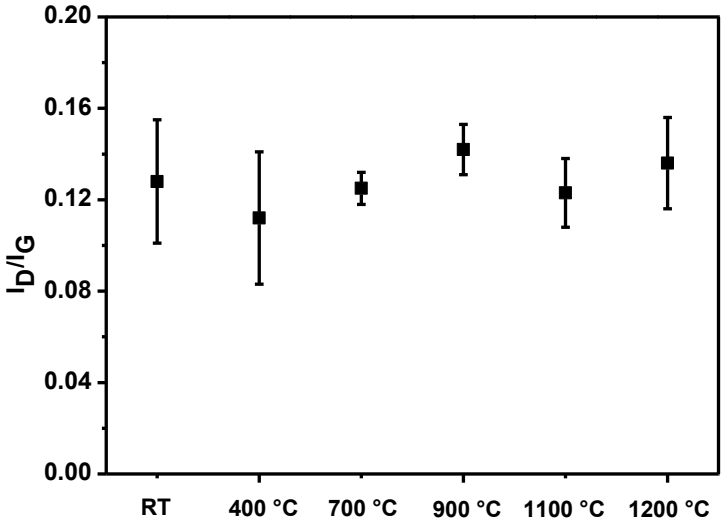

Figure 5.17. I_D/I_G ratio of purified (RT) and and thermally annealed SWCNTs (after purification) at 400 °C, 700 °C, 900 °C, 1100 °C and 1200 °C. Each value is an average based on three measurements. CNTs were excited using a 532 nm laser wavelength.

Thermogravimetric analysis (TGA) of the different samples was performed under flowing air. As it can be seen in Figure 5.18, the steam and HCl treated sample (RT) presents a higher thermal stability than the as-received material. As we already discussed in Chapter 3 this is due to the removal of the amorphous carbon and catalytic nanoparticles from the sample. Whereas amorphous carbon is more easily combusted than SWCNTs, the presence of metal catalyst nanoparticles is known to decrease the onset of combustion.[49] By having a close look at the TGA curve of the as-received material (inset in Fig. 5.18) it is possible to discern two thermal events; one corresponding to combustion of amorphous carbon at ca. 400 °C and the other corresponding to the combustion of SWCNTs (onset at 546 °C). The presence of catalytic particles also leads to a higher residue after the complete combustion of the carbonaceous material. The initial amount of impurities present in the sample of as-received SWCNTs was 4.6 wt. % (solid

residue at 880 °C). After purification it decreases to about 1.3 wt. %. The thermally annealed samples present a slightly higher onset of combustion than the purified material. Although no major differences are visible, the observed trend is that the higher the annealing temperature the higher the onset of combustion. The highest onset of combustion is presented by the sample annealed at 1200 °C (613 °C).

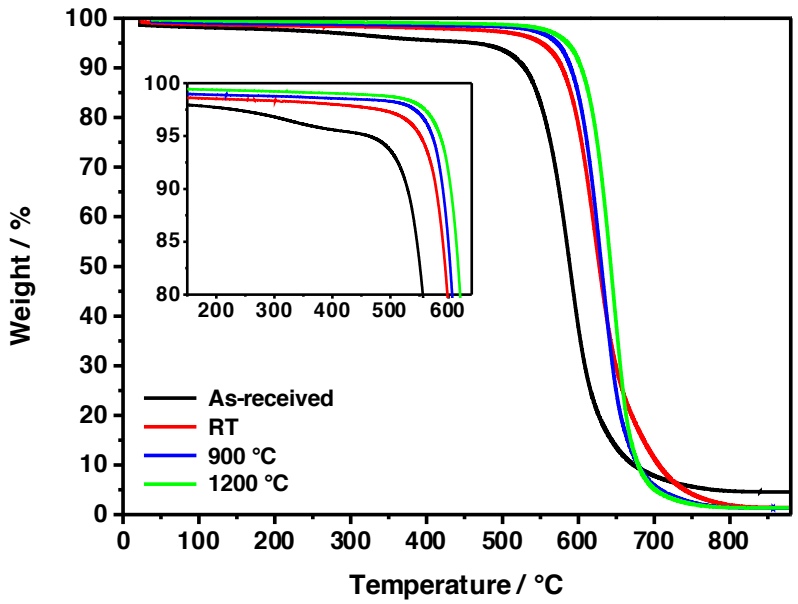

Figure 5.18. Thermogravimetric analyses of empty of as-received, purified (RT), and annealed SWCNTs (after purification) at 900 °C and 1200 °C. Measurements were performed under flowing air.

To complete this study we prepared several samples of SWCNTs filled with europium chloride ($EuCl_3$) from molten phase at different temperatures. Three temperatures: 700 °C, 900 °C and 1200 °C were selected to perform the filling experiments. All of them above the melting point of chosen payload, which is 632 °C.[26]

The $EuCl_3$@SWCNTs were analyzed by TGA under flowing air (Fig. 5.19) During the TGA of $EuCl_3$@CNTs carbon is oxidized to $CO_{2(g)}$. Thus, the remaining solid residues correspond to Eu_2O_3 obtained by oxidation of the encapsulated $EuCl_3$. The amount of residue increases with the temperature used for the filling process indicating higher amount of encapsulated material. We employed the formula reported by Ballesteros et al.[33] to calculate the filling yield of each sample from TGA residues (see Annex A.1), which turned out to be 3.1 wt. %,

7.3 wt. % and 11.8 wt. % for the filling conducted at 700 °C, 900 °C and 1200 °C, respectively. The sample prepared at the highest temperature is characterized by the highest filling yield. This is in agreement with the fact that at the highest employed temperature a higher amount of closed-ended SWCNTs are obtained (as per N_2 adsorption analysis). Based on these results we can conclude that the filling yield is temperature dependent, i.e. by controlling the temperature of the melt filling process the amount of encapsulated payload can also be controlled.

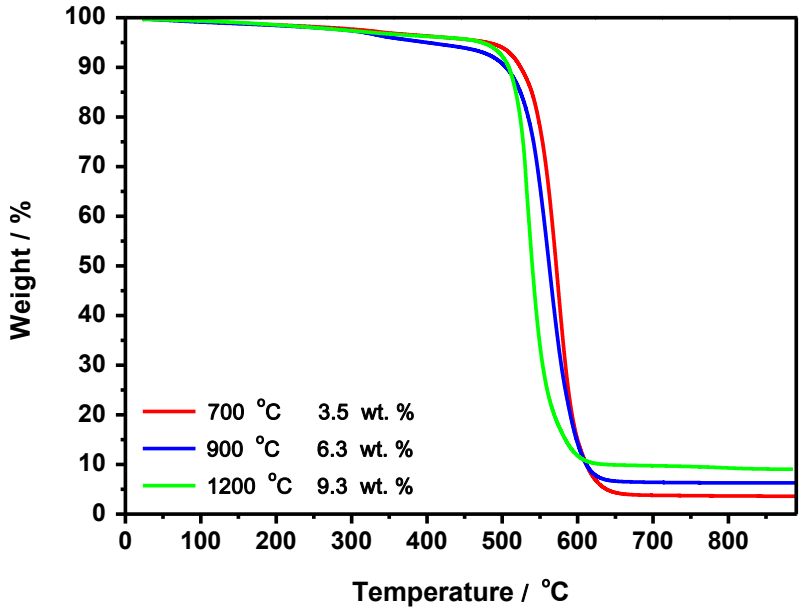

Figure 5.19. Thermogravimetric analyses of purified SWCNTs filled with $EuCl_3$ at selected temperatures: 700 °C, 900 °C and 1200 °C. Measurements were performed under flowing air.

To provide direct evidence on the encapsulation of $EuCl_3$ inside SWCNTs, the samples were characterized by means of electron microscopy techniques. To get first glimpse on the filling and the cleanness of the prepared nanocapsules scanning electron microscopy in transmission mode was used (Fig. 5.20a). High angle annular dark field images were obtained by using a specially adapted detector. This operating mode was selected for this purpose because as mentioned the contrast formation of the image is proportional to the atomic number of the elements present. Thus, europium chloride filling appears as bright lines following the shape of carbon nanotubes, which appear much dimmer. To get insights into the crystallinity of the filling and to be able to check whether the tips of SWCNTs were closed, we used high resolution transmission electron microscopy (TEM) since

the resolution of SEM is too low for this purpose. In Figure 5.20b we observe bundles of carbon nanotubes with a double-walled carbon nanotube clearly filled with crystalline nanowires of $EuCl_3$ at the center of the image. It is worth noticing that the end of the nanotube is closed, thus preventing leakage of the encapsulated payload. Energy Dispersive X-Ray Spectroscopy confirmed the presence of Eu and Cl in the sample (Fig. 5.20c). The copper peaks arise from the support grid employed for the analysis of the sample, which also contribute to the C peak.

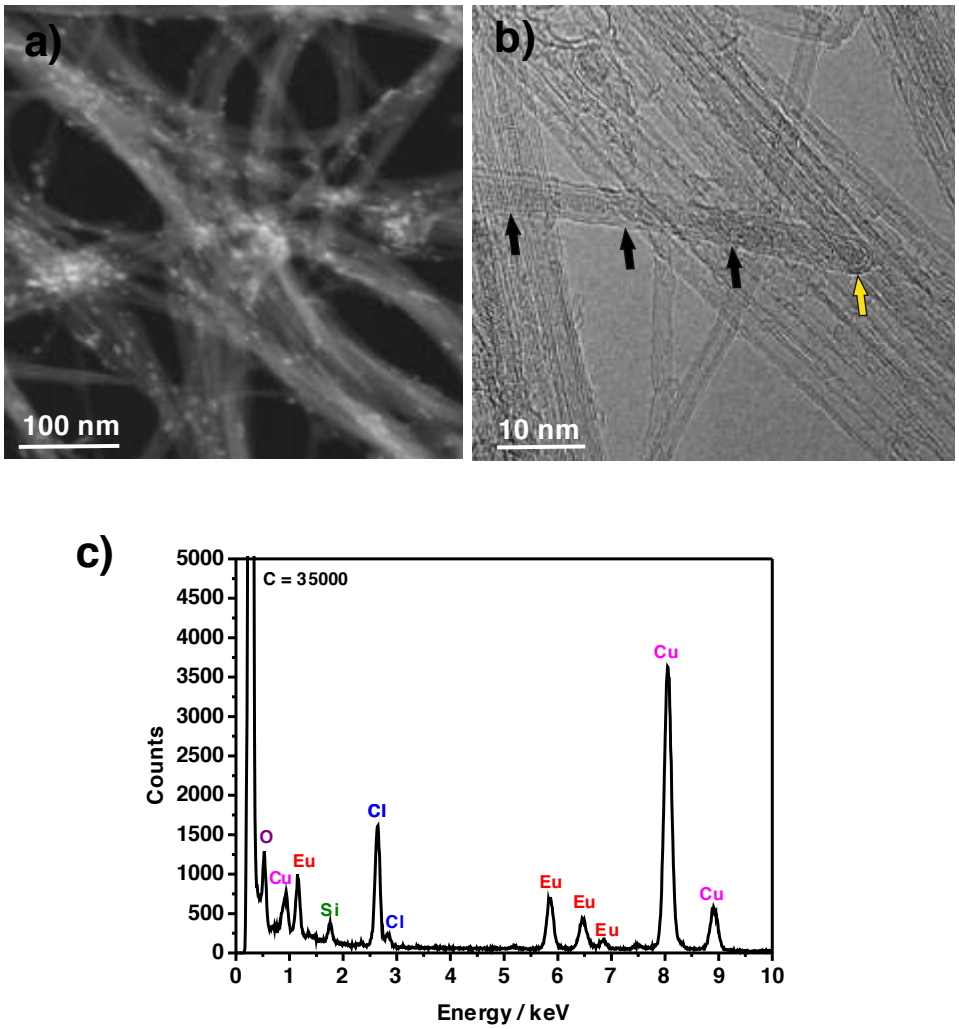

Figure 5.20. Electron microscopy images and EDX spectroscopy of $EuCl_3$@SWCNTs: a) SEM image of purified and filled carbon nanotubes in HAADF-STEM mode, b) HR-TEM image of a double-walled carbon nanotube filled with crystalline $EuCl_3$ (indicated by black arrows) showing its closed end (indicated by a yellow arrow), c) EDX spectrum of the sample confirming the presence of Eu and Cl (the carbon peak maximum was cut down for better visibility of lower intensity peaks).

5.5. Conclusions

CVD and arc discharge CNTs have been successfully filled with several payloads by high temperature melt filling. We observed the formation of lutetium halide nanowires and nanotubes inside CVD SWCNTs. To our best knowledge, the synthesis of lutetium halide nanotubes has not been reported so far. Employment of the inner cavities of carbon nanotubes as hosting templates opens up exciting horizons for the preparation of novel layered nanostructures and nanomaterials that have been difficult to synthesize by conventional bulk-scale reactions.

We have developed a sustainable system to process samples of filled SWCNTs with poor water soluble materials. The green protocol allows a 95 % reduction in water waste, which could for instance be contaminated with hazardous heavy (radioactive) elements. When developing nanocapsules for theranostics applications the proposed methodology benefits from a synergistic combination of both Soxhlet and dialysis. It allows an efficient removal of the large excess of non-encapsulated material present after filling carbon nanotubes. The methodology holds special interest for the manipulation of radioactive systems where reduction of the residual waste is a must, but can be employed for the external removal of other payloads. A quick *on-site* assessment for the proper removal of external salts has been carried out by visual inspection of the filtrate, avoiding the consumption of sample in the process. $LuCl_3$@SWCNTs has been the material of choice since the radioactive isotope ^{177}Lu is clinically employed in oncology. An efficient removal of $LuCl_3$ remaining on the exterior of SWCNTs after its encapsulation has been achieved while preserving the encapsulated payload and structural integrity of the SWCNTs. We foresee the use of such optimized purification protocol as a path towards the production of high-quality filled SWCNTs, exclusively endohedral, to be employed not only in the biomedical field but also in other applications where the presence of non-encapsulated material can be detrimental.

To complete the study, we investigated the effect of temperature on the degree of end-closing and filling of SWCNTs. Nitrogen adsorption studies show that the specific surface area of carbon nanotubes increases after purification when the pores of carbon nanotubes are unblocked. In the range between 800 °C and 1200 °C the specific surface area and the pore volume decreases, which is associated with the progressive end-closure of SWCNTs. Thermal annealing does

not affect the purity and structure of carbon nanotubes. However, according to TGA the annealed samples show a higher thermal stability than as-received SWCNTs. We successfully demonstrated, using $EuCl_3$@CNTs as an example, that the use of high temperatures has a positive effect on the filling yield from molten phase. The filling yield is correlated with the fraction of closed-ended CNTs, i.e. the more nanotubes have closed tips, the lowest the probability of washing out th encapsulated payload. In summary, by controlling the temperature we may modify the fraction of closed-ended CNTs and their filling yield.

REFERENCES

1. Shao, L., et al., *A Simple Method for the Containment and Purification of Filled Open-Ended Single Wall Carbon Nanotubes Using C_{60} Molecules.* Chemistry Communications, 2008(18): p. 2164-2166.
2. Tobias, G., Ballesteros, B., Green, M.L.H., *Carbon Nanocapsules: Blocking Materials Inside Carbon Nanotubes.* Physica Status Solidi C, 2010. **7**(11-12): p. 2739-2742.
3. Shao, L., et al., *Reversible Filling of Single Walled Carbon Nanotubes Opened by Alkali Hydroxides.* Carbon, 2006. **44**(13): p. 2855-2858.
4. Cabana, L., et al., *Carbon Nanotubes: Synthesis of PbI_2 Single-Layered Inorganic Nanotubes Encapsulated Within Carbon Nanotubes.* Advanced Materials, 2014. **26**(13): p. 2108-2108.
5. Liu, Q., et al., *Nanowires Sheathed Inside Nanotubes: Manipulation, Properties and Applications.* Progress in Materials Science, 2015. **70**: p. 1-49.
6. Ariga, K., et al., *Forming Nanomaterials as Layered Functional Structures Toward Materials Nanoarchitectonics.* NPG Asia Materials, 2012. **4**: p. e17.
7. Chuvilin, A., et al., *Self-assembly of a Sulphur-Terminated Graphene Nanoribbon Within a Single-Walled Carbon Nanotube.* Nature Materials, 2011. **10**(9): p. 687-692.
8. Nakanishi, R., et al., *Thin Single-Wall BN-Nanotubes Formed Inside Carbon Nanotubes.* Scientific Reports, 2013. **3**: p. 1385.
9. Marega, R., Bonifazi, D., *Filling Carbon Nanotubes for Nanobiotechnological Applications.* New Journal of Chemistry, 2014. **38**(1): p. 22-27.
10. Martincic, M., Tobias, G., *Filled Carbon Nanotubes in Biomedical Imaging and Drug Delivery.* Expert Opinion on Drug Delivery, 2015. **12**(4): p. 563-581.
11. Hong, S.Y., et al., *Filled and Glycosylated -Carbon Nanotubes for In Vivo Radioemitter Localization and Imaging.* Nature Materials, 2010. **9**(6): p. 485-490.

12. Strano, M.S., *Biomedical Materials: Nanoscale Radiosurgery.* Nature Materials, 2010. **9**(6): p. 467-468.
13. Spinato, C., et al., *Design of Antibody-Functionalized Carbon Nanotubes Filled with Radioactivable Metals Towards a Targeted Anticancer Therapy.* Nanoscale, 2016.
14. Lyra, M.E., et al., *Radionuclides Used in Nuclear Medicine Therapy - From Production to Dosimetry.* Current Medical Imaging Reviews, 2013. **9**(1): p. 51-75.
15. Sharipov, G.L., Gainetdinov, R.K., Abdrakhmanov, A.M., *Multibubble Sonoluminescence of Europium(III) Chloride in Heavy Water.* Russian Chemical Bulletin, 2008. **57**(9): p. 1827-1830.
16. Breen, P.J., Horrocks, W.D., *Europium(III) Luminescence Excitation Spectroscopy. Inner-Sphere Complexation of Europium(III) by Chloride, Thiocyanate, and Nitrate Ions.* Inorganic Chemistry, 1983. **22**(3): p. 536-540.
17. Yao, M., Chen, W., *Hypersensitive Luminescence of Eu^{3+} in Dimethyl Sulfoxide As a New Probing for Water Measurement.* Analytical Chemistry, 2011. **83**(6): p. 1879-1882.
18. Song, B., et al., *A Europium(III)-Based PARACEST Agent for Sensing Singlet Oxygen by MRI.* Dalton transactions, 2013. **42**(22): p. 8066-8069.
19. Karimi, M., et al., *Carbon Nanotubes Part II: A Remarkable Carrier for Drug and Gene Delivery.* Expert Opinion on Drug Delivery, 2015. **12**(7): p. 1089-1105.
20. Zhang, S., et al., *A Novel Europium(III)-Based MRI Contrast Agent.* Journal of the American Chemical Society, 2001. **123**(7): p. 1517-1518.
21. Ballesteros, B., et al., *Steam Purification for the Removal of Graphitic Shells Coating Catalytic Particles and the Shortening of Single-Walled Carbon Nanotubes.* Small, 2008. **4**(9): p. 1501-1506.
22. Tobias, G., et al., *Purification and Opening of Carbon Nanotubes Using Steam.* The Journal of Physical Chemistry B, 2006. **110**(45): p. 22318-22322.
23. De Jongh, P.E., Eggenhuisen, T.M., *Melt Infiltration: an Emerging Technique for the Preparation of Novel Functional Nanostructured Materials.* Advanced Materials, 2013. **25**(46): p. 6672-6690.
24. Xu, C., et al., *1D Lanthanide Halide Crystals Inserted Into Single-Walled Carbon Nanotubes.* Chemistry Communications, 2000(24): p. 2427-2428.
25. Brown, G., et al., *High Yield Incorporation and Washing Properties of Halides Incorporated into Single Walled Carbon Nanotubes.* Applied Physics A, 2003. **76**(4): p. 457-462.
26. Hammond, C.R., *Physical Constants of Inorganic Compounds*, in *Handbook of Chemistry and Physics*, Linde, D.R., Editor. 2004, CRC Press. p. **4**-57.
27. Zhou, W., et al., *Charge Transfer and Fermi Level Shift in p-doped Single-Walled Carbon Nanotubes.* Physical Review B, 2005. **71**(20): p. 205423.

28. Fu, Q., et al., *Selective Filling of Carbon Nanotubes with Metals by Selective Washing.* New Carbon Materials, 2008. **23**(1): p. 17-20.
29. Cook, J., et al., *Purification of Rhodium-Filled Carbon Nanotubes Using Reversed Micelles.* Chemical Communications, 1996(23): p. 2673-2674.
30. Martincic, M., et al., *Quantitative Monitoring of the Removal of Non-Encapsulated Material External to Filled Carbon Nanotube Samples.* Physical Chemistry Chemical Physics, 2015. **17**: p. 31662-31669.
31. Sloan, J., et al., *Direct Imaging of the Structure, Relaxation, and Sterically Constrained Motion of Encapsulated Tungsten Polyoxometalate Lindqvist Ions within Carbon Nanotubes.* ACS Nano, 2008. **2**(5): p. 966-976.
32. Fidiani, E., et al., *Magnetically Active and Coated Gadolinium-Filled Carbon Nanotubes.* The Journal of Physical Chemistry C, 2013. **117**(32): p. 16725-16733.
33. Ballesteros, B.n., et al., *Quantitative Assessment of the Amount of Material Encapsulated in Filled Carbon Nanotubes.* The Journal of Physical Chemistry C, 2009. **113**(7): p. 2653-2656.
34. Cattrall, R.W. and S.J.E. Slater, *The Spectrophotometric Determination of Europium(III) Using Chrome Azurol S.* Microchemistry Journal, 1971. **16**(4): p. 602-609.
35. Nishida, H., *Spectrophotometric Determination of Titanium with Chromazurol S and Hydrogen Peroxide.* Bunseki Kagaku, 1970. **19**(1): p. 30-33.
36. Diaz, E., et al., *Purification of Single-Wall Carbon Nanotubes by Functionalization and Ultracentrifugation.* Asian Journal of Chemistry, 2013. **25**: p. S17-S21.
37. Ren, X., et al., *Carbon Nanotubes as Adsorbents in Environmental Pollution Management: A Review.* Chemical Engineering Journal, 2011. **170**(2–3): p. 395-410.
38. Rawat, D.S., M.M. Calbi, and A.D. Migone, *Equilibration Time: Kinetics of Gas Adsorption on Closed- and Open-Ended Single-Walled Carbon Nanotubes.* The Journal of Physical Chemistry C, 2007. **111**(35): p. 12980-12986.
39. Wiśniewski, M., et al., *Detecting Adsorption Space in Carbon Nanotubes by Benzene Uptake.* Journal of Colloid and Interface Science, 2013. **391**: p. 74-85.
40. M. Maryam, et al., *BET Analysis on Carbon Nanotubes: Comparison Between Single and Double Stage Thermal CVD Method* Advanced Materials Research, 2013. **626**: p. 289-293
41. Birch, M.E., et al., *Properties that Influence the Specific Surface Areas of Carbon Nanotubes and Nanofibers.* Annals of Occupational Hygiene, 2013.
42. Landers, J., Gor, G.Y., Neimark, A.V., *Density Functional Theory Methods for Characterization of Porous Materials.* Colloids and Surfaces A: Physicochemical and Engineering Aspects, 2013. **437**: p. 3-32.

43. Lafi, L., Cossement, D., Chahine, R., *Raman Spectroscopy and Nitrogen Vapour Adsorption for the Study of Structural Changes During Purification of Single-Wall Carbon Nanotubes.* Carbon, 2005. **43**(7): p. 1347-1357.
44. Agnihotri, S., Rostam Abadi, M., Rood, M., *Temporal Changes in Nitrogen Adsorption Properties of Single-Walled Carbon Nanotubes.* Carbon, 2004. **42**(12-13): p. 2699-2710.
45. Furmaniak, S., et al., *Simple Model of Adsorption on External Surface of Carbon Nanotubes—a New Analytical Approach Basing on Molecular Simulation Sata.* Adsorption, 2010. **16**(4-5): p. 197-213.
46. Byl, O., Liu, J., Yates Jr, J.T., *Characterization of Single Wall Carbon Nanotubes by Nonane Preadsorption.* Carbon, 2006. **44**(10): p. 2039-2044.
47. Arai, M., et al., *Pore Characterization of Assembly-Structure Controlled Single Wall Carbon Nanotube.* Adsorption, 2007. **13**(5-6): p. 509-514.
48. Thommes, M., et al., *Physisorption of Gases, with Special Reference to the Evaluation of Surface Area and Pore Size Sistribution (IUPAC Technical Report)*, in *Pure and Applied Chemistry*. 2015. p. 1051.
49. Cabana, L., et al., *The Role of Steam Treatment on the Structure, Purity and Length Distribution of Multi-Walled Carbon Nanotubes.* Carbon, 2015. **93**: p. 1059-1067.

CHAPTER 6

COVALENT FUNCTIONALIZATION OF SINGLE-WALLED CARBON NANOTUBES

The functionalization of CNTs is indispensable for their use as diagnostic and therapeutic vectors in the biomedical field, because pristine nanotubes show very limited dispersibility in common solvents. Various chemical modifications have been proposed to enable manufacturing carbon nanotubes more compatible in physiological conditions. Pre-functionalized CNTs are suitable for further conjugation with different therapeutic and/or targeting agents.[1, 2]

Among commonly used functionalization methods the radical addition via diazonium salt (Tour reaction) is one of the most versatile and easily scalable. The extent of modification varies depending on the type of aryl diazonium salt used.[3] However, during prolonged reactions undesired processes might occur, including polymerization and solvent addition.[4] Usually, the mechanism of Tour reaction involves an electron injection from CNT to aryl diazonium and formation of an aryl radical, which binds with sidewalls of the carbon nanotube forming a stable covalent bond.[3, 5, 6] Metallic CNTs have higher electron density, thus show higher reactivity towards Tour reaction. This allows that under selective controlled conditions metallic and semiconducting SWCNTs can be separated.[7, 8] Diazonium salts can be used directly[11] or formed *in situ* by mixing aniline and isoamyl nitrite (or sodium nitrite) with CNTs in a solvent-free reaction[10, 13] or in solution using either organic solvents[9, 11] or oleum[14]. Direct reaction can be efficient at moderate or room temperature, and the activation of the reaction can be either thermal[9, 10] or electrochemical.[11, 12] On the other hand, *in situ* generation of the diazonium species avoids the necessity of isolating light-sensitive aryl diazonium salts.[9]

Cycloadditions also find wide interest in the functionalization of CNTs. In particular, 1,3-dipolar cycloaddition (Prato reaction) render CNTs remarkably soluble in most organic solvents and even in water.[15, 16] Prato reaction is an *in situ* thermal condensation of an α-amino acid and an aldehyde, forming pyrrolidine rings fused to sp^2-carbon. The functionalization occurs both on the tips

and sidewalls and it is reversible. [3, 17, 18] Various biomolecules and radionuclides have been attached on amino-modified CNTs. [2, 19]

In this chapter the functionalization of empty and metal halide filled SWCNTs has been explored. We compared reactivity of CNTs towards radical addition via diazonium salts and 1,3-dipolar cycloaddition.

6.1. Experimental conditions for the radical addition via diazonium salt (Tour reaction)

6.1.1. Tour reaction with 4-[2-(Boc-amino)methyl]aniline

The reaction was performed using 4-[2-(Boc-amino)methyl]aniline (Sigma Aldrich) as a reagent (Scheme 6.1). SWCNTs (0.83 mmol, 1 eq) were dispersed in dimethylformamide (DMF, 1 mg/mL) by sonication for 5 min. Then, 4-[2-(Boc-amino)ethyl]aniline (1.15 mmol) was added and the mixture was dispersed for another 3 min. Next, isopentyl nitrite (2.30 mmol) was added and the reaction mixture was heated up to 80 °C and stirring was continued for 2 h. The mixture was cooled to room temperature. CNTs were filtered on teflon membrane (MILIPORE®, type JHWP, pore size 0.45 µm) and washed with DMF until the solvent eluted colorless, washed again with DMF, water, methanol (MeOH), ethyl acetate (EtOAc), diethyl ether (Et_2O) and dried under vacuum.

In the case of filled SWCNTs the protocol was the same. In this case, 1 eq corresponds only to the carbon mass of samples. Thus, the mass of filled carbon nanotubes employed to the reaction was recalculated taking into account filling yield of the samples.

All the solvents used for the synthesis were of analytical grade.

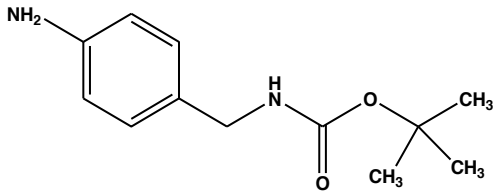

Scheme 6.1. 4-[2-(Boc-amino)methyl]aniline, Boc = *tert*-butoxycarbonyl.

6.1.2. Cleavage of Boc protecting groups

The Boc protecting groups of the 4-[2-(Boc-amino)methyl]aniline were cleaved by treatment with solution of 4 M HCl in dioxane (1 mg/mL) for overnight (12 h) at room temperature. After reaction functionalized CNTs were dispersed in water, and filtered and washed till neutral pH. Then CNTs were redispersed in DMF, filtered, and washed with water, MeOH, Et_2O, and dried under vacuum.

6.2. 1,3-dipolar cycloaddition of azomethine ylides (Prato reaction)

6.2.1. Synthesis of aminoacid

The aminoacid (AA) was synthesized form commercially available 2,2'-(ethylenedioxy)bis(ethylamine) (Sigma Aldrich) in five steps. The synthesis was inspired by the protocol of Kondratos and coworkers.[20] However, in the second step phthalic anhydride was used as protection group instead of di-tert-butyl dicarbonate (Boc_2O). As a consequence, the conditions in all the intermediate steps vary. Time and temperature of reactions were also optimized.

6.2.1.1. Synthesis of N-Boc amine: N-tert-butoxycarbonyl-2,2'-(ethylenedioxy)bis(ethylamine)

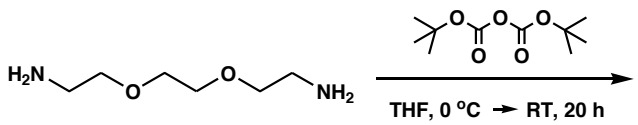

1.

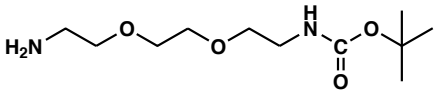

2.

Scheme 6.2. Synthesis of N-Boc amine.

2,2'-(ethylenedioxy)bis(ethylamine) (**1**) (50.0 g, 340 mmol) was dissolved in dry tetrahydrofuran (THF, 120 mL). A solution of di-tert-butyl dicarbonate (9.8 g, 45 mmol) in dry THF (120 mL) was slowly added over 40 min at 0 ˚C to the first mixture. The reaction was stirred for 21 h at room temperature (RT). Then it was concentrated in vacuum in a rotary evaporator leading to the formation of white slurry, which was re-dissolved in water (200 mL) and filtered to remove the white precipitate. The aqueous layer was extracted with DCM (200 mL x 3). The combined organic layer was backwashed with water (80 mL), then dried with Na_2SO_4, filtered and concentrated in vacuum. The residue was purified by flash column chromatography using dichloromethane: methanol (DCM/MeOH, 1:0, 1:1) to afford the product **2**, colorless viscous oil.

$C_{11}H_{24}N_2O_4$ (M.W. 248.32): yield 4% (3.3 g, 13 mmol)

^{1}H-NMR (270 MHz, $CDCl_3$) δ (ppm): 5.21 (*br*, 1H), 3.59-2.84 (*m*, 12H), 2.03 (*s*, 2H), 1.43 (*s*, 9H)

6.2.1.2. Synthesis of NBocNPht amine: tert-butyl(2-(2-(2-(1,3-dioxoisoindolin-2-yl)ethoxy)ethoxy)ethyl)carbamate

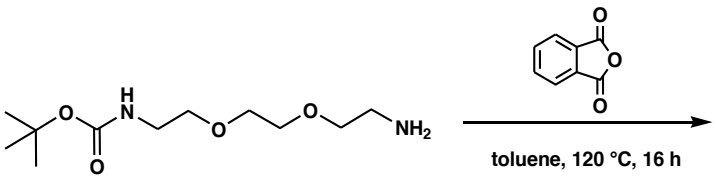

2.

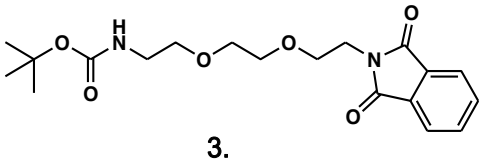

3.

Scheme 6.3. Synthesis of NBocNPht amine.

A toluene solution (110 mL) of tert-butyl(2-(2-(2-aminoethoxy) ethoxy)ethyl)carbamate (3.3 g, 13 mmol) and phthalic anhydride (1.93 g, 13 mmol) was stirred at 120 ˚C overnight. The solvent was removed under reduced pressure.

Product **3** was purified by flash chromatography using toluene: acetone (AcO) 10:3, affording golden oil.

$C_{19}H_{26}N_2O_6$ (M.W. 378.42): yield 100% (4.91 g, 13 mmol)

^{1}H-NMR (270 MHz, $CDCl_3$) δ (ppm): 7.86 (*m*, 2H), 7.76 (*m*, 2H), 5.08 (*br*, 1H), 3.60-3.20 (*m*, 12H), 1.47 (*s*, 9H)

6.2.1.3. Synthesis of NH2NPht amine: 2-(2-(2-(1,3-dioxoisoindolin-2-yl)ethoxy)ethoxy)ethanaminium

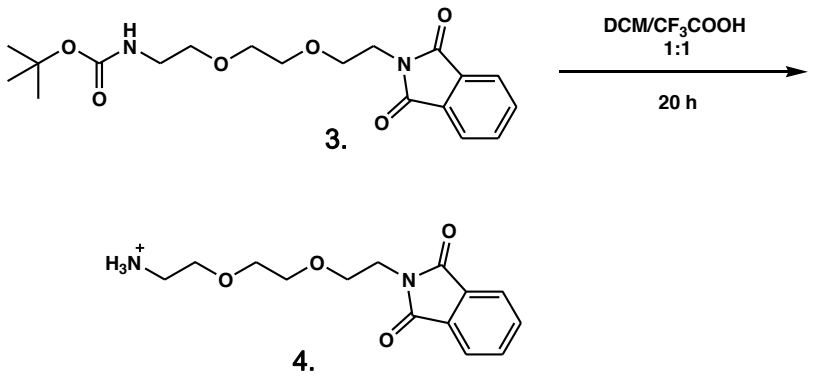

Scheme 6.4. Synthesis of NH_2NPht amine.

Compound **3** (3.2 g, 8.46 mmol) was dissolved in 15 mL of DCM and cooled down to 0 ˚C in an ice bath. Then 15 mL of trifluoroacetic acid (TFA) were added drop wise. The solution was warmed to room temperature and stirred for 24 h. After reaction solvent was evaporated. Product **4** was triturated few times with Et_2O and toluene in order to obtain white-brownish crystals, which were stored under vacuum.

$C_{14}H_{18}N_2O_4$ (M.W. 278.13): yield 97% (2.28 g, 8.20 mmol)

^{1}H-NMR (400 MHz, CD_3OD) δ (ppm): 7.85 (*m*, 2H), 7.83 (*m*, 2H), 3.89-3.20 (*m*, 12H)

6.2.1.4. Synthesis of NBenzacetateNPht

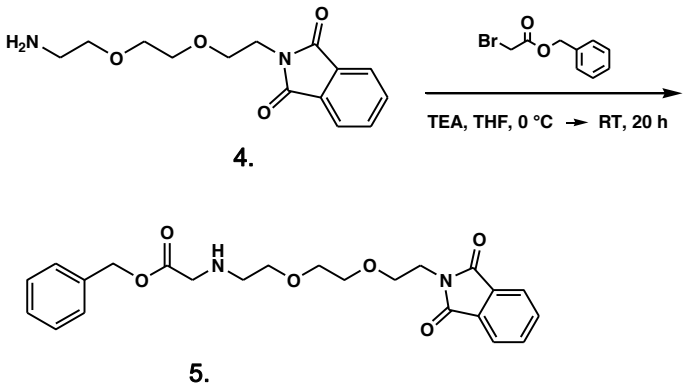

Scheme 6.5. Synthesis of NBenzacetateNPht.

Benzyl 2-bromoacetate (1.27 ml, 8.05 mmol) in THF (60 ml) was added dropwise to a solution of **4** (2.24 g, 8.05 mmol) and triethylamine (TEA, 1.35 mL, 9.66 mmol) in tetrahydrofuran (60 mL) cooled to 0 °C, over a period of 1.5 hours. The reaction mixture was allowed to warm to room temperature (RT) and stirred overnight. The solvent was removed under reduced pressure. The final product **5** was purified by flash chromatography in ethyl acetate: isopropanol (AcOEt/iPrOH, 9:1).

$C_{23}H_{26}N_2O_6$ (M.W. 426.18) yield: 86% (2.95 g, 6.92 mmol)

^{1}H-NMR (270 MHz, $CDCl_3$) δ (ppm): 7.62 (*m*, 2H), 7.49 (*m*, 2H), 7.16 (*s*, 5H), 4.95 (*s*, 2H), 3.8-2.7 (*m*, 14H), 2.1 (*br*, 1H)

6.2.1.5. Hydrogenolisis of NBenzacetateNPht

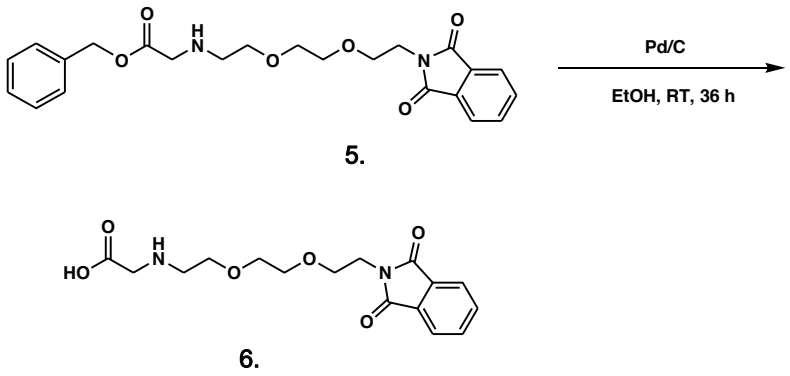

Scheme 6.6. Hydrogenolisis of NBenzacetateNPht.

Compound **5** (2.40 g, 5.63 mmol) was dissolved in methanol (90 mL). Then, Pd/C (10%, Acros) was added and the mixture was stirred under hydrogen for 24 hours. The catalyst was removed by filtration on celite and the solid was evaporated. After crystallization in AcOEt a white powder of α-aminoacid (AA) **6** was obtained.

$C_{16}H_{20}N_2O_6$ (M.W. 306.36), yield: 91% (1.56 g, 5.09 mmol)

ESI-MS: +MS: 337.1 (AA), 359.1 (AA + Na), -MS: 334.9 (AA – H), 362.8 (AA + K)

^{1}H NMR (270 MHz, CD_3OD) δ (ppm): 10.56 (*br*, 1H), 7.62 (*m*, 2H), 7.49 (*m*, 2H), 3.86-3.24 (*m*, 14H), 3.18 (*br*, 1H)

6.2.2. Functionalization with aminoacid

SWCNTs (10 mg, 1 eq) were added to *ortho*-DCB (10 mL) in a 50 mL flask and dispersed by sonication for 15 min. Then the AA (28 mg) and paraformaldehyde (15 mg) were added and dispersed by sonication for 5 min. The solution was stirred using a magnetic stirrer for 2 h at 180 ˚C. After this period of time the mixture was cooled to room temperature and dispersed by sonication for 10 min. This step was repeated 4 more times. In total 140 mg (0.42 mmol) of AA and 75 mg (2.49 mmol) of paraformaldehyde were added into the reactant mixture. Heating and stirring was continued up to 24 h. Then the resulting functionalized CNTs (f-CNTs) were filtered (membrane MILIPORE, type: JHWP, pore

size 0.45 µm) and washed up with DMF until the solvent eluted colorless, DMF + 10 % THF, Et_2O and dried at 40 ˚C.

In the case of filled SWCNTs the protocol was the same. In this case 1 eq corresponds only to carbon mass of the sample. Thus, the mass of filled carbon nanotubes employed for the reaction was recalculated taking into account the filling yield of the samples.

6.2.3. Deprotection of aminoacid

Functionalized CNTs with phthalimide protecting group (7 mg) were added to ethanol (7 mL) in a 50 mL flask and dispersed by sonication for 10 min. The hydrazine (50 mL) was added and the solution was stirred using a magnetic stirrer for 17 h at room temperature. Then the resulting deprotected f-CNTs were filtered (membrane MILIPORE, pore size 0.45 µm) and washed up with MeOH (2 x 100 mL), H_2O (100 mL), H_2O+ 1 drop of HCl (150 mL), H_2O (250 mL), AcOEt and dried at 40 ˚C.

6.3. Filling of SWCNTs with chosen payloads

As-received CVD SWCNTs (Elicarb®) were initially end-opened and purified with steam (4 h) and HCl, leading to carbon nanotube samples with a length of 420 nm. The protocol of purification and length measurements are available in Chapter 3. The content of inorganic residue was determined by thermogravimetric analysis (TGA) under flowing air.

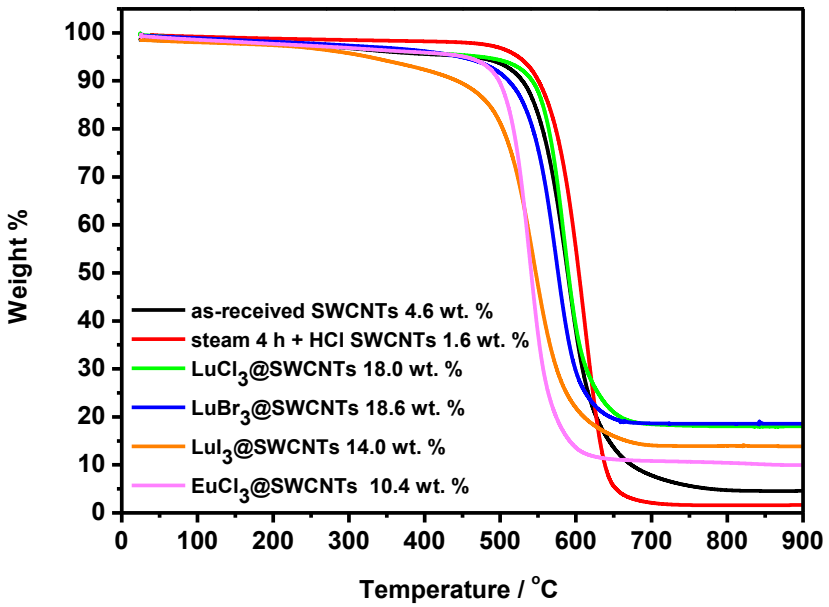

Figure 6.1. TGA under flowing air of as-received single-walled carbon nanotubes (SWCNTs), purified SWCNTs, $LuCl_3$@SWCNTs, $LuBr_3$@SWCNTs, LuI_3@SWCNTs and $EuCl_3$@SWCNTs.

The residue obtained after the complete oxidation of the sample decreased from 4.6 wt. % to 1.6 wt. % (Fig. 6.1). Besides, the steam purification also removes the amorphous carbon present in the samples enabling an efficient sidewall functionalization of CNTs.[21]

Melting filling was used in order to encapsulate metal halides (MX): lutetium (III) chloride, lutetium (III) bromide, lutetium (III) iodide and europium (III) chloride (Sigma Aldrich, anhydrous, 99.99% purity). An independent filling experiment was performed for each salt. MX was mixed with CNTs in a w/w ratio 10:1 and grinded with an agate mortar and pestle in an argon-filled glovebox. The mixture was sealed under vacuum inside a silica tube. The sample was then annealed in a horizontal furnace above the melting temperatures of the chosen payloads, in the range of 950 ˚C - 1100 ˚C during 12 h. By performing the filling experiments in this range of temperatures, the ends of the SWCNTs close on cooling, thus resulting in samples of closed-ended filled SWCNTs (see Section 1.7.2.3). Experimental details employed for the encapsulation of payloads are reported in Chapter 5. Next, filled closed-ended CNTs (MX@CNTs) were washed with hot water in order to remove external material. The filling yield of MX@CNTs

was calculated from TGA residues after the complete of oxidation samples in air (Fig 6.1) employing previously reported formula (see Annex A.1).[22] The filling yield turned out to be 23.8 wt. %, 36.6 wt. %, 35.8 wt. % and 13.3 wt. % for $LuCl_3$@SWCNTs, $LuBr_3$@SWCNTs, LuI_3@SWCNTs and $EuCl_3$@SWCNTs, respectively.

Samples were inspected by high resolution transmission electron microscopy (HRTEM, Fig. 6.2) in order to confirm the presence of filling material and lack of non-encapsulated metal halides external to the walls of CNTs. As it can be seen in the images the encapsulated metal halides can be easily discerned from the hosting carbon nanotubes. The formation of metal halide nanocrystals is observed in several images, where lattice fringes can be seen. Nanocrystals of different diameters are observed in agreement with the diameter distribution of the templating CNTs.

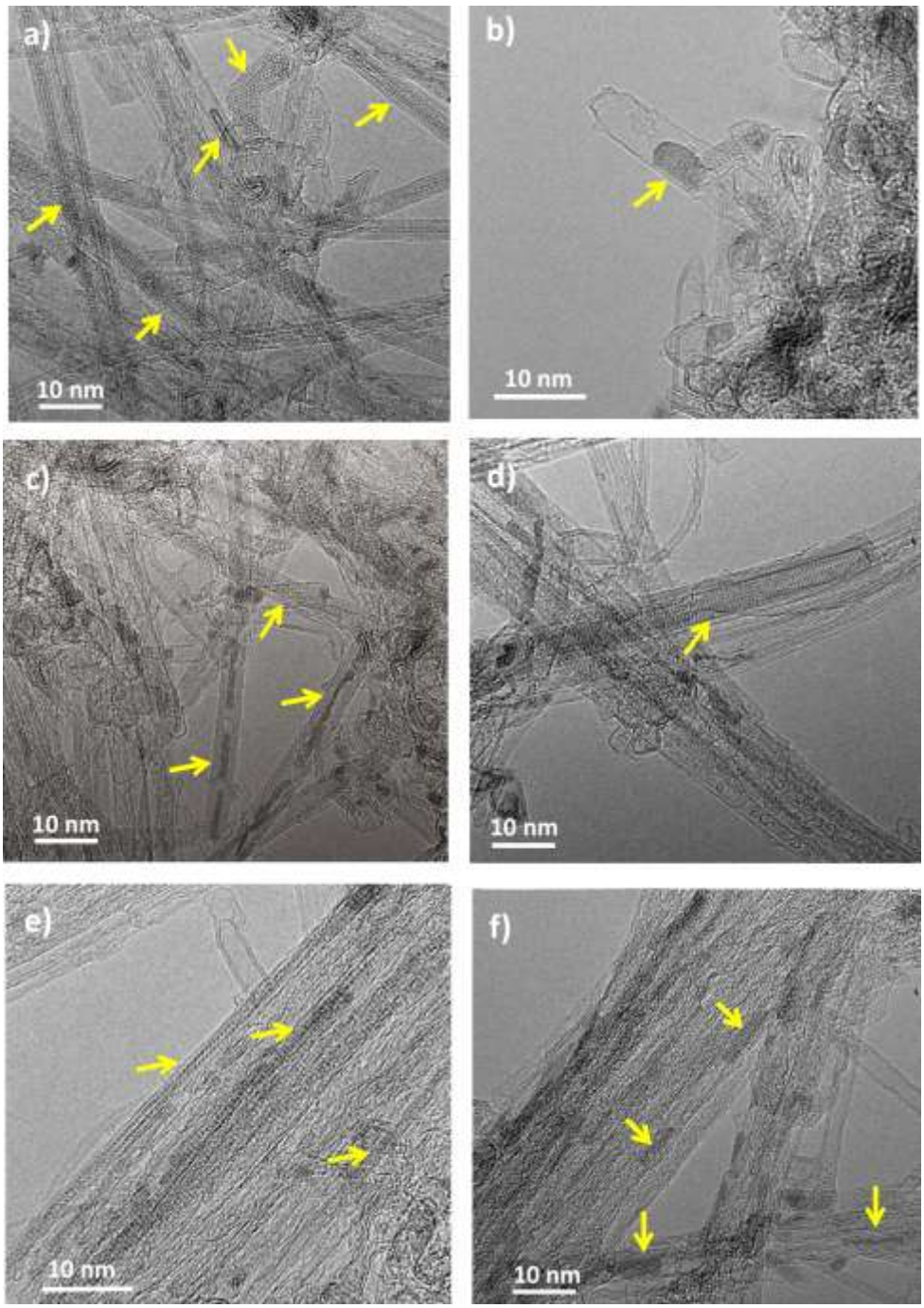

Figure 6.2. HRTEM images of a, b) $LuCl_3$@SWCNTs, c, d) $LuBr_3$@SWCNTs, e) LuI_3@SWCNTs, f) $EuCl_3$@SWCNTs. Yellow arrows point to encapsulated metal halides. Closed-ended CNTs are visible on pictures b-d).

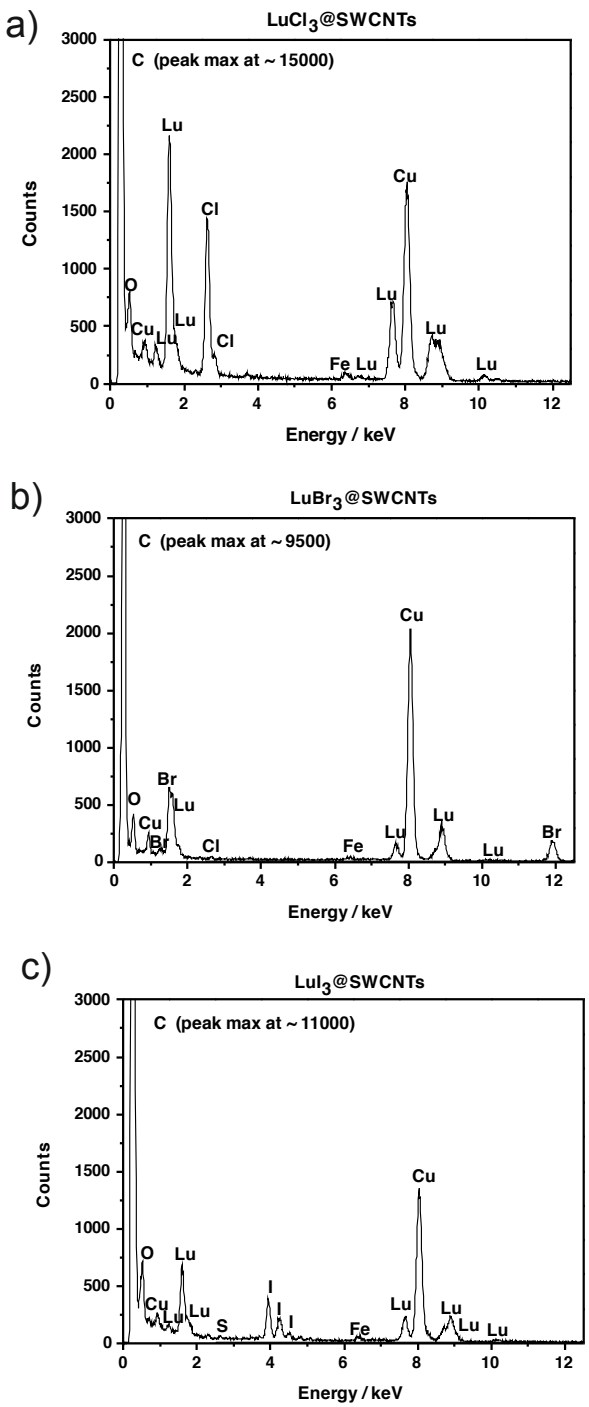

Figure 6.3. EDX analysis of lutetium halides filled SWCNTs: a) $LuCl_3$@SWCNTs, b) $LuBr_3$@SWCNTs, c) LuI_3@SWCNTs. The Cu peak arises from support.

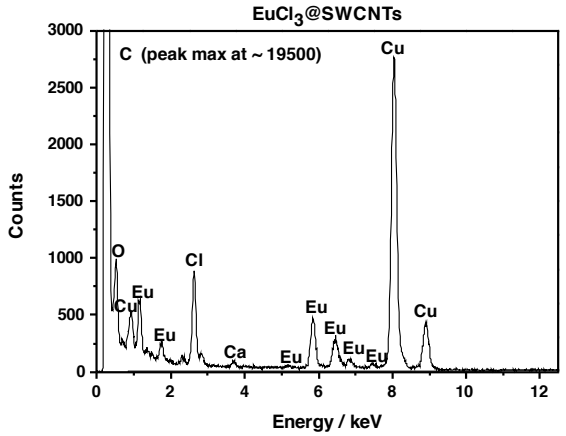

Figure 6.4. EDX analysis of $EuCl_3$@SWCNTs.

EDX of MX@CNTs (Fig. 6.3 and Fig. 6.4) gave information about the elemental composition of the samples. As it can be seen, the constituent cation (M = Lu, Eu) and anion (X = Cl, Br, I) of each metal halide is detected in the samples of filled carbon nanotubes (MX@SWCNTs) confirming that the crystals observed inside the cavities of SWCNTs by TEM do correspond to the metal halides employed in the filling experiment. The large carbon and copper signals can be assigned to the carbon coated copper grid used as support for the analyses. The iron peak comes from the catalyst used for the synthesis of carbon nanotubes.

6.4. Characterization on functionalized SWCNTs

Empty purified and MX@CNTs were functionalized by both Tour and Prato reactions. Functionalization was monitored by TGA under flowing N_2, Kaiser test and Raman spectroscopy.

6.4.1. Characterization of samples functionalized by Tour reaction

First, SWCNTs were functionalized with 4-[2-(Boc-amino)methyl]aniline (Boc-amine) in the presence of isopentyl nitrite. Then, Boc group was removed using 4 M HCl in dioxane in order to obtain amino functionalized SWCNTs (Scheme 6.7). Tour reaction was repeated twice for each type of CNTs used.

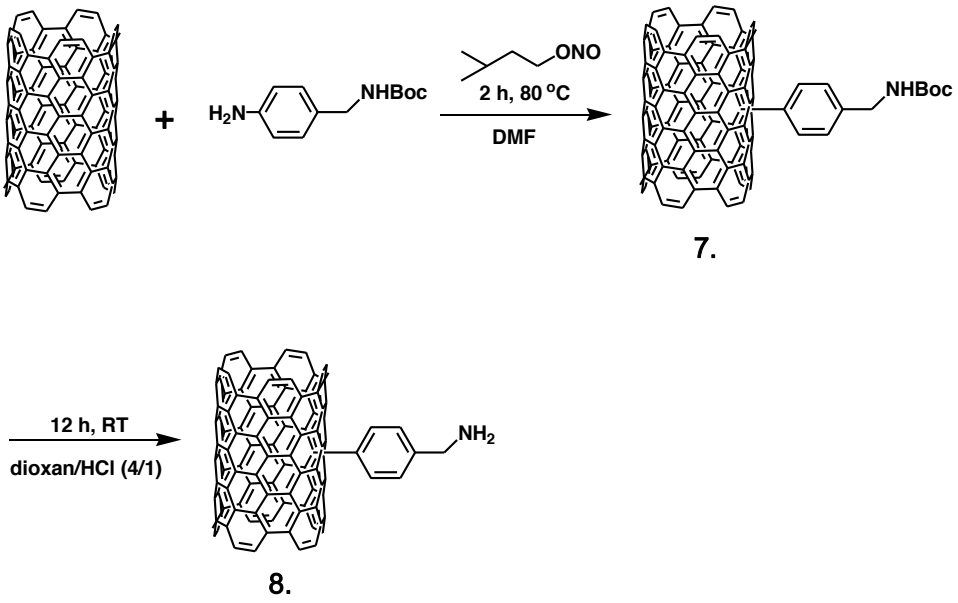

Scheme 6.7. Tour reaction (7) on SWCNTs and cleavage of Boc group in order to afford amino functionalized SWCNTs (8).

Table 6.1 summarizes the results of TGA and Kaiser test for functionalized CNTs. According to TGA empty SWCNTs show a higher degree of functionalization (ca. 700 μmol/g) than any of the MX@SWCNTs (ca. 350 - 600 μmol/g). The amount of functional groups determined by TGA was taken at 500 ˚C, as detailed in Annex A.2. It is worth noting that $EuCl_3$@SWCNTs are characterized by the highest Boc-amine loading among all the investigated filled CNTs: 692 μmol/g and 542 μmol/g. The amine loading of empty and filled SWCNTs determined by Kaiser test (fdpr-CNTs), it is similar for all types of samples, in the range ca. 200-350 μmol/g. Kaiser test is sensitive to the presence of primary amines. Therefore, where f-CNTs (compound 7) where analyzed by TGA and fdpr-CNTs (compound 8) were employed for Kaiser test. As a control, Kaiser test was also performed on f-CNTs (7), to confirm the absence of free α-amines.

Table 6.1. Functionalization degree of empty and filled SWCNTs by Tour reaction as determined from TGA in nitrogen at 500 ˚C and Kaiser test. Reactions were performed twice two for each type of samples.

Sample	Functionalization (μmol/g)		
	TGA	Kaiser test	
	f-CNTs[a] (7)	f-CNTs[a] (7)	fdpr-CNTs[b] (8)
$LuCl_3$@SWCNTs	434 359	23 17	195 +/-24 357 +/- 29
$LuBr_3$@SWCNTs	490 -	16 17	305 +/- 24 378 +/- 45
LuI_3@SWCNTs	365 324	19 17	268 +/- 33 153 +/- 29
$EuCl_3$@SWCNTs	692 542	26 12	272 +/- 27 231 +/- 34
SWCNTs	752 657	11 4	194 +/- 14 212 +/- 45

[a]**f-CNTs: functionalized carbon nanotubes,** [b]**fdpr-CNTs: functionalized carbon nanotubes with cleaved protecting group**

Raman spectroscopy is widely employed to monitor the functionalization of carbon nanotubes by looking at the intensity ratio of D and G bands, I_D/I_G. We recorded the Raman spectra of both empty and filled SWCNTs before and after being modified by Tour reaction. As it can be seen in Table 6.2, the spectra of the functionalized material always exhibit a significant increase in the intensity of the D to G ratio band. This confirms the covalent functionalization of the structure of carbon nanotubes. Upon covalent chemical modification of the sp^2 network of the nanotubes (origin of the G-band) an increase of the carbon atoms bearing sp^3 hybridization is expected (associated with the D-band).

Table 6.2. Raman I_D/I_G ratio of empty and filled SWCNTs before and after Tour reaction. Reactions were performed twice for each type of samples. Raman spectroscopy was performed using a 20 mW He–Ne laser (632 nm). Each sample was measured at 3 different spots.

Sample	Intensity I_D/I_G	
	CNTs	f-CNTs (7)
$LuCl_3$@SWCNTs	0.14 +/- 0.00	0.18 +/- 0.09 0.30 +/- 0.05
$LuBr_3$@SWCNTs	0.15 +/- 0.03	0.27 +/- 0.19 0.22 +/- 0.13
LuI_3@SWCNTs	0.15 +/- 0.04	0.23 +/- 0.10 0.26 +/- 0.03
$EuCl_3$@SWCNTs	0.11 +/- 0.01	0.20 +/- 0.09 0.27 +/- 0.03
SWCNTs	0.17 +/- 0.01	0.28 +/- 0.13 0.33 +/- 0.04

6.4.2. Characterization of samples functionalized by Prato reaction

SWCNTs were functionalized with the synthesized aminoacid (9) via 1,3-dipolar cycloaddition. Phtahalimide protecting group was cleaved with paraldehyde at 180 ˚C (Scheme 6.8).

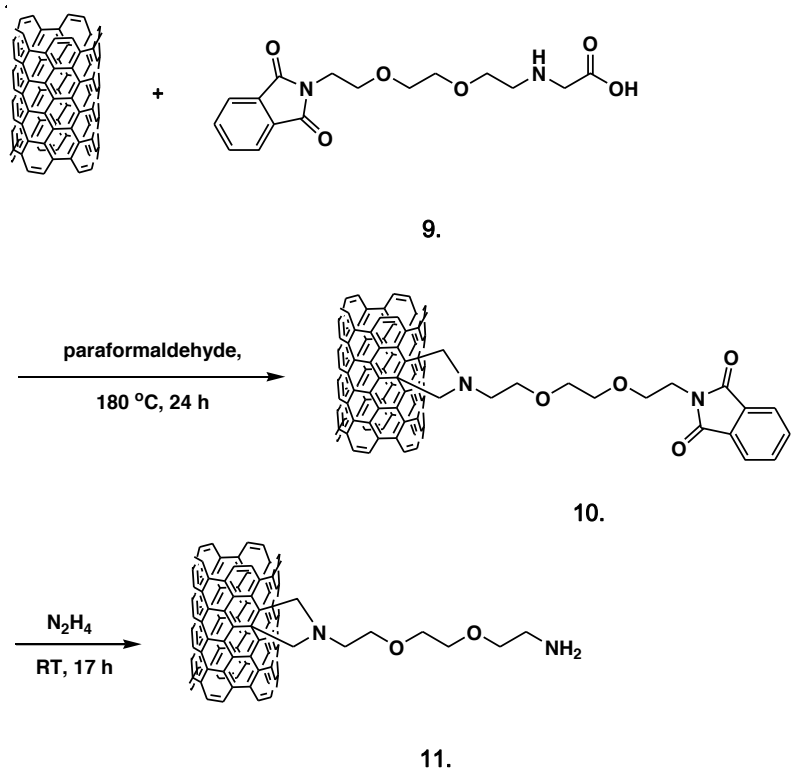

9.

10.

11.

Scheme 6.8. Prato reaction on SWCNTs (10) and cleavage of phtahalimide group in order to afford amino functionalized SWCNTs (11).

The loading of functional groups was determined on the samples of both empty and filled SWCNTs by TGA under flowing nitrogen and Kaiser test (fdpr-CNTs, compound 10), and the results are summarized in Table 6.3. In agreement with the Tour reaction, $EuCl_3$@SWCNTs are characterized by the highest functionalization, with 305 μmol/g, compared to the other MX@SWCNTs. Empty SWCNTs also reveal a similar degree of functionalization, with 294 μmol/g. Interestingly, the degree of functionalization of the LuX_3@SWCNTs seems to be dependent on the anion employed (as determined by TGA) in the order Cl > Br > I (210 μmol/g, 182 μmol/g, 146 μmol/g, respectively). According to TGA, for all analyzed samples a larger amount of functional groups are introduced when using the Tour reaction than with the Prato reaction. In contrast, Kaiser test indicates that the reaction was not efficient on the samples investigated by Prato reaction.

Table 6.3. Functionalization degree of empty and filled SWCNTs by Prato reaction as determined by TGA in nitrogen at 500 ˚C and Kaiser test.

Sample	Functionalization (μmol/g)		
	TGA	Kaiser test	
	f-CNTs[a] (10)	f-CNTs[a] (10)	fdpr-CNTs[b] (11)
$LuCl_3$@SWCNTs	210	24	18 +/- 1
$LuBr_3$@SWCNTs	192	37	23 +/- 5
LuI_3@SWCNTs	146	36	19 +/- 2
$EuCl_3$@SWCNTs	305	13	37 +/- 11
SWCNTs	294	0	17 +/- 5

[a]**f-CNTs: functionalized carbon nanotubes,** [b]**fdpr-CNTs: functionalized carbon nanotubes with cleaved protecting group**

Whereas TGA indicates that functional groups are present in the sample, the presence of amines is no detected by Kaiser test. Therefore, we next performed Raman spectroscopy of the samples to determine whether the sp^2 structure of CNTs has been altered, which as previously mentioned is an indication of the formation of covalent bonds. The D to G ratios of the samples before and after Prato reaction are summarized in Table 6.4.

In contrast to the Tour reaction, where an increase in D to G intensity ratio was observed, the I_D/I_G ratio remains practically unaltered after the Prato reaction. Therefore, non-covalent bonds seem to have been created by this reaction. The TGA weight loss observed could account for the presence of absorbed molecules of protected aminoacid.

Table 6.4. Raman I_D/I_G ratio of empty and filled SWCNTs before and after Prato reaction. Raman spectroscopy was performing using a 20 mW He–Ne laser (632 nm). Each sample was measured at 3 different spots.

Sample	Intensity I_D/I_G	
	CNTs	f-CNTs
$LuCl_3$@SWCNTs	0.14 +/- 0.00	0.10 +/- 0.01
$LuBr_3$@SWCNTs	0.15 +/- 0.03	0.14 +/- 0.02
LuI_3@SWCNTs	0.15 +/- 0.04	0.14 +/- 0.01
$EuCl_3$@SWCNTs	0.11 +/- 0.01	0.15 +/- 0.00
SWCNTs	0.17 +/- 0.01	0.13 +/- 0.00

6.5. Conclusions

We have investigated functionalization of empty purified SWCNTs and metal halide filled SWCNTs (MX@SWCNTs) using both Tour and Prato reactions. For all the employed samples, Tour reaction turned out to be much more efficient than Prato reaction, according to TGA, Raman spectroscopy and Kaiser test. Samples functionalized by radical addition via diazonium chemistry (Tour reaction) were characterized by high amine loading in the range of ca. 200-350 μmol/g (Kaiser test). In contrast, functionalization of CNTs via 1,3-dipolar cycloaddition (Prato reaction) resulted in a non-significant amount of amine loading (Kaiser test). According to TGA $EuCl_3$@SWCNTs, show the highest reactivity in both type of reactions compared to both empty and lutetium halide filled SWCNTs. Amine functionalized CNTs are a great platform for further derivatization and attachment of various functional groups. For instance, in the biomedical field they might be used for conjugation of therapeutic and/or targeting molecules.

REFERENCES

1. Prato, M., Kostarelos, K., Bianco, A. *Functionalized Carbon Nanotubes in Drug Design and Discovery.* Accounts of Chemical Research, 2008. **41**(1): p. 60-68.
2. Kostarelos, K., Bianco, A., Prato, M. , *Promises, Facts and Challenges for Carbon Nanotubes in Imaging and Therapeutics.* Nature Nanomaterials, 2009. **4**(10): p. 627-633.
3. Tasis, D., et al., *Chemistry of Carbon Nanotubes.* Chemical Reviews, 2006. **106**(3): p. 1105-1136.
4. Mamane, V.M., et al., *Chemi- vs Physisorption in the Radical Functionalization of Single-Walled Carbon Nanotubes under Microwaves.* Beilstein Journal of Nanotechnology, 2014. **5**: p. 537–545.
5. Aarón Morelos-Gómez, et al., *Nanotube Chemical Functionalization*, in *Springer Handbook of Nanomaterials*, Vajtai, R., Editor. 2013, Springer. p. 197-200.
6. Dyke, C.A., et al., *Diazonium-Based Functionalization of Carbon Nanotubes: XPS and GC-MS Analysis and Mechanistic Implications.* Synlett, 2004. **2004**(01): p. 155-160.
7. Strano, M.S., et al., *Electronic Structure Control of Single-Walled Carbon Nanotube Functionalization.* Science, 2003. **301**(5639): p. 1519-1522.
8. Kim, W.-J., Usrey, M.L., Strano, M.S., *Selective Functionalization and Free Solution Electrophoresis of Single-Walled Carbon Nanotubes: Separate Enrichment of Metallic and Semiconducting SWNT.* Chemistry of Materials, 2007. **19**(7): p. 1571-1576.
9. Bahr, J.L. , Tour, J.M., *Highly Functionalized Carbon Nanotubes Using in Situ Generated Diazonium Compounds.* Chemistry of Materials, 2001. **13**(11): p. 3823-3824.
10. Dyke, C.A., Tour, J.M. *Solvent-Free Functionalization of Carbon Nanotubes.* Journal of the American Chemical Society, 2003. **125**(5): p. 1156-1157.
11. Bahr, J.L., et al., *Functionalization of Carbon Nanotubes by Electrochemical Reduction of Aryl Diazonium Salts: A Bucky Paper Electrode.* Journal of the American Chemical Society, 2001. **123**(27): p. 6536-6542.
12. Raicopol, M., et al., *Electrochemical Reduction of Aryl Diazonium Salts: a Versatile Way for Carbon Nanotubes Functionalisation.* Surface and Interface Analysis, 2012. **44**(8): p. 1081-1085.
13. Liang, C., et al., *A Diazonium Salt-Based Ionic Liquid for Solvent-Free Modification of Carbon.* European Journal of Organic Chemistry, 2006. **2006**(3): p. 586-589.
14. Price, B.K., Hudson, J.L., Tour, J.M., *Green Chemical Functionalization of Single-Walled Carbon Nanotubes in Ionic Liquids.* Journal of the American Chemical Society, 2005. **127**(42): p. 14867-14870.

15. Georgakilas, V., et al., *Organic Functionalization of Carbon Nanotubes.* Journal of the American Chemical Society, 2002. **124**(5): p. 760-761.
16. Georgakilas, V., et al., *Amino Acid Functionalisation of Water Soluble Carbon Nanotubes.* Chemical Communications, 2002(24): p. 3050-3051.
17. Singh, P., et al., *Organic Functionalisation and Characterisation of Single-Walled Carbon Manotubes.* Chemical Society Reviews, 2009. **38**(8): p. 2214-2230.
18. Tagmatarchis, N., Prato, M., *Functionalization of Carbon Nanotubes via 1,3-dipolar Cycloadditions.* Journal of Materials Chemistry, 2004. **14**(4): p. 437-439.
19. Battigelli, A., et al., *Endowing Carbon Nanotubes with Biological and Biomedical Properties by Chemical Modifications.* Advanced Drug Delivery Reviews, 2013. **65**(15): p. 1899-1920.
20. Kordatos, K., et al., *Novel Versatile Fullerene Synthons.* The Journal of Organic Chemistry, 2001. **66**(14): p. 4915-4920.
21. Shao, L., et al., *Removal of Amorphous Carbon for the Efficient Sidewall Functionalisation of Single-Walled Carbon Nanotubes.* Chemical Communications, 2007. (47): p. 5090-5092.
22. Ballesteros, B., et al., *Quantitative Assessment of the Amount of Material Encapsulated in Filled Carbon Nanotubes.* The Journal of Physical Chemistry C, 2009. **113**(7): p. 2653-2656.

CHAPTER 7

DECORATION OF MULTI-WALLED CARBON NANOTUBES WITH GOLD NANOPARTICLES

Carbon nanotube/gold nanoparticle hybrids (CNT/AuNPs) have gained attention in catalysis,[1, 2] sensors,[3, 4] optical electronics,[5] and solar cells[6], but they especially emerged as exciting materials in nanomedicine.[7] AuNPs exhibit a high X-ray attenuation, surface plasmon resonance (SPR), good biocompatibility and nontoxicity.[8, 9] These properties have been used for the development of contrast agents for computerized tomography (CT),[10, 11] and surface-enhanced Raman scattering (SERS) for the following applications: biosensing, optical imaging and phothothermal therapy (PTT).[12-14] On the other hand, CNTs can be externally functionalized and at the same time host a chosenpayload in their hollow core. Combining the properties of CNTs and AuNPs enables the design of multimodal platforms for diagnosis and therapy.

Herein, we filled multi-walled carbon (MWCNTs) with lutetium (III) chloride by molten filling method. $LuCl_3$ was selected, because lutetium-177 is an important radioisotope used for the treatment of cancer and other diseases. Upon decay it emits ?-particles, which can kill pathogenic cells. Moreover, the radioactive half-life of ^{177}Lu is 6.64 days, which permits its shipment from production sites to hospital.[15] We modified $LuCl_3$ filled MWCNTs ($LuCl_3$@MWCNTs) with crown ethers. Crowns are of interest for anticancer therapy to complement drugs, to induce toxicities that differ from those of conventional antitumor drugs or to deliver theranostic agents.[16] Crown ethers can attract metal ions and a variety of organic neutral and ionic species inside their ring. It is also known that two crown ether molecules can sandwich an ion. In these cases, even ligand larger than the natural fit can be captured. In the context of CNTs, in the literature it has been previously reported the functionalization of CNTs with bis(benzo-crown ether)s and substituted benzocrown ethers to host alkali metals (Li^+, K^+, Cs^+).[17, 18] SWCNTs with benzo-18-crown-6 ether were employed for Pb^{2+} determination.[19] Another work describes the preparation of cation-modified (dibenzylammonium) MWCNTs assembled with crown-modified (dibenzo-24-crown-8) gold nanoparticles.[20] In

the present study we explore the use of crown-functionalized $LuCl_3$@MWCNTs as templates for the assembly of AuNPs.

7.1. Synthesis of gold nanoparticles

Usually AuNPs are prepared by reduction of chloroauric acid ($H[AuCl_4]$), although more advanced methods exist. The process involves two steps: nucleation and successive growth. When solution becomes supersaturated with gold atoms they start to precipitate in the form of sub-nanometer particles. The more gold binds together, the bigger nanoparticles are formed. The use of vigorous stirring and stabilizing agents prevent the particles from aggregation.[21, 22]

7.1.1. Seeded growth synthesis and characterization of AuNPs

The AuNPs were prepared by seeded growth method.[23] 1 mL of $HAuCl_4$ (25 mM) precursor was injected into 150 mL of sodium citrate (2.2 mM) at 100 °C. The reaction was stirred with a magnetic bar and kept at this temperature till it reached a red color. After that, the temperature of the solution was decreased to 90 °C in order to inhibit new nucleation of AuNPs, with the desired size. An additional 1 mL of sodium citrate (60 mM) and 1 mL of $HAuCl_4$ solution (25 mM) were added to the reaction mixture, and stirred for two more minutes. Colloidal AuNPs with an intense red-wine color were obtained (Fig. 7.1). When the solution cooled down, aliquots of 2 mL were extracted for characterization by transmission electron microscopy (TEM), UV-Vis spectroscopy and dynamic light scattering (DLS).

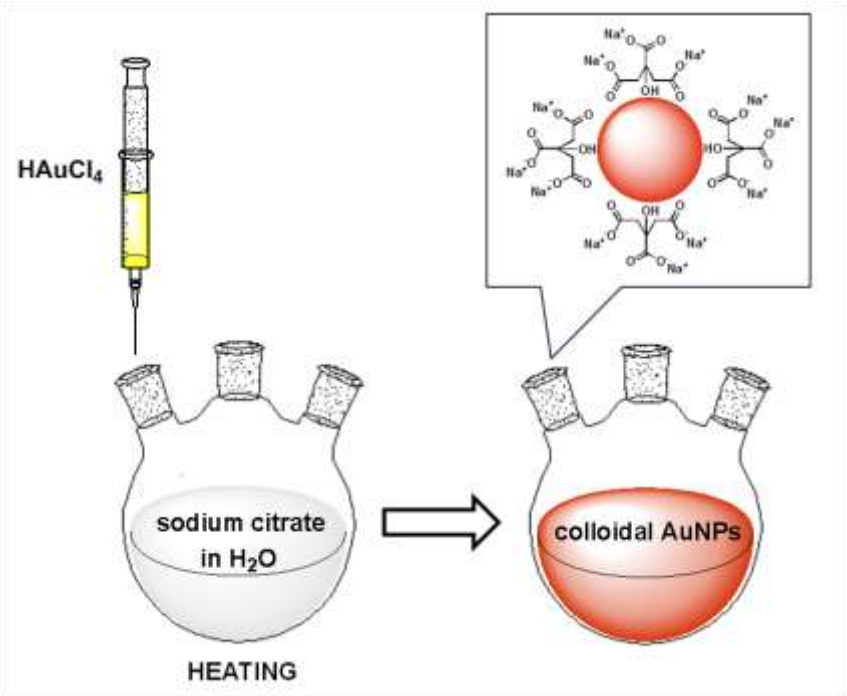

Figure 7.1. General scheme for the preparation of gold nanoparticles (AuNPs). A red colloidal solution of sodium citrate stabilized AuNPs was obtained.

Figure 7.2 shows a representative TEM image of AuNPs and the corresponding histogram of their diameter distribution, as determined from 200 measured nanoparticles. The synthesized nanoparticles have spherical shape and diameters that range between 7 nm and 27 nm with a mean diameter of 13.4 nm.

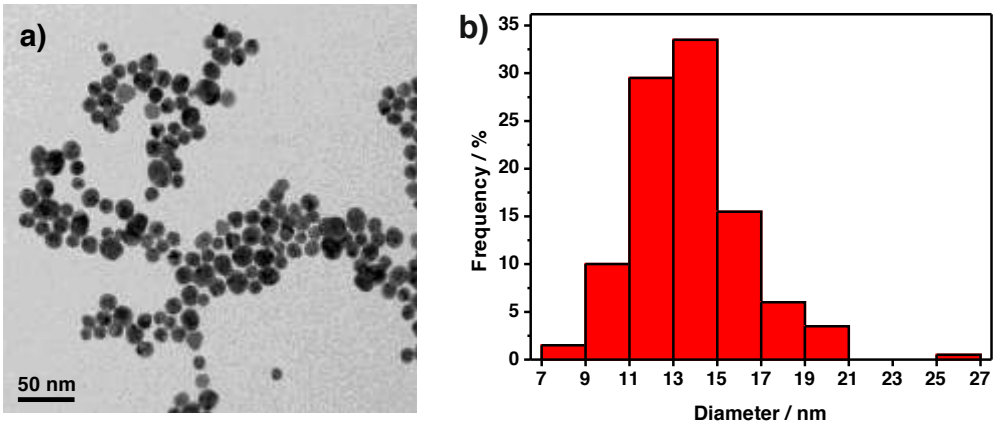

Figure 7.2. a) TEM image of the synthesized AuNPs. b) Histogram of diameter distribution of AuNPs (200 nanoparticles were measured).

Since colloidal gold consists of thousands of nanoparticles, and bearing in mind that TEM provides local information, assessing the overall sample homogeneity and size distribution from this data might be statistically poor. Therefore, we analyzed samples by bulk techniques, namely DLS and UV-Vis.

Dynamic light scattering (DLS) measurements reveled that the sample is moderately polydisperse (PDI = 0.3). Figure 6.3a, shows the relative percentage of light scattering by the particles against various size classes. Two distinct areas are visible: a high peak at 18.2 nm and a small plateau at ca. 4 µm, the latter indicating the presence of only few aggregates in the sample. When measuring nanoparticle distribution by number (Fig. 6.3b) a monomodal distribution with 99% of particles below 20 nm is obtained with a mean diameter of 10.1 nm.

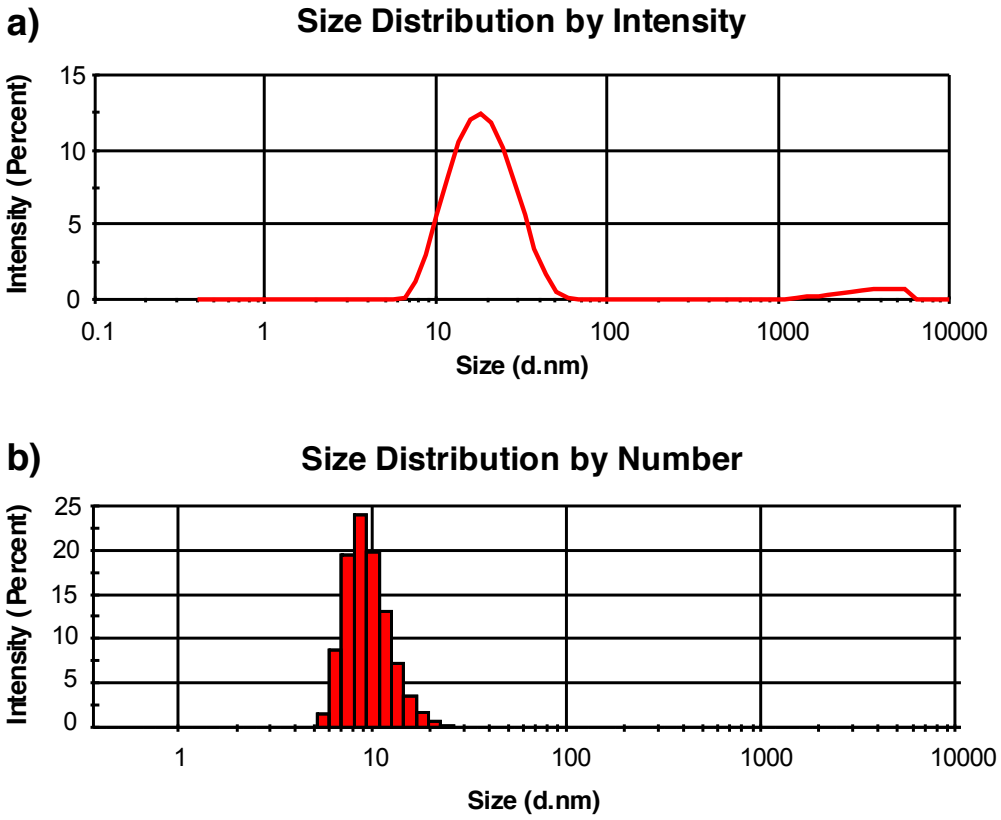

Figure 7.3. Dynamic light scattering of colloidal AuNPs: a) size distribution by intensity, b) size distribution by number. Each plot is an average of 3 independent measurements performed at room temperature during 80 s with attenuator 8 and count rate 130.6.

To complete the characterization of the prepared AuNPs, the UV-Vis absorption spectrum was recorded. As it can be seen in Figure 7.4 it has a maximum peak at 518.5 nm. This value has been assigned in literature to AuNPs with diameters in the range of 9 nm to 14 nm.[24]

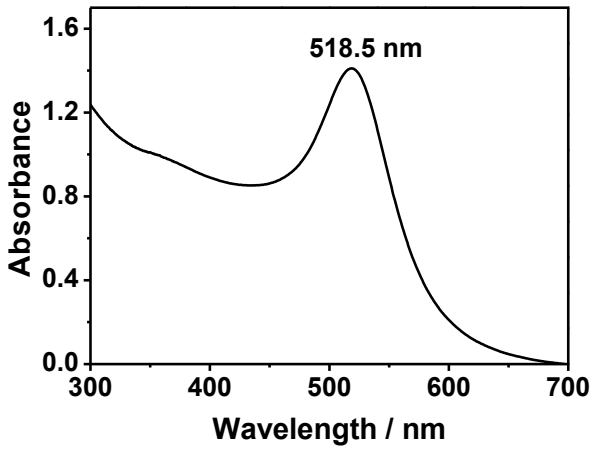

Figure 7.4. UV-Vis absorbance spectrum of synthesized AuNPs with maximum absorption at 518.5 nm.

Therefore, upon taking into account the data obtained from TEM, DLS and UV-Vis, we can conclude that most of the synthesized AuNPs have a diameter in the range ca. 9-18 nm.

7.2. Melt filling of MWCNTs with lutetium (III) chloride and characterization of sample

Chemical vapor deposition MWCNTs were supplied from Thomas Swan and Co. Ltd. They contained carbonaceous impurities and iron catalyst. The as-received MWCNTs were shortened with a mixture of concentrated H_2SO_4/HNO_3 (vol/vol 3:1), and purified by steam (1 h) and HCl. After this treatment open-ended MWCNTs with median length of ca. 225 nm were obtained (see protocol from Chapter 4). The amount of inorganic impurities present, after the complete oxidation of sample decreased from 3.5 wt. % to 0.4 wt. % (purified MWCNTs) as determined by TGA (Fig. 7.5).

Purified MWCNTs were next filled with $LuCl_3$ by molten phase filling. $LuCl_3$ (600 mg) and MWCNTs (60 mg) were ground together inside an argon filled glove box until the mixture presented a homogenous grey color. The sample was divided into three equal portions and placed inside individual silica tubes, which were sealed under vacuum before being annealed at 1100 °C during 12 h. Once the process was finished, samples were collected and mixed together. Next, they were dispersed in distilled water, placed inside a dialysis sack and washed with water in combination with a Soxhlet system in order to remove the excess of $LuCl_3$, external to the nanotubes, following the protocol described in Section 5.1.3.5. The resulting $LuCl_3$@MWCNTs were recovered by filtration onto a polycarbonate membrane. The sample was dried overnight at 100 °C.

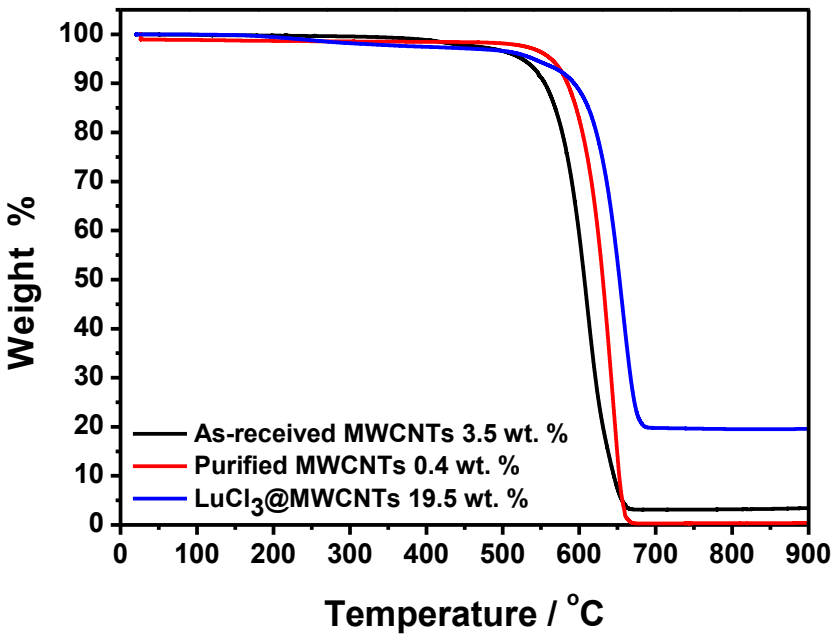

Figure 7.5. Thermogravimetric curves of: as-received, purified and $LuCl_3$ filled MWCNTs. TGA was performed under flowing air. The wt. % residues obtained after burning samples are given in the legend.

The encapsulation of $LuCl_3$ into MWCNTs was confirmed by scanning transmission electron microscopy (STEM) and high resolution transmission electron microscopy (HRTEM). As it can be seen in Figure 7.6a, SEM analysis revealed that the sample was washed properly and did not contain external $LuCl_3$, which would appear with a white contrast in this imaging modality. HRTEM images (Fig. 6b,c)

clearly indicate the presence of closed-ended and filled MWCNTs. The filling yield was determined from thermogravimetric analyses (Fig. 7.5) using a previously reported formula[25] and it was found to be 27.2 wt. %.

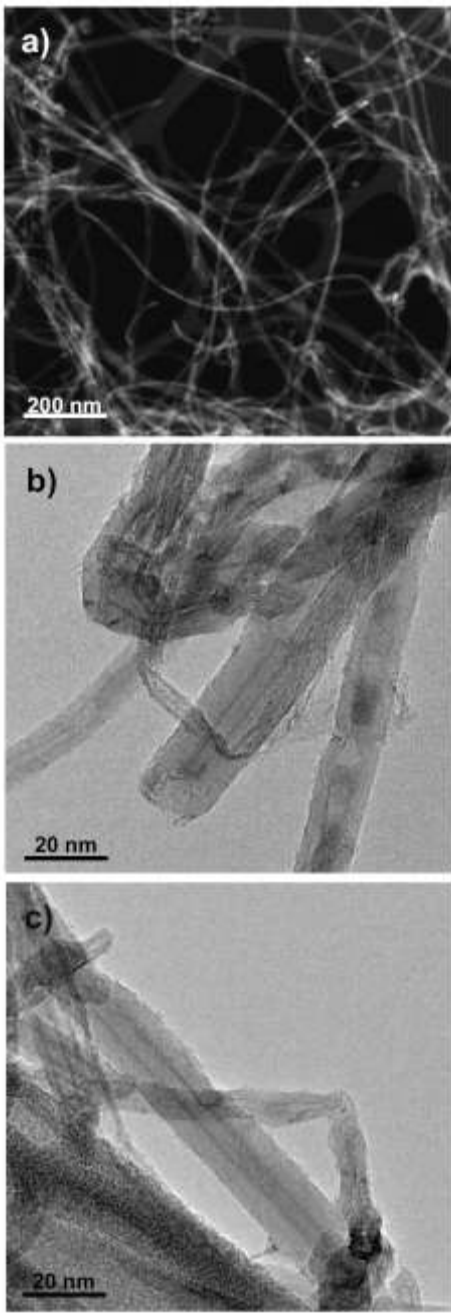

Figure 7.6. a) STEM and b, c) TEM images of $LuCl_3$@MWCNTs.

7.3. Functionalization of $LuCl_3$@MWCNTs

$LuCl_3$@MWCNTs (2.74 mmol of carbon, 45 mg of sample) were dispersed in dimethylformamide (DMF, 1 mg/mL) by sonication for several minutes. When a grey suspension was achieved, 4´-aminobenzeno-15-crown-5 (3.80 mmol) was added and the resulting mixture was sonicated for another 3 min. Then, isopentyl nitrite (7.60 mmol, 1.67 mL) was injected into the reaction, and the whole mixture was heated up to 80 °C, and stirred for 2 h. Then the solution was cooled to room temperature. Functionalized MWCNTs (f-MWCNTs) were filtered onto a teflon membrane (MILIPORE®, type JHWP, pore size 0.45 μm) and washed with DMF until the solvent eluted colorless, washed again with DMF, water, methanol (MeOH), ethyl acetate (EtOAc), diethyl ether (Et_2O) and dried in an oven at 90 °C overnight.

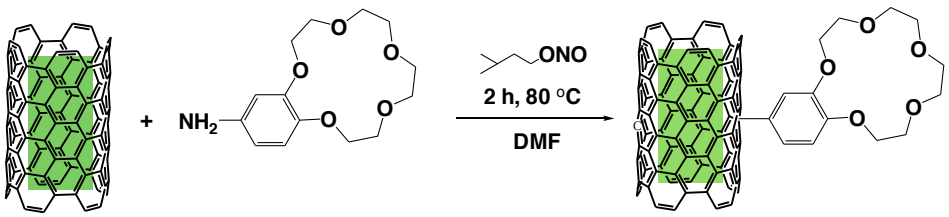

Scheme 7.1. Reaction of $LuCl_3$@MWCNTs with 4´-aminobenzeno-15-crown-5.

Functionalized MWCNTs were analyzed by TGA under flowing nitrogen in order to assess the loading of 4´-aminobenzeno-15-crown-5 (abbreviated later as crown). Figure 7.7 presents the acquired TGA data of carbon nanotubes starting from as-received material until its functionalization. We compared the weight loss for all MWCNTs derivatives at 500 °C and deduced that crown loading was 234 μmol/g (the method employed for the calculation is detailed in Annex A.2).

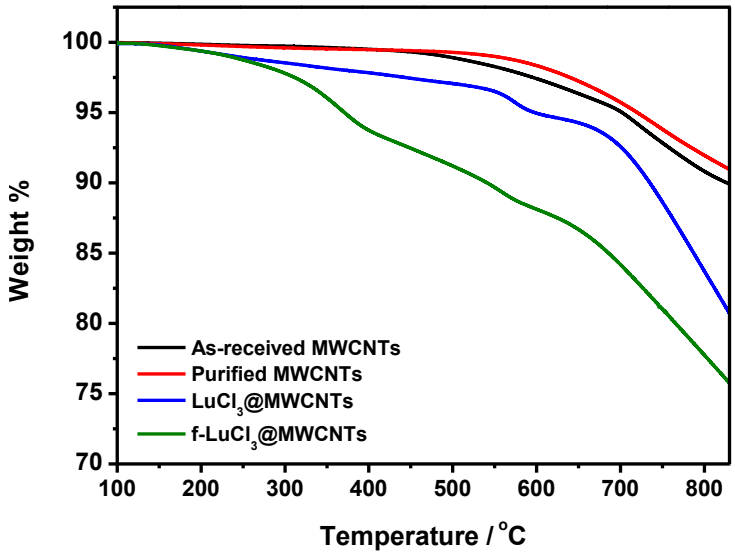

Figure 7.7. Thermogravimetric curves of: as-received, purified, $LuCl_3$ filled MWCNTs and 4´-aminobenzeno-15-crown-5 functionalized $LuCl_3$@MWCNTs. TGA was performed under flowing nitrogen.

7.4. Preparation of $LuCl_3$@MWCNTs/AuNPs hybrids

After confirming the successful functionalization of CNTs with crown, we explored the crown-CNTs chemistry to afford $LuCl_3$@MWCNTs/AuNPs hybrids. The prepared 4´-aminobenzeno-15-crown-5 functionalized $LuCl_3$@MWCNTs were dispersed in 96% ethanol, placed in a round bottom flask and sonicated using an ultrasound bath till a homogenous grey color was obtained. The concentration of CNTs was 0.075 mg/mL. Colloidal AuNPs (10 mL) were added dropwise to the dispersion of nanotubes (100 mL). The resulting mixture was sonicated for 30 seconds, shaked vigorously, and left for 15 minutes to rest. After this period of time it was filtrated onto a teflon membrane and rinsed with 200 mL of Milli-Q water. Obtained $LuCl_3$@MWCNTs/AuNPs were collected, placed into a vial and dried in the oven at 90 °C overnight.

7.5. Characterization of $LuCl_3$@MWCNTs/AuNPs hybrids

$LuCl_3$@MWCNTs/AuNPs were characterized by energy-dispersive X-ray spectroscopy (EDX), transmission electron microscopy (TEM) and scanning transmission electron microscopy (STEM).

EDX (Fig. 7.8) confirmed the presence of both, the filling material (Lu and Cl) and the external nanoparticles decorating the walls of the MWCNTs (Au peak) The presence of the sodium peak is attributed to the sodium citrate used for stabilization of the gold nanoparticles, whereas the silicon peak might arise from the EDX detector.

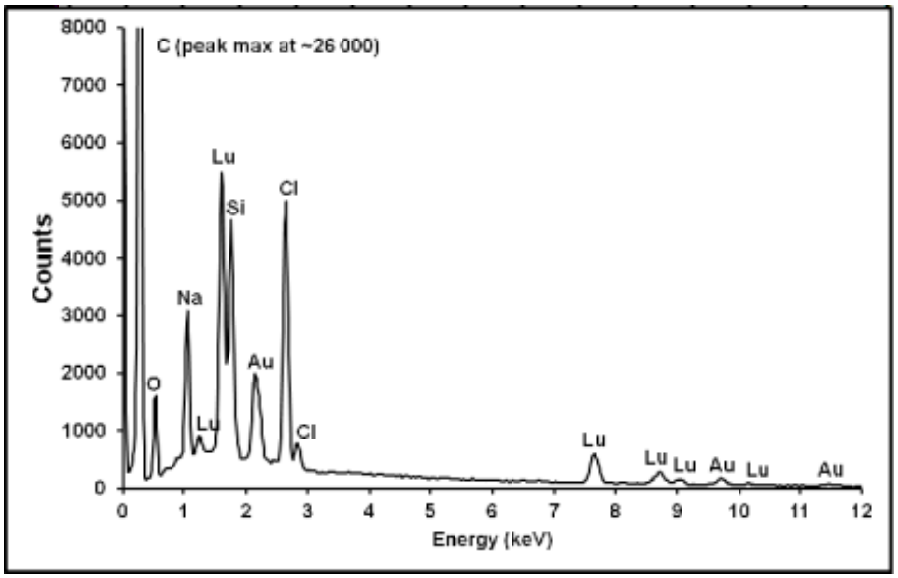

Figure 7.8. EDX analysis of $LuCl_3$@MWCNTs/AuNPs.

Electron microscopy images confirm the decoration of MWCNTs with AuNPs. The TEM image of an individual MWCNT on Figure 7.9b shows that the nanoparticles are evenly distributed along the main axis of the nanotube. HRTEM (Fig. 7.9c and d) allows to simultaneously confirm the presence of gold nanoparticles and the filling material. As discussed in Section 5.2, $LuCl_3$ can form either nanowires or inorganic nanotubes when encapsulated inside carbon nanotubes. In Figure 7.9c the layered structure of $LuCl_3$ is clearly visible (blue arrow). Both encapsulated payload and closed ends can be seen. As a guide to the eye, the different components of the sample are pointed with arrows.

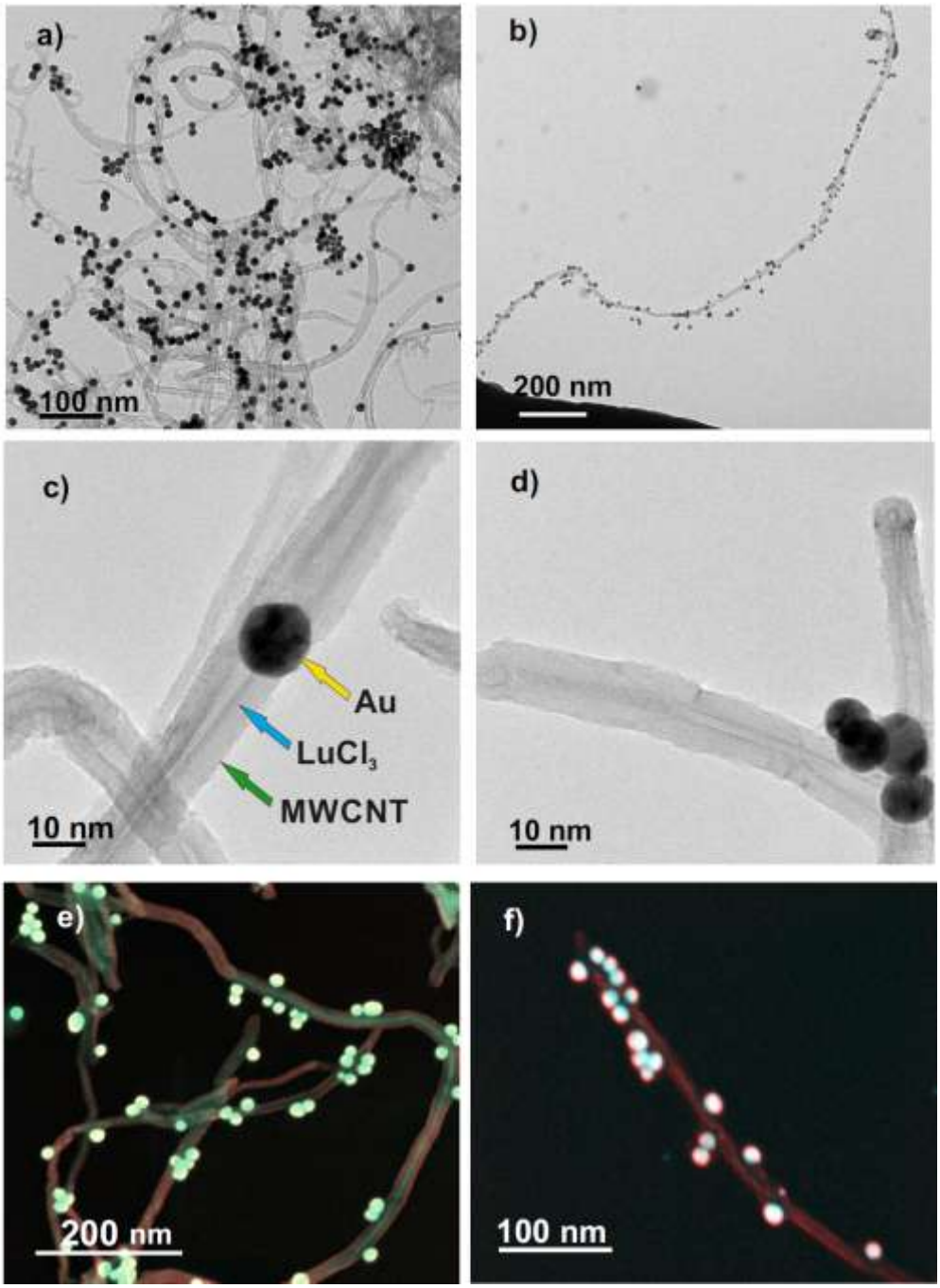

Figure 7.9. Electron microscopy of $LuCl_3$@MWCNTs/AuNPs hybrids: a,b) TEM; c, d) HRTEM; e, f) HAADF STEM.

As previously mentioned, by high angle annular dark field (HAADF) STEM analysis, the different elements present in a sample appear with different contrast, which depends on their atomic number. Images were colored in order to facilitate identification of the components of the sample. Therefore, the bright spheres in Figure 7.9e, f correspond to AuNPs, green lines to the encapsulated payload and the sidewalls of MWCNTs are red.

7.6. Conclusions

We have synthesized colloidal gold nanoparticles using a seeded growth method. The majority of the prepared AuNPs have diameters in the range of 9 nm - 18 nm as determined by TEM, DLS and UV-Vis. Purified MWCNTs were filled with $LuCl_3$ by molten filling method leading to a payload content of ca. 27 wt. % as determined by thermogravimetric analysis. We have covalently functionalized $LuCl_3$@MWCNTs with 4´-aminobenzeno-15-crown. The crown loading was determined by TGA as 234 µmol/g. Finally, f-$LuCl_3$@MWCNTs were decorated with the synthesized AuNPs. The employed protocol for the functionalization of the MWCNTs and subsequent attachment of AuNPs preserved the ends of MWCNTs closed, thus avoiding the removal of the encapsulated $LuCl_3$. Filling, end-closure and decoration were confirmed by TEM and HAADF STEM. The resulting hybrid material holds interest as multimodal nanocapsules for imaging and cancer therapy.

REFERENCES

1. Shi, Y., Yang, R., Yuet, P.K., *Easy Decoration of Carbon Nanotubes with Well Dispersed Gold Nanoparticles and the Use of theMaterial as an eEectrocatalyst.* Carbon, 2009. **47**(4): p. 1146-1151.
2. Lü, W., et al.,. *Decoration of Carbon Nanotubes with Gold Nanoparticles for Catalytic Applications.* in *MRS Proceedings*. 2004.
3. Muhammad, A., Yusof, N., Hajian, R., Abdullah, J., *Decoration of Carbon Nanotubes with Gold Nanoparticles by Electroless Deposition Process Using Ethylenediamine as a Cross Linker.* Journal of Materials Research, 2016. **31**(18): p. 2897-2905.
4. Haider, W., et al., *Gold Nanoparticle Decorated Single Walled Carbon Nanotube Nanocomposite with Synergistic Peroxidase Like Activity for d-Alanine Detection.* RSC Advances, 2015. **5**(32): p. 24853-24858.

5. Satishkumar, B.C., et al., *The Decoration of Carbon Nanotubes by Metal Nanoparticles.* Journal of Physics D: Applied Physics, 1996. **29**(12): p. 3173.
6. Kaniyoor, A., Ramaprabhu, S., *Gold Nanoparticle Decorated Multi-Walled Carbon Nanotubes as Counter Electrode for Dye Sensitized Solar Cells.* Journal of Nanoscience and Nanotechnology, 2012. **12**(11): p. 8323-8329.
7. Boisselier, E., Astruc, D., *Gold Nanoparticles in Nanomedicine: Preparations, Imaging, Diagnostics, Therapies and Toxicity.* Chemical Society Reviews, 2009. **38**(6): p. 1759-1782.
8. Dykman, L., Khlebtsov, N., *Gold Nanoparticles in Biomedical Applications: Recent Advances and Perspectives.* Chemical Society Reviews, 2012. **41**(6): p. 2256-2282.
9. Daraee, H., et al., *Application of Gold Nanoparticles in Biomedical and Dug Delivery.* Artificial Cells, Nanomedicine, and Biotechnology, 2016. **44**(1): p. 410-422.
10. Xi, D., et al., *Gold Nanoparticles as Computerized Tomography (CT) contrast agents.* RSC Advances, 2012. **2**(33): p. 12515-12524.
11. Cole, L.E, et al., *Gold Nanoparticles as Contrast Agents in X-ray Imaging and Computed Tomography.* Nanomedicine, 2015. **10**(2): p. 321-341.
12. Bao, Z., et al., *Near-Infrared Light-responsive Inorganic Nanomaterials for Photothermal Therapy.* Asian Journal of Pharmaceutical Sciences, 2016. **11**(3): p. 349-364.
13. Modugno, G., et al., *Carbon Nanomaterials Combined with Metal Nanoparticles for Theranostic Applications.* British Journal of Pharmacology, 2015. **172**(4): p. 975-991.
14. Weintraub, K., *Biomedicine: The New Gold Standard.* Nature, 2013. **495**(7440): p. S14-S16.
15. Ambikalmajan, M.R.P., Furn, F.K., *Evolving Important Role of Lutetium-177 for Therapeutic Nuclear Medicine.* Current Radiopharmaceuticals, 2015. **8**(2): p. 78-85.
16. Kralj, M., Tušek-Božić, L., Frkanec, L., *Biomedical Potentials of Crown Ethers: Prospective Antitumor Agents.* ChemMedChem, 2008. **3**(10): p. 1478-1492.
17. Kikukawa, K., et al., *New Applications of Crown Ethers. Part 6. Structural Effects of Bis(benzocrown ether)s and Substituted Benzocrown Ethers on Solvent Extraction and Complexation of Alkali-Metal Cations.* Journal of the Chemical Society, Perkin Transactions 2, 1987(2): p. 135-141.
18. Kazei, A., et al., *Functionalization of Oxidized Single-Walled Carbon Nanotubes with 4-benzo-9-crown-3 ether.* Journal of Chemical Sciences, 2012. **1124**(5): p. 1127-1135.
19. Khazaei, A., Borazjani, M.K., Moradian, K.M., *Functionalization of Oxidized Single-Walled Carbon Nanotubes with 4-benzo-9-crown-3 ether.* Journal of Chemical Sciences, 2012. **124**(5): p. 1127-1135.

20. Sainsbury, T., Fitzmaurice, D., *Carbon-Nanotube-Templated and Pseudorotaxane-Formation-Driven Gold Nanowire Self-Assembly.* Chemistry of Materials, 2004. **16**(11): p. 2174-2179.
21. Zhao, P., Li, N., Astruc, D. *State of the Art in Gold Nanoparticle Synthesis.* Coordination Chemistry Reviews, 2013. **257**(3–4): p. 638-665.
22. Herizchi, R., et al., *Current Methods for Synthesis of Gold Nanoparticles.* Artificial Cells, Nanomedicine, and Biotechnology, 2016. **44**(2): p. 596-602.
23. Bastús, N.G., Comenge, J., Puntes, V., *Kinetically Controlled Seeded Growth Synthesis of Citrate-Stabilized Gold Nanoparticles of up to 200 nm: Size Focusing versus Ostwald Ripening.* Langmuir, 2011. **27**(17): p. 11098-11105.
24. Link, S., El-Sayed, M.A., *Size and Temperature Dependence of the Plasmon Absorption of Colloidal Gold Nanoparticles.* The Journal of Physical Chemistry B, 1999. **103**(21): p. 4212-4217.
25. Ballesteros, B., et al., *Quantitative Assessment of the Amount of Material Encapsulated in Filled Carbon Nanotubes.* The Journal of Physical Chemistry C, 2009. **113**(7): p. 2653-2656.

CHAPTER 8

GENERAL CONCLUSIONS

In this thesis the development of carbon nanocapsules (closed-ended filled carbon nanotubes) has been investigated at different stages to render materials that can be directly employed for imaging/diagnosis and therapeutic studies. The general conclusions are divided by these different steps with an increased complexity: i) purification and shortening, ii) endohedral filling, iii) and exohedral functionalization of nanocapsules.

i) Purification and shortening

The role of steam on the purity, length distribution and structure of single-walled (SWCNTs) and double-walled CNTs (DWCNTs) has been studied. Steam plays an important role in the purification of CNTs. It removes amorphous carbon and graphitic shells, which in turn can be coating catalyst particles. After the steam treatment the metal particles can be easily dissolved in HCl. Besides, steam etches the most defective and outer nanotubes on samples of DWCNTs. Chemical vapor deposition and arc discharge CNTs reveal different reactivity towards steam. After 4 h of steam treatment their median length was reduced about 40% and 15%, respectively. CVD CNTs with median length of ca. 200 nm were obtained after 10 h of exposition to steam. We have shown that individual carbon nanotubes can be imaged by means of SEM by employing *ortho*-dichlorobenzene as a dispersing agent, thus allowing a fast assessment of the length distribution.

The efficiency of several protocols for shortening SWCNTs and multi-walled CNTs (MWCNTs) have been tested: steam, ball milling, concentrated sulfuric and nitric acids (H_2SO_4/HNO_3, vol/vol 3:1), and piranha (96% H_2SO_4/ 30% H_2O_2, vol/vol 4:1) to define the best route to prepare short CNTs in a high yield. As methods of choice we suggest the use of combined shortening strategies: piranha + steam 1 h + HCl for SWCNTs and H_2SO_4/HNO_3 + steam 1 h + HCl for MWCNTs. The median lengths of as-obtained nanotubes are ca. 260 nm and ca. 225 nm, respectively. The prepared samples were characterized by high purity and good structural integrity, the latter being essential for the encapsulation and protection of selected payloads.

ii) Endohedral filling of carbon nanotubes

The role of the annealing temperature on the degree of end-closure of SWCNTs has been analyzed by means of nitrogen adsorption studies. A continuous closure of the nanotubes ends is detected in the range of 800 °C to 1200 °C when annealed under vacuum, which has direct implications for the formation of carbon nanocapsules. A variety of metal halides, of interest for nanooncology, have been thus successfully encapsulated by molten phase filling in this range of temperatures in both CVD and arc discharge SWCNTs. In agreement with the nitrogen adsorption studies a higher filling yield has been obtained when employing higher temperatures for the filling experiment. We have developed a straightforward approach that allows the removal of the non-encapsulated material present after the bulk filling of CNTs, in a time efficient and environmentally friendly manner. The protocol benefits from the combination of Soxhlet and dialysis and uses water as a "green" solvent, while minimizing the residual waste. Therefore, it paths the way towards a sustainable production of carbon nanocapsules, especially when dealing with radioactive payloads.

iii) Exohedral functionalization of carbon nanocapsules

Aryl diazonium chemistry (Tour reaction) and 1,3-dipolar cycloaddition (Prato reaction) were employed to functionalize both empty and filled SWCNTs with several metal halides. CNTs reacted with 4-[2-(Boc-amino)methyl]aniline and α-aminoacid. The degree of functionalization was verified by TGA and Kaiser test, which together with Raman analyses revealed that Tour reaction is much more efficient than Prato reaction for the samples employed herein.

CNTs internally loaded and externally decorated with inorganic materials have been developed to afford dual imaging/diagnostic and therapeutic agents. Specifically, closed-ended and clean $LuCl_3$@MWCNTs were afforded by molten phase filling and washing with the above mentioned Soxhlet system. Then, CNTs were covalently modified with 4´-aminobenzeno-15-crown-5, to ca. 230 μmol/g of functional moieties, which allowed the attachment of gold nanoparticles. To the best of our knowledge this constitutes the first hybrid material, where inorganic payloads have been simultaneously loaded inside and outside CNTs walls.

PART III

ANNEXES

ANNEX A. METHODS

A.1. Calculation of the filling yield of samples of metal halide filled carbon nanotubes

Filling yield (FY) of CNTs with encapsulated payloads (A@CNTs) was calculated on the basis TGA residues in air[1]: from empty nanotubes (R_1), clean filled nanotubes (R_2) and bulk material (R_A).

$$FY\ (wt.\ \%) = \frac{100 \cdot (\mathrm{R_2} - \mathrm{R_1})}{\mathrm{R_A} - \mathrm{R_1}}\ (\mathrm{A.1})$$

R_A is the product of oxidation of a given lanthanide halide and therefore can also be theoretically calculated from the reaction: $xA_{(s)} \overset{O_2}{\rightarrow} yB_{(s)}$.

$$R_A = \frac{100 \cdot \mathrm{y} \cdot \mathrm{MW_B}}{\mathrm{x} \cdot \mathrm{MW_A}}\ (\mathrm{A.2})$$

Where *x* and *y* are stoichiometric coefficients of reaction and MW is the molar weight of the metal halide (MW_A) and metal oxide (MW_B).

A.2. Calculation of the loading of functional groups from TGA curves

The degree of the functionalization of CNTs was calculated from TGA curves at 500 °C. TGA of f-CNTs was performed in nitrogen. We compared step by step percentage weight loss of the sample for all derivatives developed from the same starting material, and divided by molecular weight of functional group:

$$FGR\ loading\ \left(\frac{\mu mol}{g}\right) = \frac{Weight\ \%\ \cdot 10^4}{MW_{FGR}\ \left(\frac{mg}{mol}\right)}\ (A.3)$$

Where: FGR loading - loading of functional groups, Weight % - TGA weight loss, MW_{FGR} - molecular weight of functional group.

A.3. Kaiser test

Kaiser test is a colorimetric test, which enables qualitative indication of presence or absence of free primary amino groups.[2] It is based on the reaction of ninhydrin with primary amines. They form a complex (Scheme A.1), which gives a characteristic purple color (Fig. A.1).

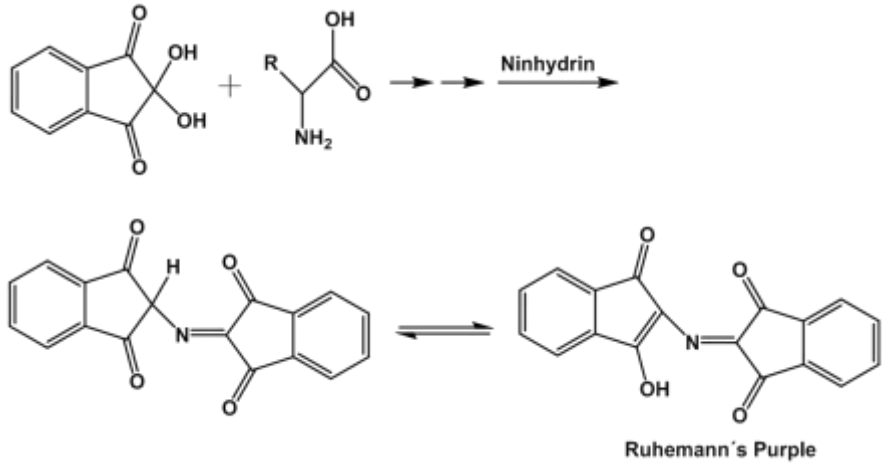

Scheme A.1. Reaction of ninhydrin with primary amines- formation of Ruherman´s purple complex.

Figure A.1. Kaiser test: left vial-control (light yellow), right- positive (purple).

Kaiser test was performed using Fluka Kaiser test kit. In a typical test, 0.2-0.3 mg of CNTs (m) were weighted. In case of filled nanotubes only the mass of carbon was taken into account. 75 µL of the kit solution of phenol (80% in EtOH) and 100 µL of the kit solution of KCN (in H_2O/pyridine) were added, and mixture was sonicated for 2 minutes. Subsequently, 75 µL of the kit solution of ninhydrin (6% in ethanol) was added and the mixture was sonicated for 30 s, and heated at 120 °C for 10 minutes. Then, it was cooled to room temperature and diluted with EtOH/H_2O (60%) to a final volume of 3 mL. After centrifugation (10 min at

8000 rpm) the absorption spectrum of the solution was measured, using as a blank a solution obtained in the same way as above but without CNTs. The value of the absorption maximum at 570 nm was used to calculate the amine loading in the CNT sample (Ɛ = 15000 M^{-1}·cm^{-1}). The amount of free amine functionalities on CNTs surface was calculated according to Lambert-Beer law:

$$NH_2\ loading\ \left(\frac{\mu mol}{g}\right) = \frac{A \cdot V\ (mL) \cdot 10^6}{\varepsilon\ (M^{-1} \cdot cm^{-1}) \cdot\ l(cm) \cdot m\ (mg)} \quad (A.4)$$

Where:
A - absorption value at 570 nm,
V - final volume (here 3 mL),
m – mass of the sample,
ε - extinction coefficient (15000 M^{-1}·cm^{-1}),
l - length of optical path.
The amine loading values reported in Chapter 6 are an average of two separate measurements.

REFERENCES

1. Ballesteros, B., et al., *Quantitative Assessment of the Amount of Material Encapsulated in Filled Carbon Nanotubes.* The Journal of Physical Chemistry C, 2009. **113**(7): p. 2653-2656.
2. Kaiser, E., et al., *Color Test for Detection of Free Terminal Amino Groups in the Solid-Phase Synthesis of Peptides.* Analytical Biochemistry, 1970. **34**(2): p. 595-598.

ANNEX B. INSTRUMENTATION

Thermogravimetric analyses (TGA) of the samples were conducted using either a NETZSCH-STA 449 F1 Jupiter or Q5000 IR instruments.

Inorganic impurities and filling yield were calculated from solid residues obtained after oxidation of the samples. Around 5 mg of each sample were analyzed in air (flow rate 25 mL/min) with a heating rate of 10 °C/min until 900 °C.

Functionalization of CNTs was determined on the basis of TGAs performed in nitrogen (flow rate 25 mL/min) using the following program: plateau at 100 °C during 20 min (to stabilize the sample, remove adsorbed gases and water residues) and ramp with a heating rate of 10 °C/min until 830 °C. Around 1 mg of CNTs was used for each measurement.

Magnetic measurements were done in a superconducting quantum interference device (SQUID) magnetometer (LOT-Quantum Design Iberia). A diamagnetic gelatin capsule was filled with 5-7 mg of sample. Data was acquired with an applied field from -15.000 Oe to +15.000 Oe at 10 K to obtain the hysteresis loops. The sample holder contribution was subtracted in all the measurements. The amount of iron in each of the analyzed samples was determined by taking into account the magnetic saturation of the bulk material (Ms_{Fe} = 221.7 emu·g^{-1}).

Raman spectra (from Chapters 2 and 3) were acquired using a LabRAM HR Raman spectrometer (Horiba Jobin-Yvon), and laser excitation energies of 2.54 and 2.33 eV (488 and 532 nm, respectively, Ar/Kr laser, Coherent) and of 1.96 eV (633 nm, He-Ne). A 50x objective was used with a laser spot of about 1 µm. The laser power was 1 mW and the spectral resolution was 1 cm^{-1}. Each sample was measured in multiple regions. Raman mapping was conducted with lateral steps of 1 µm (both in *X* and *Y* directions) on rectangular areas with varying sizes (49 data points or 900 data points for each map). The samples were measured under ambient conditions.

Raman spectra (Chapters 4-7) were also recorded with Via Renishaw microspectrometer equipped with 20 mW He-Ne laser at 633 nm using the 100x objective. The abscissa was calibrated with a silicon standard. Raman spectra were taken from the thin films prepared by dispersion samples in isopropanol and deposition on glass microscopy slides. To ensure homogeneity of the samples, three spectra were recorded from different spots on the sample.

The Raman spectroelectrochemistry was performed in a 3 electrode cell assembled in a glove box. The measured CNTs were cast on a Pt wire from their dispersion in methanol, which was employed as the working electrode. Another Pt wire was employed as a counter electrode and an Ag wire as a reference electrode. An Autolab PGSTAT (Ecochemie) potentiostat was used to apply potential. The electrolyte solution was $LiClO_4$ (0.2 M) dissolved in dry acetonitrile. The potential was ramped to ± 1.5 V in steps of 0.3 V, and Raman spectra were acquired at constant potential at every step. The high frequency component of the G^- band, the G^+, was fitted by a Lorentzian line shape, whereas the low frequency component, the G^-, was fitted using a Breit-Wigner-Fano (BWF) lineshape. The D-band was fitted by a Lorentzian lineshape.

Scanning electron microscopy (SEM) was carried out on a FEI Magellan 400L XHR using the In-Lens Detector (TLD) at a landing energy of 2 kV achieved by beam deceleration mode. In these conditions, surface sensitive images with spatial resolution below 1 nm are obtained, allowing the visualization of individual single-walled and double-walled carbon nanotubes. Samples were dispersed in *ortho*-dichlorobenzene and dropcasted onto a copper grid coated with a carbon film.

Scanning transmission electron microscopy (STEM) images were acquired on FEI Magellan XHR SEM operated at 20 kV using a High Angle Annular Dark Field (HAADF) detector. Samples were prepared by dispersion in ethanol, and dropcasted on copper lacey grids.

Atomic-resolution STEM (AR-STEM) images were obtained using aberration-corrected corrected FEI Qu-Ant-EM scanning transmission electron microscopy in the HAADF mode operating at 300 kV.

Transmission electron microscopy (TEM) images and **energy dispersive X-ray (EDX)** spectra were acquired at 20 kV on a FEI Quanta 200 FEG ESEM coupled to an Oxford Instruments EDX detection system or with a FEI Tecnai G2 F20 HRTEM at 200 kV equipped with an EDAX super ultra-thin window (SUTW) X-ray detector. TEM analyses were also performed on JEOL 1210. Samples were prepared by dispersion in ethanol, and dropcasted on copper lacey grids.

UV-Vis absorbance was recorded with a double beam UV-Vis spectrophotometer Varian Cary 5 using 1 mm-path quartz cuvettes.

Dynamic light scattering (**DLS**) was measured with Zetasizer Nano ZS.

Nuclear magnetic resonance (^{1}H-NMR) spectra were recorded in deuterated solvents using Varian Gemini – 270 MHz and Jeol JNM-EX400 – 400 MHz. Chemical shifts (δ) are reported in ppm using the residual signal of deuterated solvent as reference. The resonance multiplicity is described as *s* (singlet), *d* (doublet), *t* (triplet), *q* (quartet), *qt* (quintuplet), *m* (multiplet), *br* (broad signal). Coupling constants (*J*) are given in Hz.

Thin layer chromatography (TLC) was conducted on classical pre-coated silica aluminium sheets (TLC Silica gel 60, Merc).

Column chromatography was carried out with silica gel (Merck Kiesel gel 60, 40-60 µm, 230-400 mesh ASTM) in standard columns. All organic solvents used for the purifications were of analytical grade.

Electrospray ionization mass spectrometry (ESI-MS) was performed with Perkin-Elmer Sciex API instrument. Analytes were dissolved in methanol.

ANNEX C. LIST OF PUBLICATIONS

1. Filling Single-Walled Carbon Nanotubes with Lutetium Chloride: A Sustainable Production of Nanocapsules Free of Nonencapsulated Material. **Kierkowicz M.**, González-Domínguez J.M., Pach E., Sandoval S., Ballesteros B., Da Ros T., Tobias G. ACS Sustainable Chemistry & Engineering **2017,** 5 (3), 2501–2508. DOI: 10.1021/acssuschemeng.6b02850.

2. Effect of steam treatment time on the length and structure of single-walled and double-walled carbon nanotubes.
Kierkowicz M., Pach E., Santidrián A., Tobias-Rossell E., Kalbac M., Ballesteros B., Tobias G. ChemNanoMat **2016,** 2, 108-116. DOI : 10.1002/cnma.201500207.

3. Design of antibody-functionalized carbon nanotubes filled with radioactivable metals towards a targeted anticancer therapy.
Spinato C., Perez Ruiz de Garibay A., **Kierkowicz M.**, Pach E., Martincic M., Klippstein R., Bourgougnon M., Tzu-Wen Wang J., Ménard-Moyon C., Al-Jamal K. T., Ballesteros B., Tobias G., Bianco A. Nanoscale **2016,** 8, 12626-12638. DOI: 10.1039/C5NR07923C.

4. Carbon Nanotubes Allow Capture of Krypton, Barium, and Lead for Multichannel Biological X-Ray Fluorescence Imaging.
Serpell C. J., Rutte R. N., Geraki K. , Pach E., Martincic M., **Kierkowicz M.**, De Munari S., Wals K., Raj R., Ballesteros B. Tobias G., Anthony D. C., Davis B. G.
Nature Communications **2016,** 7, 13118. DOI: 10.1038/ncomms13118.